Biodiesel Production in Fixed-Bed Monolithic Reactors

Firth, Benjamin

Award date:
2014

Awarding institution:
University of Bath

University of Bath

Biodiesel Production in Fixed-Bed Monolithic Reactors

Thesis submitted for the degree of Doctor in Philosophy

Ben Firth

Supervisors:

Professor Stan Kolaczkowski (Lead)

Professor Matthew Davidson

Dr. Serpil Awdry

May 2014

Table of Contents

Acknowledgements

I am greatly indebted to a number of people whose help and guidance throughout my PhD has made this thesis possible.

First of all, I wish to extend my greatest thanks to Professor Stan Kolaczkowski, who has provided me with excellent supervision, and has kept me focused and encouraged throughout the project.

I would like to thank the members of the Kolaczkowski research group, particularly Umi Asli and David McClymont, for their technical assistance and knowledge.

The members of the DTC, particularly the 2009 cohort, through their friendship, advice, and troubleshooting, have enabled me to explore areas outside my own experience, and to maintain perspective on life.

Various members of the University of Bath have lent their time and expertise to aid me in this project: John Lowe was of great assistance in utilising the NMR facilities, John Mitchels was invaluable in helping with materials characterisation, and Massi Vezzoli in allowing me to use the Karl Fisher titrator. Also, I would like to thank Andy Tubb, of the University of the West of England, for use and assistance with the ICP facilities.

I would also like to acknowledge the Doctoral Training Centre at the University of Bath for providing me with the opportunity to undertake this Ph.D., and the EPSRC for providing funding.

Most of all, I wish to thank my wife, Jennifer, whose constant acceptance and support has allowed me to pursue my dreams.

Abstract

The production of biodiesel by the transesterification reaction of glycerides (rapeseed oil) with methanol, in a continuous-flow fixed-bed catalytic reactor was explored. Based on data in the literature, lanthanum oxide and strontium oxide (SrO) catalyst systems were selected for this work.

In preliminary experiments in a batch reactor (300 cm^3; with 160 cm^3 of oil), ceramic monoliths (61 cells cm^{-2}; hydraulic cell diameter = 1.1 mm) acted as catalyst supports. At the conditions tested (T= 120ºC; P = 8 bar(g); molar ratio methanol:oil = 6:1), the monoliths coated with SrO (19.6 wt% SrO), were found to be sufficiently active to proceed to the continuous flow fixed-bed trials. A study of the solubility of methanol in oil, showed that in a pressurized autoclave at 100ºC, the methanol dissolved at a 6:1 molar ratio, and at 120ºC this increased up to 9:1, providing useful information for the design of a continuous flow reactor.

The SrO slurry coated monolith was then tested in a single-tube fixed-bed reactor (i.d. = 6.2 mm; L = 200 mm). In experiments at a 7:1 molar ratio of methanol:oil, at T = 195 ºC, and P = 20 bar(g), although catalytic activity was cyclic in nature, it was maintained over a 300 h period (not continuous) of operation. This led to the performance of experiments in a multi-tubular reactor, which consisted of 5 tubes, connected in series (each tube with an i.d. = 22 mm; L = 550 mm). It was now possible to perform experiments with a longer overall length of monolith sections, and to take samples between each tube. Experiments were performed with a monolith bed length of 2300 mm and a molar ratio of methanol:oil = 7:1 (T = 150ºC, P = 15 bar(g)), with overall conversions ranging from 20 to 50%.

.

Nomenclature

Symbols:

M	Molecular weight of component "i"	g mol^{-1}
C	Concentration	mg ml^{-1}
I	Integration value (area)	-
A	Amount of component	Mol %
V	Volume	ml, L
w	Weight %	-
m	Mass	g
T	Temperature	°C
P	Pressure	bar
X	Conversion	%
d	Diameter	cm; m
z	Reactor length	cm; m
ε	Voidage	-
υ	Volumetric flow rate	ml min^{-1}
r	Reaction rate	mol m^{-2} s^{-1}
F	Molar flow	Mol s^{-1}
a	Surface area	m^2
τ	Residence time	Min

Abbreviations:

DG	Diglycerides
FAME	Fatty acid methyl esters, Biodiesel
FFA	Free fatty acids
GC	Gas Chromatography
Gly	Glycerol
MG	Monoglycerides
NMR	Nuclear magnetic resonance
SEM	Scanning electron microscopy
TG	Triglycerides

Chapter 1 Introduction

1.1 Background

Economic, social, political and environmental pressures are accelerating the search for alternative energy sources to augment or replace the use of fossil fuels. Mounting evidence of the potential impact of anthropogenic climate change through the release of greenhouse gases, such as CO_2, has moved legislatures across the world to commit to reducing these emissions through subsidies, taxes, and mandates, while consumers are increasingly demanding action from industry to reduce their impact on the environment (Pahl, 2008). Further to these issues, the majority of the world's crude oil and natural gas reserves are found in unstable geopolitical areas (Kesicki, 2010). This has made the search for viable renewables an issue of national, as well as fuel supply, security. Ultimately, the reserves of fossil fuels are finite by nature, and therefore alternatives must be found before they are exhausted – which may happen within the next century (Sharma and Singh, 2009). Biodiesel, formed by the transesterification of lipid feedstocks, offers an opportunity to generate sustainable, renewable fuel, although advances must be made for it to be a viable competitor in the energy market (Knothe *et al.*, 2005).

In this section, to put the project into its proper context, a brief introduction to diesel engines and fuels is provided. This includes discussion of the history of vegetable oils as diesel fuels, and a more in-depth examination of the science of biodiesel production. Following this is a look at the industrial processes used, the advantages and disadvantages of biodiesel, as well as the future prospects of biodiesel as a fuel. Finally, the project is introduced, along with the aims, objectives, scope and structure of the thesis.

1.2 Diesel Engines

Diesel engines are internal combustion engines which use the compression of a fuel-air mixture as the source of ignition. The expansion of the ignited gases drives the piston, which in turn transfers this energy to mechanical work. After this expansion step, a valve is opened and the piston returns to its original point, forcing the combustion mixture out as exhaust. In a four stroke diesel engine, the piston then expands a second time, drawing in a fresh batch of air through the intake valve. This valve then closes, allowing the air to be compressed to the initial ignition point, and fuel is injected to begin a second cycle. The four stroke cycle is illustrated in Figure 1.1. The fuel injection generally lasts throughout much of the power stroke, in order to create a more even delivery of power. (Smith *et al.*, 2005, Çengel and Boles, 2008)

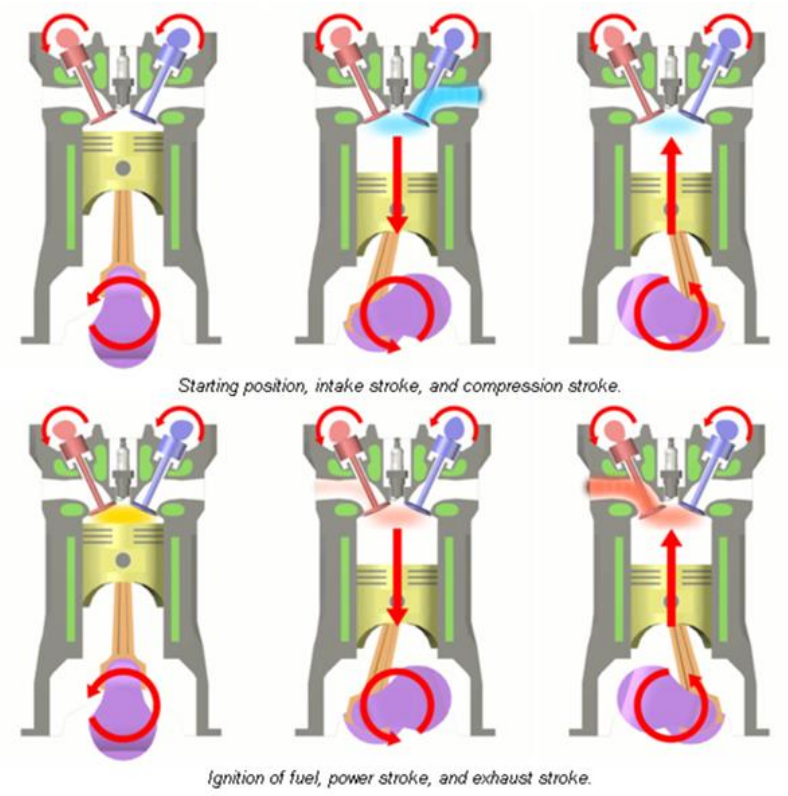

Figure 1.1 A four stroke diesel engine (Minnesota State University, 2010).

1.2.1 Thermodynamic Cycle

The diesel engine in modelled on the thermodynamic cycle known as the Diesel Cycle. It is made up of four stages, which correspond to four strokes of a diesel engine. These stages are shown in Figure 1.2. The cycle begins with isobaric heat addition (D-A), which corresponds to the ignition of the fuel and the beginning of the power stroke. A-B is isentropic expansion, which models the remainder of the power stroke. Next, isochoric heat removal is shown by line B-C, and corresponds to the exhaust stroke and air intake stroke. Although these are obviously not isochoric, their overall effect can be modelled as such. Finally, the Cycle returns to D via isentropic compression, which parallels the compression of the air prior to fuel injection. (Smith *et al.*, 2005, Çengel and Boles, 2008)

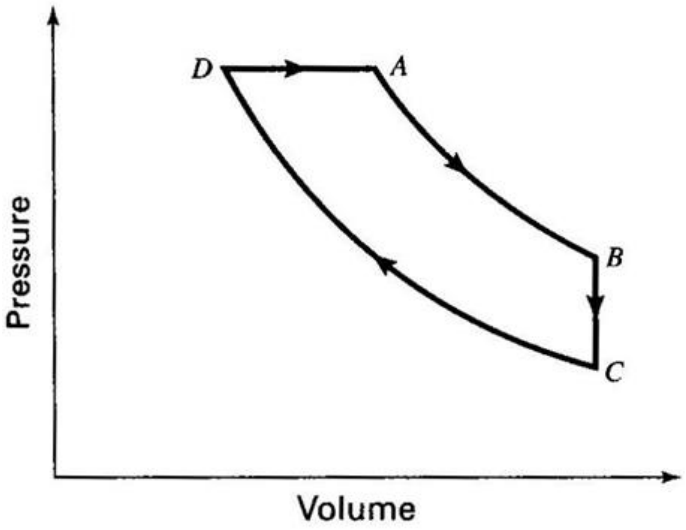

Figure 1.2 P-V diagram of the Diesel Cycle (Smith *et al.*, 2005).

1.2.2 Fuel

Generally speaking, diesel engines are fuelled by a hydrocarbon mixture of alkanes and alkenes of chain lengths between 10 and 20 carbons, and a significant amount of aromatic compounds (Clothier et al., 1993, Knothe et al., 2005). These are obtained from the fractional distillation of crude oil, within the temperature range of 160°C to 330°C (BS 2000-123:2001). Varying the ratios of components, or augmenting or replacing them, will have an effect on the properties of the fuel, and thus the

performance of the engine they are used in. The main properties to consider are calorific value, viscosity, density, and cetane number, and it is possible to use any fuel that has relatively similar properties to conventional diesel in an engine. (Knothe *et al.*, 2005).

1.2.3 Cetane Number

The cetane number of a fuel is an expression of the rate of combustion of the fuel, also known as the ignition delay. More rapid combustion leads to higher cetane numbers. The system is based on the combustion of cetane (hexadecane) and one of its isomers (2,2,4,4,6,8,8-heptamethylnonane). Cetane burns rapidly, and so its combustion delay was given a value of 100. Its isomer is highly branched, and so burns more slowly, and was given a value of 15. Diesel engines are generally designed for fuels with cetane numbers in the range of 40 to 60, with numbers outside the range leading to poor engine performance. (Knothe *et al.*, 2005)

1.2.4 Emissions

The main emissions from diesel engines are water and carbon dioxide, the products of complete combustion of a hydrocarbon fuel. However, due to incomplete combustion, as well as the oxidation of atmospheric nitrogen, carbon monoxide, hydrocarbons (HC), nitrogen oxides (NO_x), and particulate matter (PM) are produced. Additionally, sulphur dioxide is produced from any sulphur present in the fuel. Legislation currently limits the content of all of these additional components in diesel exhaust emissions, and the reductions that must be made are not at all trivial (>90% conversion of hydrocarbons at catalyst operation temperature). (Twigg, 2005)

Despite the large excess of oxygen present, the oxidation of the CO and HC in the exhaust is somewhat complicated by the low exhaust temperatures of diesel engines (Twigg, 2005). This is countered by fine dispersal of the catalyst, and the addition of zeolites to adsorb the hydrocarbons during cold start conditions. The HC later desorb at elevated temperatures, and the catalyst is able to effectively oxidise them (Twigg, 2005).

The production of NO_x in a diesel engine is caused by the high flame temperatures within the cylinder (Zheng et al., 2004). The main component at this stage is NO, some of which later oxidises through a series of free radical reactions with the HC present in the exhaust to make NO_2 (Twigg, 2005). NO_2 then reacts with atmospheric oxygen to create ozone and, along with other pollutants from vehicle exhaust, result in photochemical smog (Twigg, 2005). Because of the excess levels of oxygen in the exhaust, NO_x reduction is a major challenge, despite the fact that NO_x levels prior to the exhaust are lower than in spark ignition engines, where NO_x is reduced using a "three-way" catalyst (Wallington et al., 2006). Two approaches used for dealing with NO_x are exhaust gas recirculation (EGR) and selective catalytic reduction (SCR). The principle of EGR is to supplement the air intake of the engine with exhaust gas, and thus reduce the oxygen concentration in the engine. This in turn reduces the flame temperatures, leading to the creation of less NO_x. Unfortunately this also leads to higher levels of PM (Zheng et al., 2004). SCR uses a reductant such as ammonia to reduce the NO_x over a catalyst, although this creates the obvious need for additional hardware and storage for the system. Generally, urea is used as the ammonia source (Johnson, 2009).

Particulate matter is created by the incomplete combustion of fuel droplets after injection. Some of the fuel does not have sufficient access to oxygen, and undergoes pyrolysis. This leads to a carbonaceous core, which grows larger through agglomeration and adsorption of organic molecules (van Setten et al., 2001). These particles can cause health problems, including asthma, due to their size. PM creation has been reduced dramatically through the use of advanced fuel injector design, but the remaining particles must be dealt with. This is generally achieved by a particle filter, which catches the PM. Once full, the PM is burnt during a higher temperature regeneration period (Twigg, 2005).

1.3 Vegetable Oils as Fuel

Diesel engines are internal combustion engines which use the compression of a fuel-air mixture as the source of ignition. The expansion of the ignited gases drives the piston, which in turn transfers this energy to mechanical work (Smith *et al.*, 2005). These engines are traditionally fuelled by hydrocarbon mixtures obtained from crude oil, although any fuel with similar properties may be used (Knothe *et al.*, 2005). With increasing pressure to obtain renewable energy sources, vegetable oils and their derivatives have been investigated as potential replacements.

Vegetable oils have been used to fuel diesel engines for almost as long as they have existed. In fact, Rudolf Diesel himself used peanut oil to run one of his engines at the Paris Exhibition in 1900, and spent some of his later career investigating the potential of vegetable oils as a fuel source (Pahl, 2008). According to Knothe *et al*. (2005), he once declared that:

> *"the fact that fat oils from vegetable sources can be used may seem insignificant today, but such oils may perhaps become in course of time of the same importance as some natural mineral oils and the tar products are now… they make it certain that motor-power can still be produced from the heat from the sun, which is always available for agricultural purposes, even when all our natural stores of solid and liquid fuels are exhausted."*

1.3.1 Direct Use

Diesel engines can be run directly on pure vegetable oils. The main historical examples are during times of necessity, such as during the Second World War (Knothe *et al.*, 2005). The major advantage to the use of such oils is the ability to source them locally, and with little processing (Sidibe *et al*., 2010). However, several technical problems arise with the use of vegetable oils, such as coking of injectors, breakage due to polymerisation on various components, and severe thickening of the engine oil (Misra and Murthy, 2010). Generally, this has led the research into straight vegetable oils to focus on blends with other fuels, such as traditional petro-diesel.

1.3.2 Fuel Blends

(summarised from Knothe *et al.*, 2005)

The fuel properties of vegetable oils can be improved by diluting them in conventional diesel, and many studies have been undertaken to investigate this. Various oils were examined, primarily during the 1980s, and generally it was found that many of the same problems that affect engines running on vegetable oils also interfere with the operation of those using the oils as a diesel fuel extender; coking in particular is a major issue. Many of the blends failed to meet ASTM standards for diesel fuels, although there was also a trend of improved emissions characteristics.

1.3.3 Micro-emulsions

(summarised from Knothe *et al.*, 2005)

Another alternative for mixed fuels is to emulsify the vegetable oil in a carrier liquid, such as a lower alcohol, with the aid of an amphiphile. This allows for the fuel properties to be tailored through the addition of additives. A micro-emulsion is specifically defined as a mixture of two immiscible liquids which form a thermodynamically stable emulsion on the addition of a surfactant. This results in an improvement over vegetable oils or fuel blends with regard to engine wear and coking, but also increases fuel consumption markedly.

1.3.4 Pyrolysis

Pyrolysis is the catalytic cracking of biomass at elevated temperatures to produce smaller molecules. Pyrolysis of vegetable oils can produce fuels with similar properties to conventional gasoline or diesel (Knothe *et al*., 2005, Taufiqurrahmi and Bhatia, 2011). A typical pyrolysis product will contain a mixture of straight and cyclic alkanes, alkenes, aldehydes, ketones and carboxylic acids (Taufiqurrahmi and Bhatia, 2011). The process can be done both with and without hydrogen, with the

presence of hydrogen being important for the removal of carboxylic acids, through the formation of water (Knothe *et al.*, 2005).

1.3.5 Transesterification

Vegetable oils can also be prepared through a catalysed reaction with a primary alcohol, wherein the fatty acid chains are transesterified, resulting in the formation of fatty acid alkyl esters, generally referred to as biodiesel, and glycerol. Both acid and base catalysts may be used for the reaction, although basic catalysts tend to be more rapid. The reaction is usually carried out with methanol to give fatty acid methyl esters (FAME), which can be used in diesel engines either directly or in a blend with conventional diesel (Knothe *et al.*, 2005).

1.4 Biodiesel

Although the term “biodiesel” has been used in the past to describe various biologically derived diesel fuels, the generally accepted definition is fatty esters formed by the transesterification of triglycerides with a primary alcohol (Knothe *et al.*, 2005). The transesterification occurs sequentially, with one fatty acid chain removed from the triglyceride at a time to give diglyceride, monoglyceride, and finally glycerol co-products. The overall reaction scheme is shown in Figure 1.3. Since the turn of the millennium, global biodiesel production has grown dramatically, increasing by almost eight times from 2000-2008 in the EU, and 350 times in the US in the same time period (Knothe, 2010). European production capacity was estimated to be 20.9 million tons in 2009 (Rottig *et al*., 2010). After ethanol, biodiesel is the second most produced biofuel, and together they combine to make up 90% of the biofuel market (Rottig *et al*., 2010).

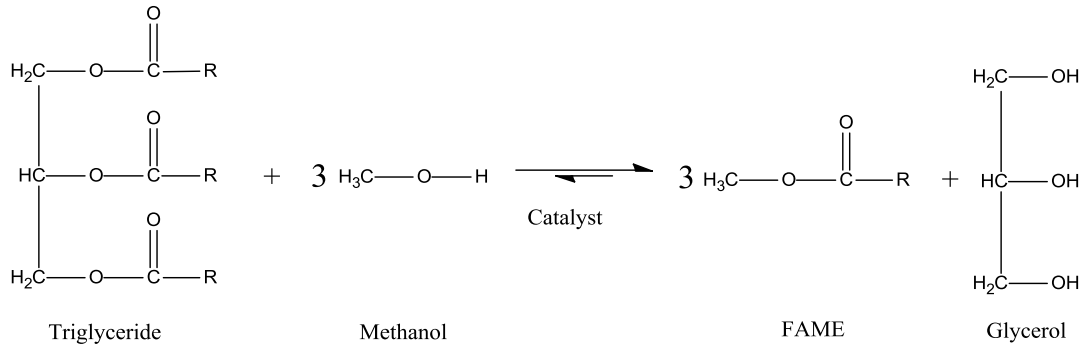

Figure 1.3 General scheme of the transesterification reaction.

1.4.1 Feedstocks

The main feedstocks for biodiesel production are a fat or oil, and a primary alcohol. Generally, methanol is chosen due to its wide availability, low cost, and the ease of obtaining anhydrous supplies. Ethanol is sometimes used, particularly where it is easily available, such as in Brazil (Rottig *et al*., 2010). The source of fat or oil will vary depending on geography, climate, and government policy. Potential sources may include wastes, such as beef tallow; however, the general constituents of the oils will be similar. Oils and fats are made of triglyceride molecules, which entail three fatty acid chains attached to a glycerol backbone by ester bonds. In addition to this, the oil may contain some amount of free fatty acids (FFA), water, and di- and monoglycerides, with less refined oil containing phospholipids and various other impurities (Srivastava and Prasad, 2000).

The fatty acid chains in a triglyceride molecule are classified by their length and the number of double bonds present, presented in that order such that 18:2 represents a fatty acid chain with 18 carbons after the ester bond, and two double bonds along the chain. Generally speaking, an increase in chain length increases the melting point of the vegetable oil, and the biodiesel produced from it, while an increase in the number of double bonds decreases their melting points. However, an increase in double bonds will also increase the molecule's susceptibility to oxidative degradation. Table 1.1 gives the general composition of various oils.

Table 1.1 Typical compositions of common oils (%) (adapted from Pinto et al., 2005)

Source	Palmitic	Palmitoleic	Stearic	Oleic	Linoleic	Other acids
	16:0	16:1	18:0	18:1	18:2	
Castor oil	-	3.0	3.0	3.0	1.2	89.8[a]
Coconut oil	6.1	-	1.9	4.9	0.8	86.3[b]
Corn oil	6.0	-	2.0	44.0	48.0	-
Cotton oil	28.6	0.1	0.9	13.0	57.2	0.2
Groundnut oil	8.5	-	6.0	51.6	26.0	-
Hazelnut kernel	4.9	0.2	2.6	81.4	10.5	0.3
Olive oil	14.6	-	-	75.4	10.0	-
Poppy seed	12.6	0.1	4.0	22.3	60.2	0.8
Rapeseed	3.5	0.1	0.9	54.1	22.3	9.1
Safflower seed	7.3	0.1	1.9	13.5	77.0	0.2
Soybean oil	11.0	-	2.0	20.0	64.0	3.0
Sunflower seed	6.4	0.1	2.9	17.7	72.8	0.1
Tallow	29.0	-	24.5	44.5	-	-

[a] 89.5% Ricinic (12-OH-oleic), 0.3% other
[b] 51.0% Lauric (12:0), 16.5% Myristic (14:0), 10.0% Capryric (8:0), 7.9% Capric (10:0), 0.5% Caproic (6:0), 0.4% other (Benjapornkulaphong *et al*., 2009)

A major advantage of vegetable oil based fuels is the ability to produce them within a region, for local distribution. The oils available will vary, as mentioned previously, with climate and geography. In general, soybean is the major oil grown in North America, while Europe produces rapeseed oil. Tropical areas such as Malaysia primarily produce palm oil. Algae is a major area of research, as various species can contain as much as 80 wt.% oil in terms of dry biomass, and it may be possible to establish algal farms on marginal or non-arable land, with the use of sea or brackish water (Chisti, 2007). However, major progress needs to be made, specifically in the areas of algal oil extraction and purification (Knothe, 2010). Figure 1.4 shows recent data on the choice of oils used for biodiesel.

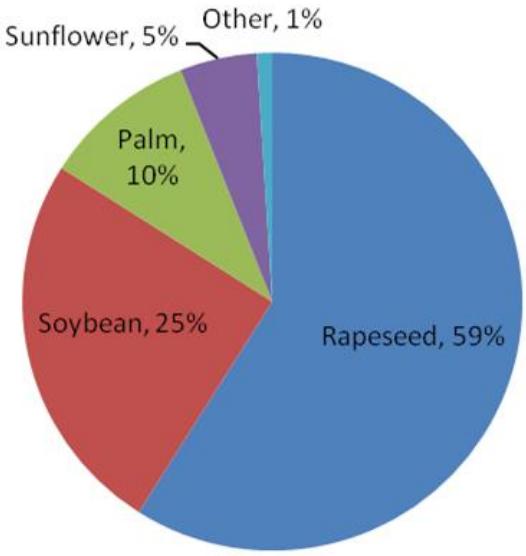

Figure 1.4 Oil sources used for biodiesel (adapted from Pahl, 2008).

Additional consideration must be given to the oil production with respect to the land area required. While many oils are under consideration as sources of oil for biodiesel, the amount of oil the plants can produce varies widely. Chisti (2007) considered the case of fuelling half of the transport needs of the United States with biodiesel grown from various crops, the result of which is shown in Table 1.2.

Table 1.2 Comparison of various oil sources (adapted from Chisti, 2007)

Source	Oil Yield (m^3 km^{-2})	Land needed for 50% of US transport (10^6 km^2)[a]
Corn	17.2	15.4
Soybean	44.6	5.84
Rapeseed (Canola)	119	2.23
Jatropha	189.2	1.4
Coconut	268.9	0.99
Oil Palm	595	0.45
Microalgae (70 wt.% oil)	13690	0.02
Microalgae(30 wt.% oil)	5870	0.045

[a] Total arable land in US is approximately $1.7x10^6$ km^2 (Central Inteligence Agency, 2011)

It is clear from this that in the long term, complete replacement of petroleum diesel with biodiesel is not feasible with conventional oil sources. However these are, and likely shall continue to be, widely used until a source such as algae is ready for mass production.

1.4.2 Catalysis

The transesterification reaction (introduced in Section 1.3.5) can be catalysed by both acid and base catalysts, which offer distinct advantages and disadvantages. Primarily, basic catalysts work much faster, with reaction rates being as much as 4000 times that of their acid counterparts (Srivastava and Prasad, 2000). Common choices for biodiesel production include alkali metal hydroxides, such as KOH and NaOH, and more active alkoxides (Helwani *et al*., 2009). However, basic catalysts are also susceptible to side reactions, namely the formation of soap in the presence of FFA or water (Knothe *et al.*, 2005). To counteract this, acid catalysts are used for less refined feedstocks. These generally include sulphuric and sulphonic acids (Abdullah *et al*., 2007). Despite the improved impurity tolerance over basic catalysts, water concentrations above 0.5% will inhibit the acid catalysed reaction, with 5% water leading to complete inhibition (Helwani *et al*., 2009).

The reaction mechanisms for both basic and acidic catalysis are described by Lotero *et al.* (2005), and are as follows:

a) Basic catalysis begins with:

   i. The donation of a proton from the alcohol, leaving a methoxide ion, in the case of methanolysis, as shown in Figure 1.5. This ion the attacks the carbonyl carbon of the triglyceride molecule, while the negative charge moves to the carbonyl oxygen, to give a tetrahedral intermediate.

   ii. This then decomposes to give biodiesel, leaving a negatively charged oxygen as the terminal atom of the now diglyceride molecule.

   iii. The proton that was initially accepted by the base now bonds with the oxygen to complete the reaction, and return the catalyst to its original

state. An identical mechanism leads to the formation of monoglyceride and finally glycerol.

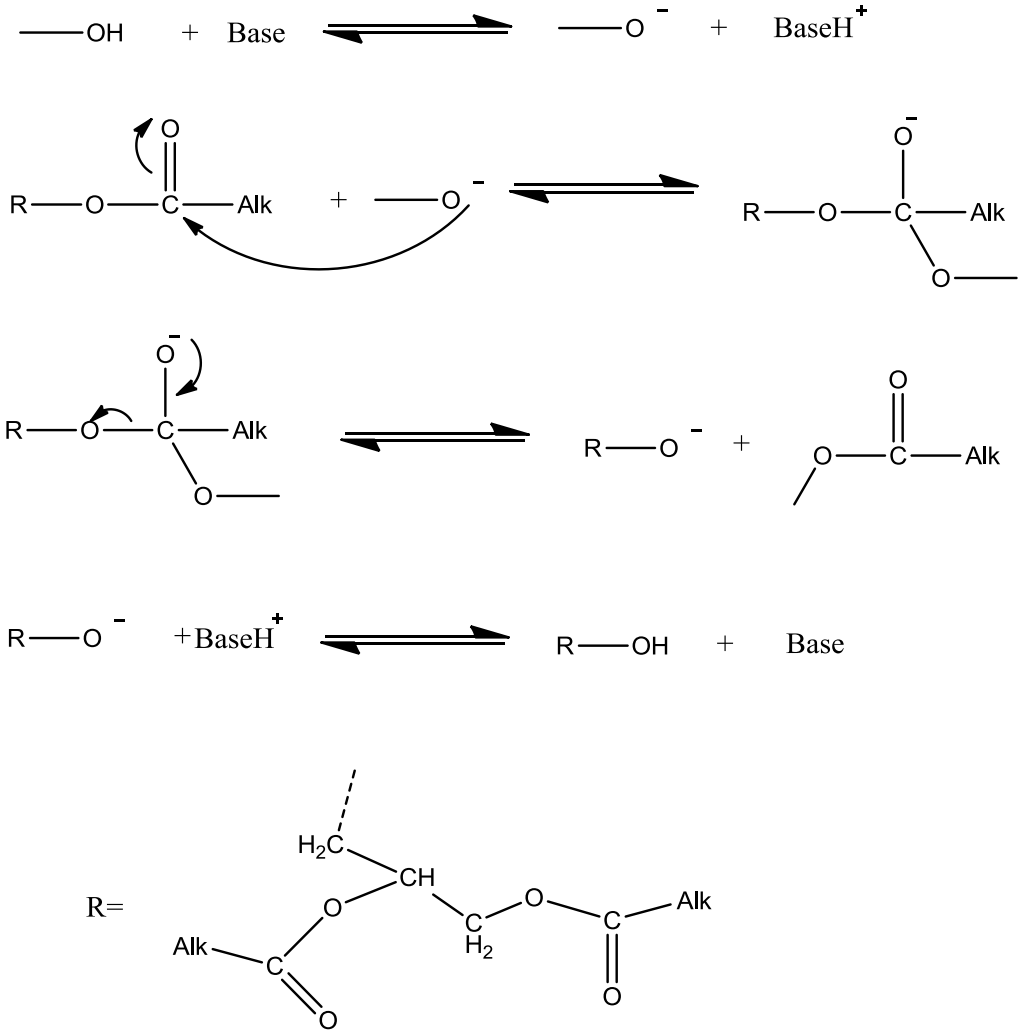

Figure 1.5 Base catalysed transesterification mechanism (adapted from Lotero *et al*., 2005).

b) The mechanism for acid catalysed transesterification begins with:

i. A proton attacking the carbonyl oxygen.

ii. A lone pair from the methanol's oxygen then attacks the carbonyl carbon, causing the double bond to break in order to balance the positive charge on the oxygen.

iii. This leads to a tetrahedral intermediate, which decomposes, with the methanol's hydrogen bonding with the glyceride's oxygen, allowing the original ester bond to break.

iv. The proton that initiated the reaction is then forced from the oxygen, reforming the double bond and thus releasing the FAME and the diglyceride. Monoglyceride and glycerol result from subsequent reactions. The reaction is shown in Figure 1.6.

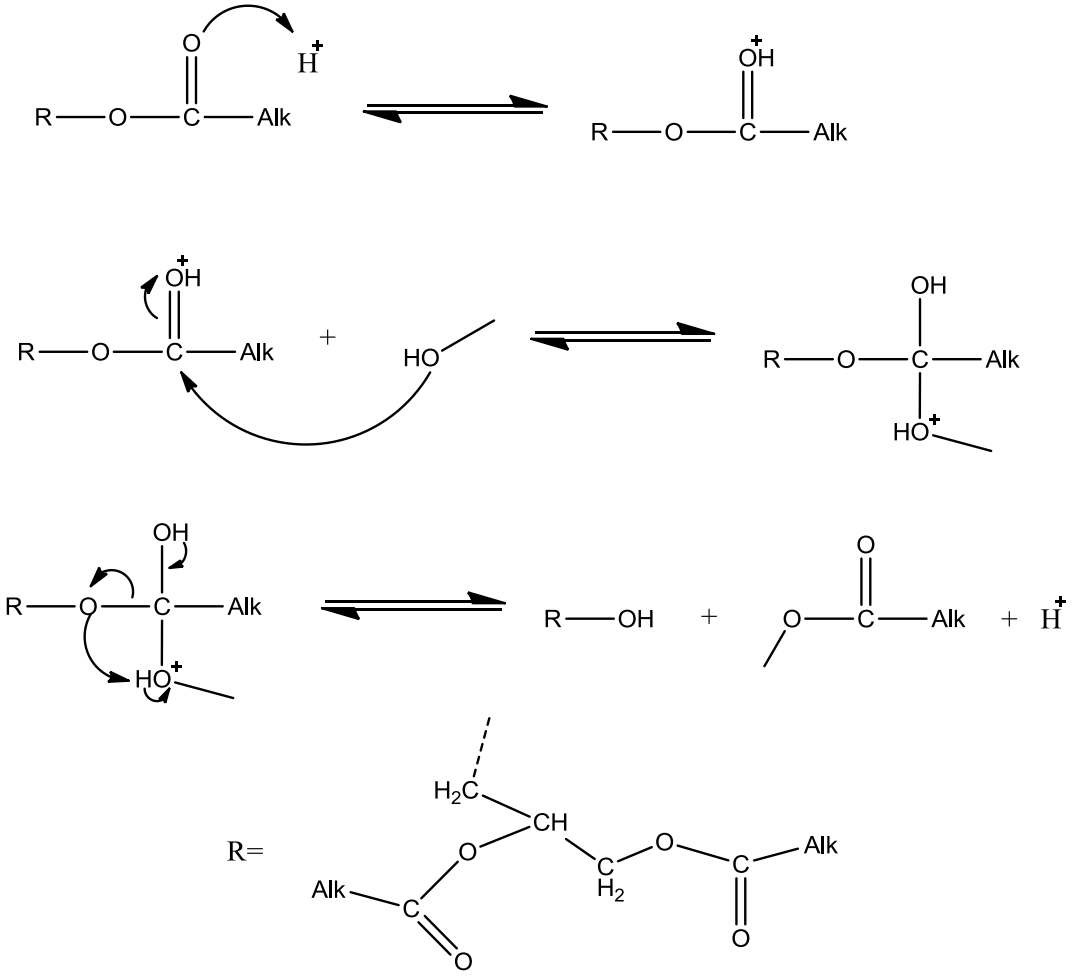

Figure 1.6 Acid catalysed transesterification mechanism (adapted from Lotero *et al*., 2005).

The catalysts discussed above are generally homogeneous, which causes various problems in downstream processing (Helwani *et al*., 2009, Knothe *et al*., 2005). First, the catalyst must be neutralised and washed out of the reaction mixture. This

leads to more complex separation requirements, due to both the need for additional reagents, as well as further drying and purification after the initial phase separation. Secondly, a waste water stream has been introduced, which must be dealt with before discharge. Another effect of this is that the catalyst must be continually replaced. For these reasons, there is a large effort in the literature to identify potential heterogeneous catalysts which can be used to process biodiesel more economically than is possible with homogeneous catalysis (Helwani *et al*., 2009, Knothe *et al*., 2005).

1.4.3 Industrial Processes

Current industrial production of biodiesel is primarily by homogeneous batch production, although there is a movement towards both heterogeneous and continuous plant design (Helwani *et al*., 2009). A typical industrial production plant will include a preliminary acid catalysed reactor to esterify the fatty acid content of the feedstock, unless a high quality oil is used (Abdullah *et al*., 2007). This must then be followed by water removal to avoid inhibiting downstream reactions (Leung, 2010). The acid must then be neutralised before the use of an alkali catalyst, which performs the bulk transesterification. This too must be neutralised, and both the biodiesel and the glycerol, after being gravity separated, must be washed with water to remove the salts. This creates further processing steps to obtain a final product. An illustration of the process is shown in Figure 1.7

Although much work has been devoted to finding new, effective heterogeneous catalysts for biodiesel production (this shall be summarised later), there appears to be only one process that has reached full industrial production, Esterfip-H, developed by the French Institute of Petroleum, and commercialised by Axens (Ondrey, 2004). Despite the existence of a heterogeneous process, plants using homogeneous technology have since been built (Gillatt, 2006). A heterogeneous process would be expected to have a much simpler design, with fewer downstream units due to the lack of impurities introduced as described for the homogeneous process. Figure 1.8 is an illustrative example of what such a process may look like.

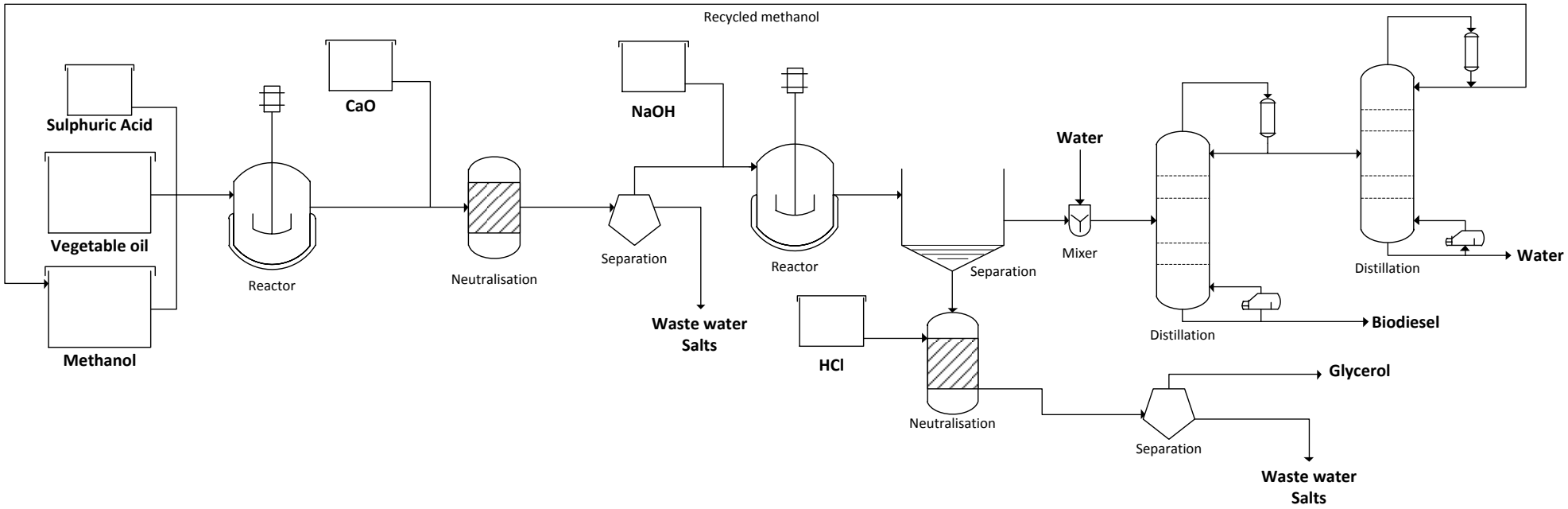

Figure 1.7 Example flowsheet of a typical homogeneous biodiesel process (adapted from Melero *et al.*, 2009).

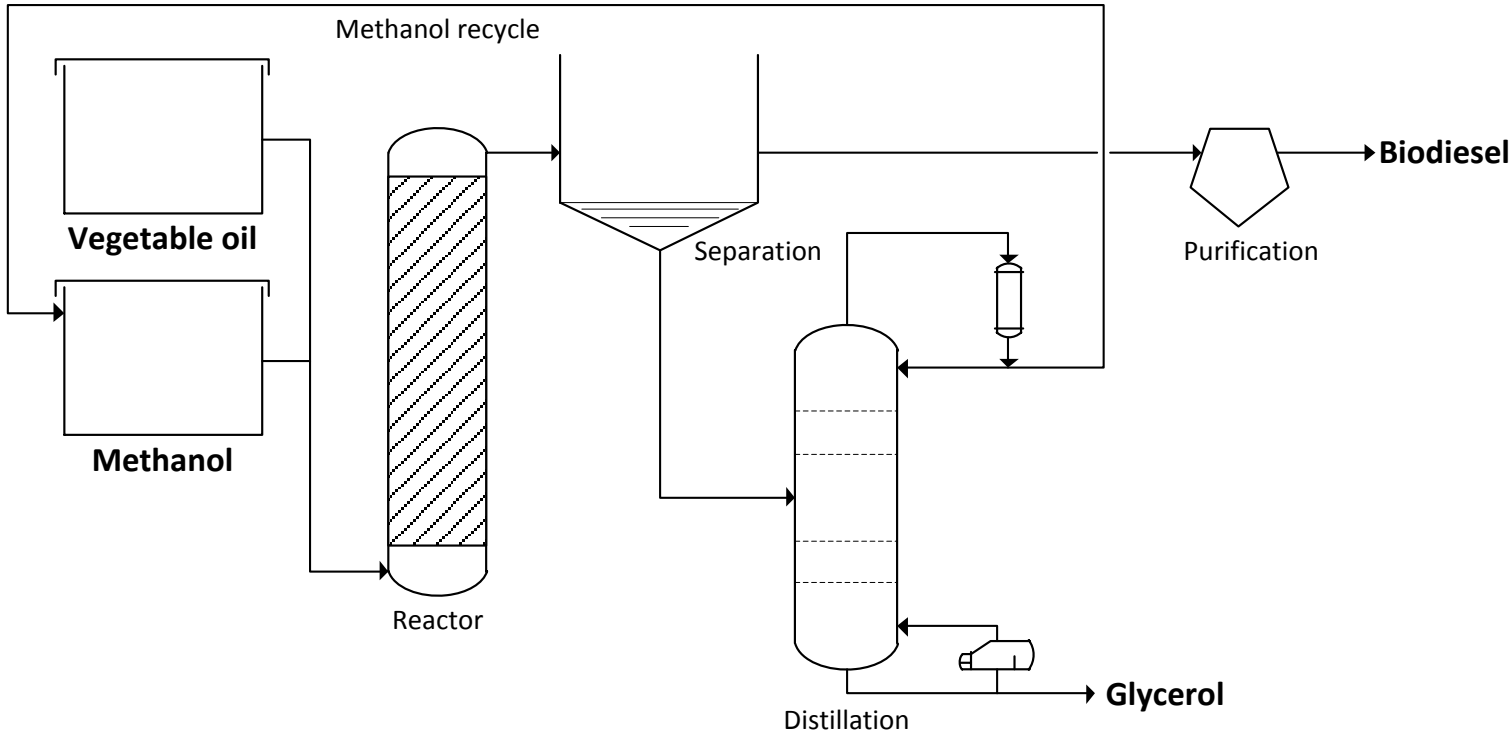

Figure 1.8 Illustrative flowsheet of a heterogeneous process (adapted from Melero *et al*., 2009).

1.4.4 Properties of Biodiesel

The properties of biodiesel compare well with conventional diesel. The main advantages to using biodiesel in an engine relate to its increased lubricity over ultra-low sulphur diesel (ULSD), which leads to improved fuel injector performance and lifetime, and the presence of oxygen within the molecule, which leads to more complete combustion (Knothe *et al.*, 2005). A comparison of the properties of rapeseed biodiesel (rapeseed methyl ester, RME) and ULSD are given in Table 1.3. Many of the differences extend to biodiesel made from other sources. The higher flash point means that biodiesel handling and storage is inherently safer that conventional diesel, while the lower sulphur content decreases the environmental impact of the fuel, and lengthens the life of the catalytic converter, for which sulphur compounds are generally a poison (Knothe *et al.*, 2005). The acceptable properties of biodiesel for automotive use are standardised (BS EN 14214:2008 + A1:2009).

Table 1.3 Properties of ULSD and RME (Bannister et al., 2010)

Property	ULSD	RME
Density at 15°C (kg m^3)	833	883.2
Kinematic Viscosity at 40°C (mm^2 s^{-1})	2.748	4.564
Flash Point (°C)	65	182
Cetane Number	52.8	49.5
Cold Filter Plugging Point (°C)	-18	-20
Net Calorific Value (MJ kg^{-1})	42.59	39.99
Sulphur Content (mg kg^{-1})	7	1.8
Carbon Content (wt. %)	86.2	77.1
Hydrogen Content (wt. %)	13.8	12.2
Oxygen Content (wt. %)	0	10.7
Acid Number (mg(KOH) g^{-1})	0.2	0.18

1.4.5 Biodiesel Blends

Biodiesel is usually sold as a blend with conventional diesel. The amount of biodiesel in the fuel is denoted by the blend number, such that a fuel containing 5% biodiesel is referred to as B5, 10% is B10, and so on. The maximum blend sold at pumps is B7 (BS EN 590:2009+A1:2010), with the average diesel fuel containing approximately about 4.5% biodiesel; a number which had been expected to continually increase over time as EU targets provide more legislative pressure (Bannister *et al*., 2010), although this may not be the case due to potential changes in the target scheme (European Commission, 2012).

1.4.6 Emissions

Following the more general discussion of diesel emissions in Section 1.2.4, it is appropriate to consider the effect of biodiesel on the environmental performance of diesel engines. It is generally reported in the literature that the use of biodiesel improves engine emissions due to more complete combustion. This is evidenced by a decrease in carbon monoxide, particulates, and hydrocarbons (Knothe *et al*., 2005, Abdullah *et al*., 2007, Demirbas, 2008).

The findings for NO_x emissions are not in agreement, although a majority of papers report that biodiesel leads to an increase compared with petroleum diesel; 65% report an increase, 29% report a decrease, and 6% report no change (Xue *et al*., 2011). Bannister *et al* (2010) found that the NO_x emissions vary with ambient temperature, and that due to lower pre-exhaust temperatures, the catalyst performance is lowered for biodiesel. This leads to better end of pipe performance for engines running on ULSD.

1.4.7 Controversies

A major aspect when considering potential biofuels is the use of food sources, or land that could otherwise be used for food, to produce biofuel feedstocks. The potential competition between the two divides opinion on how biofuels should be pursued. This is tangled into the debate over the extent to which biofuels should be pursued at all, with many claims and counterclaims regarding the net carbon reductions or increases from using biofuels and the impacts of land use changes, and the economic effects of rising demands for biofuels (Knothe, 2010).

Although it is obvious that using food sources, or land that could be used for growing food sources, to produce biofuels will reduce the world's capacity to provide for its population, the extent to which this is currently an issue is a point of contention. For example, the major spike in food prices between 2006 and 2008 was initially blamed on the increase in biofuel production for 75% of the price rise, in a report by the World Bank (Chakrabortty, 2008). However, a subsequent report by the same organisation looking back at the crisis found that 1.5% of the price rise could be attributed to biofuels – the main contributor was in fact the rising price of crude oil (Baffes and Haniotis, 2010).

The primary driver for the use of biofuels is the threat of anthropogenic global climate change relating to the carbon dioxide released by the use of fossil fuels. It is thus necessary that any replacement fuel results in a reduction of net carbon dioxide production; fuels and their precursors must be examined individually to ensure that they do indeed meet this goal. Although on the face of it, biodiesel is made from photosynthetically converted CO_2, the additional energy that is required in the agricultural cultivation, harvesting, and processing to produce the vegetable oils may lead to more energy being put into the production of the biodiesel than is made available when the fuel is burned (Abdullah *et al*., 2007). Further to the net carbon debate is the impact of changing the use of land to growing crops for biofuels, which in some cases may lead to an increase in greenhouse gas emissions (Tilman *et al*., 2009).

1.4.8 Advantages of Biodiesel

There are many reasons to advocate the increasing use of biodiesel, many of which have already been discussed. Of highest prominence is the fact that biodiesel is produced from renewable resources (especially if the alcohol used is ethanol), and has the potential to be entirely sustainable, if feedstocks are chosen and managed properly. This makes biodiesel an extremely important fuel moving forward, as reducing the use of crude oil products becomes more essential for both environmental and energy security reasons. An additional environmental benefit is the fact that biodiesel is non-toxic and biodegradable in both soil and aquatic environments (Demirbas, 2008). Biodiesel is also inherently safer than conventional diesel, due to a higher flash point and lower volatility (Knothe *et al.*, 2005).

In terms of actual use, biodiesel has many other commendable features that put it in prime position as an option for sustainable fuels. First, it can utilise current diesel infrastructure, in terms of transport, product delivery, and end use in engines. Additionally, significant improvements in emissions can be obtained for CO, HC, and PM, due to the increased combustion efficiency of oxygenated fuels, as well as a marked reduction in sulphur compounds, which both poison the catalytic converter and lead to destructive acid rain (Knothe *et al.*, 2005, Bannister *et al.*, 2010). Increased use of biodiesel also benefits the performance of various engine components, e.g. fuel injectors, as a blend as low as B1 can increase lubricity by as much as 30% (Demirbas, 2008).

1.4.9 Disadvantages of Biodiesel

It must also be noted that there are several disadvantages to the use of biodiesel, some of which may be overcome, while others are inherent to the fuel itself. Contrasting with the potential to be sustainable, improper management of oil sources can lead to devastating land use changes, such as rainforest being cleared to create room for oil plants (Nepstad and Stickler, 2008), while some production pathways require a net energy input, negating any benefit obtained from using a renewable feedstock (Abdullah *et al*., 2007). A further economic obstacle is the price of

vegetable oils, which contributes approximately 80% of the final price of biodiesel (Balat and Balat, 2008).

At the point of end use, biodiesel leads to increased fuel consumption due to lower energy density, and decreased power output, due to lower operating temperatures, compared to petrodiesel (Murugesan *et al.*, 2009). The lower temperatures also lead to decreased activity of the catalytic converter, which may result in an increase in NO_x emissions (Bannister *et al.*, 2010). Corrosion of engine components is also an issue to be considered, for example carbon steel in the fuel system is vulnerable to attack by water, which is significantly more soluble in biodiesel than conventional diesel (Knothe *et al.*, 2005).

1.4.10 Prospects of Biodiesel

The biodiesel industry grew steadily throughout the first decade of the twenty-first century, with the biofuels market being expanding with the help of government legislation, such as EU renewables targets, subsidies, and public support for "greener" technologies. As things stand, however, biodiesel is not in a position to compete economically with diesel without these factors, and so there is much need to improve the economics of biodiesel production at every stage (Chisti, 2007). Although there is room for long-term optimism, as more work is done to develop more economical and environmentally friendly oil sources, biodiesel faces a difficult path. Recent changes by the European commission may cap the incentives for producing "first generation" biofuels at 5% (European Commission, 2012), and until technologies to effectively raise and harvest algal oil sources are developed, this could limit the growth of the biodiesel market. It is, however, essential that cleaner and more economic processing technologies are ready and available as these oils sources are established.

1.5 Content and Structure of the Thesis

The current project is a continuation of earlier work done at the University of Bath, Department of Chemical Engineering, to develop a more efficient biodiesel production method, primarily through the use of heterogeneous catalysts anchored to a monolithic support structure (Asli, 2011). It is motivated by the need to address the problems discussed above, namely, through improving the economics of biodiesel production. A heterogeneous catalyst will reduce inputs and waste streams, while also improving the quality of the biodiesel and glycerol produced by the reaction.

An examination of heterogeneous catalysts is incomplete without use in a continuous setting, as many issues and challenges may be obscured in batch reactions. The previous work by Asli found that the zinc proline catalyst being used was much more promising in batch experiments than when it was tested in a continuous reactor. Thus it is imperative that reactions are carried out in both batch and continuous reactors.

1.5.1 Aims and Objectives

The primary aims of the project were to develop an improved heterogeneous catalyst system for the production of biodiesel from vegetable oils and to use this system in demonstrating a small scale continuous flow reactor. Additionally, the project aimed to add to the general knowledge in the area of heterogeneous biodiesel production with the catalyst retained in a fixed bed. Although there has been some work in that field, there appears to be only one commercialised process.

To achieve these aims, the following specific objectives were set:

- To investigate various catalysts for the transesterification of vegetable oils;
- To develop methods for fixing catalyst materials to a monolithic support structure;
- To enhance the initial mass-transfer controlled reaction step;
- To characterise the catalysts used;

- To utilise the catalysts in a continuous flow, packed bed reactor;
- To measure and interpret the rates of the transesterification reaction with the various catalysts.

1.5.2 Scope and Structure of the Thesis

The current project is primarily focused on the development of a catalytic system for biodiesel production, which will comprise a monolithic support structure carrying a catalyst. This development will include the aims listed above, and will be limited to the subcritical, conventionally-heated transesterification reaction, putting aside the biodiesel's properties and performance as a fuel. The investigation will extend to any influences on the reaction, particularly the presence of impurities in the feedstock, which will be initially limited to a mixture of rapeseed oil and methanol, although this may be expanded in order to test the capabilities of successful catalysts (e.g. the use of other oil sources and other alcohols).

The link between the various activities undertaken in the development of this thesis, and the rationale and value of the work done is presented in Figure 1.9.

In **Chapter 2**, a literature review of the various catalysts that have been investigated for vegetable oil transesterification is presented, and the reasoning behind the selection of the catalysts used for this thesis is explained.

The preliminary work done to arrive at a suitable heterogeneous catalyst is described in **Chapter 3**, beginning with an introduction to the analytical techniques used throughout the thesis and characterisation of the vegetable oil. This is then followed by the procedures and experimental equipment to develop the best method of catalyst coating, including the procurement and modification of a batch reactor. Lastly, results of the experiments undertaken and a selection of the best catalyst for use in a continuous reactor is chosen.

Chapter 4 is an examination of the extent to which methanol is soluble in vegetable oil. This includes a literature review of the work done so far on the subject, the development of an experimental rig to carry out the necessary experiments,

determination of an appropriate method for quantifying the amount of methanol in an oil sample, and a discussion of the results in the context of biodiesel production.

Chapter 5 focuses on continuous biodiesel production, beginning with a literature review. A continuous reactor from previous work (after slight modification) is used to test selected catalysts for their suitability for long-term use in a continuous setting. Further, a larger, multiple channel reactor is used to provide more information about the reaction along the length of the catalyst bed.

Finally, the conclusions from the work presented in the thesis, as well as recommendations for future work, are given in **Chapter 6**.

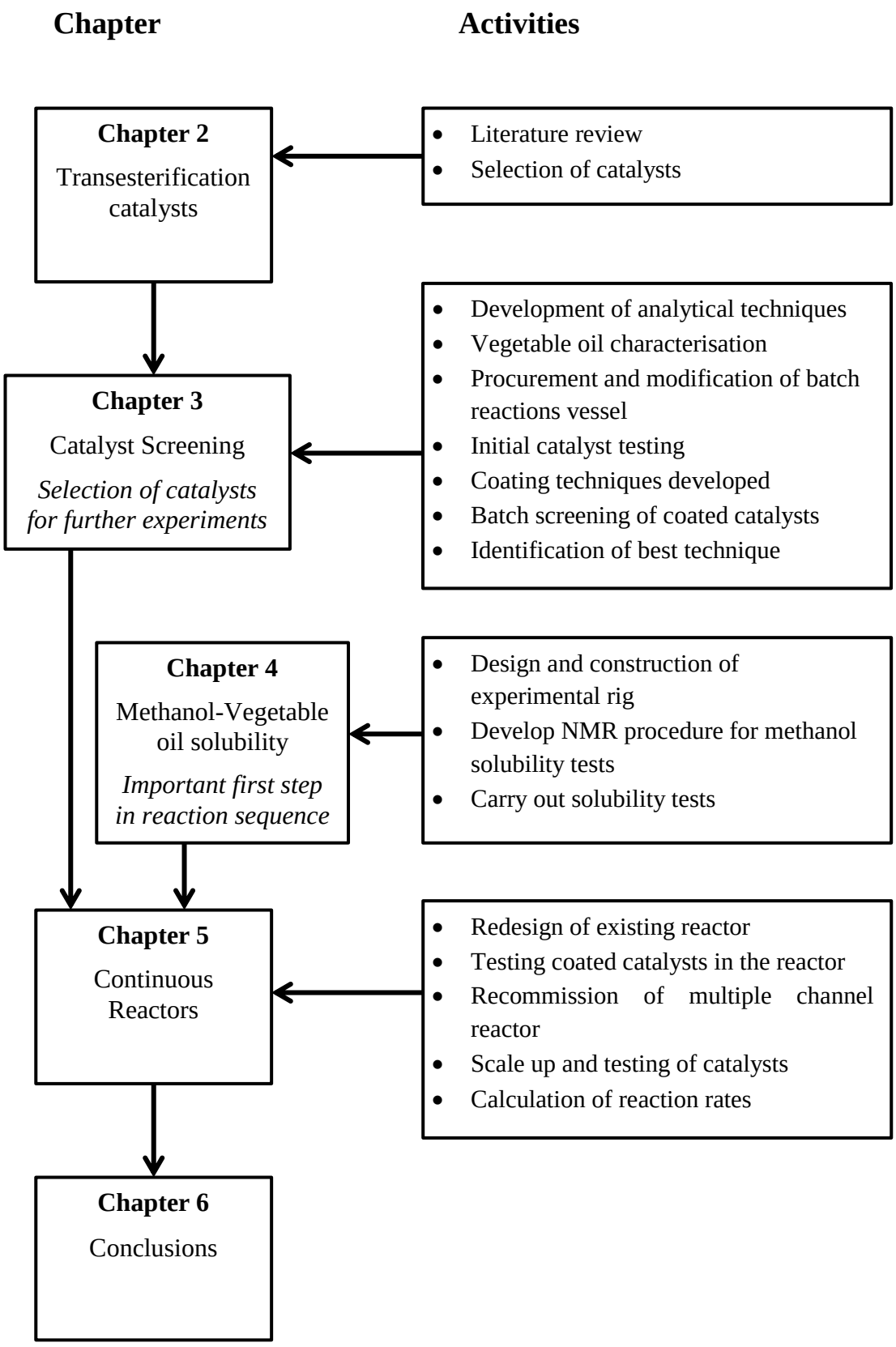

Figure 1.9 Links between activities undertaken for the thesis.

References

ABDULLAH, A. Z., RAZALI, N., MOOTABADI, H. & SALAMATINIA, B. 2007. Critical technical areas for future improvement in biodiesel technologies. *Environmental Research Letters,* 2.

ASLI, U. A. 2011. *Catalytic monoliths for biodiesel production.* Ph.D., University of Bath.

BAFFES, J. & HANIOTIS, T. 2010. Placing the 2006/08 Commodity Price Boom into Perspective. *Policy Research working paper.* World Bank.

BALAT, M. & BALAT, H. 2008. A critical review of bio-diesel as a vehicular fuel. *Energy Conversion and Management,* 49**,** 2727-2741.

BANNISTER, C. D., HAWLEY, J. G., ALI, H. M., CHUCK, C. J., PRICE, P., CHRYSAFI, S. S., BROWN, A. & PICKFORD, W. 2010. The impact of biodiesel blend ratio on vehicle performance and emissions. *Proceedings of the Institution of Mechanical Engineers, Part D: Journal of Automobile Engineering,* 224**,** 405-421.

BENJAPORNKULAPHONG, S., NGAMCHARUSSRIVICHAI, C. & BUNYAKIAT, K. 2009. Al2O3-supported alkali and alkali earth metal oxides for transesterification of palm kernel oil and coconut oil. *Chemical Engineering Journal,* 145**,** 468-474.

BS 2000-123:2001 Petroleum products - Determination of distillation characteristics at atmospheric pressure. *British Standards Institute.*

BS EN 590:2009+A1:2010 Automotive fuels - Diesel - Requirements and test methods. *British Standards Institute.*

BS EN 14214:2008 + A1:2009 Automotive fuels - Fatty acid methyl esters (FAME) for diesel engines. Requirements and test methods. *British Standards Institute.*

ÇENGEL, Y. A. & BOLES, M. A. 2008. *Thermodynamics : an engineering approach,* Boston ; London, McGraw-Hill Higher Education.

CENTRAL INTELIGENCE AGENCY. 2011. *The World Factbook 2011* [Online]. Washington, DC. Available: https://www.cia.gov/library/publications/the-world-factbook/index.html [Accessed 16/08/2011].

CHAKRABORTTY, A. 2008. Secret report: biofuel caused food crisis. *Guardian*.

CHISTI, Y. 2007. Biodiesel from microalgae. *Biotechnology Advances,* 25**,** 294-306.

CLOTHIER, P. Q. E., AGUDA, B. D., MOISE, A. & PRITCHARD, H. O. 1993. How do diesel-fuel ignition improvers work? *Chemistry Society Reviews,* 22**,** 101-108.

DEMIRBAS, A. 2008. *Biodiesel : a realistic fuel alternative for diesel engines,* London, Springer.

EUROPEAN COMMISSION 2012. Executive summary of the ipact assessment on indirect land-use change related to biofuels and bioliquids, Accompanying the document: Proposal for a directive of the European Parliament and of the council amending Directive 98/70/EC relating to the quality of petrol and diesel fuels and amending Directive 2009/28/EC on the promotion of the use of energy from renewable sources. *In:* COMMISION, E. (ed.).

GILLATT, M. 2006. *Biodiesel: Green and sustainable*. The Chemical Engineer Institution of Chemical Engineers. 781. p.29.

HELWANI, Z., OTHMAN, M. R., AZIZ, N., FERNANDO, W. J. N. & KIM, J. 2009. Technologies for production of biodiesel focusing on green catalytic techniques: A review. *Fuel Processing Technology,* 90**,** 1502-1514.

JOHNSON, T. V. 2009. Review of diesel emissions and control. *International Journal of Engine Research,* 10**,** 275-285.

KESICKI, F. 2010. The third oil price surge - What's different this time? *Energy Policy,* 38**,** 1596-1606.

KNOTHE, G. 2010. Biodiesel: Current Trends and Properties. *Topics in Catalysis,* 53**,** 714-720.

KNOTHE, G., VAN GERPEN, J. & KRAHL, J. 2005. *The biodiesel handbook,* Urbana, Ill., AOCS Press.

LEUNG, D. Y. C. 2010. A review on biodiesel production using catalyzed transesterification. *Applied energy,* 87**,** 1083-1095.

LOTERO, E., LIU, Y. J., LOPEZ, D. E., SUWANNAKARN, K., BRUCE, D. A. & GOODWIN, J. G. 2005. Synthesis of biodiesel via acid catalysis. *Industrial & Engineering Chemistry Research,* 44**,** 5353-5363.

MELERO, J. A., IGLESIAS, J. & MORALES, G. 2009. Heterogeneous acid catalysts for biodiesel production: current status and future challenges. *Green Chemistry,* 11**,** 1285-1308.

MINNESOTA STATE UNIVERSITY. 2010. *Four stroke diesel engine cycle* [Online]. Available: http://cset.mnsu.edu/engagethermo/images/Four%20Stroke%20Diesel%20Engine%20Cycle.bmp [Accessed 12/5/2010].

MISRA, R. D. & MURTHY, M. S. 2010. Straight vegetable oils usage in a compression ignition engine-A review. *Renewable & Sustainable Energy Reviews,* 14**,** 3005-3013.

MURUGESAN, A., UMARANI, C., SUBRAMANIAN, R. & NEDUNCHEZHIAN, N. 2009. Bio-diesel as an alternative fuel for diesel engines-A review. *Renewable & Sustainable Energy Reviews,* 13**,** 653-662.

NEPSTAD, D. C. & STICKLER, C. M. 2008. Managing the tropical agriculture revolution. *Journal of Sustainable Forestry,* 27**,** 43-56.

ONDREY, G. 2004. *Biodiesel production using a heterogeneous catalyst*. Chemical Engineering 10. p.13.

PAHL, G. 2008. *Biodiesel : growing a new energy economy,* White River Junction, Vt., Chelsea Green.

PINTO, A. C., GUARIEIRO, L. L. N., REZENDE, M. J. C., RIBEIRO, N. M., TORRES, E. A., LOPES, W. A., PEREIRA, P. A. D. & DE ANDRADE, J. B. 2005. Biodiesel: An overview. *Journal of the Brazilian Chemical Society,* 16**,** 1313-1330.

ROTTIG, A., WENNING, L., BROKER, D. & STEINBUCHEL, A. 2010. Fatty acid alkyl esters: Perspectives for production of alternative biofuels. *Applied microbiology and biotechnology,* 85**,** 1713-1733.

SHARMA, Y. C. & SINGH, B. 2009. Development of biodiesel: Current scenario. *Renewable & Sustainable Energy Reviews,* 13**,** 1646-1651.

SIDIBE, S. S., BLIN, J., VAITILINGOM, G. & AZOUMAH, Y. 2010. Use of crude filtered vegetable oil as a fuel in diesel engines state of the art: Literature review. *Renewable & Sustainable Energy Reviews,* 14**,** 2748-2759.

SMITH, J. M., VAN NESS, H. C. & ABBOTT, M. M. 2005. *Introduction to chemical engineering thermodynamics,* London, McGraw-Hill.

SRIVASTAVA, A. & PRASAD, R. 2000. Triglycerides-based diesel fuels. *Renewable & Sustainable Energy Reviews,* 4**,** 111-133.

TAUFIQURRAHMI, N. & BHATIA, S. 2011. Catalytic cracking of edible and non-edible oils for the production of biofuels. *Energy & Environmental Science,* 4**,** 1087-1112.

TILMAN, D., SOCOLOW, R., FOLEY, J. A., HILL, J., LARSON, E., LYND, L., PACALA, S., REILLY, J., *et al.* 2009. Beneficial Biofuels-The Food, Energy, and Environment Trilemma. *Science,* 325**,** 270-271.

TWIGG, M. V. 2005. Controlling automotive exhaust emissions: Successes and underlying science. *Philosophical Transactions: Mathematical, Physical and Engineering Sciences,* 363**,** 1013-1033.

VAN SETTEN, B., MAKKEE, M. & MOULIJN, J. A. 2001. Science and technology of catalytic diesel particulate filters. *Catalysis Reviews-Science and Engineering,* 43**,** 489-564.

WALLINGTON, T. J., KAISER, E. W. & FARRELL, J. T. 2006. Automotive fuels and internal combustion engines: a chemical perspective. *Chemical Society Reviews,* 35**,** 335-347.

XUE, J. L., GRIFT, T. E. & HANSEN, A. C. 2011. Effect of biodiesel on engine performances and emissions. *Renewable & Sustainable Energy Reviews,* 15**,** 1098-1116.

ZHENG, M., READER, G. T. & HAWLEY, J. G. 2004. Diesel engine exhaust gas recirculation - A review on advanced and novel concepts. *Energy Conversion and Management,* 45**,** 883-900.

Chapter 2 Transesterification catalysts

In this chapter, a literature review of various catalysts reported for biodiesel production is presented. Primarily, this focuses on inorganic compounds, although some other catalysts, such as enzymes, are considered. This leads to the selection of catalysts from the literature that appear to be promising in a continuous setting, but have not been sufficiently investigated.

2.1 Literature review

The literature contains a wealth of resources on catalysis for biodiesel production, with increasing focus in recent years on the development of effective heterogeneous catalysts. These catalysts range from simple metal oxides, to molecules as complex as enzymes. Most of these catalysts are reported as powders, although some work has been done on fixed catalysts. In order to provide some structure to this overview, inorganic catalysts have been classified as metal oxides, Group 1 halides, or other inorganic compounds.

Beyond the catalyst's activity, two things that are vitally important to the viability of a process are the reusability and resistance to leaching of the catalyst. Unfortunately, many papers do not take either one or both these into account. Indeed, some papers recognise that there is deactivation between experiments, but no effort is made to investigate possible leaching.

2.1.1 Metal Oxides

Metal oxides appear to be the most common heterogeneous catalysts in the literature. The metals are usually from Group 2 (of the Periodic Table), either deposited on a substrate, or used directly as a powder. A summary of some catalysts from recent years is provided in Table 2.1. The sources in the literature provide results as either conversion or yield, but rarely both, while the methods of product recovery have varied.

Table 2.1a Metal oxide catalysts from the literature

Reference	Catalyst used	Conv	Yield	Temp (°C)	Catalyst w.r.t. oil	Methanol: oil	Time (h)	Feedstock	Notes on paper
(Benjapornkulaphong *et al.*, 2009)	CaO on Al2O3		94.3%	60	10%	65:1	3	Palm oil	Significant leaching - 10% loss of catalyst in single run.
(Bournay *et al.*, 2005a)	Zn and Al oxides		98.3%	?	?	?	N/A	Rapeseed oil	98% purity glycerol obtained, complete process at pilot scale. Process appears to have been commercialised.
(Chakraborty *et al.*, 2010)	CaO on fly ash		97.7%	70	1%	6.9:1	5	Soybean oil	Catalyst was reusable 16-18 times, then lost all activity due to hydration to Ca(OH)2.
(Chen *et al.*, 2012)	SrO/SiO2	95%		65	5%	6:1	0.17	Olive oil	Conversion calculated from comparison to NaOH, which leads to conversions greater than 100%.
(de Carvalho *et al.*, 2013)	SrO	97.2%		65	1%	6:1	1	Babassu oil	Catalyst recalcined after each use - only slight drop in conversion after 6 runs.
(De Moura *et al.*, 2010)	SrO	98.5%		25	1.5	5.5:1	3	Babassu oil	3h at room temp - circulating through packed bed reactor.
(del Remedio Hernández *et al.*, 2010)	Na on hydrotalcite	92.5%	83.2%	60	7%	9:1	8	Sunflower oil	Major activity losses between runs.
(Dias *et al.*, 2012)	SrO/MgO		97.3%	67	5%	9:1	3	Soybean oil	92.6% yield after 0.5 hours. Catalyst only reusable once, after which loss of SrO leads to deactivation.
(Faungnawakij *et al.*, 2012)	SrO/MgO		96%	60	3%	6:1	1.25	Palm oil	90% yield within 0.5 hours. No activity loss after three runs, but no investigation of leaching.
(Hsin *et al.*, 2010)	Calcium containing silicate mixed oxide		100%	65	20%	520:1	2	Soybean oil	Appears to be using yield as conversion, as there is no discussion of actual product yield.
(Kim *et al.*, 2011b)	ZnO on ZrO2		78%	200	5.8%	17:1	2	Brown Grease	THF as cosolvent. Yield lowered by unidentified macromolecules in grease.
(Kim *et al.*, 2009)	Na on ZnO-Al2O3/ZSM-5		99%	62	8%	10:1	9	Soybean oil	Sodium leaches substantially, and activity is quickly lost.

Table 2.1b Metal oxide catalysts from the literature

Reference	Catalyst used	Conv	Yield	Temp (°C)	Catalyst w.r.t. oil	Methanol: oil	Time (h)	Feedstock	Notes on paper
(Koberg *et al.*, 2011)	SrO	99.8%		MW	1.8%	6:1	<0.015	Waste cooking oil	Using microwave heating, achieves very rapid conversion. No activity loss after 4 runs.
(Koberg and Gedanken, 2012)	SrO	99.7%+		MW	30%		<0.1	Castor and jatropha oil and seeds	Reaction done both with oils and directly with seeds with methanol/chloroform mixture. Similar conversions in both using microwave heating. Reusable more than 10 times.
(Lima *et al.*, 2012)	$SrZrO_3$		98.4%	60	3%	12:1	3	Soybean oil	No investigation of catalyst reuse or leaching, and no samples reported before three hours - time needed for reaction unclear.
(Liu *et al.*, 2007)	SrO		95%	65	3%	12:1	0.17	Soybean oil	Activity lasts >10 runs, only decreasing slightly.
(Luz Martinez *et al.*, 2011)	CaO nanoparticles on NaX zeolite		93.5%	60	10%	6:1	6	Sunflower oil	Conversion likely low, as long reaction time leads to less pure product. Does not last more than 2 runs.
(MacLeod *et al.*, 2008)	Group one nitrates on CaO	100%		60	5%	6:1	3	Rapeseed oil	Significant leaching, leachate is catalytically active. Catalytic activity linked to basicity of catalyst.
(Montero *et al.*, 2010)	MgO nanocrystals	80%		60	1.7%	30:1	24	Glyceryl tributyrate	Links surface structure and basicity to catalytic activity.
(Olutoye and Hameed, 2011)	Mixed Zn and Mg oxide	87%	80%	188	2.55%	9:1	4	Waste cooking oil	Catalyst lifetime extended by periodic calcination.
(Patil *et al.*, 2011)	BaO, SrO		~80%	100	2%	9:1	3	Camelina sativa oil	94% yield with BaO in 4 min under microwave heating.
(Pugnet *et al.*, 2010)	Zinc aluminate		91%	200	4%	27:1	6	Rapeseed oil	Tolerant to water, insignificant leaching.
(Puna *et al.*, 2010)	CaO		95%	60	5%	12:1	7	Soybean oil	Does not discuss leaching, but it is prevalent with alkali metals.

Table 2.1c Metal oxide catalysts from the literature

Reference	Catalyst used	Conv	Yield	Temp (°C)	Catalyst w.r.t. oil	Methanol: oil	Time (h)	Feedstock	Notes on paper
(Tantirungrotechai *et al.*, 2013)	SrO/MgO		94%	65	5%	12:1	0.5	Soybean oil	Yield practically the same as with SrO. Lost activity after one run, so was reloaded with Sr. No comparison to reusability of SrO.
(Taufiq-Yap *et al.*, 2011)	CaMgO and CaZnO	83% 81%		65	4%	15:1	6	Jatropha oil	Slight loss of activity after 6 runs for both catalysts.
(Viola *et al.*, 2012)	CaO, SrO	92%, 86%		65	5%	6:1	3	Waste cooking oil	Catalysts tested as powder in stirred vessel and as granules in packed column in batch mode. Much lower conversion on reuse.
(Xie *et al.*, 2007)	Li doped ZnO	96.3%		60	5%	12:1	3	Soybean oil	Reused catalyst had conversion of 42.7%, and has significantly reduced basicity. After regeneration this reached 83.6%.
(Yan *et al.*, 2009)	CaO-La2O3		94.3%	58	5%	20:1	1	Soybean oil	High water (~10%) and FFA (~3.6%) tolerance. No activity at 7% FFA. Catalyst apparently severely inhibited by FFA until it has been esterified.
(Yan *et al.*, 2010)	ZnO modified with La		93.7%	200	2.4%	39:1	3	Soybean oil	Also achieved 92% yield in a continuous flow reactor. Maintains activity after 70 days.
(Yang *et al.*, 2010)	10% CuO on SrO		96%	180	3%	12:1	3	Hemp seed oil	Under 3 Mpa H2 pressure, also substantial hydrogenation. Do not appear to have investigated the reusability of the catalyst.
(Yang and Xie, 2007)	ZnO loaded with SrO	94.7%		65	5%	12:1	5	Soybean oil	Conversion increased to 96.8% using THF as a cosolvent. No investigation into leaching.
(Yoosuk *et al.*, 2010)	Mg-Sr oxides		97.7%	60	5%	9:1	0.5	Palm oil	>90% yield after 15 min. Gradual dropoff of activity with reuse due to significant strontium leaching.
(Yu *et al.*, 2011)	CaO-CeO2		93%	100	9%	30:1	6	Pistacia chinensis oil	Gradual loss of activity, regenerated after 5 runs, yield back up to 91%.

The mechanism of metal oxide catalysis begins with methanol adsorbing onto the catalyst surface. The methanol is then split by the metal oxide, with the oxygen atom attracting the hydrogen from the hydroxyl unit, and the metal atom drawing the hydroxyl's oxygen, to produce the methoxide ion (Boey *et al*., 2011, Liu *et al*., 2007). The methoxide ion then desorbs, and the reaction takes place as in homogeneous catalysis, with the methoxide ion attacking the carbonyl carbon to form a tetrahedral intermediate. This then rearranges, with the C-O bond between the fatty chain and the glyceride breaking to leave the methyl ester, and a negatively charged oxygen on the glyceride, which then combines with the adsorbed hydrogen to form a hydroxyl unit. This mechanism is illustrated in Figure 2.1.

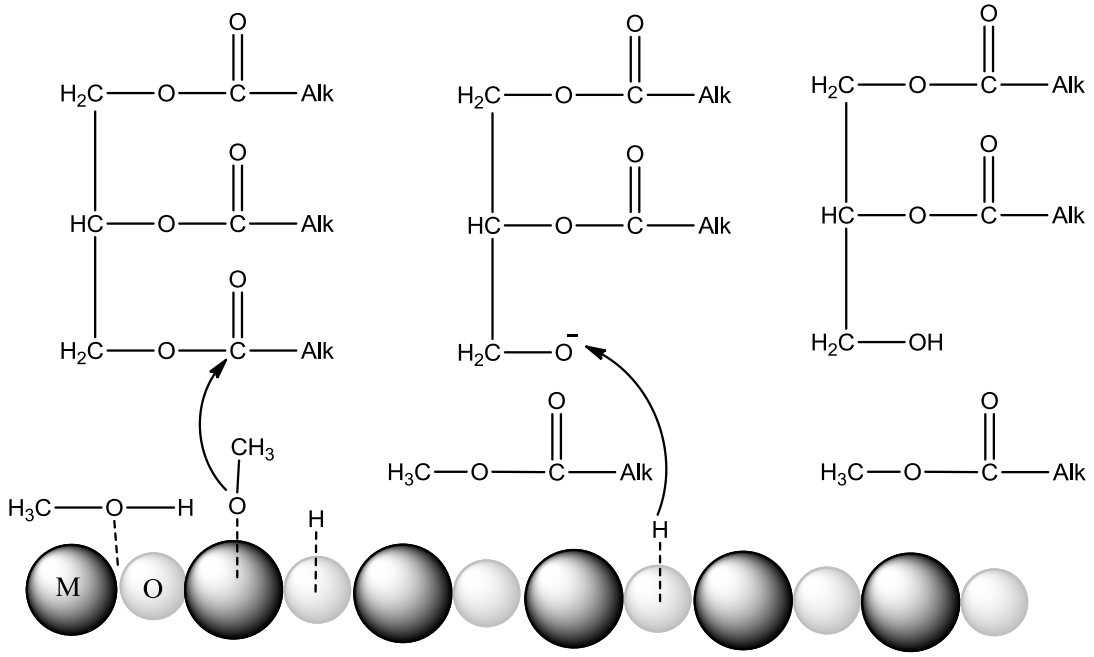

Figure 2.1 Heterogeneous base reaction mechanism.

Of particular note are reactions involving strontium oxide, which produce faster reactions than the other metal oxides in the literature, reaching a yield of 95% in half an hour at 65°C (Liu *et al*., 2007). It is also a capable catalyst at lower temperatures, reaching 98.5% conversion in three hours at room temperature (De Moura *et al*., 2010). Yoosuk *et al* (2010) report similar results with a mixed magnesium-strontium oxide, although they also report strontium leaching, with over 800 ppm strontium in

the biodiesel product. Liu *et al* (2007) do not report such leaching using pure SrO, although they report some catalyst loss, which they assume occurs during filtration, without investigating the strontium content of the biodiesel. Yang and Xie (2007) make a similar assumption with their zinc supported SrO catalyst – as activity goes down with reuse, it is hypothesised that the active sites have been deactivated or blocked. Other authors do not discuss catalyst loss, reuse, or leaching (Yang *et al*., 2010, De Moura *et al*., 2010). The British Standard (BS EN 14214:2008 + A1:2009) for FAME quality does not include a limit for strontium content, although it does limit "Group 2 metals (Ca+Mg)" to 5 mg kg^{-1}.

Also of importance is the work of Bournay *et al*. (2005a), which appears to be the basis of the Esterfip-H process mentioned earlier. The catalyst on which this process is based is a mix of zinc and aluminium oxides, and the reaction mechanism is completely heterogeneous. However, according to the corresponding patent, it does require less than 1500 ppm water in the feedstock, preferably less than 1000 ppm, and there is no mention of FFA content in the worked example or the main text (Bournay *et al.*, 2005b). This lack of flexibility means that poorer quality feedstocks will inevitably require some degree of pre-treatment.

2.1.2 Group 1 Halides

Group 1 halides adsorbed onto a support such as alumina have been the subject of a fair amount of research; many show a high activity towards transesterification. Very few of the papers surveyed investigated the reusability or the tendency of the catalyst to leach, and of those that did, only one reported a durable catalyst (Xiao *et al*., 2010). The limit for Group 1 metals (Na and K) present in the FAME product is 5 mg kg^{-1} (BS EN 14214:2008 + A1:2009). A summary of the literature on these compounds is given in Table 2.2

Table 2.2 Group 1 halide catalysts in the literature

Reference	Catalyst used	Conversion	Yield	Temp (°C)	Catalyst w.r.t. oil	Methanol: oil	Time (h)	Feedstock	Notes on paper
(Balbasi *et al.*, 2011)	KI on volvanic tufa		91.1%	220	9%	30:1	3	Sunflower oil	Tufa more active than MCM-41 when loaded with KI. No discussion of leaching or reusability.
(Boz *et al.*, 2009)	KF on gamma alumina		97.7%	65	3%	15:1	8	Canola oil (rapeseed)	K leaching into FAME in first run, large drop in activity after this.
(Gao *et al.*, 2010)	KF on Ca-Al hydrotalcite		99.7%	65	5%	12:1	3	Palm oil	97.1% yield after 1 h. No consideration of reusability or leaching.
(Hameed *et al.*, 2009)	KF on activated carbon		80.2%	175	3%	8.85:1	1	Waste cooking oil	Used modelling to predict optimum conditions. No consideration of reusability or leaching.
(Ni *et al.*, 2010)	CsF on alumina		47%	65	3.7%	?	24	Sunflower oil	Using a circulating reactor. CsF almost completely stripped from alumina - no activity in reuse.
(Samart *et al.*, 2009)	KI on mesoporous silica		90.1%	70	5%	16:1	8	Soybean oil	Reduction in activity after 1 use, no investigation into leaching.
(Verziu *et al.*, 2009)	CsF on alumina	65%	40%	75	1.4%	4:1*	2	Sunflower oil	Catalysts stable for 5 runs of 5 minutes each under microwave heating - unclear how this compares to full length reaction.
(Wan *et al.*, 2008)	KF on MgO		79.4%	65	7%	12:1	5	Rapeseed oil	No investigation of catalyst reuse or leaching.
(Xiao *et al.*, 2010)	KF on Ca-Mg-Al hydrotalcite	98.3%		65	N/A	30:1	N/A	Palm oil	Continuous, packed-bed reactor, using isopropyl ether as cosolvent. Conversion steady after 8 h.
(Xie and Li, 2006)	KI on alumina	96%		65	2.5%	15:1	8	Soybean oil	No consideration of reusability or leaching.

*Molar ratio calculated from the reported numbers gives a value of 5.2:1.

2.1.3 Other Inorganic Compounds

There are a wide variety of other inorganic heterogeneous catalysts, although they can generally be classified by either acidic or basic sites. These include simple compounds (Cordeiro *et al.*, 2008, Liu *et al.*, 2008), conventional homogeneous catalysts adsorbed onto a porous solid (Borges *et al*., 2011, Mutreja *et al*., 2011, Su *et al*., 2010), natural and waste materials (Chakraborty *et al*., 2011, Ilgen, 2011, Deka and Basumatary, 2011), and more complex molecular structures (Cantrell *et al*., 2005, Narasimharao *et al*., 2007, Pesaresi *et al*., 2009). Table 2.3 contains a summary of some of the work on these catalysts. The work of Chakraborty *et al*. (2011) and Deka and Basumatary (2011) raise the interesting possibility of utilising biomass waste as a cheap catalyst source, potentially making catalyst lifetime a less important consideration due to more favourable economics. Muthu *et al*. (2010) demonstrate that sulphated zirconia is capable of handling large amounts of FFA in an oil. This may also be a promising material, as sulphated zirconia is an established industrial catalyst (Kiss *et al*., 2006).

Table 2.3a Other inorganic catalysts

Reference	Catalyst used	Conv	Yield	Temp (°C)	Catalyst w.r.t. oil	Methanol: oil	Time (h)	Feedstock	Notes on paper
(Borges *et al.*, 2011)	Porous silica (pumice) impregnated with KOH		93.2%	60	5%	18:1	2	Sunflower oil	Maintains activity over 5 regenerations.
(Brito *et al.*, 2009)	Hydrotalcite		100%	140	6%	24:1	6	Sunflower oil	Slight loss of activity after 2 runs. Use viscosity as indicator of conversion.
(Cantrell *et al.*, 2005)	[Mg(1-x)Alx(OH)2]x+(CO3)x/n 2- hydrotalcite	74.8%	~75%	60	1.6%	30:1	3	Glyceryl tributyrate	No investigation into reusability or leaching.
(Chakraborty *et al.*, 2011)	Waste fish scales (mainly hydroxyapatite), calcined		97.7%	70	1%	6.27:1	5	Soybean oil	High basicity. Lasted 30 h with slight deactivation, although the clarity of the results seem somewhat suspect.
(Chen *et al.*, 2008)	Sr modified hydroxyapatite	85%		70	5.6%	9:1	5	Soybean oil	No reuse experiments or investigation into leaching.
(Cordeiro *et al.*, 2008)	Zinc hydroxide nitrate		95.7%	150	?	48:1	2	Palm oil	Also, esterifying lauric acid for 2h @ 140 yields 97.4%.
(Deka and Basumatary, 2011)	Burnt banana trees		96%	32	20%	695:1	3	Yellow oleander	Catalyst made of K and Na chlorides and carbonates, as well as various trace level metals, and carbon. Appears to conflate yield and conversion.
(Ilgen, 2011)	Dolomite (Ca and MgCO3)		91.78%	67.5	3%	6:1	3	Canola oil (rapeseed)	Reused 3 times before loss of activity.
(Li *et al.*, 2011)	KOH on Neodymium oxide		92.41%	60	6%	14:1	1.5	Soybean oil	Catalyst appears to be reusable.
(Li *et al.*, 2009)	Zn1.2H0.6PW12O40 nanotubes	97.2%		65	2.3%	70:1	12	Waste cooking oil	FFA and water tolerant.
(Liu *et al.*, 2008)	Calcium ethoxide		95.0%	65	3%	12:1	1.5	Soybean oil	Also an effective catalyst with ethanol. Slight leaching, but no reason to suspect homogeneous reaction.

Table 2.3b Other inorganic catalysts

Reference	Catalyst used	Conv	Yield	Temp (°C)	Catalyst w.r.t. oil	Methanol: oil	Time (h)	Feedstock	Notes on paper
(Muthu *et al.*, 2010)	Sulphated Zirconia	94%*		65	1%	9:1	2	Neem oil	*FFA conversion, primarily concerned with improving current technology, by removing FFAs before homogeneous reaction.
(Mutreja *et al.*, 2011)	KOH impregnated MgO	98%		65	4%	22:1	0.33	Mutton fat	Reaction time increases significantly with addition of FFA or water.
(Narasimharao *et al.*, 2007)	Cs-doped heteropolytunstate salts	100%, 50.2%		60	1.7%	30:1	6	Palmitic acid, glyceryl tributyrate	No leaching, slight activity loss with time.
(Pesaresi *et al.*, 2009)	Cs-doped H4SiW12O40	94%, 34%	> 98%, 81%	60	1.7%	30:1	6	Palmitic acid, glyceryl tributyrate	Also, 62-86% conversion of FFA. Report higher conversion with other catalysts, but they have homogeneous mechanism.
(Peter *et al.*, 2002)	Zinc arginate on silica		80%	125	?	6:1	0.33	Sunflower oil	No investigation into leaching, propose a two reactor scheme, with glycerol removal between.
(Qiu *et al.*, 2011)	ZrO2 loaded with C4H4O6HK		98.03%	60	6%	16:1	2	Soybean oil	Slight leaching and slow decline in activity across multiple runs.
(Sreeprasanth *et al.*, 2006)	Fe-Zn double metal cyanide complex	99%		170	3%	15:1	8	Various oils, inc. high FFA	Tolerant of FFA and water, no noticeable leaching.
(Su *et al.*, 2010)	NaOH on hydrotalcite	95%		65	20%	6:1	6	Canola (rapseed) oil	No investigation into reusability or leaching, primarily concerned with screening support materials.
(Tonetto and Marchetti, 2010)	Me/Al2O3 (Me=Ca, Na, K), K/Al2O3 on coridierite monolith	100%	94.7%, 97.1%, 98.9%, 59.1%	120	1% for powder, 0.5% for monolith	32:1	6	Soybean oil	First three yields correspond to powdered catalyst, final yield is for coated monolith. Significant leaching, possibly indicating homogeneous mechanism.
(Zieba *et al.*, 2010)	Zn5(OH)8(NO3)2-2H2O	76%	48.7%, 21.1%	50	5%	29:1	3	Triacetin, Castor oil	No conversion given for castor oil. Activity loss due to pore clogging, washing restored activity.

2.1.4 Other Catalysts

A variety of other catalysts are used in the literature, ranging from zeolites to ionic liquids. A number of groups report work on ion exchange resins, particularly proton or cation exchange membranes, where high conversions of at least 94% are reported (Kiss *et al*., 2006, Shi *et al*., 2010, Feng *et al*., 2011). A major advantage of these appears to be their tolerance of FFA, with all the papers surveyed using a highly acidic feedstock, although they are also all susceptible to water, with very low limits of water tolerance. The resins appear to be reusable to various degrees, with Shi *et al*. reporting 5 reuses, and Feng *et al*. running a continuous reactor for 500 h without conversion of the FFA in acidified oil dropping below 98%.

Carrero *et al* (2011) report the use of ZSM-5 and beta zeolites for the transesterification of algal oil, which has a high FFA and polar lipid (e.g. phospholipids) content. The best yield reported was 50%, after four hours at 115°C. Unfortunately, no discussion of reusability is included in the article. Macia-Aguillo *et al*. (2010) functionalised carbon spheres with sulphonic acid to produce a catalyst for the esterification of oleic acid with ethanol. After 24 h at 55°C, a conversion of 55% and a yield of 87% were attained. The catalyst's activity decreased after each run.

Immobilised lipase has also been used for the transesterification reaction, as well as the esterification of oils. The enzymes can be immobilised on various media, such as diatomaceous earth (Shah *et al*., 2004), crystalline precipitates (Kumari *et al*., 2007), porous silicates (Dizge *et al*., 2009, Kawakami *et al*., 2009), or simply by agglomeration (Kumari *et al*., 2007). These work at moderate temperatures, although reactions take as long as 24 h to obtain yields over 90%.

2.1.5 Monolithic Catalysts

Monolithic catalyst supports have been used in the literature for biodiesel production. The current project stems from the work of Asli (2011) to fix zinc proline to a cordierite monolith. The catalyst was coated directly onto the cordierite surface by dipping monolith pieces into a suspension of zinc proline (Kolaczkowski *et al*., 2009), which had shown great promise as being both FFA and water tolerant (Chuck, 2007). Unfortunately, zinc proline was found to leach excessively and rapidly lost activity (Asli, 2011).

Tonetto and Marchetti (2010) also explored the possibility of using cordierite monoliths, transesterifying soybean oil with a potassium catalyst. Potassium carbonate was mixed into a bohemite-water slurry, and coated onto the bare monolith before calcination. The monolith pieces were fitted to the impeller of an overhead stirrer in a reactor vessel, and the reaction carried out at 120°C for 6 h. Unfortunately, despite the 98.9% yield obtained with a powdered catalyst, the monolithic system only achieved a 59.1% yield, and showed signs of leaching and deactivation after just one run.

Other monoliths studied in the literature include supports for immobilised lipases (Dizge *et al*., 2009, Kawakami *et al*., 2009). Dizge *et al*. first formed a polymeric silica monolith in a mould *via* a sol-gel method, to ensure high porosity. The lipase was then immobilised on the surface, and the monolith was used in 10 consecutive 24 h reactions. The experiments involved mixing the oil and methanol in a flask and circulating the mixture through a reactor holding the monolith; 90.2% yields were obtained. Kawakami *et al*. used a similar method to immobilise lipase to a sol-gel derived silica monolith, although their reaction medium was oil and methanol dissolved in n-hexane. It is difficult to ascertain the effectiveness of the reaction, as FAME production is discussed in terms of concentration, without mentioning the concentration of the feed stream.

2.2 Catalyst Selection

The general literature regarding heterogeneous catalysis for biodiesel production may be summarised as follows:

- A wide variety of materials can be used to transesterify natural oils with primary alcohols to yield biodiesel.
- Catalysts generally can be characterised as having either acidic or basic sites.
- Experiments have been done at a range of methanol:oil ratios and temperatures – there does not appear to be a generally accepted standard.
- The reusability and ruggedness of the catalyst are often not considered.
- The costs of constant filtration or other separation steps necessitated by simple, non-structured catalysts, such as powders, are often ignored.
- Conditions, such as methanol:oil ratio and catalyst loading are often increased to provide better yields in batch experiments, which may mask the inactivity of some catalysts relative to others in the literature.

Thus, there is much room for research into structured catalytic reactors for continuous biodiesel production, with a primary focus on extending the useful life and flexibility of the catalyst. Experiments should be carried out within a reasonable range of others in the literature. Catalyst loading should be minimised as far as possible, preferably less than 5% with respect to oil in a batch reaction. Additionally, the amount of methanol used should be chosen with due regard to scaling up, instead of maximising the lab-scale yield – molar excesses in the hundreds will only increase process costs, and so a ratio of around 6:1 should be used where possible.

Despite the promise that strontium catalysts show for transesterification, there is relatively little literature on the subject[1] (Zabeti *et al.*, 2009). A thorough investigation into the possibility of incorporating strontium oxide into a heterogeneous catalyst should be undertaken. Broader than this is the general need for the study of structured catalysts for the biodiesel production process.

[1] This literature review contains all of the relevant publications from a Web of Science search for the terms "strontium AND (biodiesel OR transester*)", 30/10/13

The doped lanthanum catalysts developed by Kim *et al* (2011a) were also chosen, as they reported good long-term stability and tolerance to impurities. However, it appears that limited work was done optimising the catalyst, so it was decided that this would be undertaken, in order to determine if it should be developed into a catalyst coating on a structured catalyst.

References

ASLI, U. A. 2011. *Catalytic monoliths for biodiesel production.* Ph.D., University of Bath.

BALBASI, M., BARTAN, A., AR, I. & GURU, M. 2011. Development of low cost heterogeneous catalysts for biodiesel processes. *Energy Sources, Part A: Recovery, Utilization and Environmental Effects,* 33**,** 1035-1047.

BENJAPORNKULAPHONG, S., NGAMCHARUSSRIVICHAI, C. & BUNYAKIAT, K. 2009. Al2O3-supported alkali and alkali earth metal oxides for transesterification of palm kernel oil and coconut oil. *Chemical Engineering Journal,* 145**,** 468-474.

BOEY, P.-L., MANIAM, G. P. & HAMID, S. A. 2011. Performance of calcium oxide as a heterogeneous catalyst in biodiesel production: A review. *Chemical Engineering Journal,* 168**,** 15-22.

BORGES, M. E., DIAZ, L., ALVAREZ-GALVAN, M. C. & BRITO, A. 2011. High performance heterogeneous catalyst for biodiesel production from vegetal and waste oil at low temperature. *Applied Catalysis B: Environmental,* 102**,** 310-315.

BOURNAY, L., CASANAVE, D., DELFORT, B., HILLION, G. & CHODORGE, J. A. 2005a. New heterogeneous process for biodiesel production: A way to improve the quality and the value of the crude glycerin produced by biodiesel plants. *In:* International Conference on Gas-Fuel '05. Elsevier, 190-192.

BOURNAY, L., HILLION, G., BOUCOT, P., CHODORGE, J.-A., BRONNER, C. & FORESTIERE, A. 2005b. *Process for producing alkyl esters from a vegetable or animal oil and an aliphatic monoalcohol*. US6878837 (B2).

BOZ, N., DEGIRMENBASI, N. & KALYON, D. M. 2009. Conversion of biomass to fuel: Transesterification of vegetable oil to biodiesel using KF loaded nano-gamma-Al(2)O(3) as catalyst. *Applied Catalysis B-Environmental,* 89**,** 590-596.

BRITO, A., BORGES, M. E., GARIN, M. & HERNANDEZ, A. 2009. Biodiesel Production from Waste Oil Using Mg-Al Layered Double Hydroxide Catalysts. *Energy & Fuels,* 23**,** 2952-2958.

BS EN 14214:2008 + A1:2009 Automotive fuels - Fatty acid methyl esters (FAME) for diesel engines. Requirements and test methods. *British Standards Institute.*

CANTRELL, D. G., GILLIE, L. J., LEE, A. F. & WILSON, K. 2005. Structure-reactivity correlations in MgAl hydrotalcite catalysts for biodiesel synthesis. *Applied Catalysis A: General,* 287**,** 183-190.

CARRERO, A., VICENTE, G., RODRIGUEZ, R., LINARES, M. & DEL PESO, G. L. 2011. Hierarchical zeolites as catalysts for biodiesel production from Nannochloropsis microalga oil. *Catalysis Today*.

CHAKRABORTY, R., BEPARI, S. & BANERJEE, A. 2010. Transesterification of soybean oil catalyzed by fly ash and egg shell derived solid catalysts. *Chemical Engineering Journal,* 165**,** 798-805.

CHAKRABORTY, R., BEPARI, S. & BANERJEE, A. 2011. Application of calcined waste fish (Labeo rohita) scale as low-cost heterogeneous catalyst for biodiesel synthesis. *Bioresource Technology,* 102**,** 3610-3618.

CHEN, C.-L., HUANG, C.-C., TRAN, D.-T. & CHANG, J.-S. 2012. Biodiesel synthesis via heterogeneous catalysis using modified strontium oxides as the catalysts.

CHEN, W., HUANG, Z., LIU, Y. & HE, Q. 2008. Preparation and characterization of a novel solid base catalyst hydroxyapatite loaded with strontium. *Catalysis Communications,* 9**,** 516-521.

CHUCK, C. J. 2007. *Lewis acid catalyst design for the transesterification of lower quality feedstocks for biodiesel production.* Ph.D., University of Bath.

CORDEIRO, C. S., ARIZAGA, G. G. C., RAMOS, L. P. & WYPYCH, F. 2008. A new zinc hydroxide nitrate heterogeneous catalyst for the esterification of free fatty acids and the transesterification of vegetable oils. *Catalysis Communications,* 9**,** 2140-2143.

DE CARVALHO, L. M. G., ABREU, W. C. D., SILVA, M. D. G. D. O. E., LIMA, J. R. D. O., OLIVEIRA, J. E. D., MATOS, J. M. E. D., MOURA, C. V. R. D. & MOURA, E. M. D. 2013. Heterogeneous catalysis afford biodiesel of babassu, castor oil and blends. *Journal of the Brazilian Chemical Society,* 24**,** 550-557.

DE MOURA, C. V. R., DE CASTRO, A. G., DE MOURA, E. M., DOS SANTOS, J. R. & MOITA NETO, J. M. 2010. Heterogeneous catalysis of babassu oil monitored by thermogravimetric analysis. *Energy and Fuels,* 24**,** 6527-6532.

DEKA, D. C. & BASUMATARY, S. 2011. High quality biodiesel from yellow oleander (Thevetia peruviana) seed oil. *Biomass and Bioenergy,* 35**,** 1797-1803.

DEL REMEDIO HERNÁNDEZ, M., REYES-LABARTA, J. A. & VALDÉS, F. J. 2010. New Heterogeneous Catalytic Transesterification of Vegetable and Used Frying Oil. *Industrial & Engineering Chemistry Research,* 49**,** 9068-9076.

DIAS, A. P. S., BERNARDO, J., FELIZARDO, P. & CORREIA, M. J. N. 2012. Biodiesel production by soybean oil methanolysis over SrO/MgO catalysts: The relevance of the catalyst granulometry. *Fuel Processing Technology,* 102**,** 146-155.

DIZGE, N., AYDINER, C., IMER, D. Y., BAYRAMOGLU, M., TANRISEVEN, A. & KESKINLER, B. 2009. Biodiesel production from sunflower, soybean, and waste cooking oils by transesterification using lipase immobilized onto a novel microporous polymer. *Bioresource Technology,* 100**,** 1983-1991.

FAUNGNAWAKIJ, K., YOOSUK, B., NAMUANGRUK, S., KRASAE, P., VIRIYA-EMPIKUL, N. & PUTTASAWAT, B. 2012. Sr-Mg Mixed Oxides as Biodiesel Production Catalysts. *Chemcatchem,* 4**,** 209-216.

FENG, Y., ZHANG, A., LI, J. & HE, B. 2011. A continuous process for biodiesel production in a fixed bed reactor packed with cation-exchange resin as heterogeneous catalyst. *Bioresource Technology,* 102**,** 3607-3609.

GAO, L., TENG, G., XIAO, G. & WEI, R. 2010. Biodiesel from palm oil via loading KF/Ca-Al hydrotalcite catalyst. *Biomass & Bioenergy,* 34**,** 1283-1288.

HAMEED, B. H., GOH, C. S. & CHIN, L. H. 2009. Process optimization for methyl ester production from waste cooking oil using activated carbon supported potassium fluoride. *Fuel Processing Technology,* 90**,** 1532-1537.

HSIN, T.-M., CHEN, S., GUO, E., TSAI, C.-H., PRUSKI, M. & LIN, V. S. Y. 2010. Calcium containing silicate mixed oxide-based heterogeneous catalysts for biodiesel production. *Topics in Catalysis,* 53**,** 746-754.

ILGEN, O. 2011. Dolomite as a heterogeneous catalyst for transesterification of canola oil. *Fuel Processing Technology,* 92**,** 452-455.

KAWAKAMI, K., TAKAHASHI, R., SHAKERI, M. & SAKAI, S. 2009. Application of a lipase-immobilized silica monolith bioreactor to the production of fatty acid methyl esters. *Journal of Molecular Catalysis B-Enzymatic,* 57**,** 194-197.

KIM, M., DIMAGGIO, C., YAN, S., SALLEY, S. O. & NG, K. Y. S. 2011a. The effect of support material on the transesterification activity of CaO-La2O3 and CaO-CeO2 supported catalysts. *Green Chemistry,* 13**,** 334-339.

KIM, M., DIMAGGIO, C., YAN, S., WANG, H., SALLEY, S. O. & SIMON NG, K. Y. 2011b. Performance of heterogeneous ZrO2 supported metaloxide catalysts for brown grease esterification and sulfur removal. *Bioresource Technology,* 102**,** 2380-2386.

KIM, M., YAN, S., SALLEY, S. O. & NG, K. Y. S. 2009. The effect of sodium on the catalytic activity of ZnO-Al2O3/ZSM-5 and SnO-Al2O3/ZSM-5 for the transesterification of vegetable oil with methanol. *Catalysis Communications,* 10**,** 1913-1919.

KISS, A. A., DIMIAN, A. C. & ROTHENBERG, G. 2006. Solid acid catalysts for biodiesel production - Towards sustainable energy. *Advanced Synthesis & Catalysis,* 348**,** 75-81.

KOBERG, M., ABU-MUCH, R. & GEDANKEN, A. 2011. Optimization of bio-diesel production from soybean and wastes of cooked oil: Combining dielectric microwave irradiation and a SrO catalyst. *Bioresource Technology,* 102**,** 1073-1078.

KOBERG, M. & GEDANKEN, A. 2012. Direct Transesterification of Castor and Jatropha Seeds for FAME Production by Microwave and Ultrasound Radiation Using a SrO Catalyst. *BioEnergy Research,* 5**,** 958-968.

KOLACZKOWSKI, S. T., ASLI, U. A. & DAVIDSON, M. G. 2009. A new heterogeneous ZnL2 catalyst on a structured support for biodiesel production. *Catalysis Today,* 147**,** S220-S224.

KUMARI, V., SHAH, S. & GUPTA, M. N. 2007. Preparation of biodiesel by lipase-catalyzed transesterification of high free fatty acid containing oil from Madhuca indica. *Energy and Fuels,* 21**,** 368-372.

LI, J., WANG, X., ZHU, W. & CAO, F. 2009. Zn1.2H0.6PW12O40 Nanotubes with double acid sites as heterogeneous catalysts for the production of biodiesel from waste cooking oil. *ChemSusChem,* 2**,** 177-183.

LI, Y., QIU, F., YANG, D., LI, X. & SUN, P. 2011. Preparation, characterization and application of heterogeneous solid base catalyst for biodiesel production from soybean oil.

LIMA, J. R. D. O., GHANI, Y. A., DA SILVA, R. B., BATISTA, F. M. C., BINI, R. A., VARANDA, L. C. & DE OLIVEIRA, J. E. 2012. Strontium zirconate heterogeneous catalyst for biodiesel production: Synthesis, characterization and catalytic activity evaluation. *Applied Catalysis A: General,* 445–446**,** 76-82.

LIU, X. J., HE, H. Y., WANG, Y. J. & ZHU, S. L. 2007. Transesterification of soybean oil to biodiesel using SrO as a solid base catalyst. *Catalysis Communications,* 8**,** 1107-1111.

LIU, X. J., PIAO, X. L., WANG, Y. J. & ZHU, S. F. 2008. Calcium ethoxide as a solid base catalyst for the transesterification of soybean oil to biodiesel. *Energy & Fuels,* 22**,** 1313-1317.

LUZ MARTINEZ, S., ROMERO, R., LOPEZ, J. C., ROMERO, A., SANCHEZ MENDIETA, V. & NATIVIDAD, R. 2011. Preparation and characterization of CaO nanoparticles/NaX zeolite catalysts for the transesterification of sunflower oil. *Industrial & Engineering Chemistry Research,* 50**,** 2665-2670.

MACIA-AGULLO, J. A., SEVILLA, M., DIEZ, M. A. & FUERTES, A. B. 2010. Synthesis of carbon-based solid acid microspheres and their application to the production of biodiesel. *ChemSusChem,* 3**,** 1352-1354.

MACLEOD, C. S., HARVEY, A. P., LEE, A. F. & WILSON, K. 2008. Evaluation of the activity and stability of alkali-doped metal oxide catalysts for application to an intensified method of biodiesel production. *Chemical Engineering Journal,* 135**,** 63-70.

MONTERO, J. M., BROWN, D. R., GAI, P. L., LEE, A. F. & WILSON, K. 2010. In situ studies of structure-reactivity relations in biodiesel synthesis over nanocrystalline MgO. *Chemical Engineering Journal,* 161**,** 332-339.

MUTHU, H., SELVABALA, V. S., VARATHACHARY, T. K., SELVARAJ, D. K., NANDAGOPAL, J. & SUBRAMANIAN, S. 2010. Synthesis of biodiesel from neem oil using sulfated zirconia via tranesterification. *Brazilian Journal of Chemical Engineering,* 27**,** 601-608.

MUTREJA, V., SINGH, S. & ALI, A. 2011. Biodiesel from mutton fat using KOH impregnated MgO as heterogeneous catalysts. *Renewable Energy,* 36**,** 2253-2258.

NARASIMHARAO, K., BROWN, D. R., LEE, A. F., NEWMAN, A. D., SIRIL, P. F., TAVENER, S. J. & WILSON, K. 2007. Structure-activity relations in Cs-doped heteropolyacid catalysts for biodiesel production. *Journal of Catalysis,* 248**,** 226-234.

NI, J., ROONEY, D. & MEUNIER, F. C. 2010. CsF and alumina: A mixed homogeneous-heterogeneous catalytic system for the transesterification of sunflower oil with methanol. *Applied Catalysis B-Environmental,* 97**,** 269-275.

OLUTOYE, M. A. & HAMEED, B. H. 2011. Synthesis of fatty acid methyl ester from used vegetable cooking oil by solid reusable Mg1-x Zn1+xO2 catalyst. *Bioresource Technology,* 102**,** 3819-3826.

PATIL, P., GUDE, V. G., PINAPPU, S. & DENG, S. 2011. Transesterification kinetics of Camelina sativa oil on metal oxide catalysts under conventional and microwave heating conditions. *Chemical Engineering Journal,* 168**,** 1296-1300.

PESARESI, L., BROWN, D. R., LEE, A. F., MONTERO, J. M., WILLIAMS, H. & WILSON, K. 2009. Cs-doped H4SiW12O40 catalysts for biodiesel applications. *Applied Catalysis A: General,* 360**,** 50-58.

PETER, S. K. F., GANSWINDT, R., NEUNER, H. P. & WEIDNER, E. 2002. Alcoholysis of triacylglycerols by heterogeneous catalysis. *European Journal of Lipid Science and Technology,* 104**,** 324-330.

PUGNET, V., MAURY, S., COUPARD, V., DANDEU, A., QUOINEAUD, A. A., BONNEAU, J. L. & TICHIT, D. 2010. Stability, activity and selectivity study of a zinc aluminate heterogeneous catalyst for the transesterification of vegetable oil in batch reactor. *Applied Catalysis a-General,* 374**,** 71-78.

PUNA, J. F., GOMES, J. F., CORREIA, M. J. N., SOARES DIAS, A. P. & BORDADO, J. C. 2010. Advances on the development of novel heterogeneous catalysts for transesterification of triglycerides in biodiesel. *Fuel,* 89**,** 3602-3606.

QIU, F., LI, Y., YANG, D., LI, X. & SUN, P. 2011. Heterogeneous solid base nanocatalyst: Preparation, characterization and application in biodiesel production. *Bioresource Technology,* 102**,** 4150-4156.

SAMART, C., SREETONGKITTIKUL, R. & SOOKMAN, C. 2009. Heterogeneous catalysis of transesterification of soybean oil using KI/mesoporous silica. *Fuel Processing Technology,* 90**,** 922-925.

SHAH, S., SHARMA, S. & GUPTA, M. N. 2004. Biodiesel preparation by lipase-catalyzed transesterification of Jatropha oil. *Energy and Fuels,* 18**,** 154-159.

SHI, W., HE, B. & LI, J. 2010. Esterification of acidified oil with methanol by SPES/PES catalytic membrane. *Bioresource Technology,* In Press, Corrected Proof.

SREEPRASANTH, P. S., SRIVASTAVA, R., SRINIVAS, D. & RATNASAMY, P. 2006. Hydrophobic, solid acid catalysts for production of biofuels and lubricants. *Applied Catalysis a-General,* 314**,** 148-159.

SU, E.-C., LI, Y.-L., TSENG, H.-H. & WU, S.-P. 2010. Influence of supports structure on the synthesis of biodiesel from canola oil. *In:* 2010 International Conference on Environmental and Agriculture Engineering, ICEAE 2010, August 1, 2010 - August 3, 2010, Kyoto, Japan. Association for Computing Machinery, 89-91.

TANTIRUNGROTECHAI, J., THEPWATEE, S. & YOOSUK, B. 2013. Biodiesel synthesis over Sr/MgO solid base catalyst. *Fuel,* 106**,** 279-284.

TAUFIQ-YAP, Y. H., LEE, H. V., HUSSEIN, M. Z. & YUNUS, R. 2011. Calcium-based mixed oxide catalysts for methanolysis of Jatropha curcas oil to biodiesel. *Biomass and Bioenergy,* 35**,** 827-834.

TONETTO, G. M. & MARCHETTI, J. M. 2010. Transesterification of Soybean Oil Over Me/Al2O3 (Me = Na, Ba, Ca, and K) Catalysts and Monolith K/Al2O3-Cordierite. *Topics in Catalysis,* 53**,** 755-762.

VERZIU, M., FLOREA, M., SIMON, S., SIMON, V., FILIP, P., PARVULESCU, V. I. & HARDACRE, C. 2009. Transesterification of vegetable oils on basic large mesoporous alumina supported alkaline fluorides-Evidences of the nature of the active site and catalytic performances. *Journal of Catalysis,* 263**,** 56-66.

VIOLA, E., BLASI, A., VALERIO, V., GUIDI, I., ZIMBARDI, F., BRACCIO, G. & GIORDANO, G. 2012. Biodiesel from fried vegetable oils via transesterification by heterogeneous catalysis. *Catalysis Today,* 179**,** 185-190.

WAN, T., YU, P., GONG, S., LI, Q. & LUO, Y. 2008. Application of KF/MgO as a heterogeneous catalyst in the production of biodiesel from rapeseed off. *Korean Journal of Chemical Engineering,* 25**,** 998-1003.

XIAO, Y., GAO, L. J., XIAO, G. M. & LV, J. H. 2010. Kinetics of the Transesterification Reaction Catalyzed by Solid Base in a Fixed-Bed Reactor. *Energy & Fuels,* 24**,** 5829-5833.

XIE, W. & LI, H. 2006. Alumina-supported potassium iodide as a heterogeneous catalyst for biodiesel production from soybean oil. *Journal of Molecular Catalysis a-Chemical,* 255**,** 1-9.

XIE, W., YANG, Z. & CHUN, H. 2007. Catalytic properties of lithium-doped ZnO catalysts used for biodiesel preparations. *Industrial and Engineering Chemistry Research,* 46**,** 7942-7949.

YAN, S., DIMAGGIO, C., MOHAN, S., KIM, M., SALLEY, S. O. & NG, K. Y. S. 2010. Advancements in heterogeneous catalysis for biodiesel synthesis. *Topics in Catalysis,* 53**,** 721-736.

YAN, S. L., KIM, M., SALLEY, S. O. & NG, K. Y. S. 2009. Oil transesterification over calcium oxides modified with lanthanum. *Applied Catalysis a-General,* 360**,** 163-170.

YANG, R., SU, M., LI, M., ZHANG, J., HAO, X. & ZHANG, H. 2010. One-pot process combining transesterification and selective hydrogenation for biodiesel production from starting material of high degree of unsaturation. *Bioresource Technology,* 101**,** 5903-5909.

YANG, Z. & XIE, W. 2007. Soybean oil transesterification over zinc oxide modified with alkali earth metals. *Fuel Processing Technology,* 88**,** 631-638.

YOOSUK, B., KRASAE, P., PUTTASAWAT, B., UDOMSAP, P., VIRIYA-EMPIKUL, N. & FAUNGNAWAKIJ, K. 2010. Magnesia modified with strontium as a solid base catalyst for transesterification of palm olein. *Chemical Engineering Journal,* 162**,** 58-66.

YU, X., WEN, Z., LI, H., TU, S.-T. & YAN, J. 2011. Transesterification of Pistacia chinensis oil for biodiesel catalyzed by CaO-CeO2 mixed oxides. *Fuel,* 90**,** 1868-1874.

ZABETI, M., WAN DAUD, W. M. A. & AROUA, M. K. 2009. Activity of solid catalysts for biodiesel production: A review. *Fuel Processing Technology,* 90**,** 770-777.

ZIEBA, A., PACUZA, A. & DRELINKIEWICZ, A. 2010. Transesterification of triglycerides with methanol catalyzed by heterogeneous zinc hydroxy nitrate catalyst. Evaluation of variables affecting the activity and stability of catalyst. *In,* 2540 Olentangy River Road, P.O. Box 3337, Columbus, OH 43210-3337, United States. American Chemical Society, 634-645.

Chapter 3 Catalyst Screening

In this chapter, experimental work to arrive at a useful transesterification catalyst is described. First, the analytical tools used throughout the work in this thesis are introduced, including a review of the techniques used in the literature to analyse the transesterification. The oil used in the experimental work is characterised, and the methods of materials characterisation are introduced. After this, the screening of powder catalysts is discussed, which forms the basis of which catalysts were chosen for attempting to coat onto monolithic supports. Various coating methods are then explored, with some attention given to understanding why some failed, and others succeeded. Finally, the catalysts are chosen for use in the continuous reactors described in Chapter 5.

In order to maintain a consistent oil quality across all experiments, Horeco Select brand rapeseed oil was purchased from Macro Ltd (Bristol) in 15L and 20L containers.

3.1 Analysis

The transesterification reaction can be followed using a number of analytical techniques, including gas chromatography, nuclear magnetic resonance (NMR), spectroscopy high-performance liquid chromatography, infra-red spectroscopy, and other methods (Monteiro *et al*., 2008). Methods for which equipment is available for this project are discussed below.

Gas chromatography (GC) is a well-established analytical method for biodiesel (Knothe *et al.*, 2005). Generally, the sample must be silylated, by the addition of a trimethylsilyl-containing molecule, which reacts with the free hydroxyl groups of the glycerides, leading to cleaner peaks and longer column life (Plank and Lorbeer, 1995). After addition of the internal standards, the solution is diluted and injected into the GC, which allows the determination of the individual components of a reaction mixture, i.e. mono, di, and triglycerides, as well as FAME and glycerol.

^{1}H-NMR spectroscopy can be used to monitor the progress of the reaction, by comparison of the methylene hydrogen atoms adjacent to the ester bond in the triglyceride and the terminal methoxy group next to the ester in the FAME molecules (Monteiro *et al*., 2008). The advantage of this is the simplicity and speed of the analysis, although it appears that the mono and diglycerides are indistinguishable from triglycerides.

Thermo-gravimetric analysis was used by de Moura *et al*. (2010), based on the different boiling temperatures of FAME and triglycerides. This method allowed them to monitor the conversion of the reaction, and comparison with NMR and GC data showed very strong correlations, and without the need for additional solvents that the others have. Similar to NMR, this method is simple, but only effective for the investigation of conversion, and does not reveal the concentrations of the intermediates.

3.1.1 Gas Chromatography

Figure 3.1 Gas chromatograph and workstation PC.

Gas chromatography was carried out using an HP Agilent 5890 Series II chromatograph (shown in Figure 3.1) and Data Apex Clarity data acquisition and processing software. The chromatograph was equipped with a guard column (1 m x 0.53 mm, non-polar fused silica, Sigma Aldrich), a Thermo-Scientific TR-Biodiesel (G) column (10 m x 0.32 mm ID, with 0.1 μm DB-5 coating), and a Flame Ionisation Detector (FID). Injections of 0.5 μL were used, with the GC set at the conditions given in Table 3.1.

Table 3.1 GC conditions

Parameter	Setting
Initial oven temperature	65°C
Injector temperature	Oven track mode
Hold time 1	2 minute
Temperature ramp rate 1	15°C min^{-1}
Oven temperature 2	180°C
Hold time 2	-
Temperature ramp rate 2	7.5°C min^{-1}
Oven temperature 3	270°C
Hold time 3	-
Temperature ramp rate 3	15°C min^{-1}
Final temperature	330°C
FID temperature	300°C

The FID was supplied with hydrogen and air, at flow rates of 33 and 400 mL min^{-1} respectively. Helium, at a flow rate of 30 mL min^{-1}, was used as the carrier gas. Injections were carried out manually, as was the sending of the start signal to the equipment. The methods and materials used were based on the procedure given by Plank and Lorbeer (1995).

Samples were prepared for GC by the trimethylsilylation of any hydroxyl groups with n-methyl-n-trimethylsilyltrifluoroacetamide (MSTFA), as this improves the clarity of results, as well as increasing the lifetime of the column (Plank and Lorbeer, 1995). Initially, the samples and subsequent additions were half the concentration described below, but this was increased to the method described to improve the response of the apparatus. Injections of 0.5 μL were used. The sample preparation procedure is as follows:

- Take 60 μL sample and dilute it up to 1.5 mL in pyridine;
- Put 360 μL of this into a GC vial;
- Add 60 μL butanetriol (4 mg mL^{-1} in pyridine), to verify complete trimethylsilylation;
- Add 60 μL tricaprin (8 mg mL^{-1} in pyridine) internal standard;
- Add 120 μL MSTFA, cover and shake the vial and leave to stand at room temperature for half an hour;
- Dilute sample up to 1.5 mL in n-heptane.

3.1.1.1 GC Calibration

The gas chromatography software was calibrated using a series of samples of known concentrations. Monoolein and diolein solutions (5 mg mL^{-1} in pyridine) were purchased from Sigma Aldrich as models for monoglycerides and diglycerides, respectively. Glycerol (99%) was also purchased from Sigma Aldrich. The rapeseed oil was used as the triglyceride calibrant.

- A pure FAME sample was made by transesterifying 160 mL oil with 40 mL methanol using 1.5 mL sulphuric acid (96%, Sigma Aldrich) as the catalyst. The mixture was refluxed in a round-bottomed flask overnight.

- About 50 mL of ester-containing phase was recovered using gravity settling, and re-reacted overnight with 30 mL methanol using 0.7 g NaOH as catalyst.

- This was then neutralised with 0.6 mL sulphuric acid, and then washed with water and heptane to effect a solvent extraction.

- The aqueous phase was discarded and the organic phase was washed twice more with water.

- The organic phase was then recovered in a rotary evaporator. An uncalibrated GC of this product revealed some mono- and diglycerides, and so 15 mL of the product was added to 1.0 g silica gel powder (70-230 mesh, Sigma Aldrich), as this has been identified as a suitable adsorbent for biodiesel purification (Mazzieri *et al.*, 2008). This mixture was stirred for 2 hours, and then centrifuged for 5 minutes at 3000 rpm.

- The supernatant was removed and filtered through a 0.22 μm syringe driven filter.

As can be seen in Figure 3.2, the final product contained no triglycerides (peaks above 19 minutes), and only a small amount of intermediates (12 to 18 minutes). Integrating the FAME peaks (7 to 12 minutes) and comparing this value to the integral of the intermediates' peaks gives a level of impurities of less than 1.1%. This was deemed to be acceptable for the purposes of the calibration.

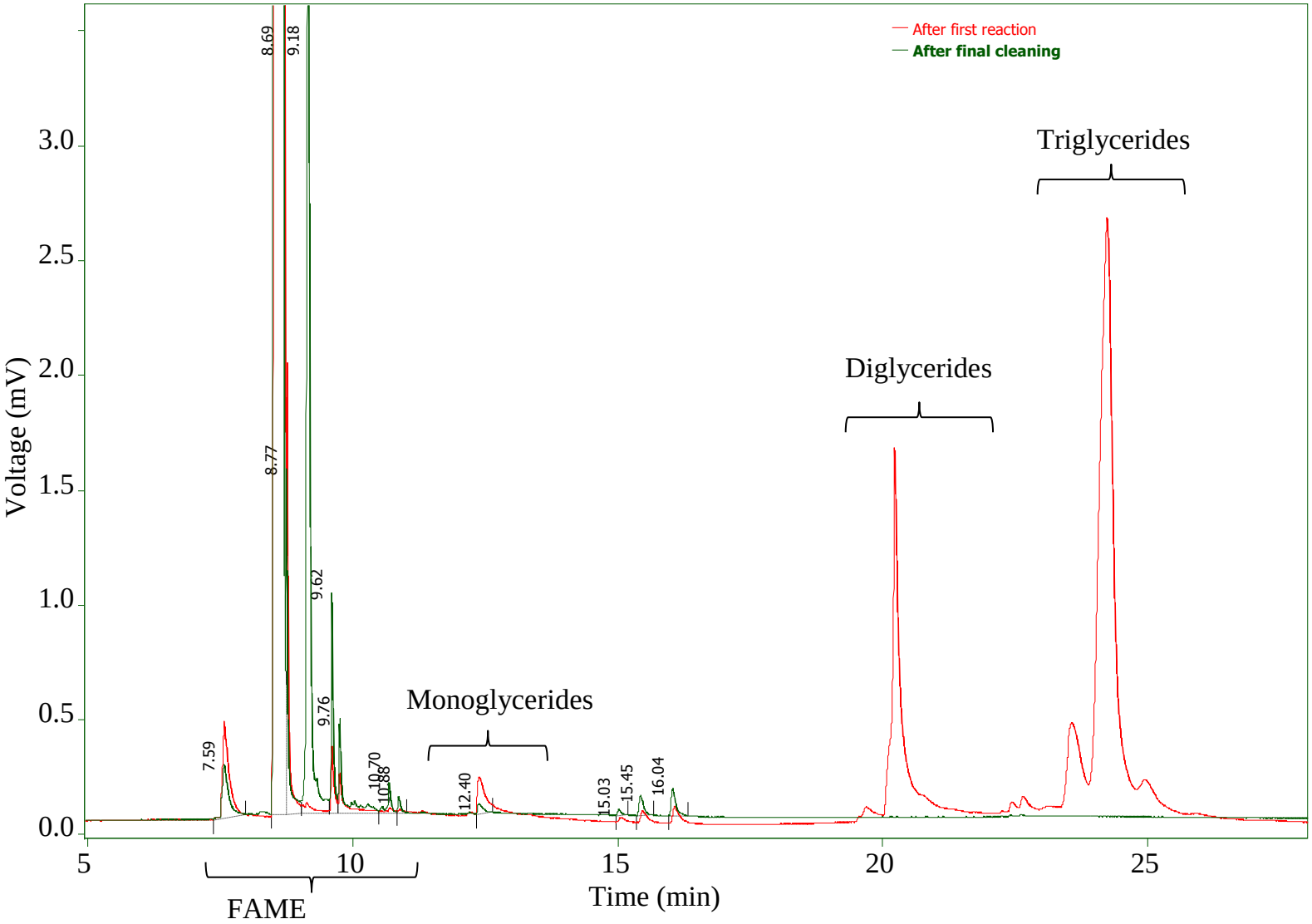

Figure 3.2 Chromatograms of product after initial reaction (red) and final FAME standard (green).

The yield of each component was obtained from the GC software in terms of wt.%, and so this was converted to mol % using equation (3.1).

$$mol\% = \frac{w_i M_i}{\sum(w_i M_i)} \tag{3.1}$$

Where:

M = molecular weight

w = Weight %

i = reaction component:

The calibration standards were prepared using these materials, with five levels being selected as the best guess of the likely ranges of products to be found in a given sample, given in Table 3.2. These were then mixed with the internal standards and derivatised with MSTFA, as described in Section 3.1.1. Injections of 0.5 µL were performed, and the Clarity chromatogram software used to process the calibration.

Table 3.2 GC calibration standards

Component	GC calibration concentrations (mg ml^{-1})				
	Level 1	Level 2	Level 3	Level 4	Level 5
Trigrlyceride	8	3	1	0.2	0.08
Diglyceride	1.6	0.8	0.2	0.05	0.01
Monoglyceride	1.6	0.8	0.2	0.05	0.01
FAME	8	3	1	0.2	0.08
Glycerol	4	2	0.5	0.1	0.04

Through the course of experiments, it was noted that the size of the glycerol peak often did not correspond to the degree of conversion. As an example, the results of a

series of samples from a high-conversion experiment are shown in Figure 3.3. It should be noted that the maximum possible yield of FAME and glycerol are 75% and 25% respectively. These results show that the glycerol would appear in the GCs at both substantially higher and lower values than would be expected for the degree of conversion.

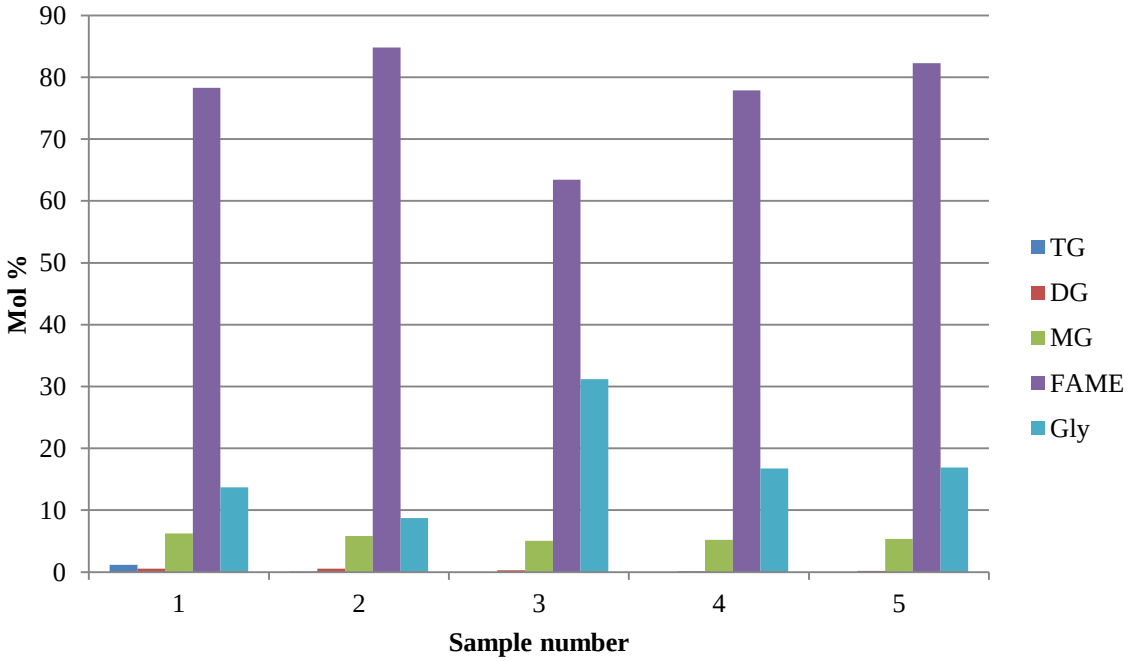

Figure 3.3 High conversion result showing inconsistent glycerol results.

In order to deal with this inconsistency with regard to the glycerol peak, it was decided that the glycerol concentration should be estimated by mass balance from the concentration of the other products. This process is represented in Equation (3.2).

$$C_{Gly} = \frac{C_{FAME} - C_{DG} - 2C_{MG}}{3} \tag{3.2}$$

The results displayed in Figure 3.3 were reprocessed using this equation in order to estimate the actual glycerol content, and close the mass balance. The results of this modification are shown in Figure 3.4.

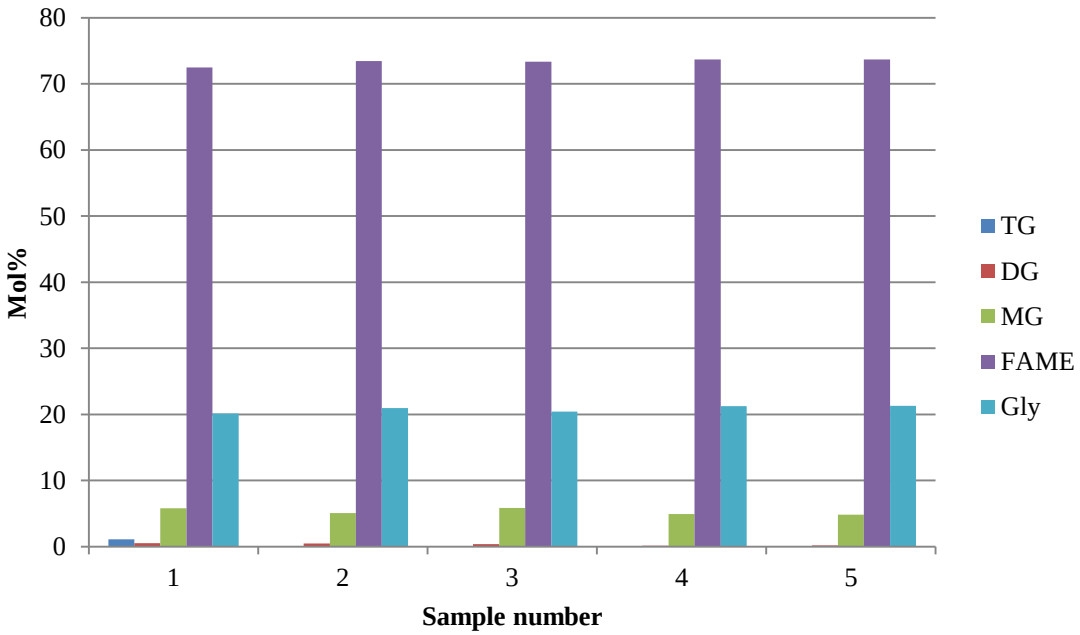

Figure 3.4 High conversion results with glycerol mass balance applied.

The application of this mass balance for glycerol appears to be an appropriate response to this issue. There seems to be a minimal effect on di- and monoglycerides (note that these are separate samples in an experiment, and so there would be natural variation between them), which suggests that they do not separate heavily into the glycerol phase, which could substantially vary the amount of these intermediates in the sample. It is hypothesised that the main source of this glycerol error is at the point of liquid sample from the two phase mixture.

3.1.1.2 GC Repeatability

In order to determine the repeatability of GC injections, a sample from an experiment with intermediate conversion was taken, and made up into three separate GC samples. Each sample was then injected 5 times. A sample chromatogram is shown in Figure 3.5 on the page 64. FAME peaks are labelled “F”, monoglycerides “M”, diglycerides “D”, and triglycerides “T”.

The peaks were integrated using Clarity Lite to give the amount of each component in the sample, based on the amplitude of the response, as well as the breadth of the peaks. These were then processed to obtain the molar composition of the samples. These are presented in Table 3.3.

Table 3.3 Mol% of transesterification components from three repeatability samples

	Sample A		
Peak	Average	Standard Deviation	St. Dev.%
TG	27.29	0.25	0.93
DG	10.71	0.09	0.86
MG	6.86	0.11	1.63
FAME	47.46	0.17	0.36
Gly	7.68	0.10	1.27
	Sample B		
TG	27.14	0.50	1.84
DG	10.69	0.08	0.74
MG	6.84	0.06	0.93
FAME	47.59	0.43	0.90
Gly	7.74	0.21	2.67
	Sample C		
TG	27.38	0.21	0.77
DG	10.92	0.10	0.92
MG	6.88	0.04	0.64
FAME	47.28	0.21	0.45
Gly	7.53	0.13	1.68

For each injection set the standard deviation appears to be acceptably small. In addition, a direct comparison between the separate samples shows them to be acceptable – for the most part, the amount of each component in a given sample is within one standard deviation of the other samples. It can be inferred from this that the GC analysis method can be said to be repeatable, and thus comparative analysis between two chromatographs produced using the equipment in the laboratory should be valid.

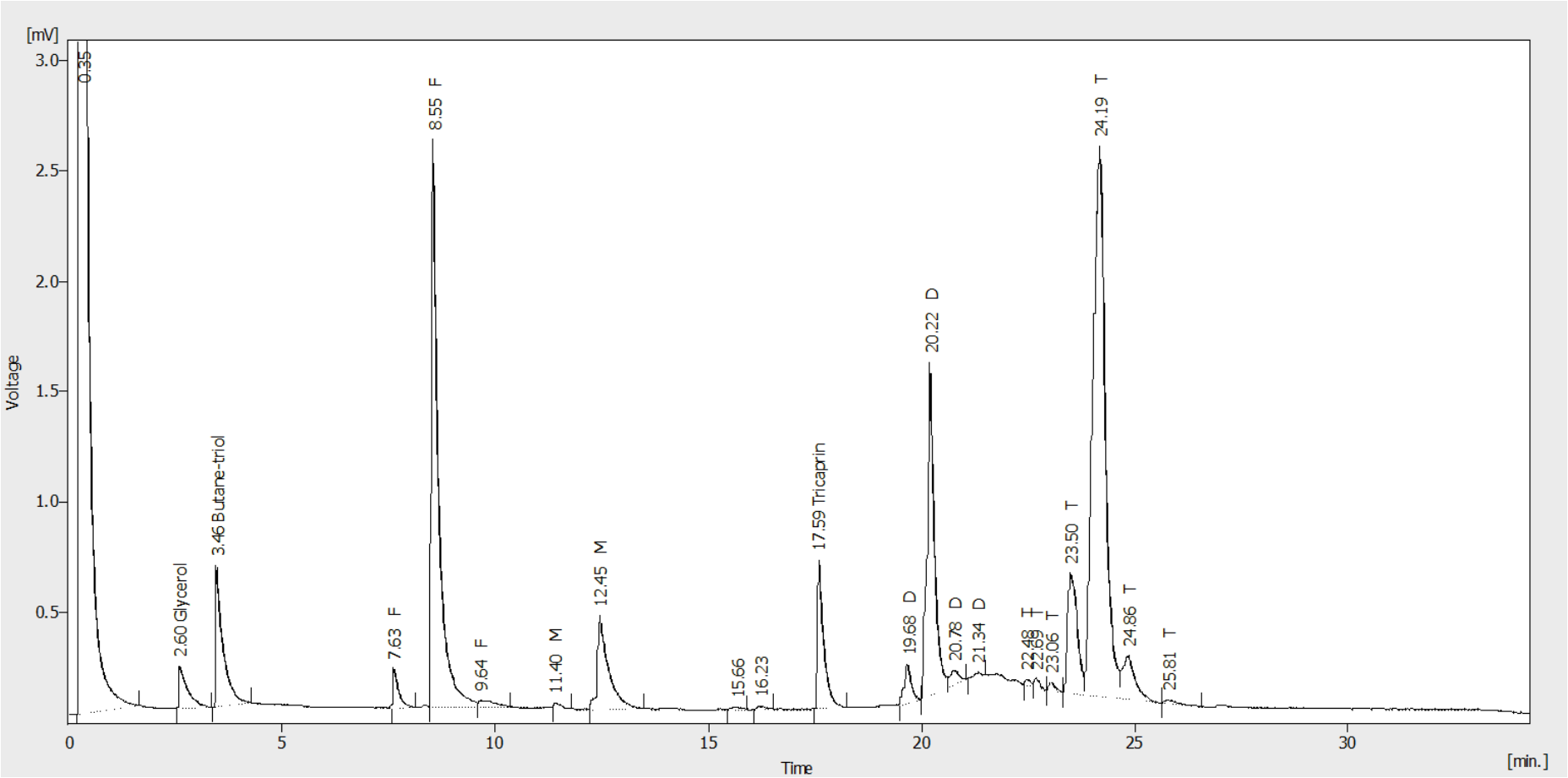

Figure 3.5 Example Gas Chromatograph of a transesterification sample.

3.1.2 Oil Characterisation

The density of the rapeseed oil was found by weighing 100 mL in a volumetric flask. The density of the oil was found to be 913 kg m^{-3} at 21°C.

3.1.2.1 Fatty Acid Profile

The fatty acid profile of the rapeseed oil was investigated by H^1-NMR, as developed by Knothe and Kenar (2004), and described below. The method identifies the main fatty acids expected in rapeseed oil; i.e. Palmitic (16:0), Stearic (18:0), Oleic (18:1), Linoleic (18:2), and Linolenic (18:3). A spectrum was obtained in deuterated chloroform on a Bruker 300 MHz spectrometer. The peaks were then integrated, with the peaks corresponding to the two pairs of protons on the outer glyceride carbons between 4.1 and 4.35 ppm being given a value of 4. The spectrum is shown in Figure 3.6 on the following page.

The peaks were identified, and the integration values are given in Table 3.4. The olefinic peak represents the single protons either side of a double bond. The proton attached to the middle glyceride carbon is also part of this peak, and so the integration value is one less than the value obtained from the spectrum. Allylic protons are those on the methylene (CH_2) immediately next to a double bond, while bis-allylic are those that have a double bond on both sides. The CH_2 peak represents the protons attached to saturated carbons, and the two CH_3 peaks are the terminal methyl groups of the fatty acids, with the methyl group of the Linolenic fatty acid chain being shifted away from the rest.

Table 3.4 Identification of NMR peaks

Peak name	Chemical shift	Integration value, *I*
Olefinic	5.3-5.4	7.51
Allylic	2.0-2.1	11.04
Bis-allylic	2.7-2.8	2.11
CH_2	1.2-1.4	55.03
CH_3, 18:3	0.95-1.0	1.03
CH_s, rest	0.8-0.95	8.21

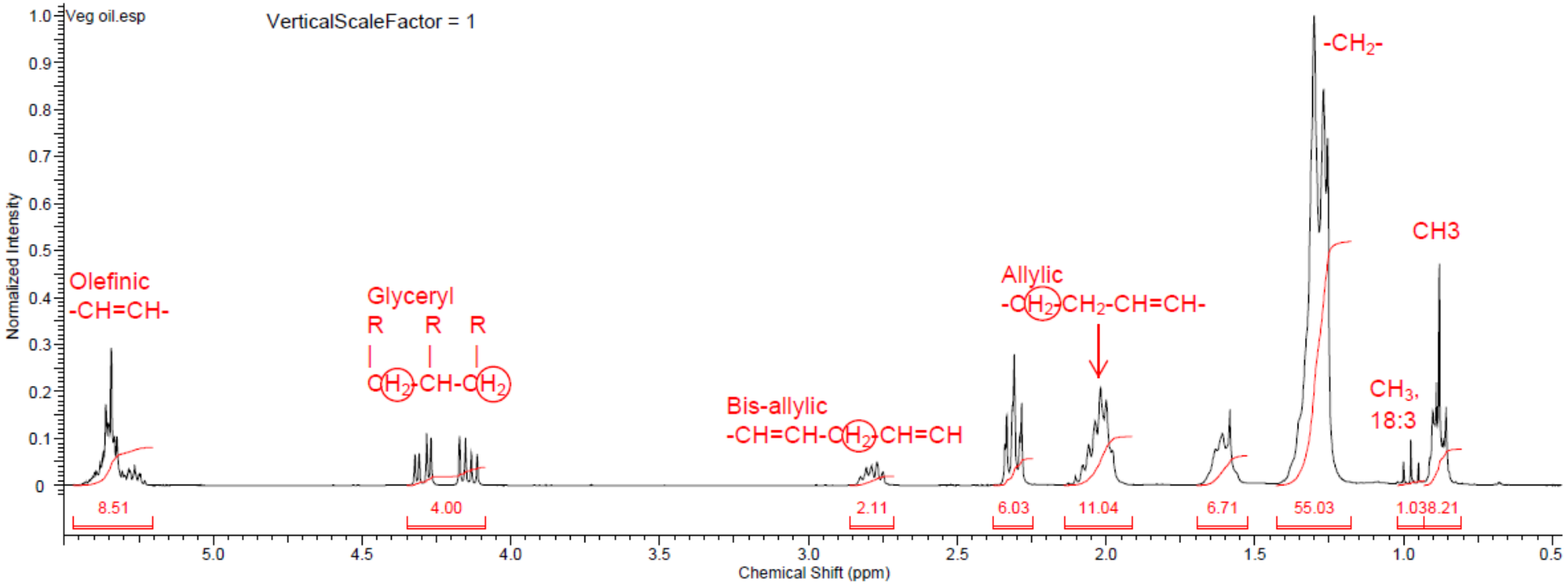

Figure 3.6 H^1-NMR spectrum of rapeseed oil.

In order to ascertain the composition from these numbers, they must be compared with the maximum possible integration values, assuming that the fatty acid profile were entirely made up of a single component. These represent the number of protons corresponding to the given fatty acid chain. These maximum values are given in Table 3.5.

Table 3.5 Maximum possible integration values

Protons	18:1	18:2	18:3
Olefinic	6	12	18
Allylic	12	12	12
Bis-allylic	0	6	12

The maximum integration values are then used to find the composition of the unsaturated fatty acid chains by using the following weighted average equations:

$$I_{olefinic} = 6A_{18:1} + 12A_{18:2} + 16A_{18:3} \quad (3.3)$$

$$I_{allylic} = 12A_{18:1} + 12A_{18:2} + 12A_{18:3} \quad (3.4)$$

$$I_{bis} = 6A_{18:2} + 12A_{18:3} \quad (3.5)$$

Where:

I = the integration value

A = the amount of the component identified by the subscript in mol %

However, the amount of 18:3 can also be found by comparing the integration peak of the terminal methyl group for it with the total methyl integration value:

$$A_{18:3} = \frac{I_{CH_3,18:3}}{I_{CH_3,18:3} + I_{CH_3,rest}} \tag{3.6}$$

This gives the amount of 18:3 as 11.1%. This is then substituted into equation (3.5) to find the amount of 18:2, which is 12.9%. These can then be substituted into equation (3.4) to obtain the amount of 18:1; 68.0%. The total unsaturates are simply the sum of these, or 92.0%.

It is then necessary to find the distribution of the final 8.0% between 16:0 and 18:0. First, the methylene protons are attributed to the unsaturated fatty chains as follows:

$$I_{CH_2,unsat} = 60A_{18:1} + 42A_{18:2} + 24A_{18:3} \tag{3.7}$$

The multipliers are the number of methylene protons contained in a molecule of triglyceride made entirely of each fatty acid. This gives an integration value of 48.87. The total CH_2 peak had an integration value of 55.03, which leaves the saturates' contribution to the integration value at 6.16. The theoretical total value for saturates if all they were entirely composed of 16:0 is given by:

$$I_{16:0} = 72A_{sat} \tag{3.8}$$

This gives $I_{16:0}$ as 5.76. Similarly, if the saturates were entirely composed of 18:0:

$$I_{18:0} = 84A_{sat} \tag{3.9}$$

This gives $I_{18:0}$ as 6.72. The actual integration value of the saturates falls somewhere in the middle. Thus, taking x to be the fraction of 18:0 in the saturates, the contributions are as worked out by the following equation:

$$I_{CH_2,sat} = I_{18:0}x + I_{(16:0)}(1 - x) \tag{3.10}$$

Substituting in the values above and rearranging for x gives 0.42. Recalling that the total amount of saturates is 8.0%, this means the amount of 16:0 is 4.7%, and the amount of 18:0 is 3.3%. A summary of the fatty acid profile and an estimate of the molar mass of oil from this are given in Table 3.6.

Table 3.6 Fatty acid profile of rapeseed oil

Fatty acid chain	Composition
16:0	4.7%
18:0	3.3%
18:1	68.0%
18:2	12.9%
18:3	11.1%
Molar Mass	879.8 g mol^{-1}

3.1.2.2 Free Fatty Acid Content

The acid value of the oil was obtained by titration with sodium hydroxide in the presence of a pH indicator, following the British Standard procedure (BS EN ISO 660:2009). The indicator used was phenolphthalein (10 g L^{-1}) in ethanol, while the sodium hydroxide solution was made to 0.1 mol L^{-1} in 96% ethanol.

- 25 mL of 0.1 mol L^{-1} nitric acid in ethanol was prepared by diluting 1.25 mL 2M standard solution in a volumetric flask.
- This was then titrated with the NaOH solution in the presence of 0.1 mL indicator to calibrate the concentration of the titrant.
- A solvent mixture was prepared, comprising equal volumes of toluene and propan-2-ol, and 60 mL of this was taken and neutralised with the NaOH in the presence of 0.3 mL indicator.
- 20.08g oil was added to this mixture and titrated. This solution required 0.4 mL of the NaOH solution to achieve a colour change lasting 15 seconds.

The free fatty acid content, w_{FAA}, is expressed as a wt % is given by the following equation:

$$w_{FAA} = \frac{V\ C\ M \times 100}{1000m} \tag{3.11}$$

Where:

V = volume of NaOH solution used (ml)

C = Concentration of NaOH solution (mol L^{-1})

M = Molar mass of fatty acid (g mol^{-1})

m = Mass of test portion (g)

The molar mass of fatty acid is found from a weighted average using the fatty acid profile obtained in Section 3.1.2.1; for a value of 280.6 g mol^{-1}. Substituting this, and the quantities given above into the equation gives w_{FFA} = 0.06% (2 d.p.).

3.1.2.3 Water Content

Karl Fisher titrations were used to analyse the water content of samples. This method is an electrochemical titration performed in an automatic titrator designed for the purpose. The general procedure given by British Standards for vegetable oils was used (BS 8534:2008):

- The cathode was filled with Hydranal Coulomat CG (Sigma Aldrich).
- The anode filled with a 50:50 mix of Hydranal Coulomat AG (Sigma Aldrich) and chloroform (Sigma Aldrich) dried over molecular sieves.
- A 100 μL aliquot of sample was introduced into the anode, and the titration run to completion.

Two oil samples were analysed, one from a new batch of rapeseed oil, and the other from the final portion of an almost exhausted batch. The moisture contents were 127.7 and 383.2 ppm.

3.1.3 Materials Analysis

3.1.3.1 Electron Microscopy

Electron microscopy was carried out using a JEOL SEM6480LV scanning electron microscope and a JEOL FESEM6301F field emission scanning electron microscope. Samples were coated in carbon, chromium or gold for high vacuum images, or left uncoated for work at low vacuum. X-ray backscatter measurements were collected using an Oxford INCA X-ray Analyser equipped on the JEOL SEM6480LV.

3.1.3.2 Raman Spectroscopy

Raman spectroscopy was carried out using a Renishaw inVia microscope. A green laser at 532 nm was used for most samples, while a red laser at 785 nm was used for samples susceptible to heat damage.

3.1.3.3 Particle Sizing

Particle sizing of slurries was performed using a Malvern Mastersizer X. Absolute ethanol was used as the liquid carrier.

3.2 Experiments at Atmospheric Pressure (Reflux Reactor)

Before screening of monolithic catalysts could take place, it was necessary to examine the effectiveness of the catalysts to be considered and to compare them to traditional homogeneous catalysts, which are usually used under reflux. Thus, certain reactions were undertaken under reflux conditions using both homogeneous and powdered catalysts. The reaction stoichiometry, as described earlier, is given in Figure 3.7.

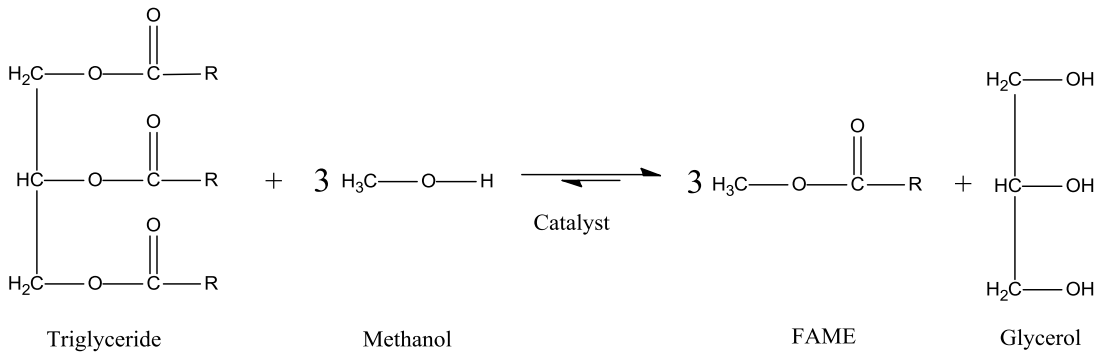

Figure 3.7 General transesterification reaction scheme.

The simplest method for the transesterification of biodiesel is to heat and stir the mixture of oil, methanol and catalyst in a round-bottomed flask under methanol reflux. The availability of methanol for this reaction is related to its solubility in oil (discussed further in Chapter 4), and thus rigorous stirring is necessary. For this reaction, a 6:1 molar ratio of methanol to oil is generally used (Knothe *et al.*, 2005), and this provides a sufficient excess of methanol to reach full conversion. Using this ratio, and taking the distribution of fatty acid chains given in Section 3.1.2.1 to calculate the molar mass of oil, the transesterification reaction was carried out using the equipment illustrated in Figure 3.8, as follows:

- 160 mL oil was added to a round-bottomed flask and heated to 65°C with stirring;
- Once the oil was up to temperature, 40 mL methanol was measured out;

- If the catalyst was soluble in methanol (for example, KOH), then it was dissolved in the alcohol. If not, then the catalyst was added separately, after the methanol;
- 1.5g of catalyst was used, representing a 1 wt.% catalyst loading;
- The methanol was added to the flask, and a reflux condenser attached;
- The stirring speed was adjusted to ensure complete mixing of the phases;
- Samples were taken at intervals for analysis.

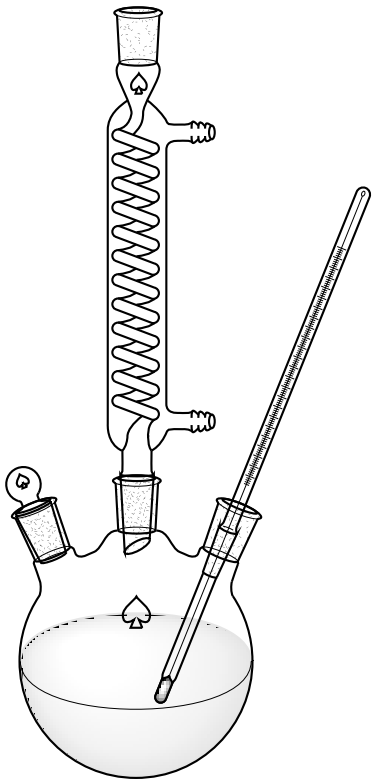

Figure 3.8 Glassware setup for reflux reaction.

3.2.1 Strontium Oxide Screening

Powdered strontium oxide (Sigma Aldrich) was used as received to verify the literature reports of the efficacy of SrO as a biodiesel catalyst. The reaction was carried out as described in Section 3.2 with the powdered catalyst being added last, as it is not significantly soluble in methanol. Samples were taken every 30 seconds for the first five minutes, every minute for the next five minutes, and then at 15 and 20 minutes. These were immediately quenched in water to remove the methanol from the oil and prevent further reaction. After being left to separate under gravity, an aliquot of the top organic phase was taken for GC analysis, and was processed as described in Section 3.1.1.

The results of this experiment are given in Figure 3.9, along with a comparison to the kinetic data for KOH obtained from literature (Vicente *et al.*, 2006), details of which are provided in Appendix A. Figure 3.9 shows that a yield of 100% FAME was obtained within 15 minutes of reaction, but with an initial delay of about four minutes. After this delay the rate of reaction is on a similar scale to that of the homogeneous KOH.

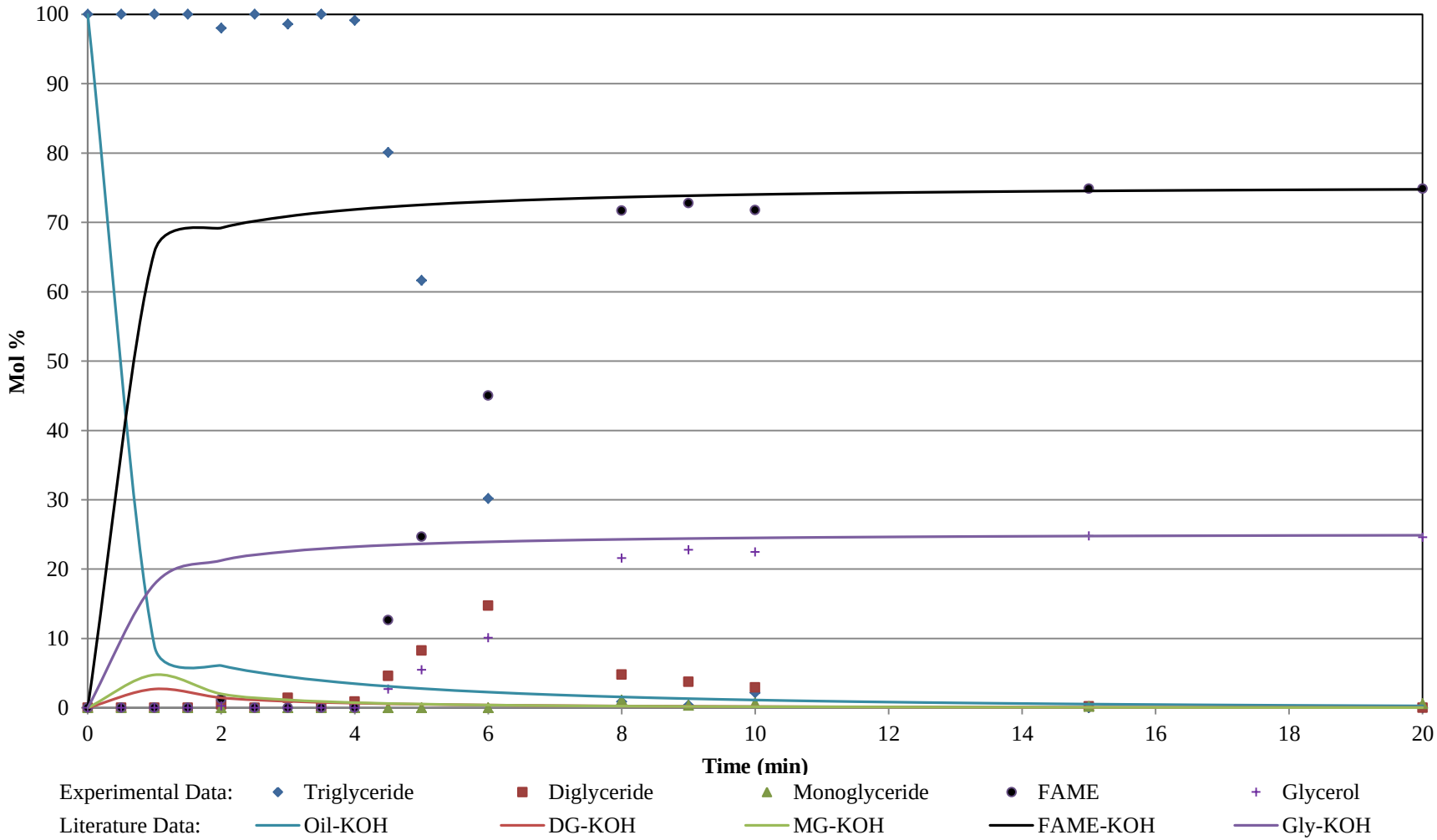

Figure 3.9 SrO catalysed rapeseed oil transesterification, 65°C, reflux, 1 wt% catalyst, and literature data of KOH catalysis provided for comparison.

3.2.1.1 Strontium Hydroxide Screening

As both a precursor to SrO, and a likely product of catalyst deactivation, it was of interest to determine the efficacy of strontium hydroxide as a biodiesel catalyst. As such, strontium hydroxide hexahydrate (Sigma Aldrich) was used as received following the reflux procedure, and the results are shown in Figure 3.10.

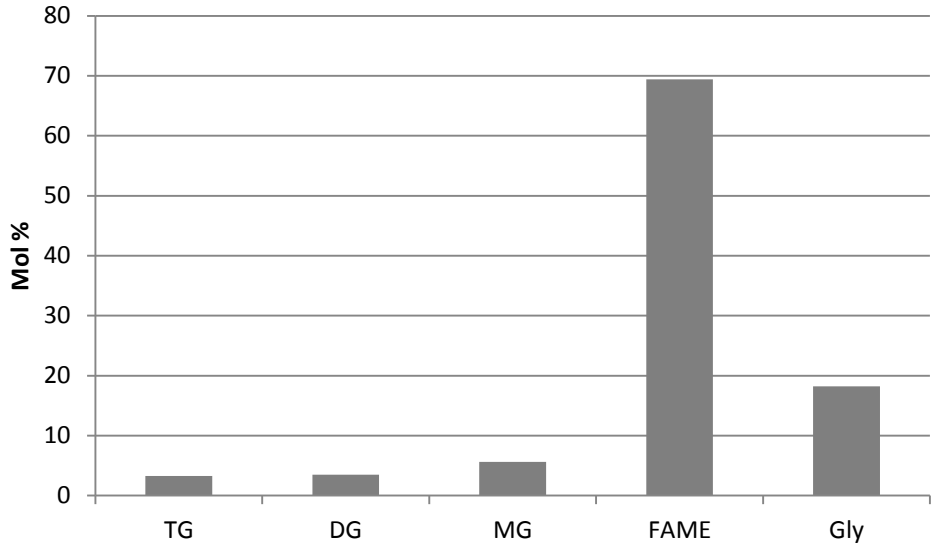

Figure 3.10 Results of strontium hydroxide catalysed transesterification, T=65°C, 24 hours.

Although strontium hydroxide is catalytically active for transesterification, it did not reach full conversion after 24 hours, unlike SrO, which only required 15 minutes. However, it is useful to note that one of the likely products of catalyst "poisoning" in strontium oxide is itself a catalyst.

3.2.2 Calcium/Cerium Catalysts Supported on Lanthanum Oxide

Calcium and cerium doped on lanthanum oxide are reported to be transesterification catalysts with a degree of tolerance for water and free fatty acids in the oil (Kim *et al.*, 2011). However, the literature does not include an optimisation of the catalysts, in terms of the proportions of the components. Thus, a range of catalysts were prepared and tested in order to see if a significant improvement could be made on the reported formulation.[2]

3.2.2.1 Catalyst Preparation

Catalysts were prepared following the method used by Kim *et al.* (2011):

- Solutions of 1M calcium nitrate and cerium nitrate were prepared;
- A total of 11.8 mL of these solutions at the desired ratio were added to 9 g lanthanum oxide;
- The mixture was stirred and kneaded;
- The mixture was left to dry in air for 24 hours;
- The dried catalyst was then calcined in air, first heated to 500°C at a rate of 10°C/min, held for an hour, then heated up to 750°C, at the same rate;
- The catalyst was then left to cool overnight before being stored under nitrogen to reduce any reactions with atmospheric water or carbon dioxide.

One interesting effect that should be noted is that with an increase in the amount of cerium solution added, the solution undergoes an exothermic reaction, wherein the paste becomes very viscous, before cooling and returning to a less viscous state.

The Raman spectra of a range of Ca:Ce ratios on La_2O_3 are shown in Figure 3.11. The appearance of a new peak at 575 with increasing cerium suggests that there is a

[2] N.B. The work in section 3.2.2 was carried out in collaboration with Chris Daniels (University of Bath) during his undergraduate research project.

new phase being formed, perhaps a mixed cerium/lanthanum oxide, based on the observations described above.

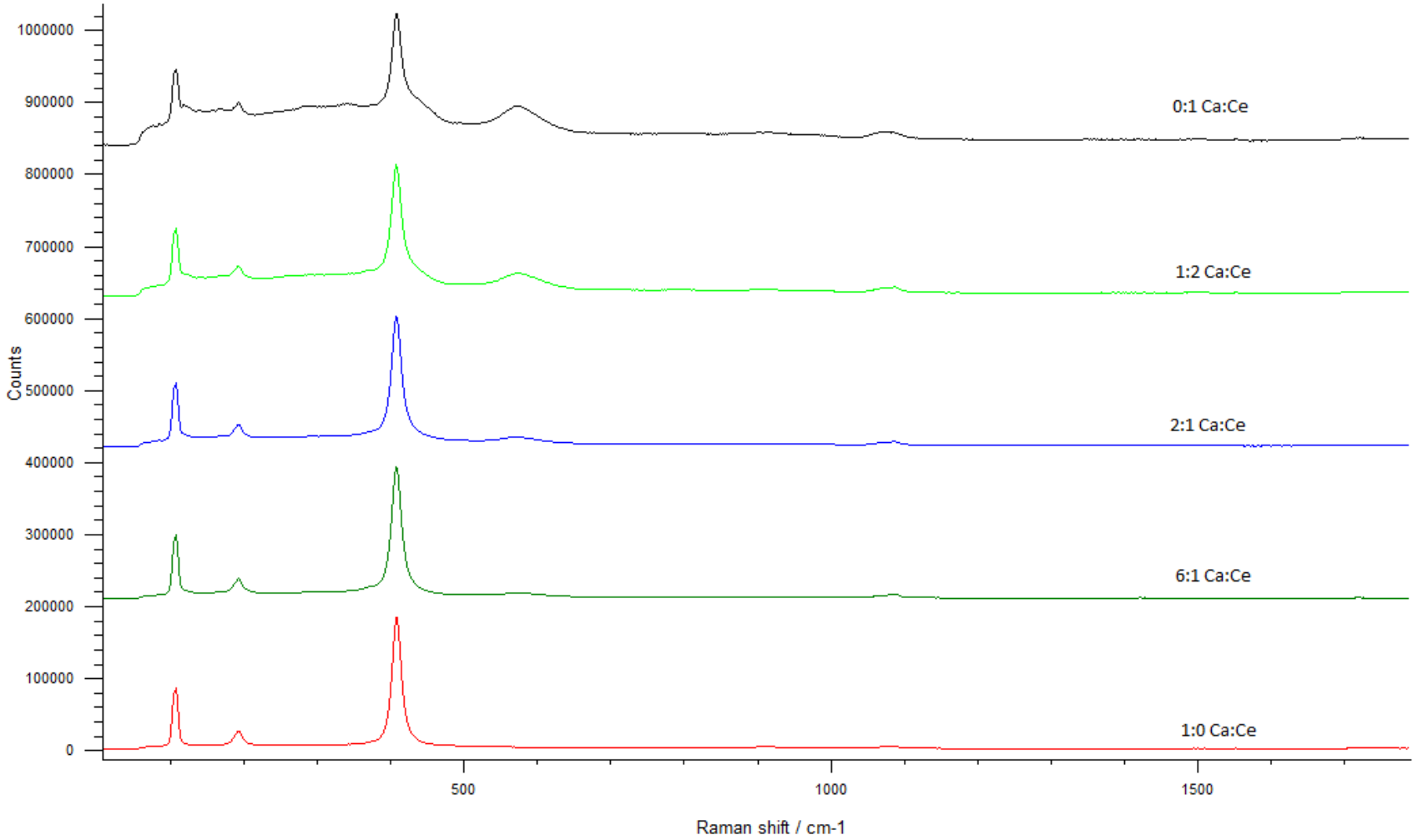

Figure 3.11 Raman spectra of a range of Ca/Ce doped catalysts.

3.2.2.2 Effect of Calcium:Cerium ratio

The catalyst reported by Kim *et al.* (2011) used a mixture of cerium and calcium nitrate of 2.4:9.4. An obvious question that arises from this is what the optimal ratio of cerium to calcium is. This was investigated by producing a range of catalysts, including the original one from the literature, and comparing them in the reflux reaction setup. The results of these experiments are shown in Figure 3.12.

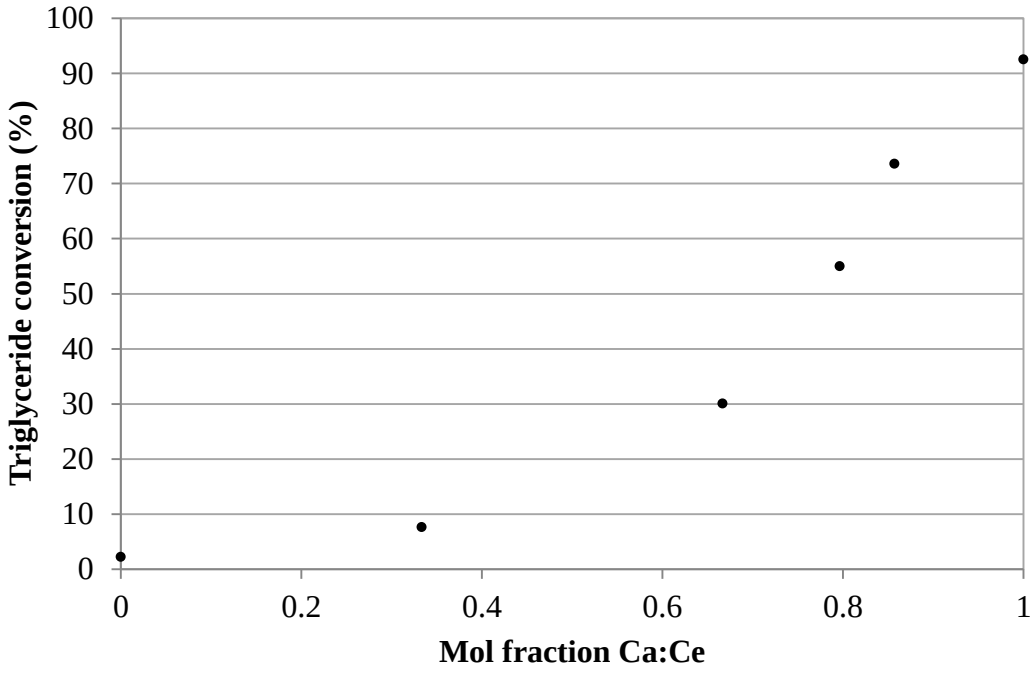

Figure 3.12 Effect of calcium:cerium content on La_2O_3 on conversion of triglycerides, 24 hours, 65°C, 1.5 wt% catalyst loading.

It can be clearly seen from these results that increasing the calcium loading on the La_2O_3 increases the activity of the catalyst, while cerium does not appear to contribute any activity. The role of cerium is unclear, as it may contribute to the heterogeneous stability of the calcium on the support, or may in fact contribute nothing of value to the system. In order to ascertain whether cerium inhibits the reaction, a catalyst was prepared with the cerium solution replaced with water. The results of this are shown in Figure 3.13.

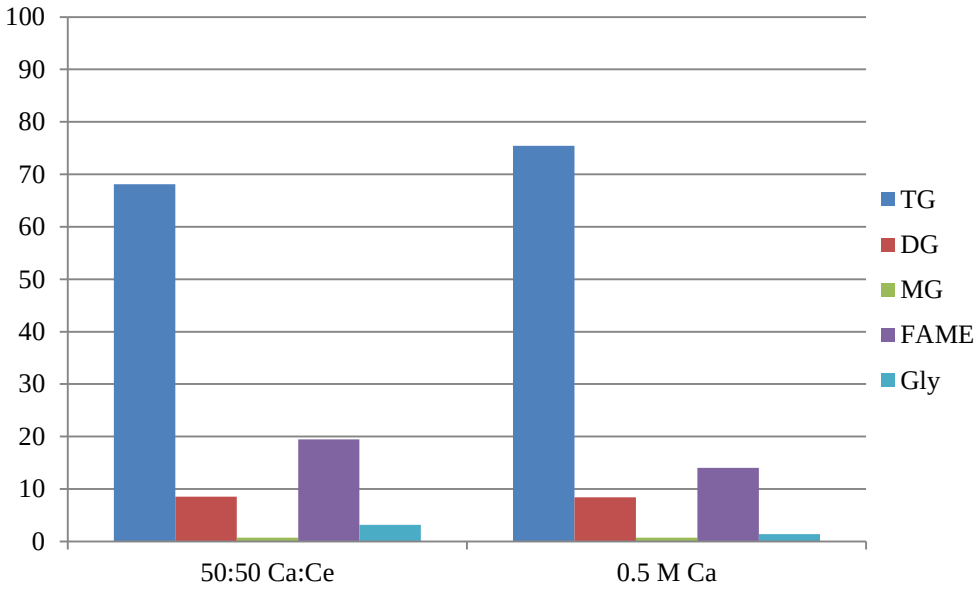

Figure 3.13 Effect of cerium on the activity of calcium, 65°C, 24 hours.

There appears to be a small advantage to adding cerium to the catalyst, despite the fact that cerium on lanthanum oxide by itself does not provide any notable level of activity. Two scenarios seem possible; one is that the calcium and cerium interact to increase activity; the other is that the cerium acts to make the calcium more available for reaction. The latter would likely be through pore blocking in the La_2O_3, preventing some of the calcium from becoming inaccessible. It is also possible, considering the apparent reaction between $Ce(NO_3)_2$ and La_2O_3, that the morphology of the support structure is altered by the addition of cerium.

3.2.2.3 Effect of Calcium Concentration

The effect calcium loading was tested by making a range of calcium nitrate solutions, from 0.5M to 2M. The catalyst was then prepared as described. The results from these catalysts are given in Figure 3.14

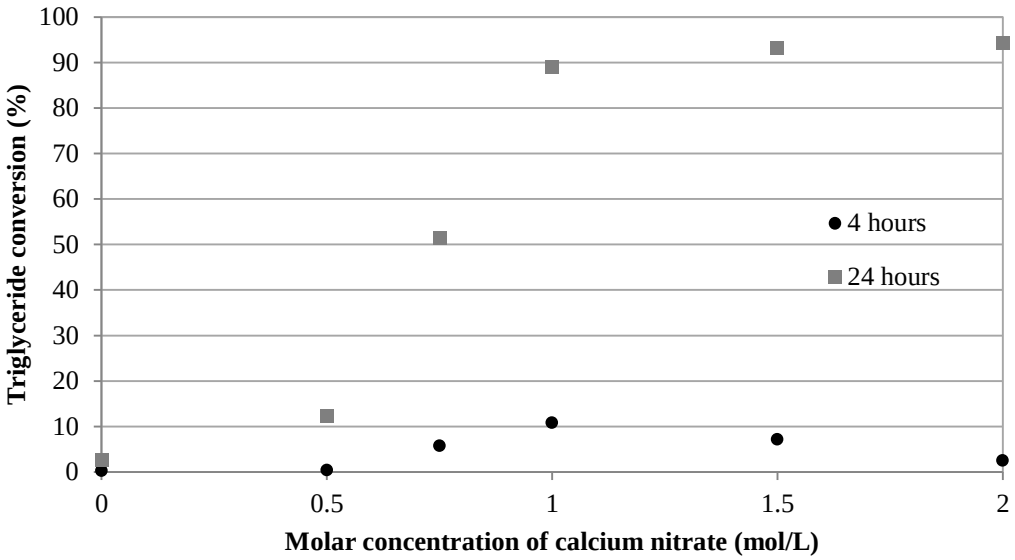

Figure 3.14 Effect of calcium loading on conversion.

There appears to be an optimal solution concentration, at around 1M, in terms of initial reaction rate. However, after a full 24 hour reaction, the higher concentrations lead to a higher conversion. This is possibly due to more leaching over time with the higher loadings.

3.2.3 Catalyst Selection

The activity of strontium oxide has been shown to be significant – even reasonably comparable to homogeneous catalysts. It was thus an obvious choice to proceed with attempts to coat SrO onto a support structure for eventual use in a continuous reactor.

While the activity of the lanthanum supported catalysts has been successfully increased, it still requires quite a long reaction at 65°C in order to approach an acceptable level of conversion. While interesting as an academic study, this does not lend itself to a continuous process, wherein reducing the residence time is paramount. The high yields seen by Kim *et al.* in under 3 hours was not achieved in this case, possibly due to the lower catalyst loading and the lower methanol: oil ratio. It was thus decided that the catalyst would not be advanced to the coating stage of the project.

3.3 Experiments at Elevated Pressure (Batch Autoclave)

The reflux procedure is limited in that it cannot be used at temperatures above the atmospheric boiling point of the alcohol (as the equipment is open to the atmosphere), and is geometrically impractical for testing monolith pieces. It was thus recognised that for data to be collected for monolithic catalysts, it was necessary to obtain an appropriate reactor. It should be noted that there is a potential side-reaction at higher temperatures, wherein two methanol molecules dehydrate to form dimethyl ether. However, this reaction generally will not occur non-catalytically below 300°C, and catalytic reactions require temperatures in excess of 200°C to be effective (Sabour *et al.*, 2014).

Initially, a pressure vessel was sourced from within the department to perform elevated temperature reactions, and to test monolith pieces. This vessel entailed a stainless steel sealed reaction vessel, a magnetic-driven overhead stirrer, a PTFE liner, and a mantle heater with a PID controller. This was modified to include a sampling tube and valve assembly, so the reaction mixture could be sampled throughout the course of an experiment. However, when this vessel was taken to the manufacturer for servicing and testing, the walls of the reactor were found to be compromised due to micro-fractures throughout the metal, apparently caused by its past use. It was recommended that the vessel be condemned, and so it became necessary to specify and source a new vessel.

3.3.1 Pressure Vessel Specification

It was decided that the new vessel should be capable of taking liquid samples, as well as monitoring the temperature of the reaction medium. After correspondence with Scientific and Medical Supplies Ltd, a 300mL stainless steel reactor was agreed upon, ordered, and acquired. This reactor includes a dip-tube that reaches the bottom of the vessel and connects to two needle valves on the lid, a thermowell that fits a 1/8” (3.2mm) temperature probe from a stirrer hotplate controller, a pressure gauge with a needle valve to sample/release gas in the headspace, and a burst disc safety fitting.

3.3.2 Modifications

In order to prepare the reactor for the batch testing of monoliths it was recognised that certain additions needed to be made to the reactor. Because the oil and methanol mixture is immiscible, stirring is necessary. Thus a method of keeping the monolith pieces from being broken by the magnetic stirrer bar was devised; a piece of steel mesh was shaped to fit at the bottom of the reactor, fixed to the diptube assembly, creating a shelf above the stirrer on which the monoliths can sit with another piece of mesh on top to prevent them from moving. This is shown in Figure 3.15. To make sampling possible, one of the needle valves was fitted with a 1/16” (1.6 mm) metal tube to direct liquid samples into a vial.

Figure 3.15 Catalyst shelf, with monoliths being loaded onto it on right.

3.3.2.1 Methanol Injection Chamber

It was also recognised that, because much of the reaction could occur while the vessel was raised to temperature, a method would need to be introduced to control the starting point of the reaction. It was decided that the simplest way to do this

would be to introduce the methanol to the system after the oil and steel vessel had been brought to temperature. This would be done by attaching an injection chamber to the reactor from which the methanol could be injected by a positive pressure of nitrogen. Thus, the other needle valve connected to the diptube was fitted with a 1/4" (6.4 mm) steel tube, which connects *via* Swagelok adapters to a vertical 1" (2.5 mm) tube, cut at 200 mm height, which acts as the holding chamber for the methanol, with a volume of 70 mL. The top of the tube was connected to a 1/4" tube adapter, which can in turn be connected to a nitrogen cylinder. The injection chamber can be filled with methanol *via* syringe, and then, after the nitrogen is connected and charged, methanol can be added to the reactor by simply opening the needle valve. By maintaining a nitrogen pressure higher than the vapour pressure of methanol at the reaction temperature, the vaporisation of the alcohol can be supressed. A one-way check valve was used to prevent methanol vapour from travelling up the nitrogen line. The pressure vessel, injection chamber, and final construction are shown in Figure 3.16.

Figure 3.16 Pressure vessel, injection chamber, and final assembly with sample port.

3.3.2.2 Initial Vessel Testing

In order to demonstrate the safe operation of the pressure vessel, two tests were carried out. First, the vessel was pressurised with 8 bar nitrogen. All fittings were then leak tested, and found to be properly sealed. The valves were then closed, and the nitrogen supply shut off, and the vessel was left for four hours. On return, the vessel was found to have held the pressure with no apparent loss.

The second test involved developing a safe method of injection and sampling, to reduce the risk posed by a high temperature, pressurised system. First, the vessel and injection chamber were filled with water, sealed, and nitrogen pressure applied to the water in the injector. Then, the valve was opened to inject the water into the vessel, and excess nitrogen was allowed in to create pressure in the vessel headspace. Liquid sampling was then tested by slowly opening the needle valve of the sample port. This was found to be satisfactory for finely controlling the sample rate. Through the injection chamber, nitrogen was used to flush out both the sample dip tube and the sample port. This was also found to work well, and will allow confidence that the samples are representative of the bulk.

3.4 Monolith Coating

Monolith pieces, both bare and alumina coated were cut to size from a larger cylindrical block. First, the block was cut into 10 mm thick sections. Then a 6 mm i.d. hole punch was used to cut out pieces of the desired size. Before coating, all monolith pieces were placed under a hot air gun for 10 minutes in order to remove any adsorbed species from the surface. After this, they were weighed on a microbalance, in order to calculate the catalyst loading after deposition. The pieces were then coated as described in the relevant procedures, and re-weighed. All loadings refer to the weight per cent of the total weight.

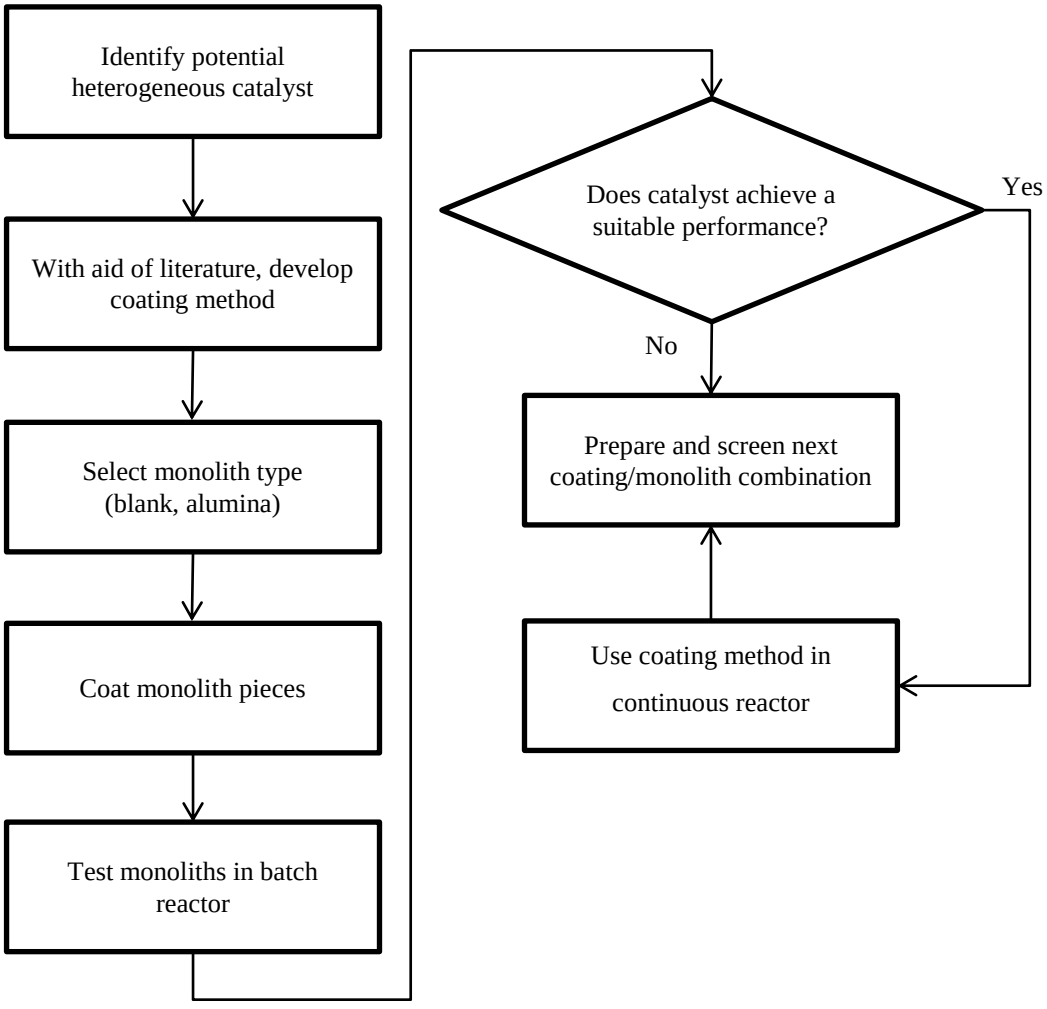

Figure 3.17 Decision process for developing and testing monolithic catalysts.

3.4.1 Monolith Details

The cordierite monoliths used in this project were obtained from a well-known catalyst manufacturer. A photograph of a monolith section is given in Figure 3.18.

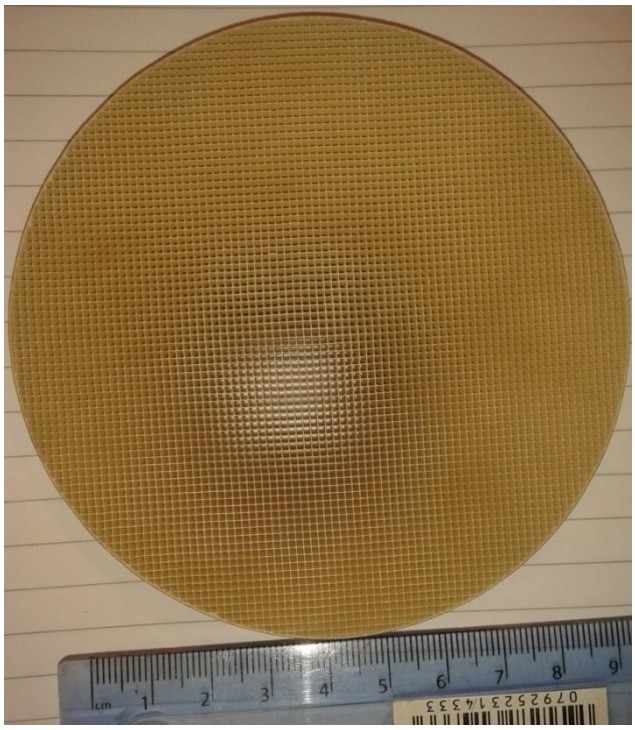

Figure 3.18 Photograph of monolith section.

This picture was then processed using the image processing software imageJ to count the number of cells in a given area. The monolith's basic characteristics are given in Table 3.7.

Table 3.7 Basic monolith characteristics

Parameter	Value	Unit
Cell density	61.3	Cells cm^{-2}
Wall thickness	0.17	mm
Cell diameter	1.1	mm
Voidage	73.4	%
External surface area	3130	$m^2\ m^{-3}$

3.4.2 Strontium Oxide Coatings

Having been shown to be an effective catalyst as a powder, methods of coating strontium oxide onto a support were investigated. These were derived from methods in the literature as well as the expertise within the research group.

3.4.2.1 Method 1: Nitrate to Oxide

- A solution of strontium nitrate was made by dissolving 25 g nitrate in 50 mL distilled water.
- The monolith pieces were then submerged in this solution for half an hour, before being removed and the channels cleared with compressed air.
- The monoliths were then placed in a crucible and calcined in air at 1100°C to decompose the strontium nitrate to strontium oxide, according to the reaction given in equation (3.12).

$$2Sr(NO_3)_{2\,(s)} \xrightarrow{\text{heat}} 2SrO_{(s)} + 2NO_{2\,(g)} + O_{2\,(g)} \qquad (3.12)$$

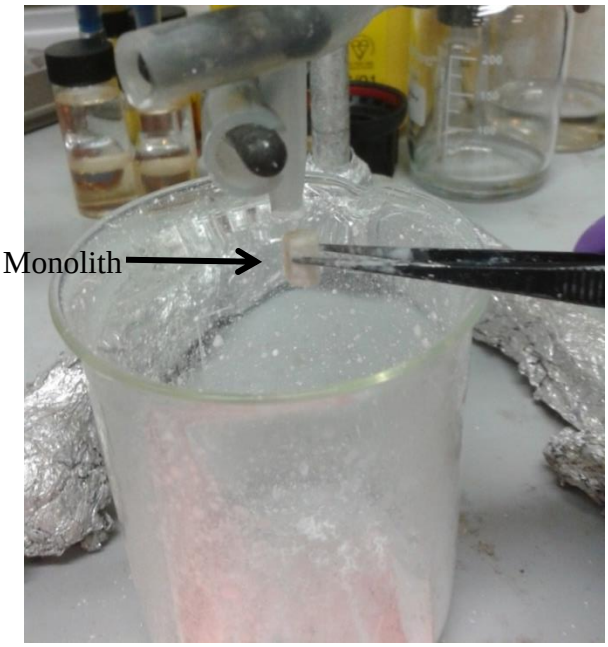

Figure 3.19 Monolith piece being cleared with compressed air.

3.4.2.2 Method 2: Nitrate to Oxide *via* Hydroxide

In order to provide an impregnation method with a lower calcination temperature, a method was developed based on the reaction between strontium nitrate and potassium hydroxide to form $Sr(OH)_2$, as described by equation (3.13). This was necessary due to the insolubility of strontium hydroxide.

- A 1 M solution of strontium nitrate was prepared (8.83 g in 40 mL distilled water), and the monolith pieces submerged for 10 minutes.
- After removal, liquid was cleared from the channels before submerging in a 2 M solution of KOH (4.48 g in 40 mL).
- The channels were cleared again to removed excess liquid, then the monoliths were dipped multiple times in 96% ethanol to wash any remaining KOH.
- The monoliths were placed in a furnace under a flow of nitrogen at 720°C to decompose the hydroxide to strontium oxide, as in equation (3.14). The nitrogen was used to prevent the formation of strontium carbonate (Glasson and Sheppard, 1968).

$$Sr(NO_3)_{2\,(aq)} + KOH_{(aq)} \rightarrow 2Sr(OH)_{2\,(s)} + 2KNO_{3\,(aq)} \tag{3.13}$$

$$Sr(OH)_{2\,(s)} \xrightarrow{\text{heat}} SrO_{(s)} + H_2O_{\,(g)} \tag{3.14}$$

3.4.2.3 Method 3: Strontium Hydroxide Slurry Coating

An alternative to catalyst impregnation is to directly coat the cordierite monolith substrate with a washcoat of the catalyst material. This is done by creating a slurry of the catalyst material in a suitable solvent via wet ball-milling, ideally down to a particle size of around 5µm (Nijhuis *et al.*, 2001). The binding may be improved by adding a binding agent of significantly smaller particle size, such as colloidal alumina or silica.

Strontium hydroxide slurries were carried out as follows:

- Strontium hydroxide octahydrate and de-ionised water were placed into a 500 mL ball-milling drum about 1/3 full of appropriate grinding media;
- The mixture was milled on a Capco Ball Mill Model 2VS at speed setting 7 for 20-24 hours;
- The particle size of the slurry was characterised using a Malvern Mastersizer, with absolute ethanol as the continuous phase;
- The slurry was then transferred into a beaker with a magnetic stirrer bar, to prevent separation under gravity;
- Additives, such as colloidal silica, silica gel, or titania were added in desired proportion.

Monoliths were then coated in the slurry coat as follows:

- The slurry was placed in a glass beaker and stirred using a magnetic stirrer to prevent the particles from settling out;
- The monolith pieces were placed under a hot-air gun to drive off any adsorbed species, before being placed in a sealed container and weighed;
- The monoliths were submerged in the slurry for 10 seconds;
- Excess slurry was removed using a jet of pressurised air;

- The monolith pieces were then dried in air before being placed in an oven to dry fully at 60°C;
- After each coating, the slurry was closed with laboratory film to prevent evaporation;
- The coating procedure was then repeated for the desired number of coats (usually three);
- The monoliths were placed in a quartz tube in a furnace and heated to 720°C at 5°C min^{-1} under a flow of nitrogen to obtain an SrO coating, following the stoichiometry given earlier in equation (3.14).

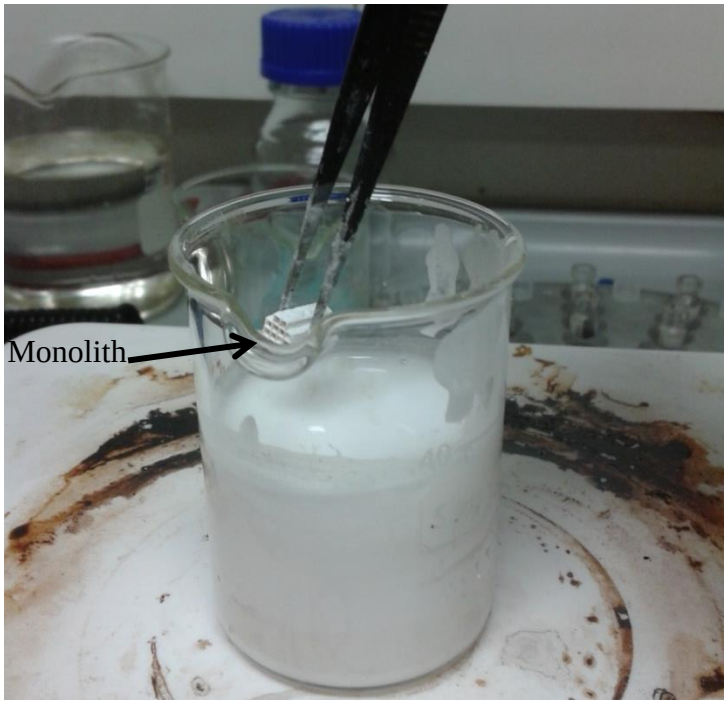

Figure 3.20 Monolith piece being dipped in slurry.

3.5 Batch Pressure Vessel Procedure

The monolith pieces (usually ten) were loaded onto the shelf in the pressure vessel, and the vessel was charged with 160 mL oil, as well as a magnetic stirring flea. The lid was securely fastened and all valves closed. The methanol injection chamber was fixed to the lid, and charged with 40 mL methanol (for a methanol:oil ratio of 6:1). The nitrogen line was then fitted, and the reactor heated to the reaction temperature (120°C). The methanol was then injected into the reactor and the timer started. Samples were removed by opening the sample valve, and the dip tube cleared by opening the injection valve. Because the injection chamber was unheated, it was found that this led to a large temperature drop in the reactor (~30°C). However, this was deemed preferable to heating the reactants together from ambient conditions.

3.6 Results and Discussion

Both blank and coated monoliths were tested in the pressurised batch reactor, as well as examined *via* SEM.

3.6.1 Blank Runs

Blank runs were undertaken using monoliths supports without catalyst coatings. The GC results and representative images from SEM samples are given in Figure 3.21 through Figure 3.24.

Generally, neither support structure is particularly active, although the cordierite is slightly more so than the alumina. The cordierite can generally be described as non-porous, being made of a large collection of sintered crystals. The alumina coating is significantly more structured, with a wide range of particle sizes, presenting much more space between the features.

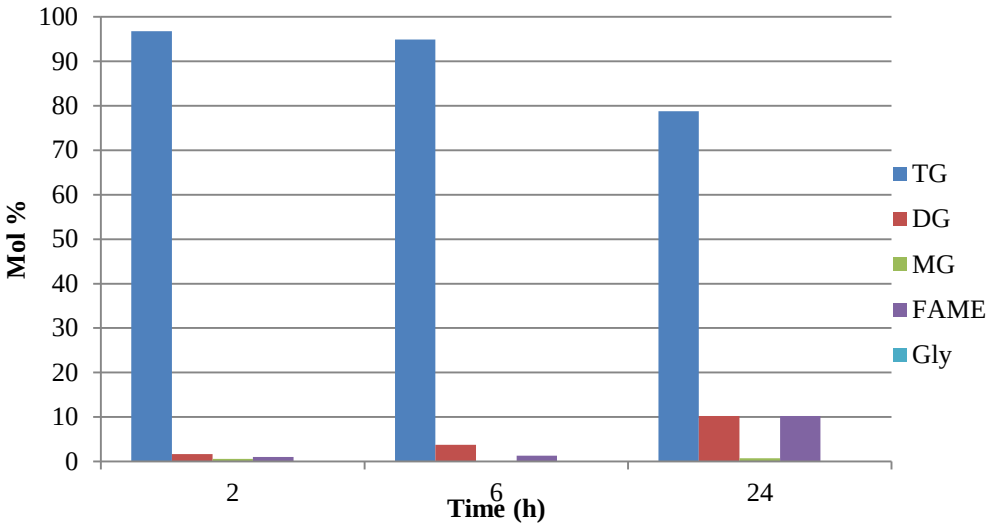

Figure 3.21 Blank run with bare monolith, T = 120°C, P = 8 bar.

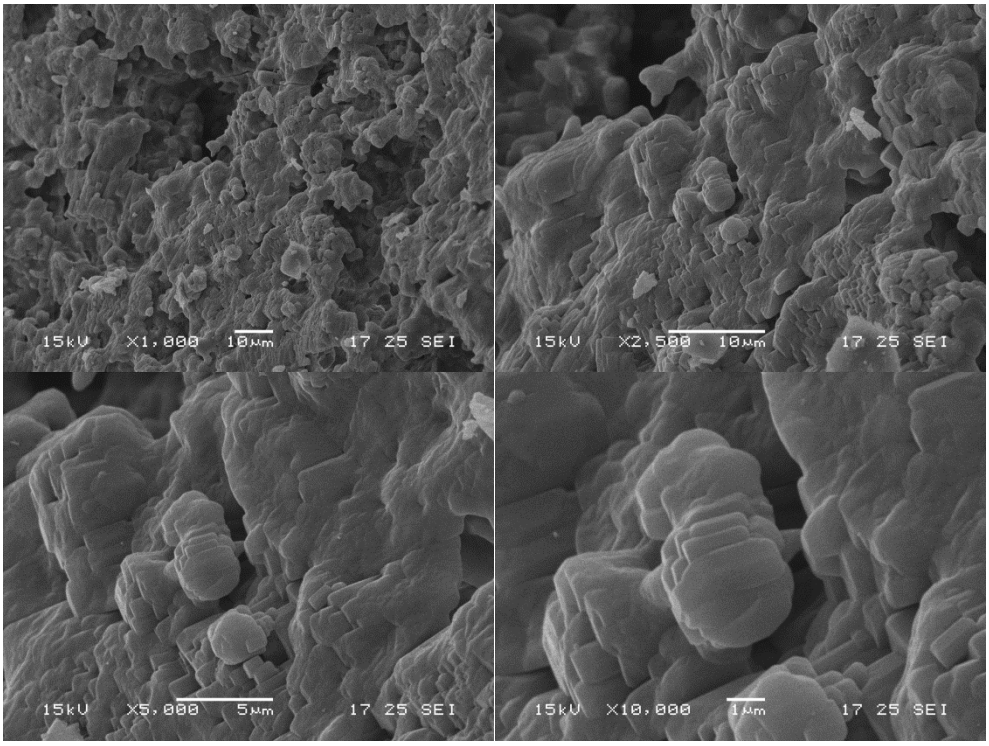

Figure 3.22 Representative SEM images of blank cordierite monolith.

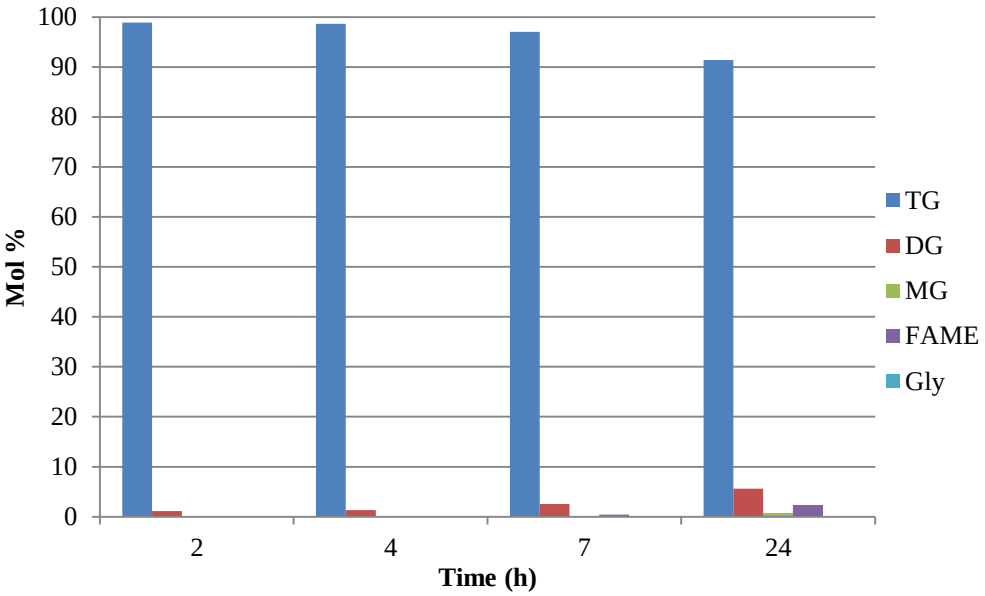

Figure 3.23 Blank run with alumina coated monolith, T = 120°C, P = 8 bar.

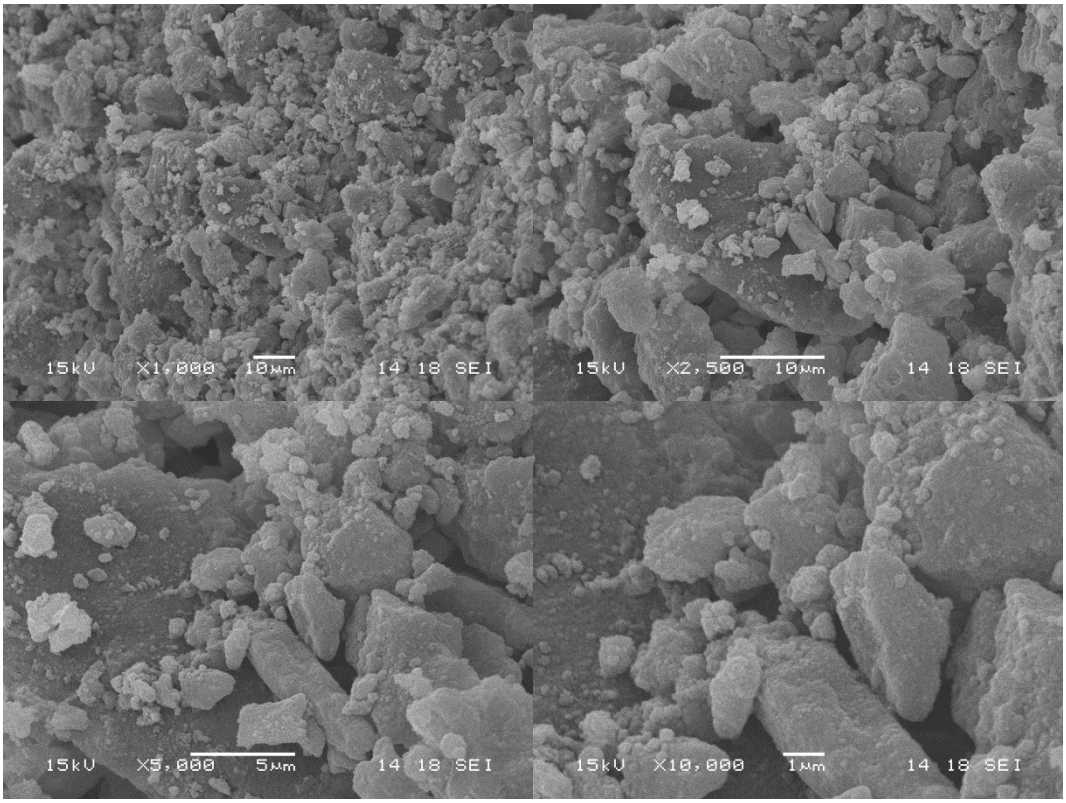

Figure 3.24 Representative SEM images of alumina coated monolith.

3.6.2 Strontium Oxide Coatings

Experiments will now be described using the three different coating methods.

3.6.2.1 Method 1

Coating Method 1 (see Section 3.4.2.1) was used on both bare monolith and alumina. The bare monolith coating achieved a loading of 10.6 wt%, which is equivalent to 0.062 wt% with respect to oil. The results of the bare monolith screening are shown in Figure 3.25.

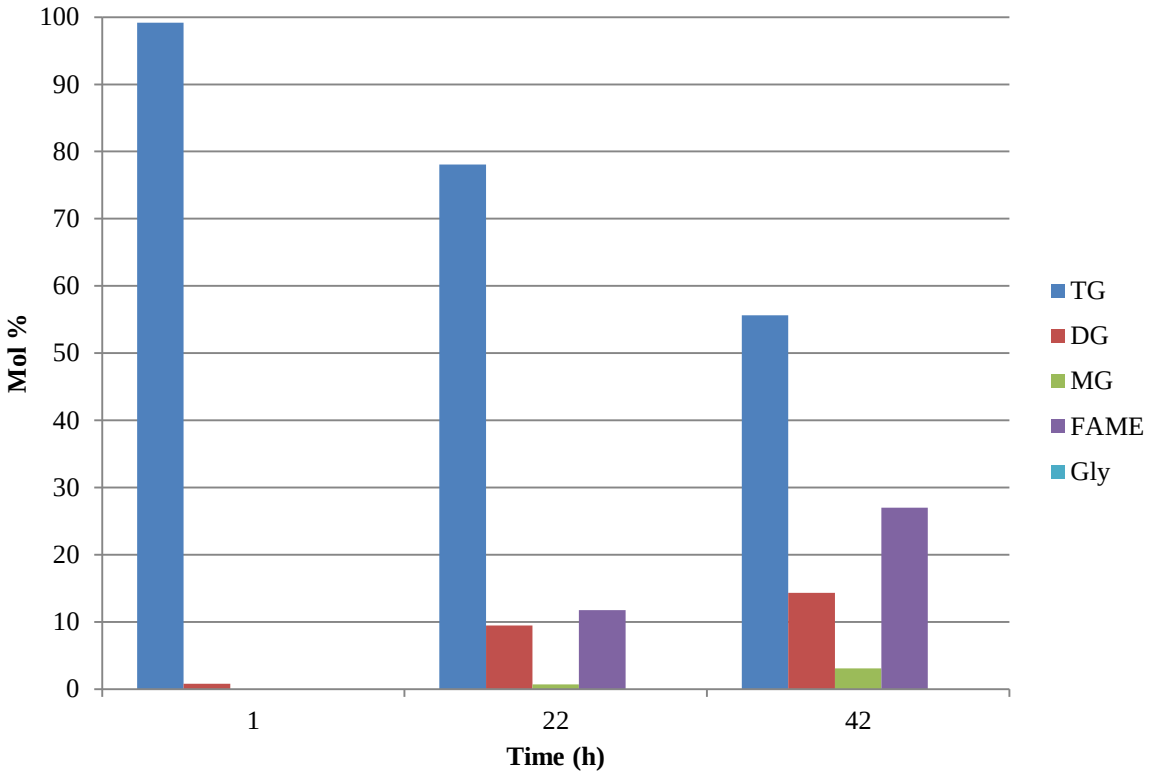

Figure 3.25 SrO Method one on bare monolith, T = 120°C, P = 8 bar.

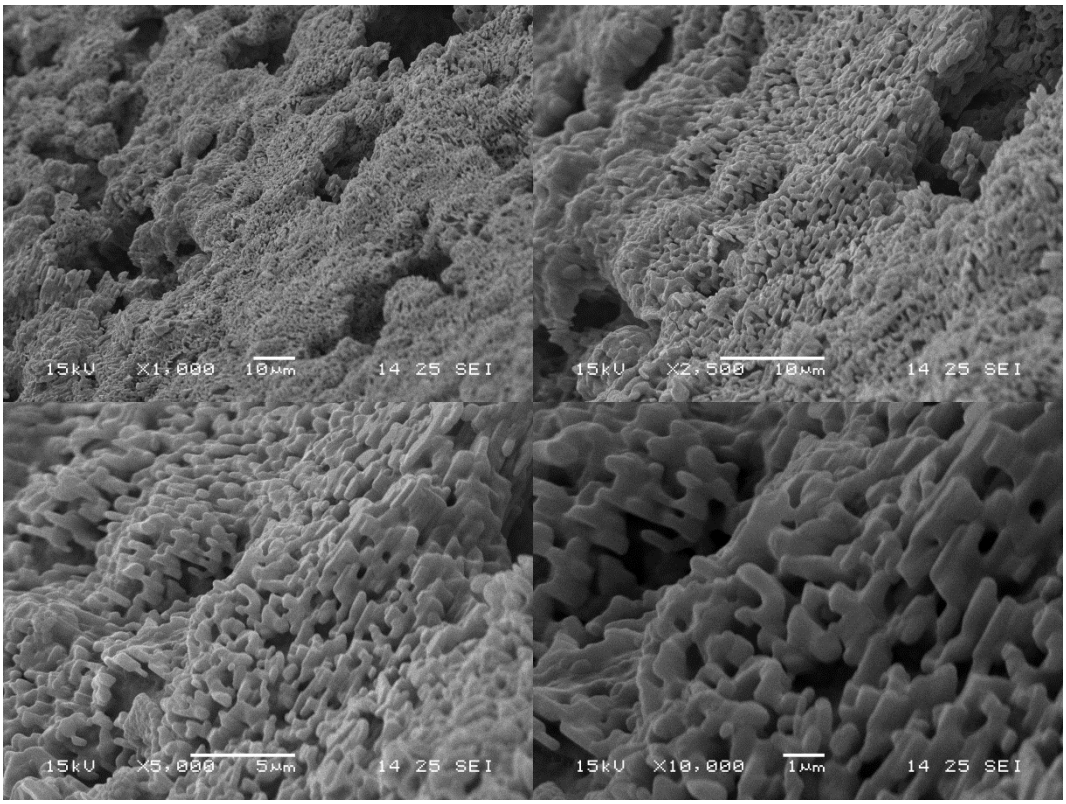

Figure 3.26 Representative SEM images of coating Method 1 on blank monolith.

There is some increase in activity once the monoliths are loaded with strontium oxide using this method. The SEMs also reveal a major change in the surface structure as that observed in the blank monoliths. This is due to the high calcination temperature, which appears to have changed the morphology of the cordierite crystals.

When Method 1 was used on alumina coated monolith, a slight green tint appeared to cover the surface of the monolith. This was deemed to be due to impurities present on the crucible, and so the method was repeated using a clean crucible, but yielded the same results. This was hypothesised to be strontium aluminate, which is reported to have this distinct green colour. This is reported in the literature to be chemically inert. The loading on the monoliths was 13.0%, with a total catalyst loading with respect to oil at 0.17 wt%. The results of this reaction are shown in Figure 3.27.

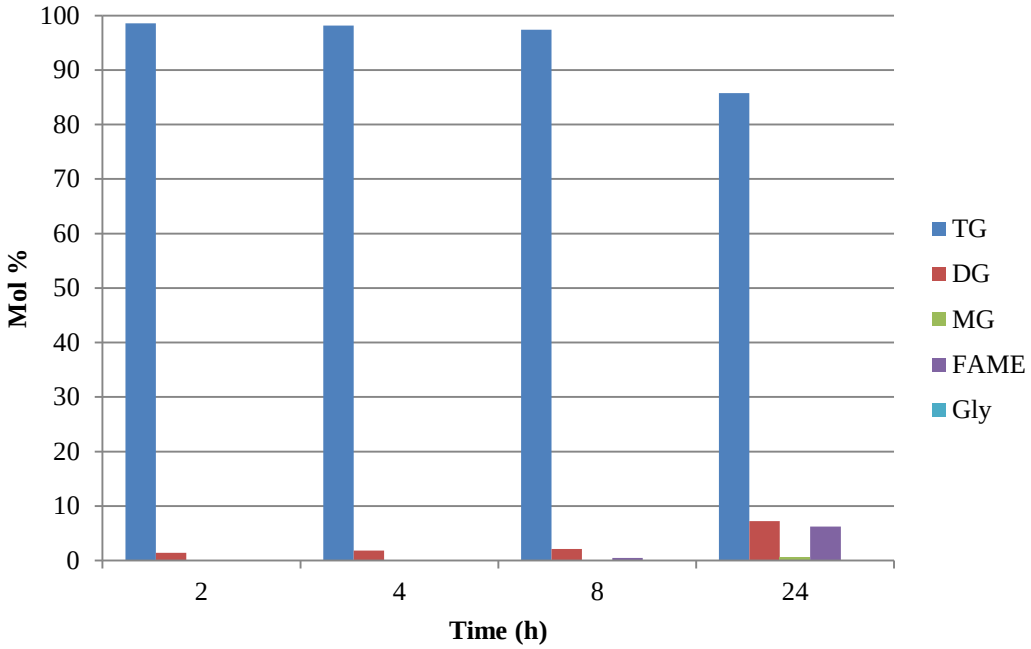

Figure 3.27 SrO Method 1 on alumina coated monolith, T = 120°C, P = 8 bar.

3.6.2.2 Method 2

Alumina monoliths were coated following Method 2 (see Section 3.4.2.2) in order to provide a lower calcination temperature and avoid the formation of strontium aluminate, although it should be noted that the nitrogen flow ran out at some point during the cooling stage. A loading of 6.2% was obtained, which was equivalent to 0.078 wt% with respect to oil. The results from the batch experiment are shown in Figure 3.28.

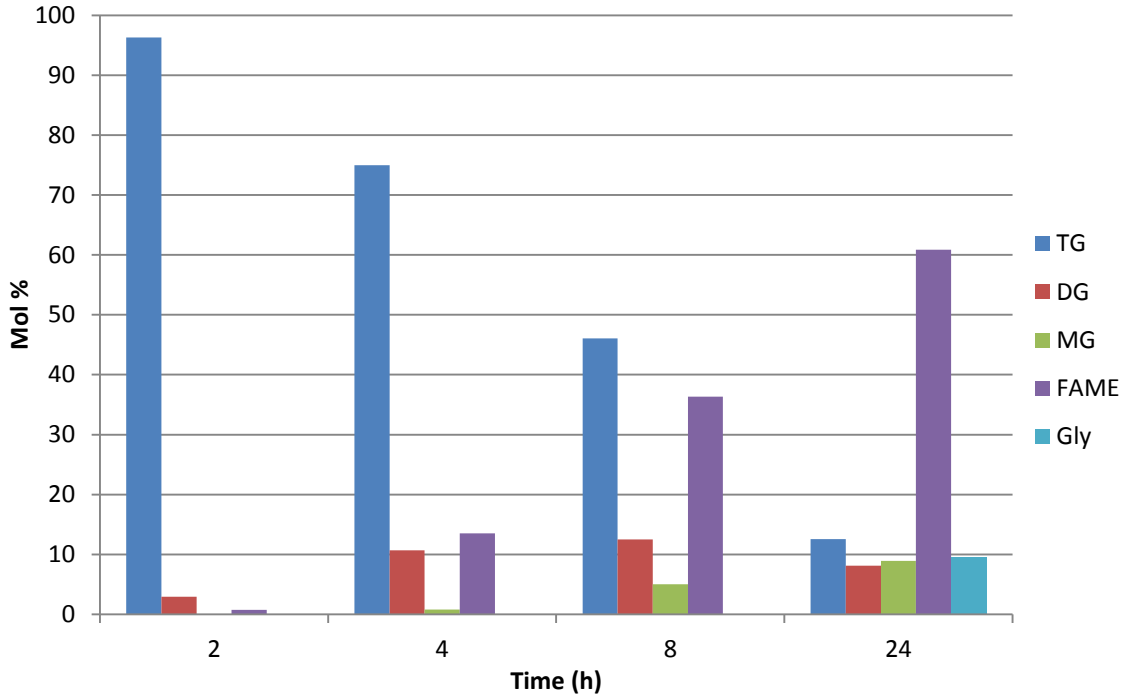

Figure 3.28 SrO Method 2 on alumina monolith, T = 120°C, P = 8 bar.

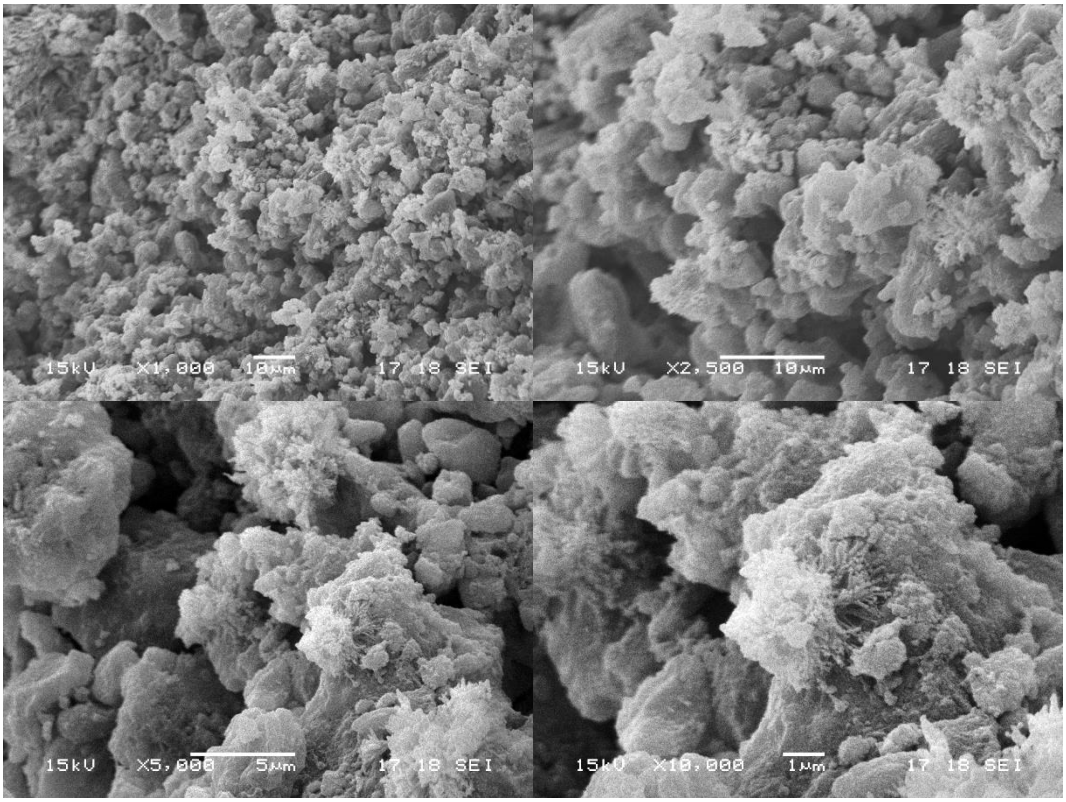

Figure 3.29 Representative SEM images of Method 2 on alumina.

Method 2 produced much more increased conversion of triglyceride, which was attributed to the well dispersed catalyst coating, as seen in the tendril-like formations shown in the SEMs. These were found to be fairly uniform throughout the monolith surface.

During the coating process, it was noted that dipping the monoliths in KOH resulted in some channels becoming blocked. Thus, it was decided to introduce a drying step between the nitrate and KOH steps. This took the form 10 minutes of heating under the hot air gun.

Because of the relative success of this coating method, it was determined a further batch should be coated and used in the continuous reactor (introduced fully in Chapter 5). An initial run was undertaken with a bed length of 190 mm, and a SrO loading of 5.7 wt%, 1 mL min^{-1} oil and 0.3 mL min^{-1} methanol, and a temperature of 120°C. The results are shown in Table 3.8.

Table 3.8 Results in mol % from continuous Run 1

Time (h)	TG	DG	MG	FAME	Glycerol
1	99.2	0.8	0.0	0.0	0.0
2	98.5	1.5	0.0	0.0	0.0
3	98.7	1.3	0.0	0.0	0.0

The catalyst was left in the reactor overnight, and then the reaction restarted with a lower flowrate of 0.1 mL min^{-1} oil, 0.03 mL min^{-1} methanol, with results in Table 3.9.

Table 3.9 Results in mol % from continuous Run 1, at reduced flow

Time (h)	TG	DG	MG	FAME	Glycerol
2	97.5	1.6	0.0	0.9	0.0

The temperature was then raised to 195°C, with the results in Table 3.10.

Table 3.10 Results in mol % from continuous Run 1, reduced flow and higher temperature

Time (h)	TG	DG	MG	FAME	Glycerol
1	71.1	6.4	0.6	18.4	3.6

To determine if the cause of the low conversion was a bad catalyst, a new batch was made, skipping the newly introduced drying stage to identify if this was the source of the problem. Enough pieces were loaded with catalyst to do both a batch experiment and a continuous run. The loading of these monoliths was 6.0 wt%. A repeat of the batch experiment yielded lower conversions, as shown in Figure 3.30.

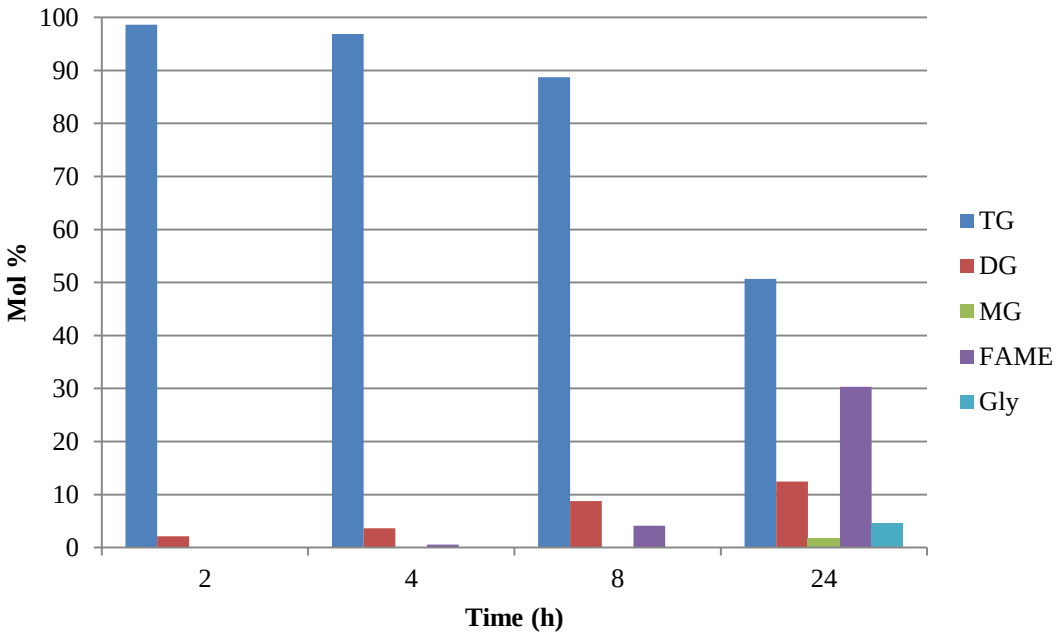

Figure 3.30 Repeat batch experiment for Method 2 on alumina.

The continuous run with this batch was with a flow rate of 0.1 mL min^{-1} oil, 0.04 mL min^{-1} methanol, 200 mm bed length (6.0% loading), at 120°C produced similar conversions to the first continuous run, as shown in Table 3.11.

Table 3.11 Results from continuous run 2

Time (h)	TG	DG	MG	FAME	Glycerol
1	98.9	1.1	0.0	0.0	0.0
2	95.7	4.3	0.0	0.0	0.0
3	94.8	5.2	0.0	0.0	0.0

From these results, it is clear that the original catalyst was not being reproduced. It was noted that there were a few equipment differences between the first catalyst and the subsequent attempts to reproduce it:

- The original catalyst was calcined under nitrogen in a stainless steel tube, however, this was found to be depositing a residue on later catalysts, and was thus replaced with a quartz tube.

- The original stainless steel tube used a different thermocouple than the quartz tube.

It was thus theorised that the original catalyst may have had some steel-related substance deposited on the surface, which acted as an effective catalyst, or that the temperature in the original catalyst calcination was different. To answer the first question, samples of the original catalyst and of the first attempt to reproduce it were examined using x-ray backscattering SEM.

Compositional SEM and x-ray backscatter analysis were performed under low vacuum at 15kV with uncoated samples from the original catalyst batch, as well as a sample from the first attempt to recreate it. Compositional SEM images of the inner track of a monolith channel were taken of each, and are shown in Figure 3.31 and Figure 3.32.

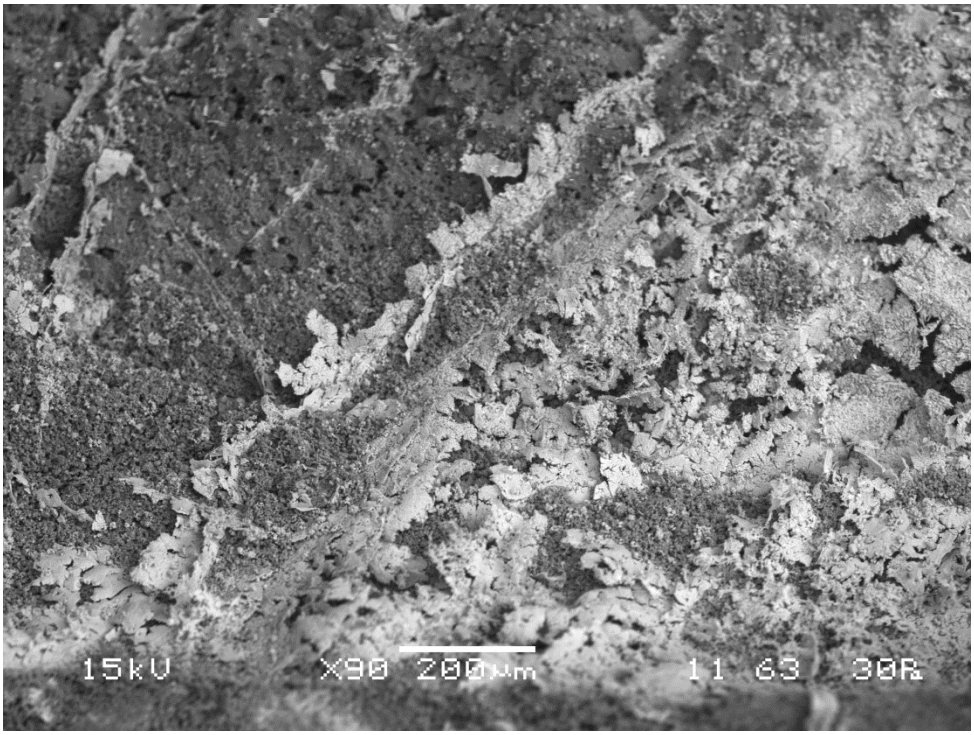

Figure 3.31 SEM image of original successful catalyst.

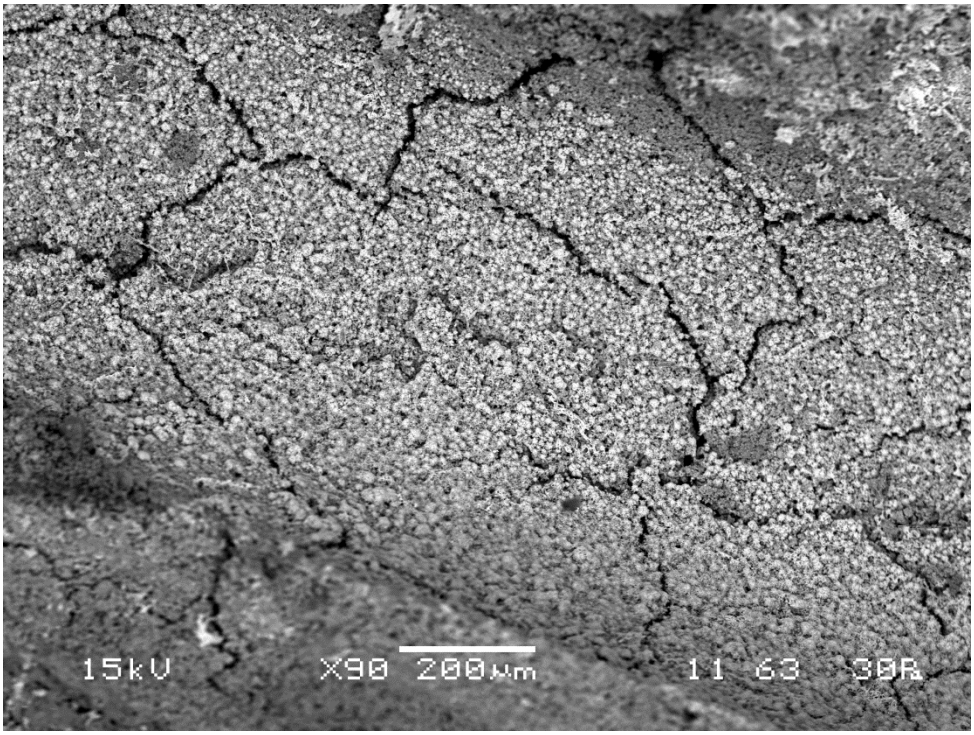

Figure 3.32 SEM image of first attempt to recreate successful catalyst.

In these images, the lighter coloured areas are strontium rich, while the darker areas are aluminium rich. Comparing these images, it can be clearly seen that the original catalyst is predominately made of larger flakes and plates, with some smaller particles on the surrounding alumina. The second catalyst, meanwhile, has a much more uniform coating of smaller particles. An examination of the different phases of these catalysts was done by x-ray backscatter.

First, the original catalyst (Sample 1) was examined. A portion of the catalyst was chosen as representative, and is shown in Figure 3.33. Three phases were identified in this image: the lighter areas; the darker, flat areas; and the darker, rough areas. Six spectra were obtained from each of these areas, and the spectra fitted to elemental energy levels using the x-ray backscatter processing program INCA. The spectra locations are indicated in Figure 3.34.

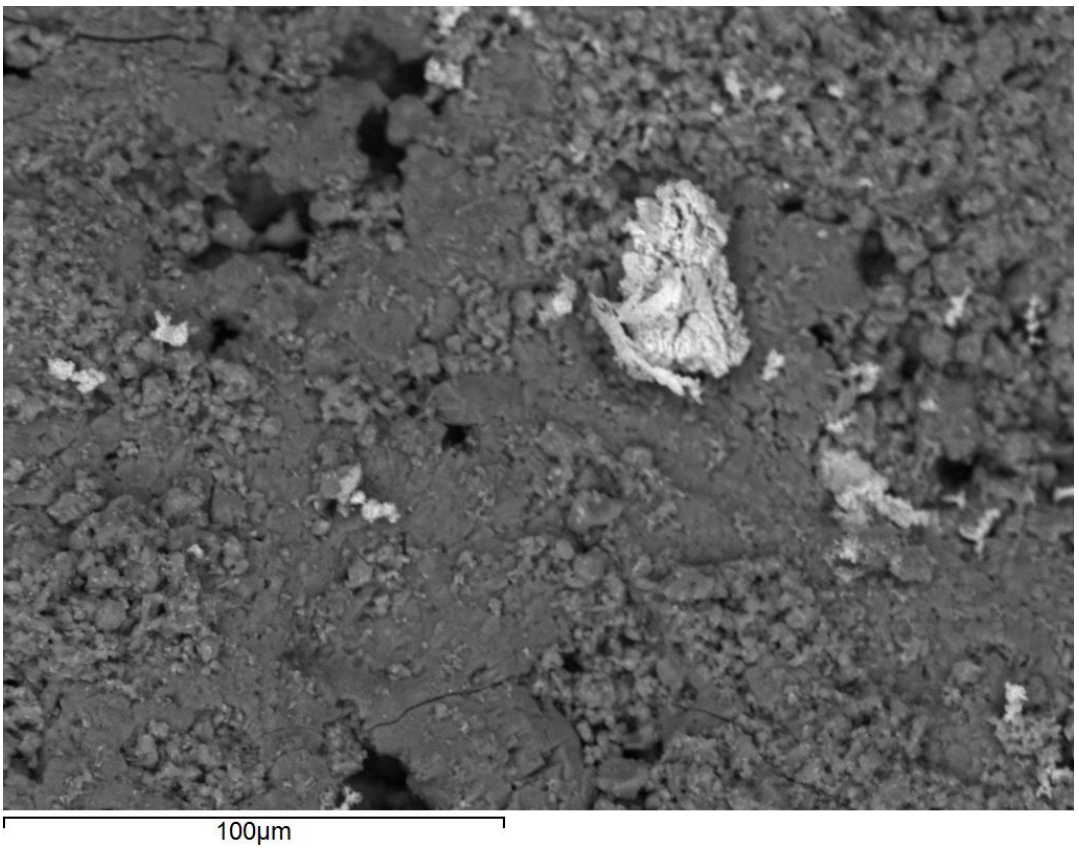

Figure 3.33 Representative compositional SEM of Sample 1.

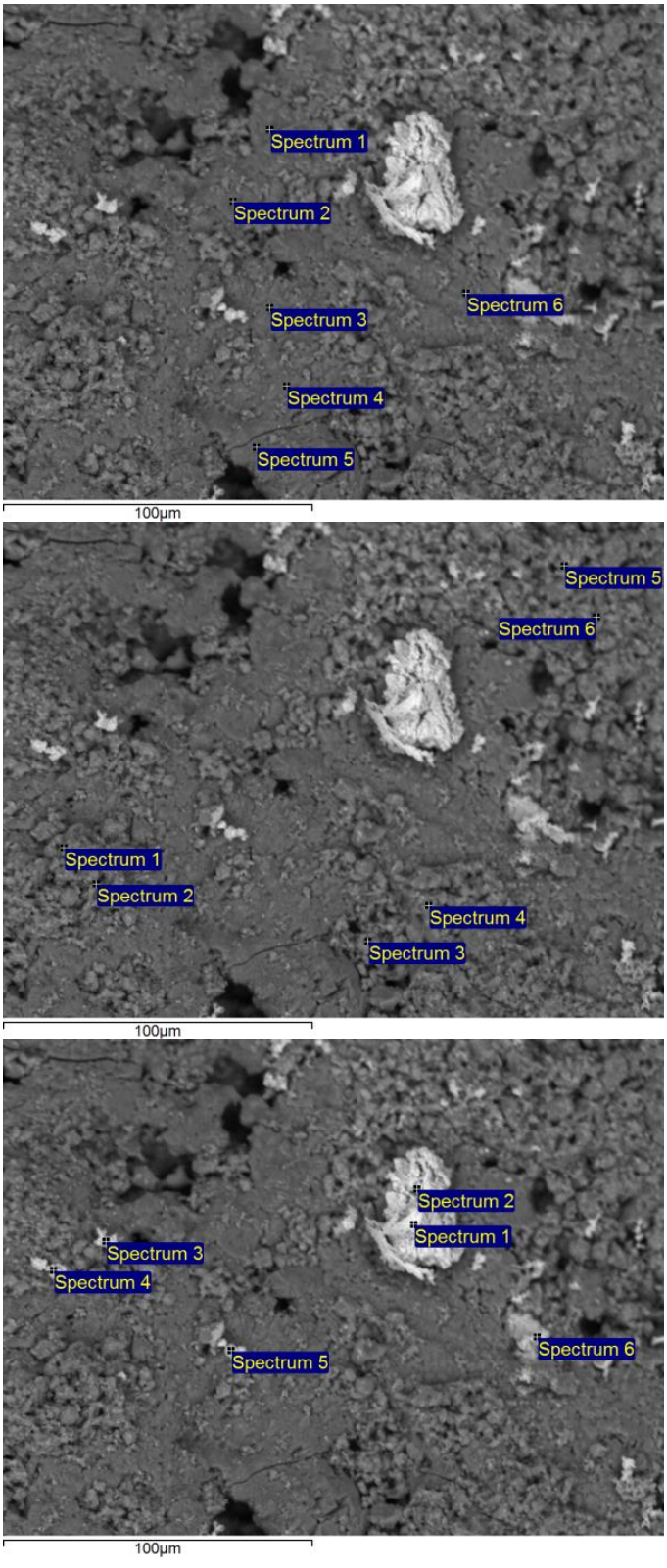

Figure 3.34 X-ray backscatter spectra locations for Sample 1.

The results from these spectra are given in Table 3.12 through Table 3.14.

Table 3.12 Elemental composition of dark, flat phase of Sample 1

Spectrum	O	Mg	Al	Si	K	Sr
Spectrum 1	66.77	4.35	14.24	12.98	0.47	1.19
Spectrum 2	60.23	5.11	16.95	16.09	0.78	0.84
Spectrum 3	60.7	4.7	17.6	15.89	0.49	0.62
Spectrum 4	61.32	5.67	15.29	16.83	0.44	0.46
Spectrum 5	60.63	5.64	15.4	17.33	0.51	0.49
Spectrum 6	66.17	5.26	13.25	14.36	0.38	0.59
Mean	62.64	5.12	15.45	15.58	0.51	0.7
Std. deviation	2.99	0.52	1.62	1.63	0.14	0.28

Table 3.13 Elemental composition of dark, rough phase of Sample 1

Spectrum	O	Mg	Al	Si	K	Sr
Spectrum 1	69.42	0.42	17.92	9.15	1.7	1.4
Spectrum 2	64.71	0.43	23.16	8.44	2	1.25
Spectrum 3	64.65	0.54	22.03	9.54	2	1.24
Spectrum 4	65.96	0.66	21.29	8.94	1.91	1.24
Spectrum 5	64.07	0.14	21.97	9.43	2.1	2.27
Spectrum 6	51.37	0.45	30.88	10.62	3.66	3.02
Mean	63.36	0.44	22.88	9.35	2.23	1.74
Std. deviation	6.18	0.17	4.31	0.73	0.72	0.75

Table 3.14 Elemental composition of lighter phase of Sample 1

Spectrum	O	Mg	Al	Si	K	Sr
Spectrum 1	71.65	0.88	7.57	3.7	0.69	15.5
Spectrum 2	73.88	0.54	5.52	2.52	0.5	17.05
Spectrum 3	70.23	1	12.52	6.25	0.94	9.06
Spectrum 4	73.77	1.03	9.81	5.08	0.8	9.51
Spectrum 5	73.76	1.22	7.68	4.75	0.7	11.88
Spectrum 6	67.76	0.69	7.34	3.67	0.77	19.77
Mean	71.84	0.89	8.41	4.33	0.73	13.8
Std. deviation	2.49	0.25	2.43	1.31	0.15	4.33

A representative piece of the second batch of the catalyst (Sample 2) was observed using the same methods. The area inspected is shown in Figure 3.35, and the spectra locations are shown in Figure 3.36. Seven locations were chosen for both the lighter areas and the darker areas between.

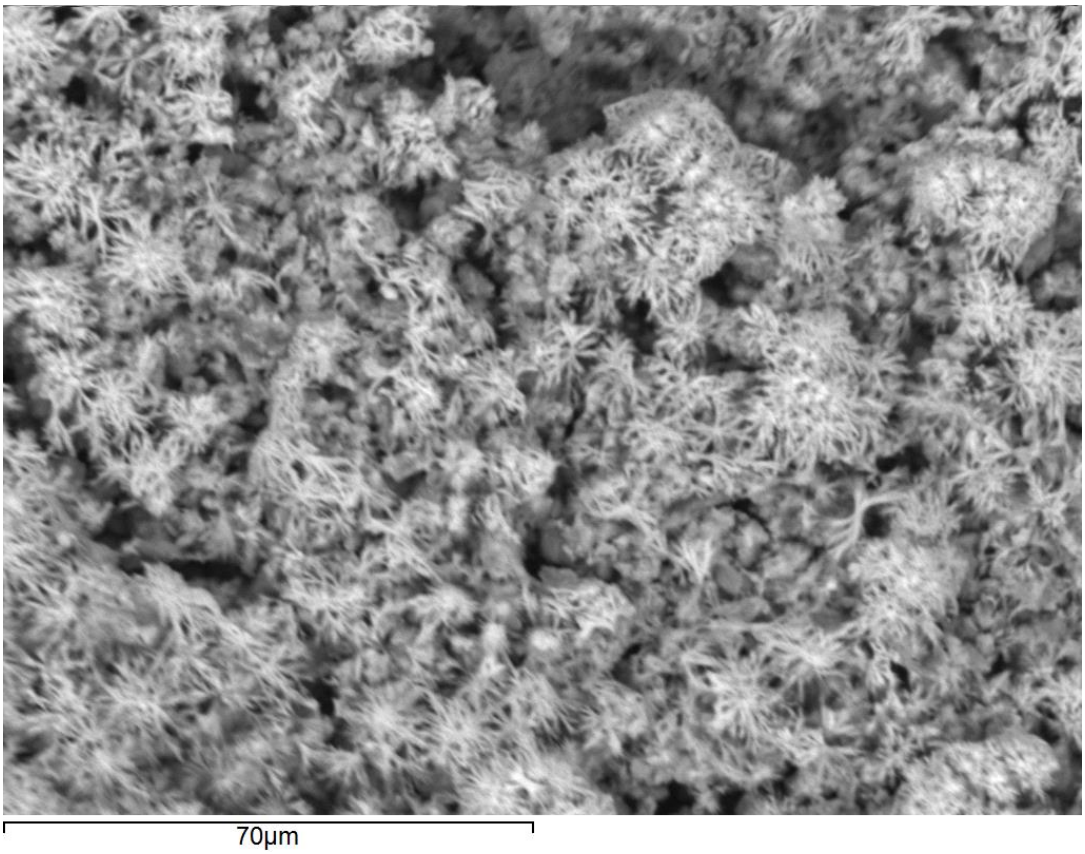

Figure 3.35 Representative compositional SEM of Sample 2.

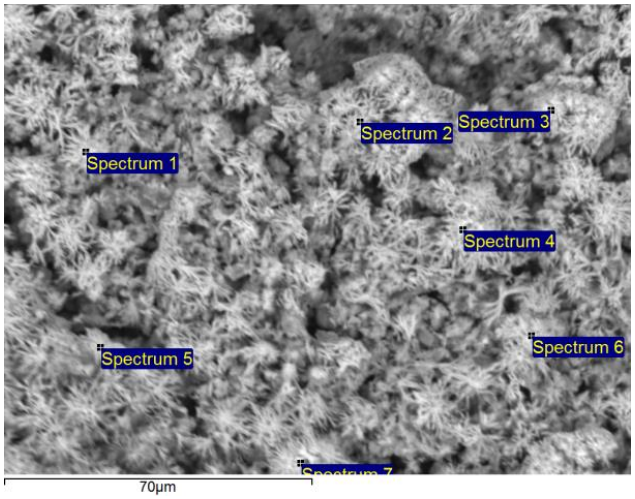

Figure 3.36 X-ray backscatter spectra locations for Sample 2.

The compositional analysis of these spectra are given in Table 3.15 and Table 3.16.

Table 3.15 Elemental composition of lighter phase of Sample 2

Spectrum	O	Al	Si	K	Sr
Spectrum 1	71.21	4.37	2.73	0.88	20.8
Spectrum 2	70.69	5.06	2.66	1.08	20.52
Spectrum 3	69.08	4.32	2.38	0.92	23.3
Spectrum 4	69.87	4.13	2.6	0.77	22.63
Spectrum 5	71.23	4.72	2.73	0.96	20.35
Spectrum 6	70.34	4.5	2.82	0.95	21.4
Spectrum 7	66.56	6.8	3.81	1.38	21.45
Mean	69.85	4.84	2.82	0.99	21.49
Std. deviation	1.64	0.91	0.46	0.19	1.1

Table 3.16 Elemental composition of darker phase of Sample 2

Spectrum	O	Mg	Al	Si	K	Sr
Spectrum 1	50.37	-	28.08	7.92	3.56	10.06
Spectrum 2	59.5	-	16.66	6.49	4.03	13.32
Spectrum 3	61.59	2.96	14.75	11.89	4.13	4.68
Spectrum 4	74.08	-	5.55	2.79	1.1	16.47
Spectrum 5	56.65	-	16.51	9.09	3.95	13.8
Spectrum 6	61.49	-	16.84	6.92	3.38	11.36
Spectrum 7	65.79	-	18.36	5.01	1.9	8.95
Mean	61.35	N/A	16.68	7.16	3.15	11.23
Std. deviation	6.84	N/A	6.10	2.70	1.09	3.54

The primary difference between the two samples appears to be the presence of magnesium in Sample 1; although one spectrum of Sample 2 did show energy peaks corresponding to magnesium, the rest did not. It appears to be most likely that the source of the magnesium is the original alumina coating, and the much more dense strontium coating of Sample 2 served to obscure most of that. No other source of magnesium was used in the laboratory, and so cross contamination from other work seems unlikely. It appears that similar amounts of potassium remained after the washing step, which would preclude that as the source of activity in Sample 1.

It appears that the initial success of this method was in fact an anomaly. This may have been caused by a few factors. It seems unlikely that the catalyst itself was contaminated, as no other significant metal appears in the x-ray spectra. Contamination from the steel tube would likely have left traces of iron and chromium on the catalyst. Thus, any contamination was likely in the reactor itself. This cannot be tested as the reactor was washed between runs, and any possible contamination was obviously removed, as future results were unaffected. However, it is also possible that the original catalyst was in fact active, but the method was too unrepeatable to obtain more catalysts with similar activity.

Indeed, the presence of aluminium and magnesium in higher quantities in Sample 1 suggest that there may have been significant interaction between the metals, leading to a material with significantly higher catalytic activity that Sample 2. However, reformulating such a material was not deemed a beneficial undertaking for achieving the project's goals.

3.6.2.3 Method 3

Blank monoliths were coated according to Method 3 (see Section 0), with 2.7 wt% colloidal silica (Ludox AS40, Sigma Aldrich) added to a 30 wt% $Sr(OH)_2$ slurry. The monoliths were coated three times, and then calcined. The particle sizing results for the slurry are given in Figure 3.37.

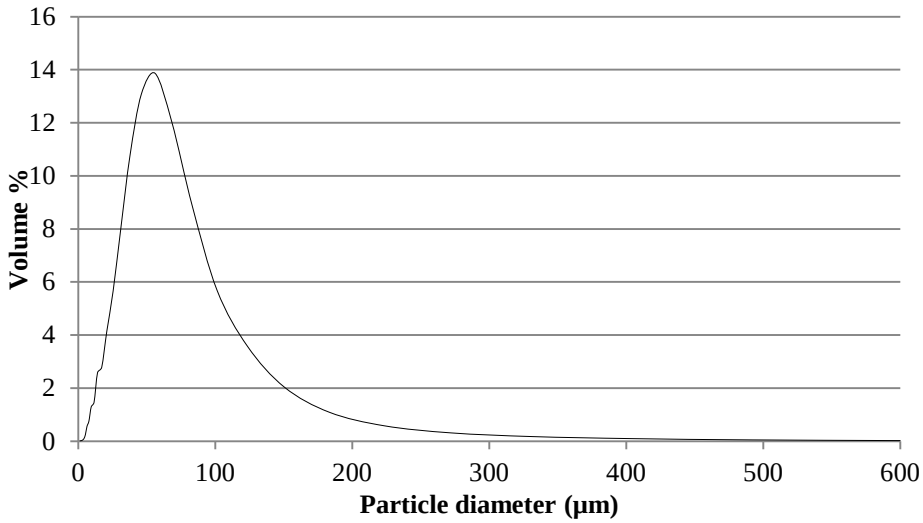

Figure 3.37 Slurry particle sizes.

After calcination, the coating was 19.6 wt%, which is a catalyst loading in the reactor of 0.28 wt% with respect to oil. The results of the initial screening are shown in Figure 3.38.

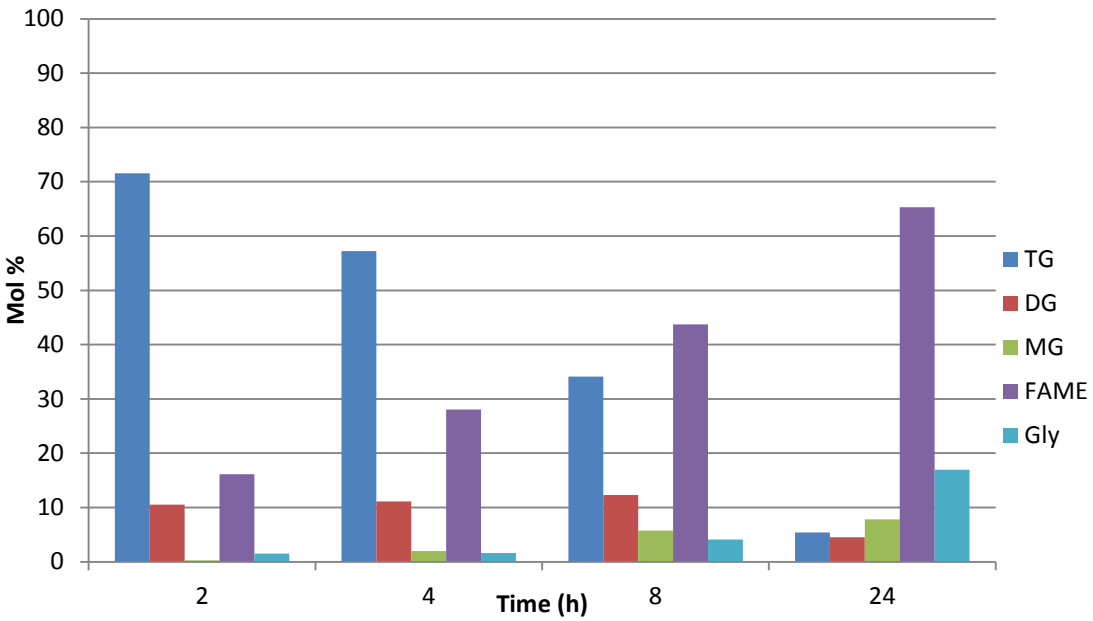

Figure 3.38 Method 3 on blank monolith, T = 120°C, P = 8 bar.

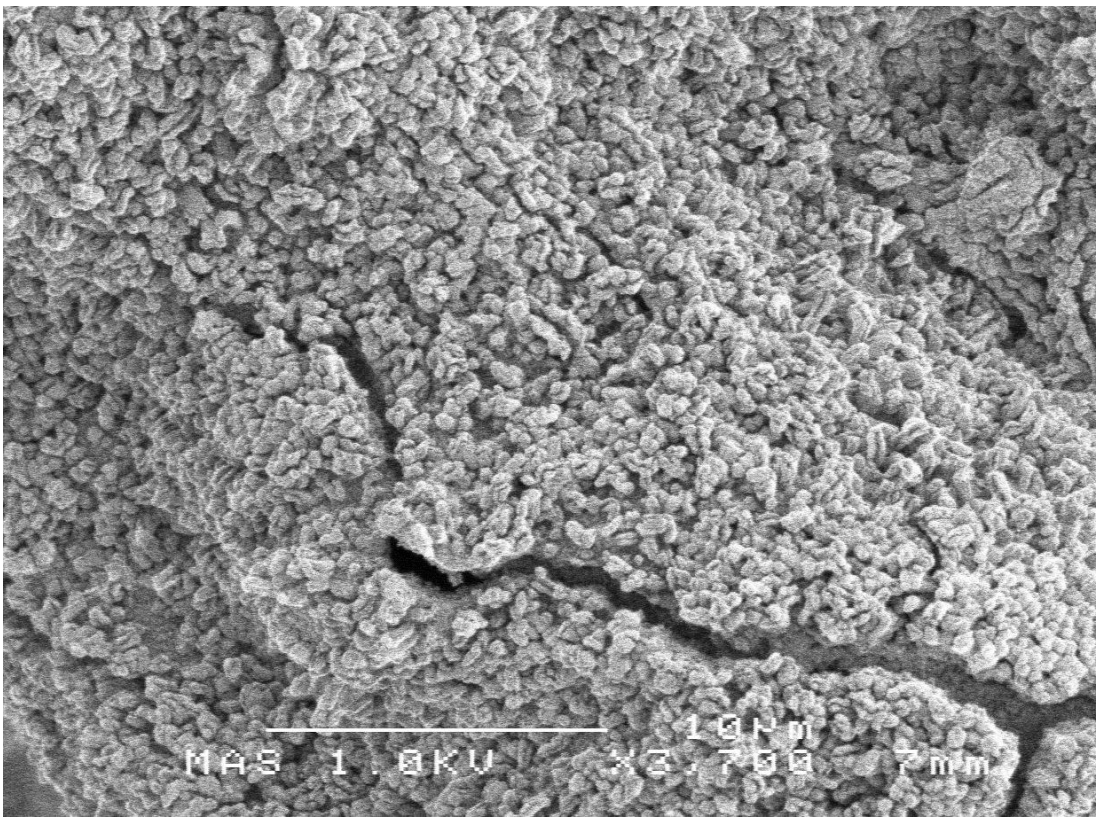

Figure 3.39 FESEM image of SrO Method 3 on blank monolith.

This coating was quite active for the transesterification, although, as can be seen in Figure 3.39, the coating was fractured. This resulted in poor adhesion to the monolith, which was evident from the ease with which the coating was removed from the monolith under even slight impact. However, due to the high activity, it was decided that this coating method would be carried over to the continuous reactor. This, and the further development of the coating method, is described in Chapter 5.

3.6.3 Consideration of Experimental Errors

In order to have confidence in the experimental methods and results, it is necessary to consider to possible sources of errors in the work.

Temperature

Temperatures were measured in two settings. The first was the furnace. This was done using a K-type thermocouple, which was calibrated in a professionally serviced thermocouple calibration furnace, and found to be accurate within 0.5°C across a range of temperatures. The other temperature measurement was carried out using the thermocouple from the stirrer hotplate, which was inserted into the diptube assembly of the autoclave. This was calibrated against a mercury thermometer, and found to be accurate within 1°C. These would not affect the reliability of the experiments.

Composition

Reaction composition was determined by GC. As discussed in 3.1.1.2, the GC was found to be repeatable, and had a standard deviation of less than 2.7% for all components, with most measurements having a standard deviation of less than 1%. This would not affect the reliability of the experiments.

Weighing

Catalyst samples were weighed in a microbalance, both before and after coating. This microbalance had a precision of 0.00001g, and was calibrated yearly by a professional balance servicing company. This would not affect the reliability of the experiments.

3.7 Conclusions

- Analytical methods were investigated and developed for use in the project.

- Catalysts identified as promising candidates in Chapter 2 were investigated as powders under reflux conditions. While strontium oxide exhibited impressive activity, reaching 100% conversion in 15 minutes, Ca/Ce doped lanthanum oxides were not found to be sufficiently active for investigation in a continuous setting.

- Three methods of coating strontium oxide onto a monolithic support were studied at T = 120°C, P = 8 bar, and a methanol:oil ratio of 6:1. Conventional impregnation coatings were outperformed by the slurry coating method. This coating method was chosen for further investigation.

- The slurry coating exhibited poor mechanical stability, which will be addressed in Chapter 5.

References

BS 8534:2008 2008. Animal and vegetable fats and oil - Determination of water content (pyridine free). *British Standards Institute.*

BS EN ISO 660:2009 Animal and vegetable fats and oils - Determination of acid value and acidity. *British Standards Institute.*

DE MOURA, C. V. R., DE CASTRO, A. G., DE MOURA, E. M., DOS SANTOS, J. R. & MOITA NETO, J. M. 2010. Heterogeneous catalysis of babassu oil monitored by thermogravimetric analysis. *Energy and Fuels,* 24**,** 6527-6532.

GLASSON, D. R. & SHEPPARD, M. A. 1968. Reactivity of lime and related oxides .19. Production of strontium oxide. *Journal of Applied Chemistry,* 18**,** 327-+.

KIM, M., DIMAGGIO, C., YAN, S., SALLEY, S. O. & NG, K. Y. S. 2011. The effect of support material on the transesterification activity of CaO-La2O3 and CaO-CeO2 supported catalysts. *Green Chemistry,* 13**,** 334-339.

KNOTHE, G. & KENAR, J. A. 2004. Determination of the fatty acid profile by H-1-NMR spectroscopy. *European Journal of Lipid Science and Technology,* 106**,** 88-96.

KNOTHE, G., VAN GERPEN, J. & KRAHL, J. 2005. *The biodiesel handbook,* Urbana, Ill., AOCS Press.

MAZZIERI, V. A., VERA, C. R. & YORI, J. C. 2008. Adsorptive Properties of Silica Gel for Biodiesel Refining. *Energy & Fuels,* 22**,** 4281-4284.

MONTEIRO, M. R., AMBROZIN, A. R. P., LIAO, L. M. & FERREIRA, A. G. 2008. Critical review on analytical methods for biodiesel characterization. *Talanta,* 77**,** 593-605.

NIJHUIS, T. A., BEERS, A. E. W., VERGUNST, T., HOEK, I., KAPTEIJN, F. & MOULIJN, J. A. 2001. Preparation of monolithic catalysts. *Catalysis Reviews - Science and Engineering,* 43**,** 345-380.

PLANK, C. & LORBEER, E. 1995. Simultaneous determination of glycerol, and mono-, di- and triglycerides in vegetable oil methyl esters by capillary gas chromatography *Journal of Chromatography A,* 697**,** 461-468.

SABOUR, B., PEYROVI, M. H., HAMOULE, T. & RASHIDZADEH, M. 2014. Catalytic dehydration of methanol to dimethyl ether (DME) over Al-HMS catalysts. *Journal of Industrial and Engineering Chemistry,* 20**,** 222-227.

VICENTE, G., MARTINEZ, M. & ARACIL, J. 2006. Kinetics of Brassica carinata oil methanolysis. *Energy and Fuels,* 20**,** 1722-1726.

Chapter 4 Methanol-Vegetable Oil Solubility

In this chapter, the mutual solubility of methanol and vegetable oil is investigated. First, a literature review is presented wherein the solubilities of various mixtures of reactants, products, and intermediates are explored. This is followed by the design and construction of an experimental rig for obtaining samples of liquid mixtures at elevated temperatures, and the development of an NMR method for analysing the samples.

4.1 Introduction

While there is much written in the literature relating to biodiesel production about the use of co-solvents, mixing methods, and the phase in which the homogeneous reaction takes place, there is a significant lack of reliable data regarding the solubility of methanol in vegetable oils. There are a number of studies on the solubility of various multi-component systems, including the reactants, products and co-solvents. Few of these extend the temperature range examined beyond the boiling point of methanol.

4.1.1 Solubility Studies

Čerče *et al*. (2005) investigated the solubility of methanol and rapeseed, mink (a bi-product of fur production), and sunflower oil from 20-75°C. Significantly more methanol is soluble in oil than *vice versa*, with approximately 12 wt% methanol was dissolved in the rapeseed oil at 75°C, compared with about 2% oil in the methanol. Subsequent measurements with varying amounts of FAME show that the reaction mixture can become homogeneous during the reaction, particularly at higher temperatures.

Resa *et al.* (2002) examine the mixing enthalpies of C-1 through C-4 alcohols at 25°C. Generally, the mixing of alcohols with vegetable oils is endothermic, which is hypothesised to be caused by the oil disrupting the hydrogen bonds between the

alcohol molecules. Methanol was found to be soluble in oil up to 50 mol%, which corresponds to about 3.5 wt%.

4.1.2 Multi-Component Systems

A number of studies focus on the interaction of products and intermediates with the reactants and each other (Andreatta *et al.*, 2008, Liu *et al.*, 2008a, Liu *et al.*, 2009, Liu *et al.*, 2008b, Zhou *et al.*, 2006). Generally, it can be said that initially a two-phase system is formed by the methanol-oil mixture, which becomes homogeneous at some point during the reaction, and returns to two-phase once a critical amount of glycerol has been produced. At the end of the reaction, the glycerol and FAME form two immiscible layers with practically no glycerol in the FAME, a negligible amount of FAME in the glycerol, and the methanol primarily in the glycerol phase (Andreatta *et al.*, 2008).

An illustration of these stages, based on this overview of the literature, is given in Figure 4.1. Such an explanation is generally supported by unquantified observations in the literature (Dasari *et al.*, 2003). In the case of homogeneous catalysis, both sulphuric acid and potassium hydroxide preferentially dissolve in the glycerol phase, particularly at lower temperature and with increased methanol (Chiu *et al.*, 2005).

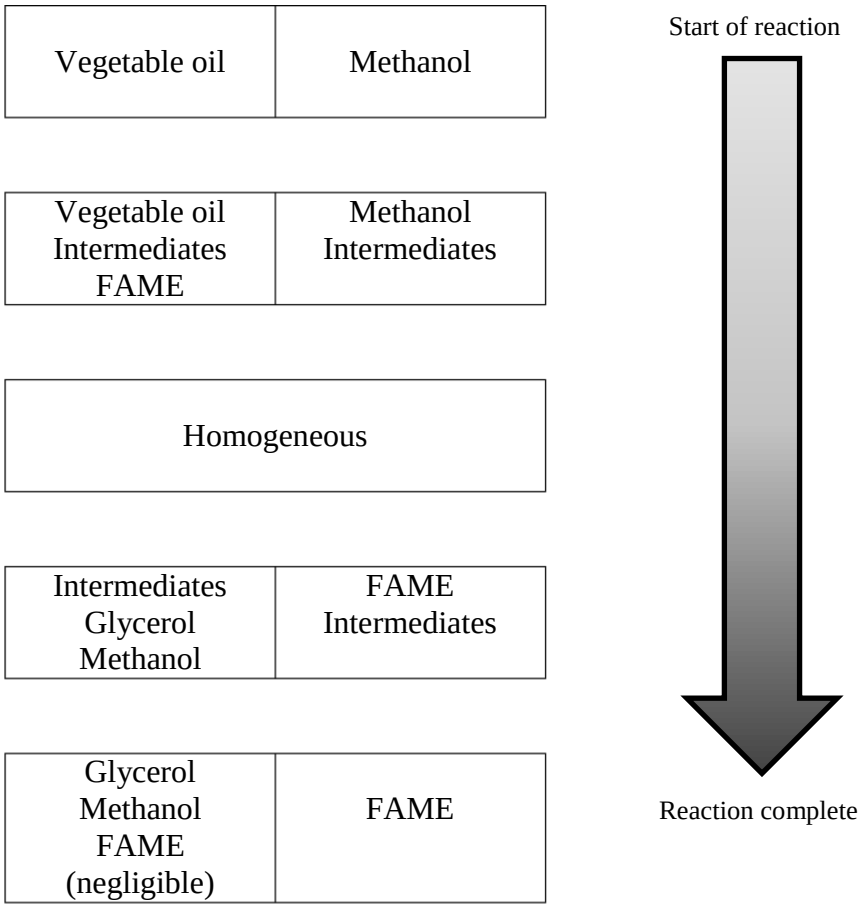

Figure 4.1 Illustration of the phases present throughout the course of a transesterification reaction.

4.1.3 Co-Solvents

In order to produce a homogeneous reaction phase, many researches have opted to use co-solvents, such as tetrahydrofuran (Mahajan *et al.*, 2007), long chain alcohols (Dunn and Bagby, 1994), and ethers (Boocock *et al.*, 1996). Generally the reaction rate is increased, particularly at the beginning where solvent free systems are severely limited by mass transfer between the phases. However, the co-solvent must be removed at the end of the reaction, which may be an energy intensive process.

4.1.4 Sonication

An alternative to the use of co-solvents is using sonication instead of conventional mixing. This can improve mass transfer significantly, which increases the overall

reaction rate. It is also claimed in the most cited paper on the subject, that sonication leads to lower soap formation (Stavarache *et al.*, 2005). However, this was judged by comparing the yields of biodiesel after purification for conventional mixing and sonication, and the conclusion reached is that more of the yield is lost in washing the conventionally stirred sample, and this must be due to higher soap formation. There is insufficient description of the purification process to determine if the difference is due to soap or simply better laboratory practice being applied to the sonicated sample. There is also no attempt to quantify the soap production in the two cases, nor is any alternative reaction mechanism for sonication suggested.

4.1.5 Reaction Phase

Although mainly studied in the case of homogeneous catalysis, the location of the reaction phase is also of great interest for heterogeneous processes. It has been claimed that the reaction takes place in the methanol phase (Zhou *et al.*, 2006), the methyl ester-oil phase (Dasari *et al.*, 2003), and at the interface (Ataya *et al.*, 2007). A more compelling case has been made that the reaction occurs primarily in a thin boundary layer on the methyl ester-oil side of the interface (Narváez *et al.*, 2009), when considering the exaggerated effect of increasing the catalyst concentration in the methanol and the low solubility of oil in the same.

4.1.6 Conclusions

An essential question for the reaction engineering of a heterogeneous system for biodiesel production is the mutual solubility of the reactants. With increased solubility will come improved mass transfer, and, subsequently, an increase in the observed reaction rate (Noureddini and Zhu, 1997). With regard to the current project, if the reaction mixture is a single phase entering the reactor, the result would be increased conversion and efficiency, as well as simplified modelling, as no consideration will be needed for phase behaviour or location of the reaction.

4.2 Experimental Materials and Procedures

It was determined that there is insufficient data regarding the solubility of methanol and oil, and as such an investigation should be undertaken to fill this void. In order to be of direct use, the temperature range would need to extend up to at least 120°C. It was also recognised that the vessel used to carry out these experiments would be most useful if it were transparent. Thus, a glass vessel rated up to 10 bar was procured from Ace Glass Ltd (New Jersey, USA).

4.2.1 Equipment Design

A PTFE lid was purchased in conjunction with the glass vessel, and incorporated a ¼" (6.2 mm) female NPT thread, which allowed for connection to standard compression fittings. This was used to connect the vessel to a 10 bar nitrogen line. In order to ensure safe operation of the equipment, a non-return valve, pressure gauge and pressure relief valve were fitted. In addition, a Perspex shield was fabricated to protect lab users from any flying glass in the event of an explosion, and a full risk assessment was carried out on the experiment. For optimal accuracy, temperature was monitored via an internal thermocouple. A diagram of the apparatus is shown in Figure 4.2

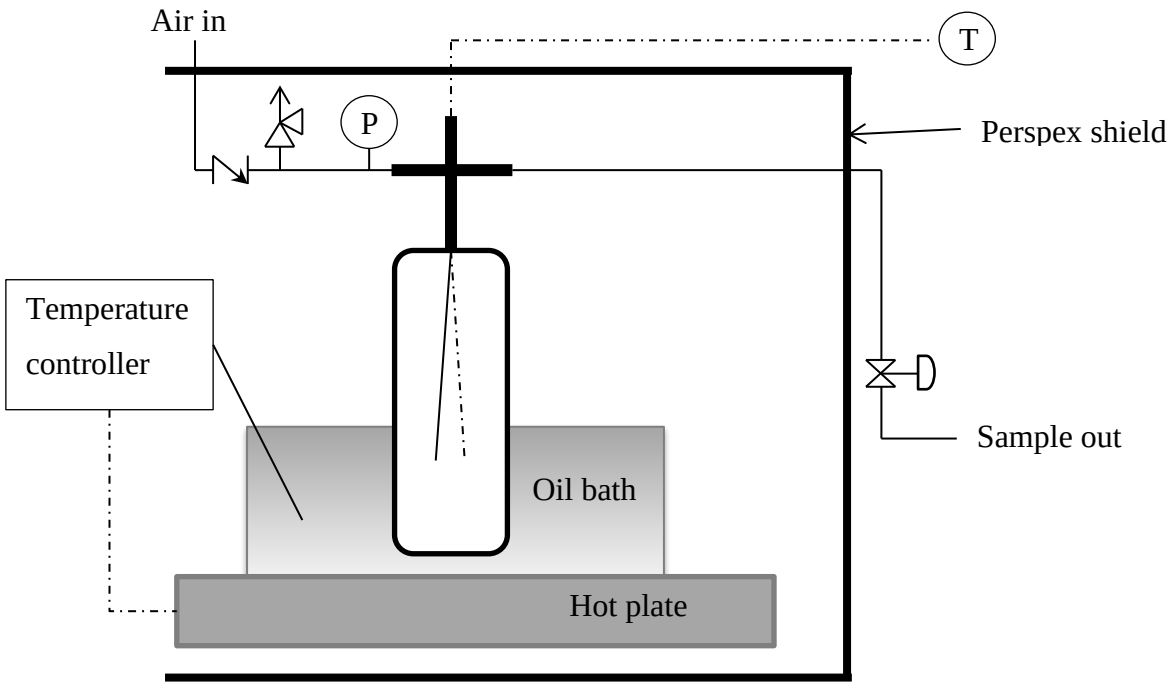

Figure 4.2 Diagram of the solubility test apparatus.

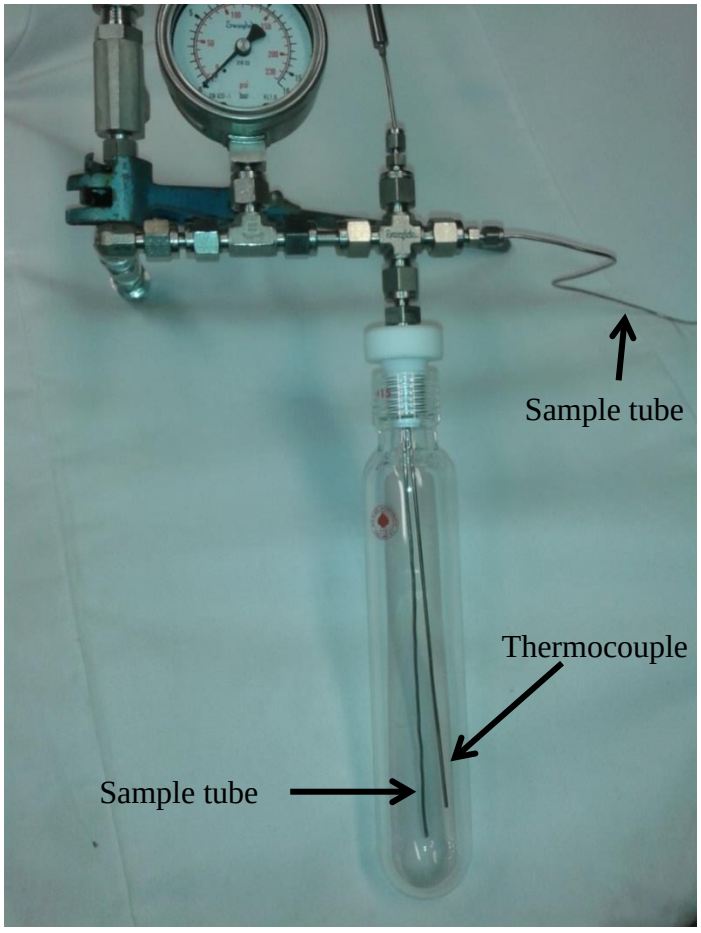

Figure 4.3 Photograph of solubility apparatus.

4.2.2 Experimental Procedure

The procedure for the solubility experiments was as follows:

- The vessel was charged with the desired amount of vegetable oil and methanol, along with a magnetic stirring flea;
- The vessel was connected to the nitrogen line;
- The temperature controller on the hotplate was set at the desired temperature, and the stirrer was set at a speed which provided satisfactory mixing;
- The pressure was increased by opening the nitrogen valve, if necessary, to maintain the methanol as a liquid;
- Once the apparatus reached the set temperature, the vessel was left stirring for an additional hour before the stirrer was turned off;
- The liquid was left to separate under gravity for an hour;
- A sample was drawn off, with the first 2 mL being discarded;
- The methanol to oil ratio in the sample was measured by two different means; NMR spectroscopy and by weighing the bulk sample before and after the methanol had been evaporated. These methods are described in more detail below.

After sampling, a sufficient amount of deuterated chloroform was added to create a clear single phase. Three aliquots were then taken from this, diluted in deuterated chloroform and analysed by NMR.

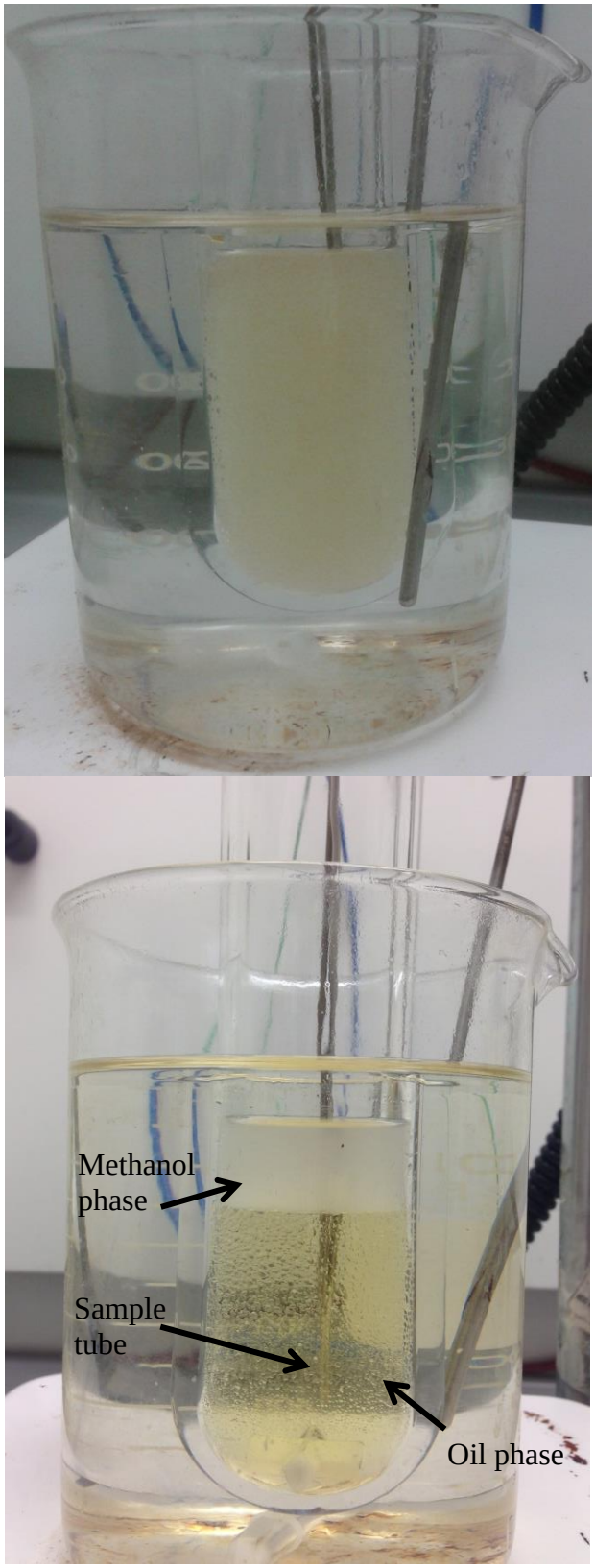

Figure 4.4 Photograph of solubility apparatus in use, stirred (top), and after phase separation (bottom).

4.3 Results and Discussion

The samples taken were analysed by NMR, after a modified method had been developed. The method was then confirmed by calibration, and used to calculate the solubility of methanol in oil.

4.3.1 NMR Calibration

Proton NMR spectra were analysed, with the pair of doublets at 3.8-4.2 from the glyceride proton pairs being given a value of 4. The methanol peak at 3.26 was then integrated, and this was then converted to weight %. An example NMR spectrum is shown in Figure 4.5.

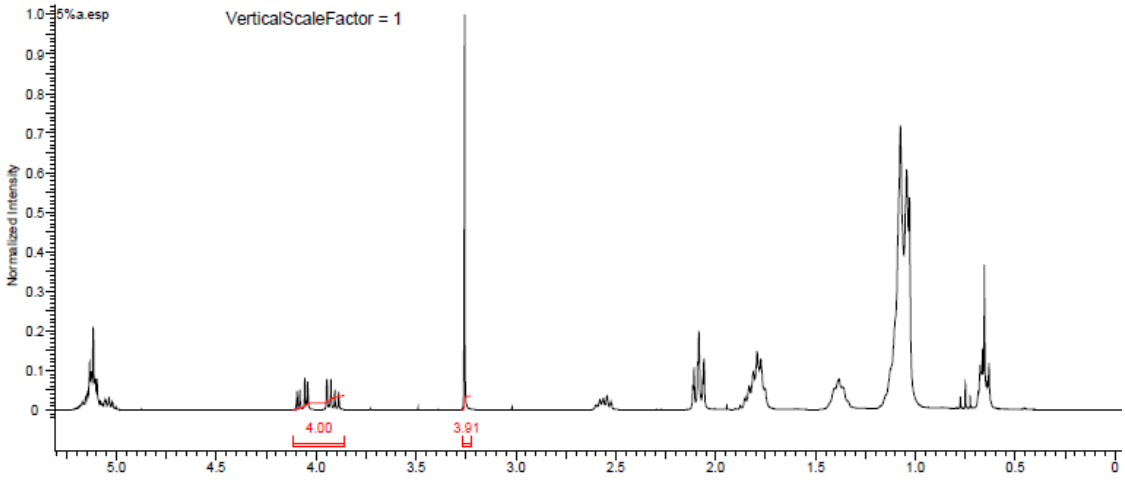

Figure 4.5 Example spectrum for NMR analysis of methanol solubility.

The value from this integration was then divided by three, as there are three protons represented by that peak, and the molecular weights of oil and methanol used to find the weight per cent using the following formula:

$$w_{MeOH} = \frac{\frac{I_{MeOH}}{3} \times M_{MeOH}}{M_{oil} + \left(\frac{I_{MeOH}}{3} \times M_{MeOH}\right)} \times 100 \quad (4.1)$$

In order to verify the accuracy of NMR for quantifying the methanol to oil ratio, a series of calibration experiments was undertaken. The results of the initial tests are given in Table 4.1.

Table 4.1 Initial NMR calibration

Weight %	Value obtained by NMR	Standard Deviation
1	0.91	0.09
5	4.36	0.15
10	8.01	0.91

From this, it was clearly seen that this method was not acceptable, and so an investigation was undertaken to find the source of the inaccuracy.

4.3.1.1 Time Constant Test

If the delay time between scans in a proton NMR is too short, the protons in a sample may have insufficient time to relax, and thus the signal will be smaller than expected. In order to check this, a set of NMR experiments was set up, whereby the delay time was incrementally increased to find the response of the protons in both the vegetable oil and the methanol. A 5 wt% methanol calibration sample was used. The resulting response curves for the glyceride protons and the methyl protons are shown in Figure 4.6 and Figure 4.7

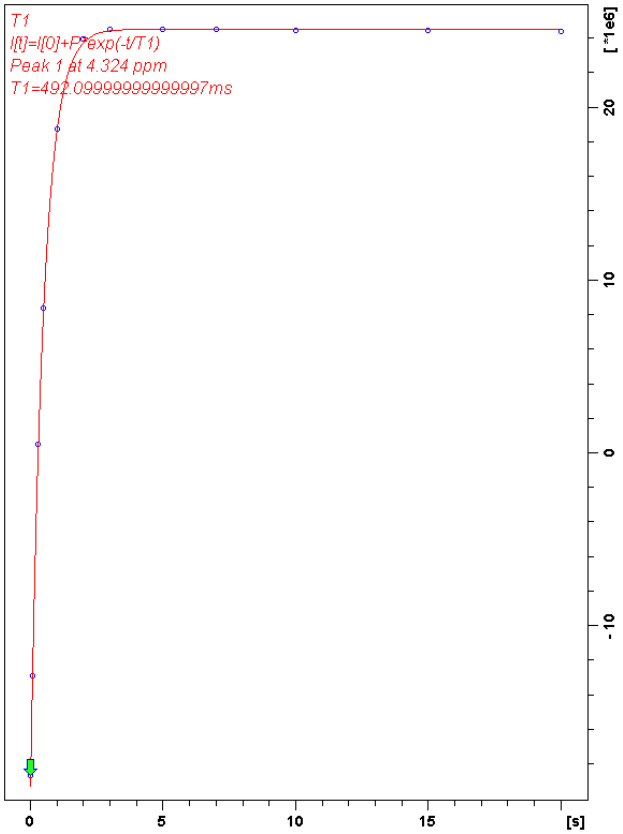

Figure 4.6 Vegetable oil delay time response curve.

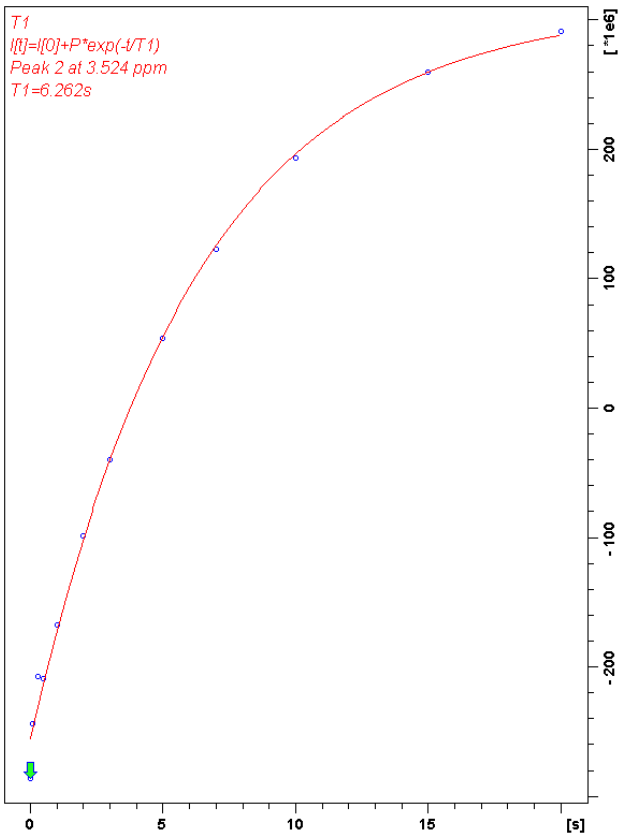

Figure 4.7 Methanol delay time response curve.

From these curves, it is clear that the vegetable oil protons had fully relaxed within the four second delay time that is the standard on the 300 MHz machine used. However, the methanol relaxation time is much greater, and so a new method was created with a delay time of 40 seconds.

4.3.2 Calibration using modified NMR method

Calibration samples were prepared of known amounts of methanol in oil ranging from 5 to 30 wt%. Three NMR samples were then prepared from each of these and subsequently measured with the modified NMR method. The resulting calibration is shown in Figure 4.8.

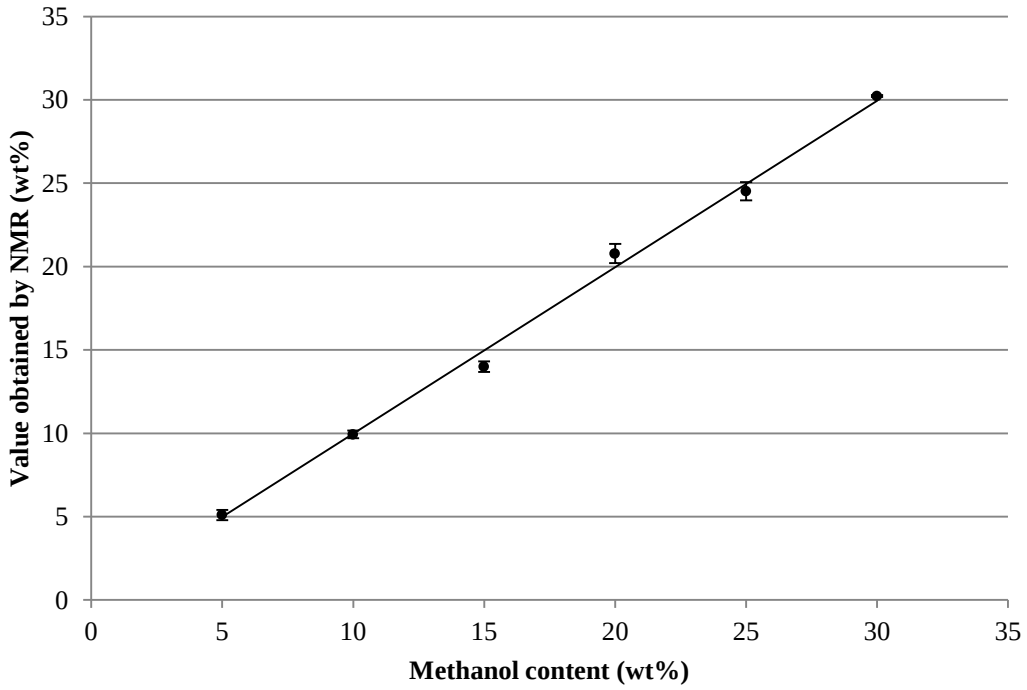

Figure 4.8 Calibration test of modified NMR method.

4.3.3 Solubility as a Function of Temperature

A series of solubility experiments was done using the described method, with 25 mL oil and 15 mL methanol, from 20 to 130°C at a pressure of 7 to 10 bar. The results from these experiments are given in Figure 4.9, along with lines representing common methanol:oil ratios relating to biodiesel production.

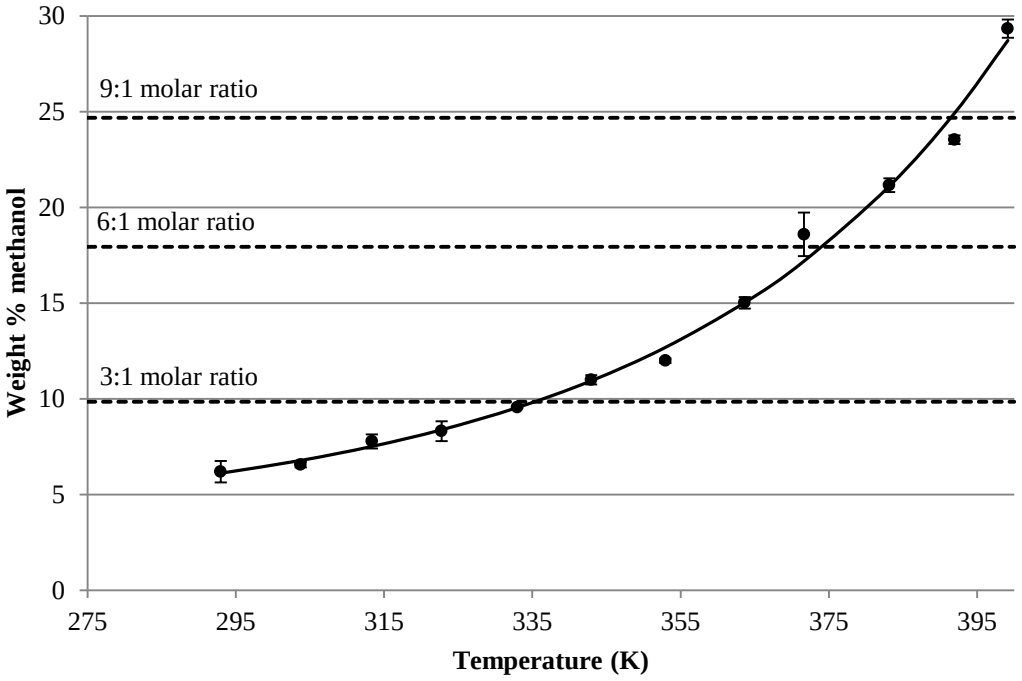

Figure 4.9 Methanol solubility in rapeseed oil with temperature, P = 7 to 10 bar.

A correlation was developed from the data, and is shown be the trend line, which has an R^2 value of 0.9921:

$$wt\% = e^{5.196\times10^{-5}T^2-0.02139T+3.617} \quad (4.2)$$

It should be noted that this correlation can only be considered applicable within the experimental range investigated.

From these results, it is clear that above 100°C a 6:1 molar ratio, which is widely used for transesterification reactions (Knothe *et al.*, 2005), will be single phase. Thus, significant mass transfer improvements should be possible in systems operating above these temperatures, as phase boundaries would not need to be overcome. Additionally, a 9:1 molar ratio can be expected to be single phase at temperatures approaching 120°C.

There is, however, the potential that other parameters can have an effect on the mutual solubility of the components, which would also impact the applicability of the data presented in Figure 4.9. To confirm that the data was not also a function of the experimental pressure and methanol:oil ratio in the apparatus, these were examined at fixed temperatures.

4.3.4 Solubility as a Function of Pressure

The apparatus was charged with 25 mL oil and 15 mL methanol, as before, stirred and heated to 80°C. The pressure was raised to a set point, and then held at temperature for about an hour. A sample was then taken, and the process repeated for four total pressures. 80°C was chosen as the temperature in order to minimise the vapour pressure (and thus increase the available pressure range), while also providing significant solubility. The results of these experiments are shown in Figure 4.10.

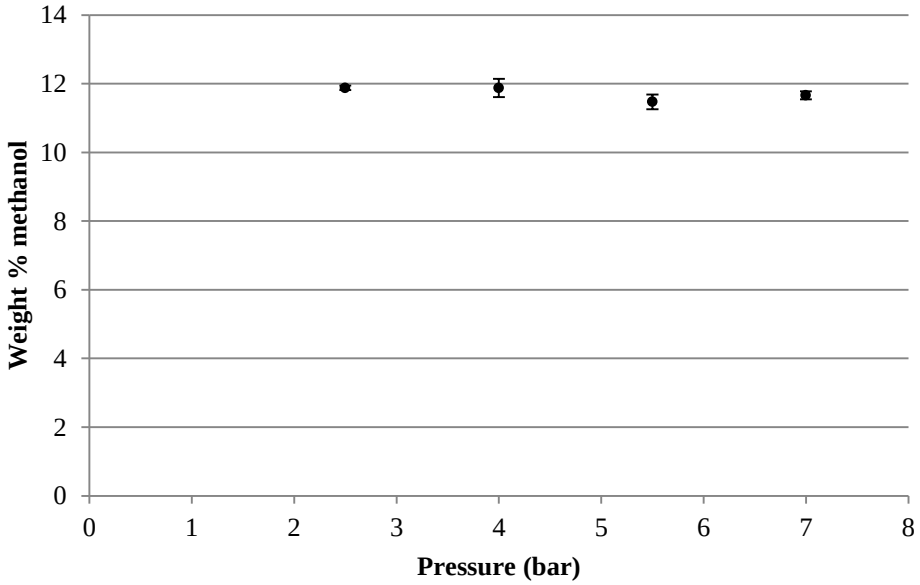

Figure 4.10 Methanol solubility in oil with pressure, T = 80°C.

There appears to be no effect of pressure on solubility, which is to be expected in a liquid-liquid system, unless there was a significant change in molar volume with mixing. It can thus be concluded with a degree of confidence that the solubility data presented in Figure 4.9 can be taken as being independent of pressure.

4.3.5 Solubility as a Function of Methanol:Oil Ratio

The other main possibility is that a varying ratio of methanol to oil would alter the uptake of methanol into the oil. Thus, experiments were carried out by charging the reactor with a constant amount oil and a range of methanol quantities, from 30 to 60 wt% with respect to oil. The experiments were then carried out as previously described, with the results shown in Figure 4.11.

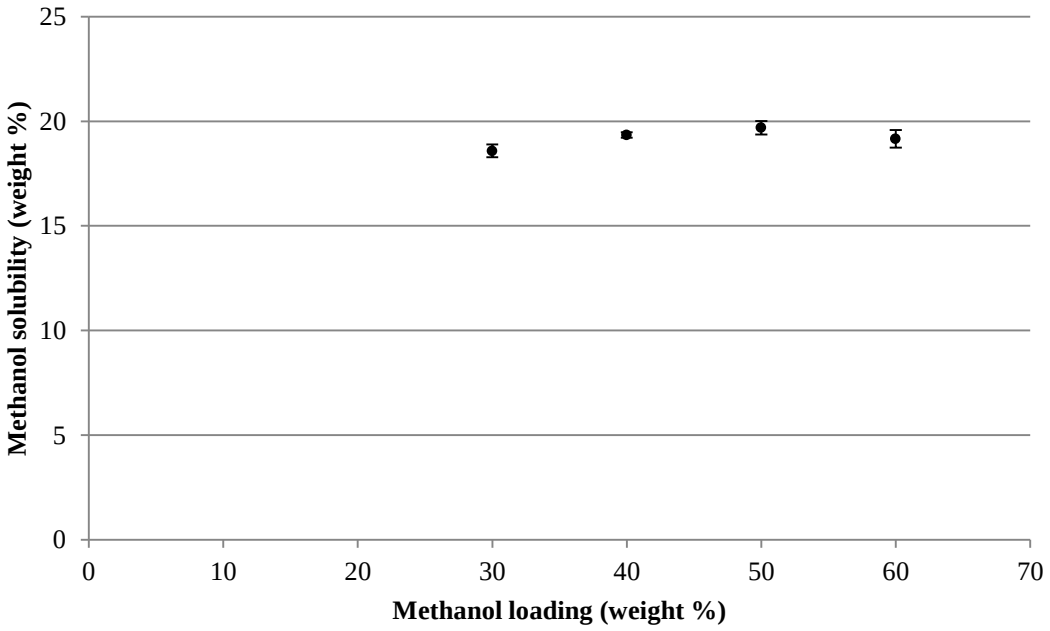

Figure 4.11 Methanol solubility in oil with varying methanol loading, T = 110°C, P = 8 bar.

There is no significant trend, and any variations are likely explained by small variations in experimental conditions between the runs, such as temperature, or a slight reaction occurring, which would be masked in the NMR spectra as the methyl peak of FAME appears at the same shift as the methyl peak of the methanol. Ultimately, the lack of change with methanol loading in the reactor can be taken as evidence that the solubility data in Figure 4.9 is valid across a range of methanol:oil ratios in the system.

4.4 Conclusions

The significance of the data presented in this chapter is best considered in terms of the transesterification reaction:

- Under reflux conditions at 65°C, the methanol dissolved at a 3:1 molar ratio, or just sufficient for the stoichiometric reaction.
- At 100°C this had increased to 6:1, and at 120°C it had reached 9:1.
- This would allow for rate improvements beyond that provided by the higher temperatures, as higher methanol solubility should lead to lower diffusional resistance in a heterogeneous system.

Combining the lack of effect of methanol to oil ratio and of pressure on the system, it can be concluded that the dependence of solubility on temperature should be consistent across a range of different systems. It should of course be noted that different oil types, and even different sources of the same oil type, will inevitably show variations in their capacities to dissolve methanol (Čerče *et al.*, 2005).

In the context of the reactors used in Chapter 5, the data here would suggest that the temperature ranges used should be within a single-phase regime at the reactor entrance. Thus, initial conversion should be unaffected by the need for phase interaction.

References

ANDREATTA, A. E., CASÁS, L. M., HEGEL, P., BOTTINI, S. B. & BRIGNOLE, E. A. 2008. Phase Equilibria in Ternary Mixtures of Methyl Oleate, Glycerol, and Methanol. *Industrial & Engineering Chemistry Research,* 47**,** 5157-5164.

ATAYA, F., DUBÉ, M. A. & TERNAN, M. 2007. Acid-Catalyzed Transesterification of Canola Oil to Biodiesel under Single- and Two-Phase Reaction Conditions. *Energy & Fuels,* 21**,** 2450-2459.

BOOCOCK, D., KONAR, S. & SIDI, H. 1996. Phase diagrams for oil/methanol/ether mixtures. *Journal of the American Oil Chemists' Society,* 73**,** 1247-1251.

ČERČE, T., PETER, S. & WEIDNER, E. 2005. Biodiesel-Transesterification of Biological Oils with Liquid Catalysts: Thermodynamic Properties of Oil−Methanol−Amine Mixtures. *Industrial & Engineering Chemistry Research,* 44**,** 9535-9541.

CHIU, C.-W., GOFF, M. J. & SUPPES, G. J. 2005. Distribution of methanol and catalysts between biodiesel and glycerin phases. *Aiche Journal,* 51**,** 1274-1278.

DASARI, M. A., GOFF, M. J. & SUPPES, G. J. 2003. Noncatalytic alcoholysis kinetics of soybean oil. *Journal of the American Oil Chemists Society,* 80**,** 189-192.

DUNN, R. O. & BAGBY, M. O. 1994. Solubilization Of Methanol And Triglycerides - Unsaturated Long-Chain Fatty Alcohol Medium-Chain Alkanol Mixed Amphiphile Systems. *Journal of the American Oil Chemists Society,* 71**,** 101-108.

KNOTHE, G., VAN GERPEN, J. & KRAHL, J. 2005. *The biodiesel handbook,* Urbana, Ill., AOCS Press.

LIU, X., PIAO, X., WANG, Y. & ZHU, S. 2008a. Liquid–Liquid Equilibrium for Systems of (Fatty Acid Ethyl Esters + Ethanol + Soybean Oil and Fatty Acid Ethyl Esters + Ethanol + Glycerol). *Journal of Chemical & Engineering Data,* 53**,** 359-362.

LIU, X., PIAO, X., WANG, Y. & ZHU, S. 2009. Model Study on Transesterification of Soybean Oil to Biodiesel with Methanol Using Solid Base Catalyst†. *The Journal of Physical Chemistry A,* 114**,** 3750-3755.

LIU, Y., LU, H., LIU, C. & LIANG, B. 2008b. Solubility Measurement for the Reaction Systems in Pre-Esterification of High Acid Value Jatropha curcas L. Oil. *Journal of Chemical & Engineering Data,* 54**,** 1421-1425.

MAHAJAN, S., KONAR, S. & BOOCOCK, D. 2007. Variables Affecting the Production of Standard Biodiesel. *Journal of the American Oil Chemists' Society,* 84**,** 189-195.

NARVÁEZ, P., SÁNCHEZ, F. & GODOY-SILVA, R. 2009. Continuous Methanolysis of Palm Oil Using a Liquid–Liquid Film Reactor. *Journal of the American Oil Chemists' Society,* 86**,** 343-352.

NOUREDDINI, H. & ZHU, D. 1997. Kinetics of transesterification of soybean oil. *Journal of the American Oil Chemists' Society,* 74**,** 1457-1463.

RESA, J. M., GONZÁLEZ, C., FANEGA, M. A., ORTIZ DE LANDALUCE, S. & LANZ, J. 2002. Enthalpies of mixing, heat capacities, and viscosities of alcohol (C1–C4) + olive oil mixtures at 298.15 K. *Journal of Food Engineering,* 51**,** 113-118.

STAVARACHE, C., VINATORU, M., NISHIMURA, R. & MAEDA, Y. 2005. Fatty acids methyl esters from vegetable oil by means of ultrasonic energy. *Ultrasonics Sonochemistry,* 12**,** 367-372.

ZHOU, H., LU, H. & LIANG, B. 2006. Solubility of Multicomponent Systems in the Biodiesel Production by Transesterification of Jatropha curcas L. Oil with Methanol. *Journal of Chemical & Engineering Data,* 51**,** 1130-1135.

Chapter 5 Continuous Reactors

In this chapter, the use of structured heterogeneous catalysts for transesterification is considered. First, a few examples are provided of other work on continuous biodiesel production. Then the catalyst developed in Chapter 3 is tested in a single channel reactor, and further developed as needed. Finally, the peformance of the improved catalyst in a larger, multi-tubular reactor rig is explored. This provides both additional data, and demonstrates the possibility of scaling up such a continuous catalytic process.

5.1 Introduction

Bournay *et al*. (2005a) developed a zinc aluminate catalytic system that is now used in the commercialised industrial Esterfip-H process. As of 2007, the process was used in plants across Europe at a total capacity of 1.3 million tonnes year^{-1}, with more being commissioned in both North America and Asia (Marshall, 2007). This process produces high purity products, with almost 100% conversion, 99% FAME purity, and 98% glycerol purity (Ondrey, 2004). The apparent lack of water tolerance (Bournay *et al.*, 2005b), and the lack of information about FFA leads one to conclude that high purity, and thus presumably higher cost, feedstocks are required. The process involves two fixed-bed reactors loaded with extruded catalysts, operates at 190-210°C and 40-70 bar, a methanol oil ratio of roughly 30:1, and a residence time of around 2 hours (Bournay *et al.*, 2005b).

On a smaller scale, the McGyan process (McNeff *et al*., 2008) has been developed to pilot-plant stage, producing around 13,000 tonnes year^{-1} (Anthony, 2009). This process uses supercritical methanol over a spherical zirconia catalyst in a packed bed at high temperatures (up to 360°C) and pressures (up to 160 bar), and is extremely tolerant of both water and FFA (Krohn *et al*., 2011). It remains to be seen how competitive a process using supercritical conditions will be, as it inherently will require higher capital and operating costs, although the residence time of 30 s (Krohn *et al*., 2011) should help minimise the required reactor size.

At a laboratory scale, Xiao *et al*. (2010) report the use of KF on Ca-Mg-Al hydrotalcite in the transesterification of palm oil, maintaining a conversion over 98% for 8 h at 1.6 ml min^{-1}, using isopropyl ether as a co-solvent. The reduced mass transfer limitations allowed for simpler modelling of the reactor kinetics.

Kim *et al.* (2011) report the use of a packed bed filled with $CaO\text{-}CeO_2$ on La_2O_3. The rig is operated at 80°C and 6.8 atm., with a methanol:oil ratio of 12:1 and a residence time of 73 minutes. This system achieved a yield of 88-90% over the course of 200 hours, with leaching reduced to acceptable levels after 144 hours.

Another laboratory scale reactor was constructed by Asli (2011), and was used to test zinc proline coated monoliths. The reaction was primarily performed at a flow rate of 0.11 ml min^{-1} oil, a 12:1 oil: methanol ratio, and at 195°C and 20 bar. Unfortunately the catalyst suffered from excessive leaching, and rapidly lost activity.

5.1.1 Summary

Although there is a wealth of literature on heterogeneous catalysts for biodiesel production, far fewer works were found that utilised them in a continuous reactor. The main issues to consider are achieving an adequate residence time, and avoiding catalyst leaching. Continuous reactors can reveal much more about the robustness of the catalyst than batch experiments.

5.2 Single Channel Monolithic Reactor

Previous work within the group at the University of Bath (Asli, 2011) resulted in the design and construction of a continuous fixed bed reactor, which consisted of a vertical heated tube that could be loaded with monolith pieces, two HPLC pumps for the oil and methanol, and a back-pressure valve to ensure the vaporisation of methanol was supressed. The reactor was operated at a flow rate of between 0.1 and 2.9 mL min^{-1}, and was designed to hold a monolith section as long as 400 mm. A schematic of the reactor is given in Figure 5.1.

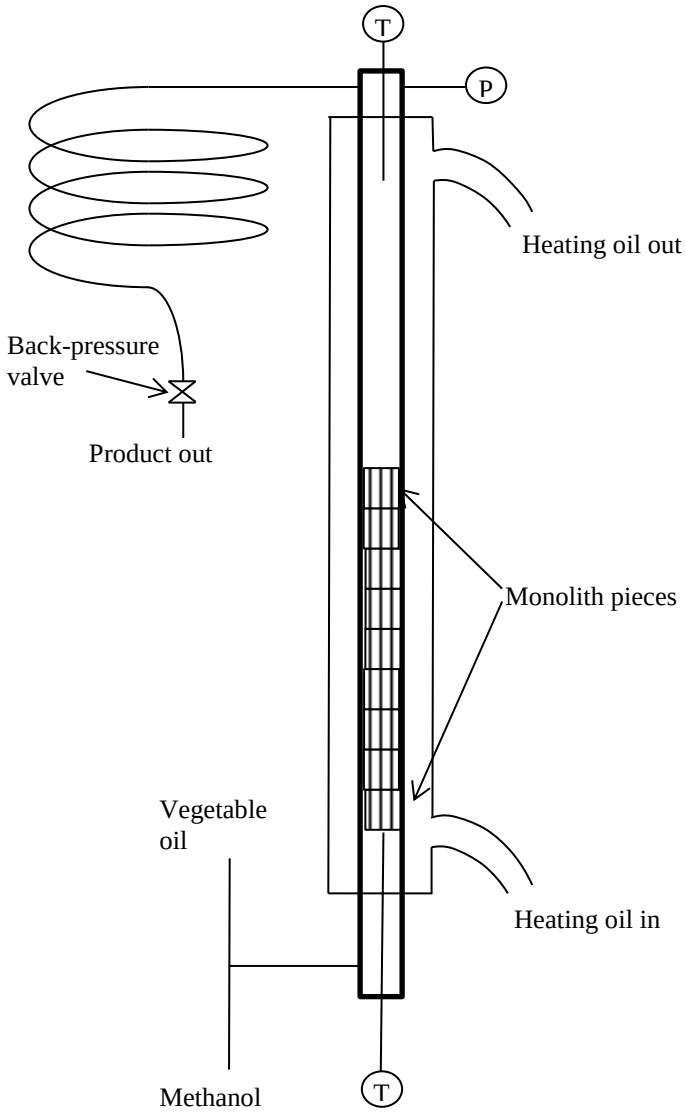

Figure 5.1 Continuous reactor schematic diagram.

The reactor section was built from 3/8” (9.5 mm) stainless steel tubing, with an internal diameter of 6.1mm. The reaction section was heated by an oil jacket supplied by a heating oil bath with a pump delivering 7 L min^{-1} of heating oil. After the reactor outlet, the product was passed through a 1/8” (3.2 mm) diameter cooling coil before the back pressure valve. A picture of the reactor is shown in Figure 5.2.

Figure 5.2 Continuous reactor, with view of loaded monolith inside the reactor at top right.

5.2.1 General Procedures

As discussed in Section 2.2, a 6:1 molar ratio of methanol and oil is considered sufficient to drive the transesterification reaction to completion, and thus was chosen for the batch experiments. However, this ratio is more difficult to attain across the range of discrete settings available on the pumps of the continuous reactor, and thus a volumetric ratio of 0.3:1 was chosen, which corresponds to a molar ratio of 7.14:1.

The reactor was operated according to the following procedures:

<u>Loading and set-up</u>

- The bottom fitting of the reactor was removed, allowing access to the reactor tube;
- Catalysts were loaded into the bottom of the reactor – the top and bottom of the catalyst section was capped with a small piece of quartz wool to protect the back-pressure valve from any particles that had broken off from the catalyst, with a blank monolith piece to hold it in place;
- The bottom fitting of the reactor, complete with thermocouple, was placed back onto the reactor, with the thermocouple holding the monoliths in the reactor.

<u>Start-up</u>

- The back-pressure valve was fully opened;
- The reactor was charged with methanol, using the "prime" feature on the pump, until liquid began to drip from the outlet;
- The back-pressure valve was then adjusted until the operating pressure of had been reached (usually 20 bar);
- The methanol pump was then turned off;

- The pumps were then started at an initial flow rate of 1 ml min^{-1} oil and 0.3 ml min^{-1} methanol;
- The oil heater was turned on, and set at the desired reaction temperature;
- Once the temperature had been reached, the reactor was left for at least 70 minutes (roughly three times the residence time of the reactor) to allow the methanol:oil ratio within the reactor to establish at the desired conditions.

Reaction and sampling

- Once the start-up sequence was complete, a sample at the initial flow rate of 1 ml min^{-1} oil and 0.3 ml min^{-1} methanol was taken, if desired;
- The flow rate or temperature were then changed to the desired values for the next experiment, after which the reactor was left for at least one residence time, to establish steady-state;
- Samples were taken by removing the product reservoir, and placing a sample vial under the outlet to catch the product;
- Samples were then processed by GC, as described in Section 3.1.1
- Reaction conditions were then changed again for the next sample, if desired.

Shut down

- After the final sample, the product reservoir was replaced, and the heater turned off;
- The oil and methanol pumps were then turned off;
- The methanol pump was put on "prime" to flush out the remaining reaction mixture for 5-10 minutes;

- The methanol pump was then turned off, and the reactor left to cool.

Results were converted to mol %, as described by Equation (3.1). Further to this, the conversion of triglyceride was calculated from these values using the following equation:

$$X = \left(1 - \frac{mol\%_{TG}}{mol\%_{TG} + mol\%_{DG} + mol\%_{MG} + mol\%_{Gly}}\right) \times 100 \quad (5.1)$$

Where:

X = conversion of triglycerides, %

TG, DG, MG, and Gly represent tri-, di- and mono- glycerides, and glycerol, respectively.

5.2.2 Original Slurry Coated Monoliths

As mentioned in Section 1.6.2.3, SrO Method 3, wherein monoliths were coated with a slurry of $Sr(OH)_2$ and water, was chosen as a catalyst to test further in the continuous reactor. So, 20 monolith pieces from the original slurry-coated batch were placed in the continuous reactor, for a total weight of 2.70g, approximately 0.53g of which was the coating. The void volume of the reactor is calculated as follows:

$$V = \frac{\pi d^2}{4} z\varepsilon \quad (5.2)$$

Where:

V = Reactor volume (ml)

d = Reactor diameter (cm)

z = Reactor length (cm)

ε = Catalyst voidage

With a diameter of 0.62 cm, a length of 20 cm, and a voidage of 73.4%, the reactor has a fluid volume of 4.43 ml. The residence time within the reactor can then be calculated:

$$\tau = \frac{V}{\upsilon} \tag{5.3}$$

Where:

τ = Residence time within the reactor (min)

υ = Volumetric flow rate (ml min^{-1})

As an example, a flow rate of 1 ml min^{-1} oil and 0.3 ml min^{-1} methanol will have a residence time of 3.4 minutes in this case.

Initially, the reactor was run at 120°C, at flow rates of 1 ml min^{-1} oil and 0.3 ml min^{-1} methanol, which was then lowered to 0.5 ml min^{-1} oil and 0.15 ml min^{-1} methanol. The compositions of the resultant products are shown in Figure 5.3.

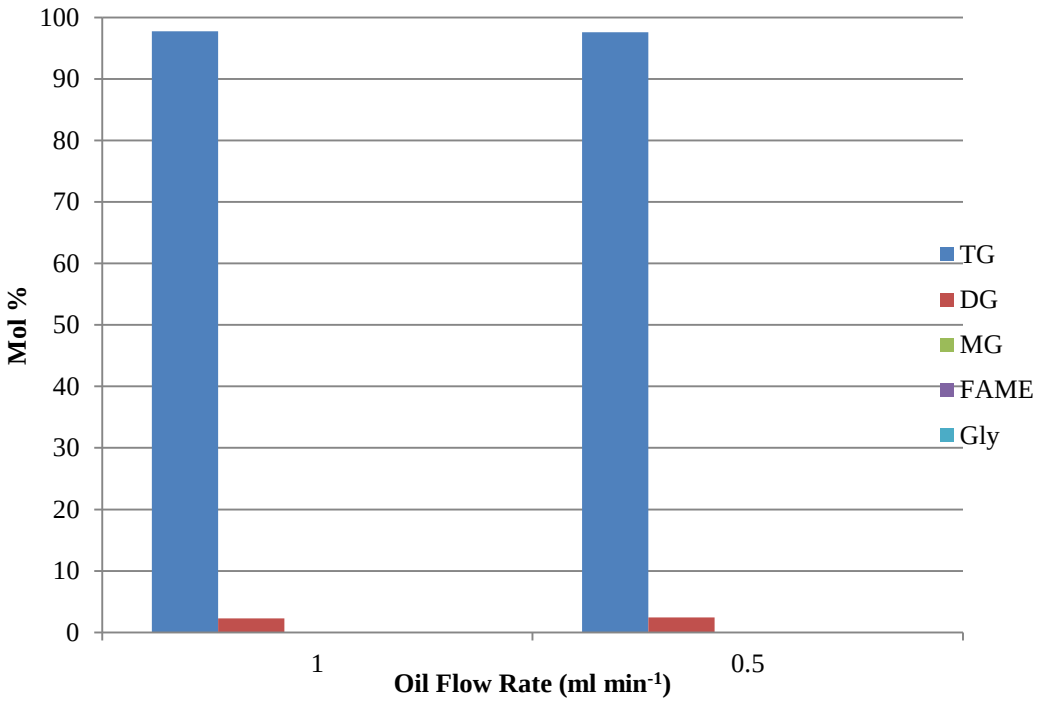

Figure 5.3 Initial continuous reaction results, first slurry coat, T = 120°C, P = 20 bar.

The conversion under these conditions clearly was insufficient for further study, and so the temperature was raised to 195°C, and the flow rates were lowered to 0.1 ml min^{-1} oil and 0.03 ml min^{-1} methanol – similar to the conditions used by Asli (2011) in the previous work with the reactor. A sample was taken at 1 ml min^{-1} oil, before the flow rate was reduced, and then after the reactor had run at 0.1 ml min^{-1} oil for sufficient time. The results of this are shown in Figure 5.4.

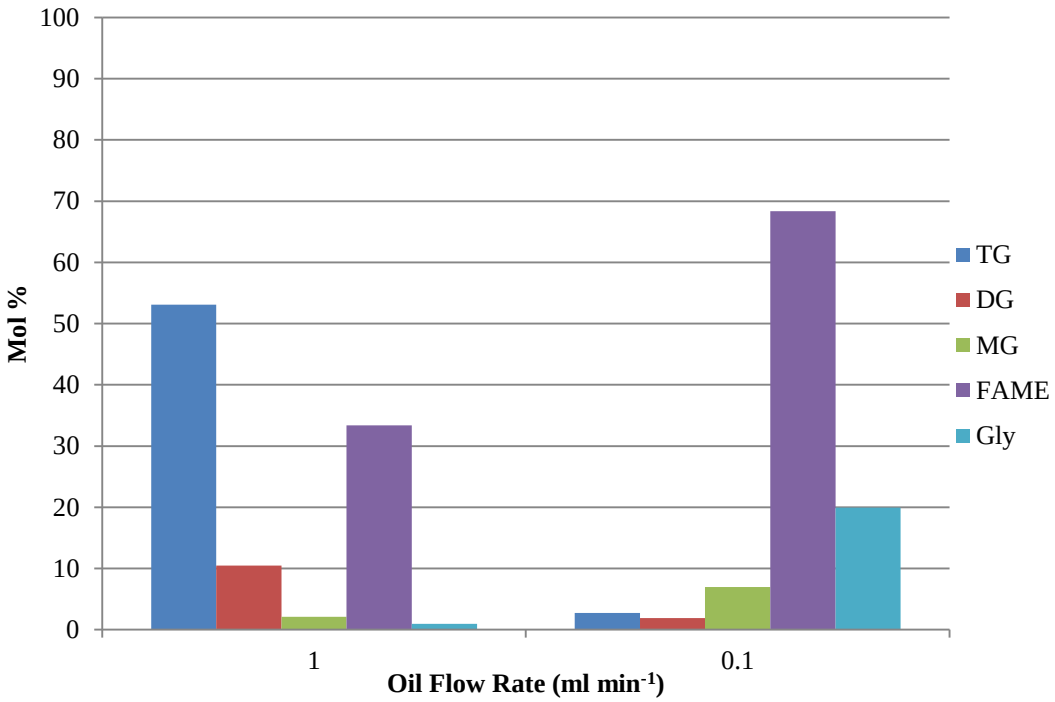

Figure 5.4 Initial continuous results, first slurry coat, T = 195°C, P = 20 bar.

Thus, it was decided that a flow rate of 0.1 ml min^{-1} oil at 195°C would provide a good baseline for reactions over time, while other conditions could be tested before returning to the baseline. The catalyst was tested over the course of 17 days, and the results of this are shown in Figure 5.5, with the intervals during which intermediate experiments were undertaken labelled. The reaction time was counted as the time for which the pumps and heater were online, and thus ignores the time spent between runs. At a flow rate of 0.1 mL min^{-1} oil and 0.03 mL min^{-1} methanol, this equates to a residence time within the catalytic section of about 34 minutes.

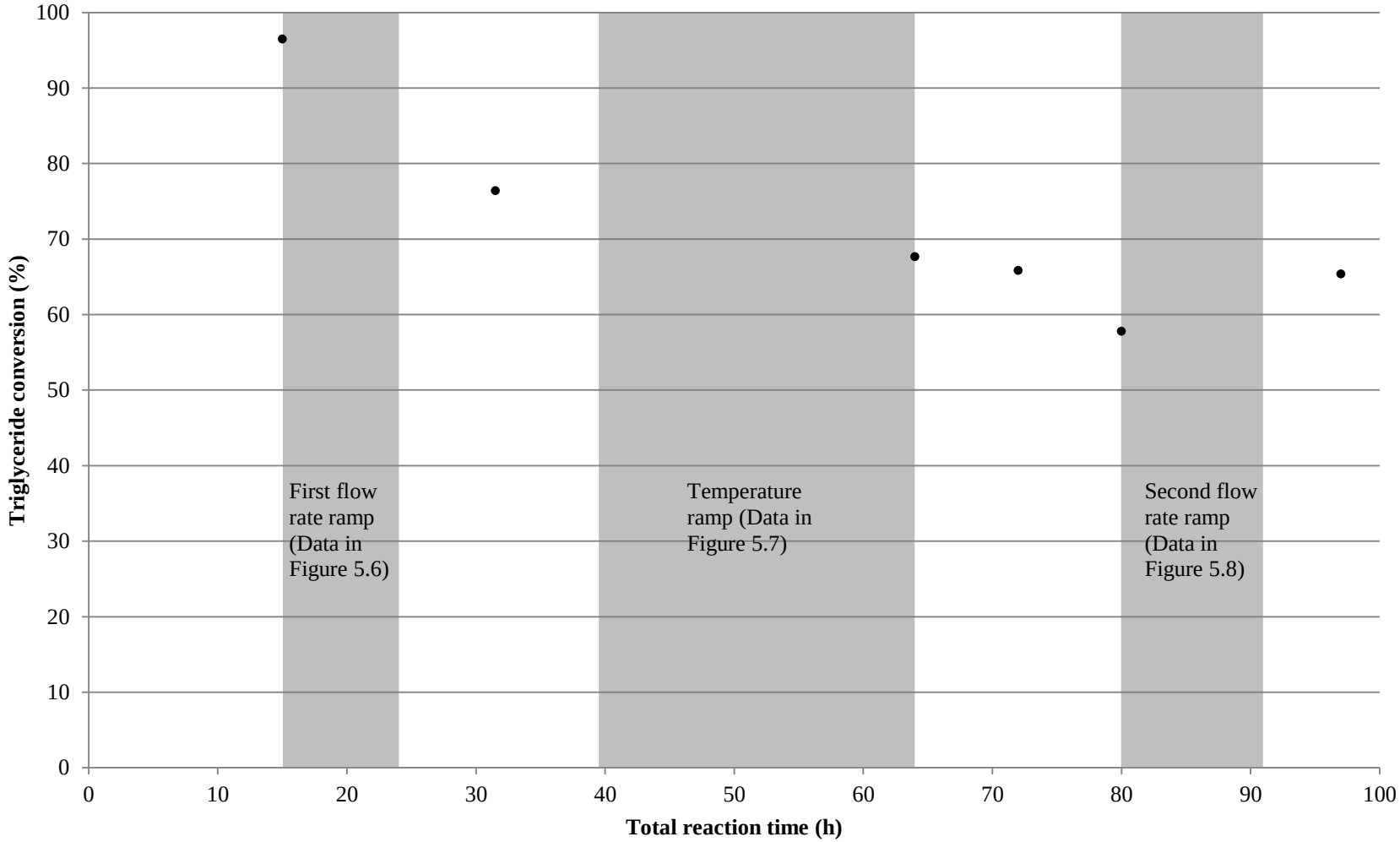

Figure 5.5 Conversion with total time on stream, 0.1 ml min^{-1} oil, T = 195°C, P = 20 bar.

5.2.2.1 First Flow Rate Ramp

In order to try and ascertain the effect of flow rate on conversion, the flow rate was increased over the course of two experimental days (i.e. with a shutdown stage included), from 0.1 mL min^{-1} to 0.7 mL min^{-1} oil. The results of this are shown in Figure 5.6.

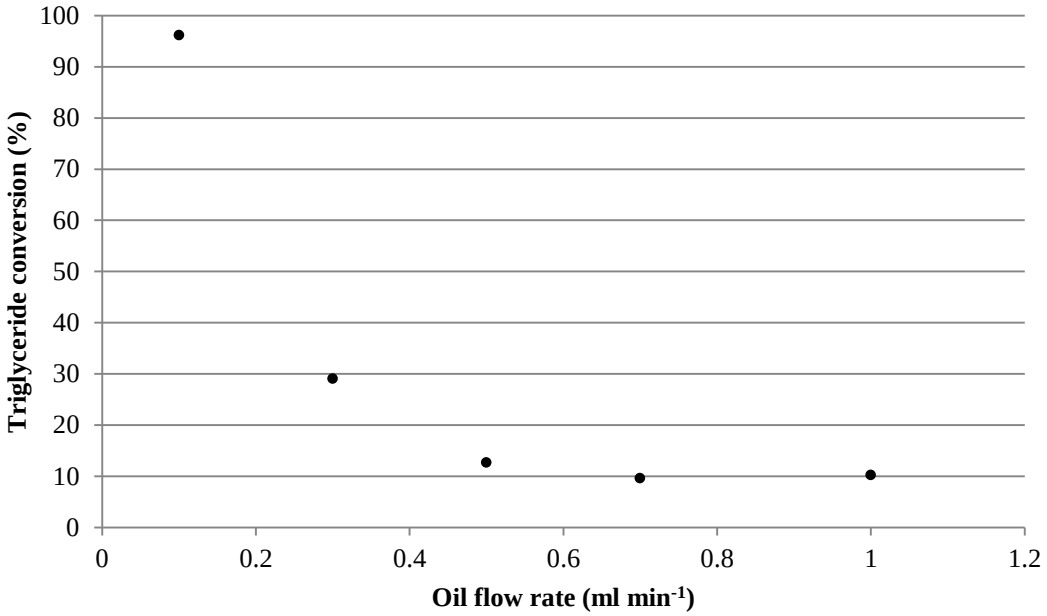

Figure 5.6 Effect of oil flow rate on conversion, T = 195°C, P = 20 bar.

There is a dramatic drop in conversion, which may be somewhat attributed to the drop in baseline activity as the catalyst aged, as seen in Figure 5.5. In order to better quantify the catalyst activity, the overall average reaction rate was obtained for each flow rate.

$$-r_{TG} = \frac{F_{TG,out} - F_{TG,in}}{z\, a_s} \tag{5.4}$$

Where:

r = Overall average reaction rate (mol m^{-2} s^{-1})

$F_{TG,\,in}$ = Molar flow of triglycerides at reactor inlet (mol s^{-1})

$F_{TG,\,out}$ = Molar flow of triglycerides at reactor outlet (mol s^{-1})

z = Length of reactor section (m)

a_s = Specific area of catalyst (m^2 m^{-1})

The specific area of the catalyst can be found by dividing the geometric external surface area of the monolith support, 3130 m^2 m^{-3}, by the cross-sectional area of the reactor tube:

$$a_s = \frac{a_g}{\pi \frac{d^2}{4}} \tag{5.5}$$

Where:

a_g = Geometric external surface area of the monolith (m^2 m^{-3})

Thus, with a diameter of 0.0061 m, the catalyst sections of the reactor have a specific area of 0.0915 m^2 m^{-1}. The average reaction rates for the range of flow rates are shown in Figure 5.7.

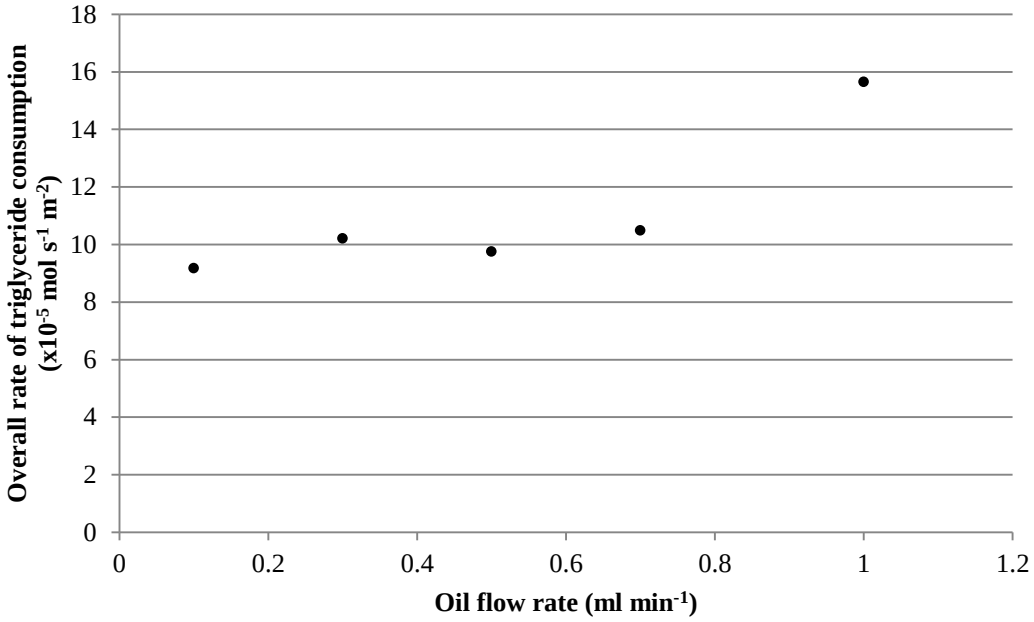

Figure 5.7 Overall average reaction rates at a range of flow rates, T = 195°C, P = 20 bar.

It would normally be expected that the overall reaction rate would increase with increasing flow rates, for two reasons. First, the higher flow rates would tend to improve mass transfer. Secondly, the shorter residence time at higher flows would result in less conversion, and thus a higher reactant concentration. This would increase the rate, assuming the reaction follows positive-order kinetics.

In this case, the reaction rate does not increase at oil flow rates of 0.5 and 0.7 ml min^{-1}. This unusual behaviour may be due to variability in catalyst activity, although it is also possible that other factors have an effect, such as the solubility and diffusivity of the components changing with composition. However, the general upward trend is seen, and so a second flow rate ramp was planned in order to ascertain the repeatability of this phenomenon.

5.2.2.2 Temperature Ramp

Temperature is of course a major factor in the rate of reaction, and so the temperature was varied over the course of four experimental runs. This was done between 140°C and 195°C at an oil flow rate of 0.1 mL min^{-1}, and the results are shown in Figure 5.8.

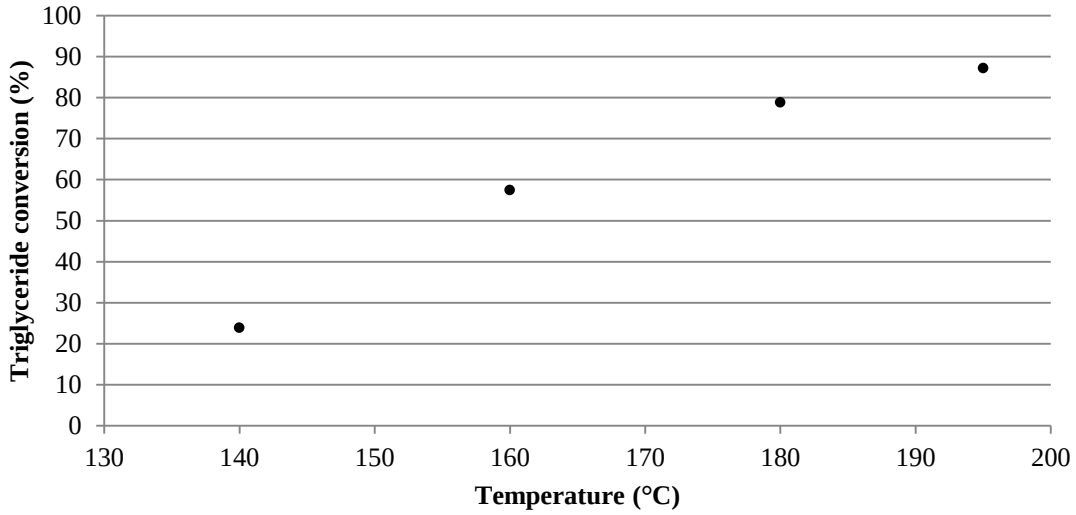

Figure 5.8 Effect of temperature on conversion, 0.1 ml min^{-1} oil, P = 20 bar.

Although the reactor was mostly operated at a fairly high temperature of 195°C, it is important to note that the catalyst is still active at lower temperatures. While it may be possible to design a reactor to operate in the lower temperature ranges, such a system would require a residence time much larger than the reactor used here.

The results from these experiments were also used to generate an Arrhenius plot, assuming that the reaction follows first order kinetics. The rate constants are found using the following equation, which is derived from Equation (5.4):

$$k = \frac{v}{z\, a_s} \ln\left(\frac{C_{TG,in}}{C_{TG,out}}\right) \tag{5.6}$$

Where:

k = Reaction rate constant (m s^{-1})

υ = Volumetric flow rate (m^3 s^{-1})

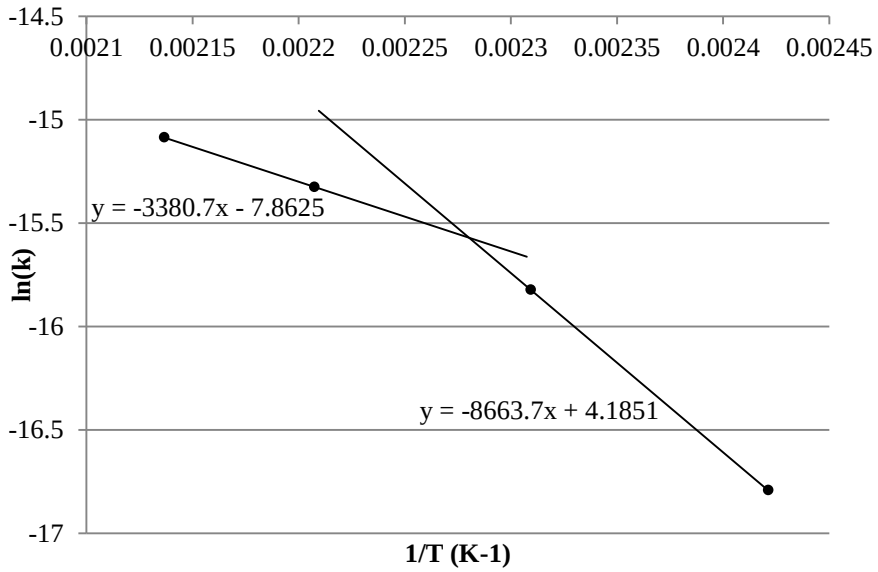

Figure 5.9 Arrhenius Plot for the temperature ramp experiments

The plot appears to show two separate trends, which would indicate a mass transfer controlled zone at lower temperatures, and a reaction controlled zone at higher temperatures. From the equation of the lines, for lower temperatures, the pre-exponential factor is 65.7 m s^{-1}, and the apparent activation energy is 72.0 kJ mol^{-1}, while at higher temperatures they are 0.000385 m s^{-1} and 28.1 kJ mol^{-1} respectively.

5.2.2.3 Second Flow Rate Ramp

A second flow rate ramp was undertaken once the catalytic activity appeared to have stabilised. The results are shown in Figure 5.10.

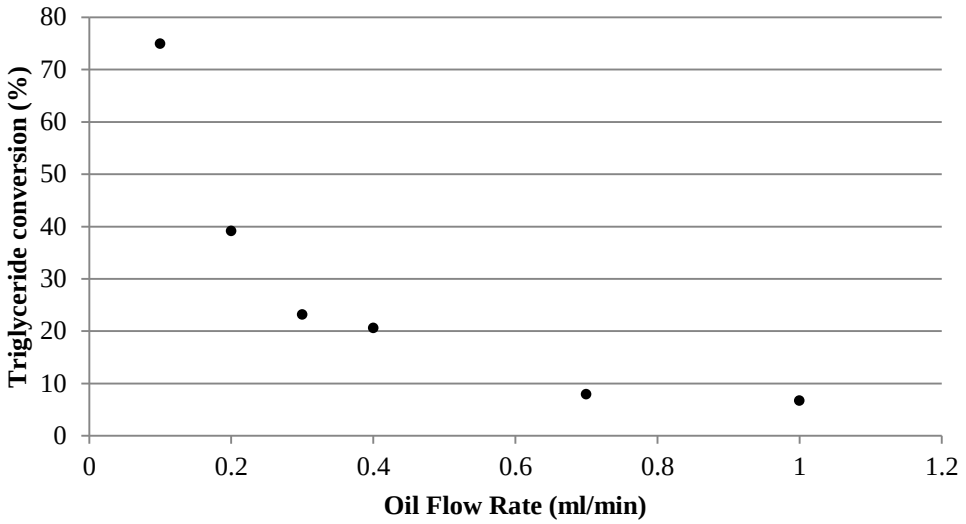

Figure 5.10a Effect of flow rate on conversion (second ramp), T = 195°C, P = 20 bar.

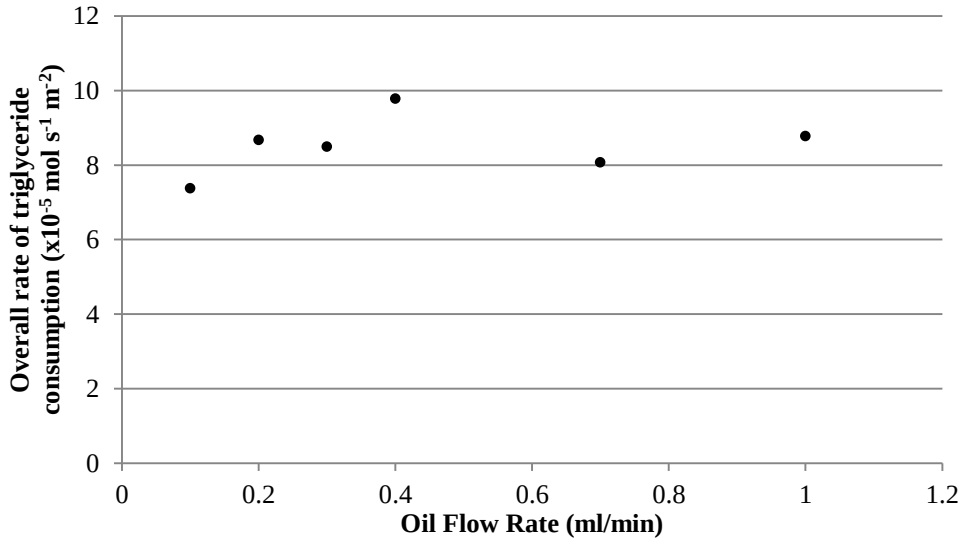

Figure 5.10b Effect of flow rate on reaction rate (second ramp), T = 195°C, P = 20 bar.

Unlike the first flow rate ramp experiment, there is a less dramatic drop in conversion with increased flow rate. However, the average reaction rate at 0.7 ml min^{-1} oil drops off, whereas it would normally be expected to be the highest. Again, this may be caused by variations in activity, but it appears that the positive effect of flow rate at lower conversions is counteracted by other factors.

5.2.3 Slurry Coat Development

As discussed earlier in Section 3.6.2.3, the slurry coating method suffered from a lack of mechanical stability, with the catalyst layer flaking away from the support under light handling. The separation of the coating layer from the monolithic support can be seen in Figure 5.11, as there are comparatively large gaps between the materials.

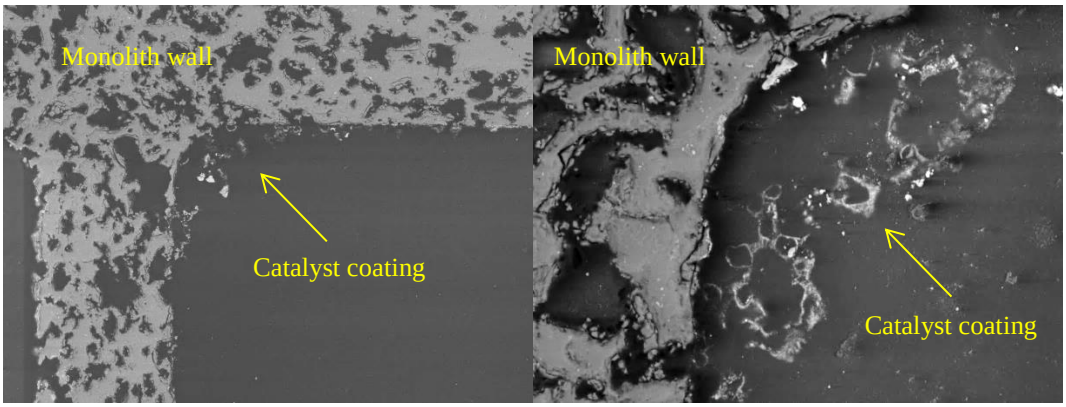

Figure 5.11 SEM images of slurry coating, showing lack of anchoring to the support.

Thus, the formulation of the slurry was refined in order to improve the adhesion of the coating:

- A 30 wt% $Sr(OH)_2$ slurry was ball milled, and was separated into four batches. To three of these were added silica gel (Sigma Aldrich) and/or titania nano-powder (<100 nm, mixture of anatase and rutile, Sigma Aldrich), up to a total of 3 wt%. One batch was left blank.

- The monoliths were then coated 3 times and calcined, according to the method described in Section 3.4.2.3.

- The monoliths were then placed into beakers of methanol and sonicated in an ultrasonic bath for five minutes.

- The monoliths were then rinsed in clean methanol, dried under a flow of nitrogen, and weighed to calculate the loss of material. The results are given in Figure 5.12.

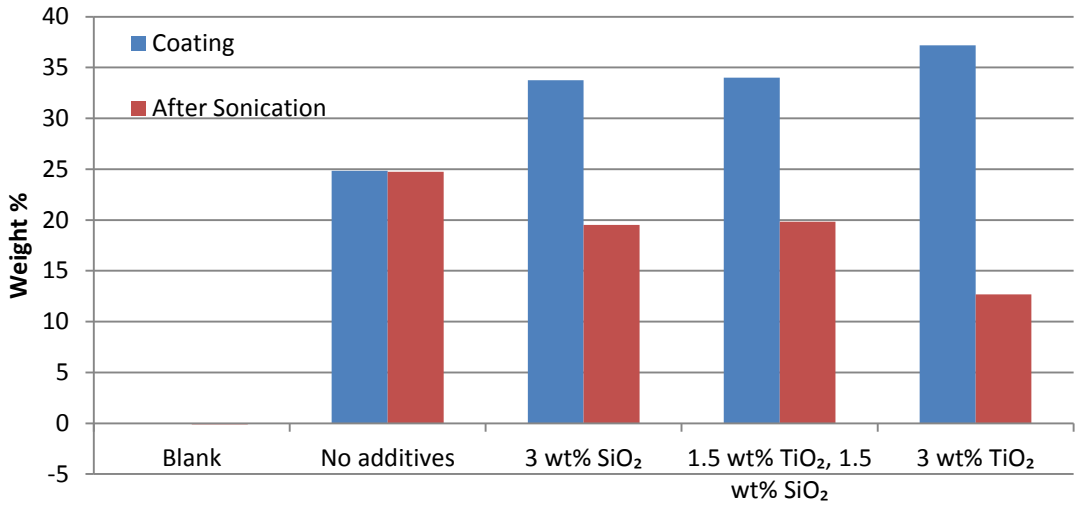

Figure 5.12 Slurry coat formulations mechanical testing.

The formulations with additives formed white coatings which flaked off easily upon contact, and clearly did not withstand sonication. The batch without additives was obviously the most stable, with minimal mass loss on sonication. Interestingly, this batch had the same appearance as uncoated monoliths (see Figure 5.13), raising the possibility of a chemical interaction between the cordierite and the coating. Additionally, this meant that there was no apparent coating to break away from the monolith. It was thus decided that a 30 wt% slurry of strontium hydroxide would be used with no additives for future monolith coatings.

Figure 5.13 Additive-free SrO coated monoliths.

5.2.3.1 Slurry Coat Repeatability

Monoliths coated with the improved method were checked to ensure they had this "uncoated" appearance. Although most did, occasional monoliths had a thick white layer after calcination. An example of this is shown in Figure 5.14. The cause of this appeared to be calcination temperature, as the monoliths were closest to the furnace inlet. Calcining these pieces a second time did not rectify the coating, as they remained white and fragile.

Figure 5.14 Improperly calcined monoliths.

It was hypothesised that the variable coating could be caused by either using a mixture of monoliths from different original blocks, or by variations in the extent of pre-coating desorption under hot air. Thus, monoliths were taken from two different blocks, and half of the pieces from each were treated with hot air before coating, with the rest not. The monoliths were then alternately placed in the furnace tube, so that the position in the furnace could be separated from the coating conditions. The results of this are given in Table 5.1.

Table 5.1 Coating results of different monolith conditions

Position in furnace	1	2	3	4	5	6	7	8	9	10	11	12
Monolith Block	A	B	A	B	A	B	A	B	A	B	A	B
Hot air treated	N	N	Y	Y	N	N	Y	Y	N	N	Y	Y
Coating result	W	W	W	W	M	M	G	G	G	G	G	G

Notes: G = Good coating, as desired; M = Mixed, with a gradient along the piece; W = White, with a fragile white coating. Furnace position is from the gas inlet of the furnace tube.

These results indicate that the furnace position is the influential factor in determining the quality of the catalyst coating. More monoliths from this same batch were stored under nitrogen and calcined at 710°C and 730°C, in order to discern if the initial temperature of the furnace tube caused the unsatisfactory coating. Neither of those later calcinations yielded satisfactory monoliths. This indicates that there is also a limited amount of time during which calcination should take place, although further work is needed to determine the direct cause of this.

As the coating is a manual procedure, small variances between dip-coating, channel clearing, and general handling are inevitable. Thus, a batch of monoliths was split into four lots of six pieces. These were then coated in the same slurry, calcined together and weighed. The resulting loadings are given in Table 5.2.

Table 5.2 Slurry coating repeatability

Lot	Monoliths (g)	Coated monoliths (g)	Coating weight %
1	0.64351	0.85791	24.99
2	0.62275	0.82001	24.06
3	0.63286	0.85503	25.98
4	0.63323	0.83572	24.23
		Average	24.82
		St. dev.	0.76

The catalyst loadings are quite consistent across a batch. This allows a degree of confidence that the availability of catalyst along the length of the reactor can be considered to be constant.

5.2.3.2 Catalyst Coating Location

Successfully coated monoliths were analysed by SEM. First, the monolith pieces were imbedded in resin, and then ground down to produce a cross-sectional sample of the material. An example of this is shown in Figure 5.15. A section of the sample was analysed by x-ray backscatter, and the Sr content is highlighted in red.

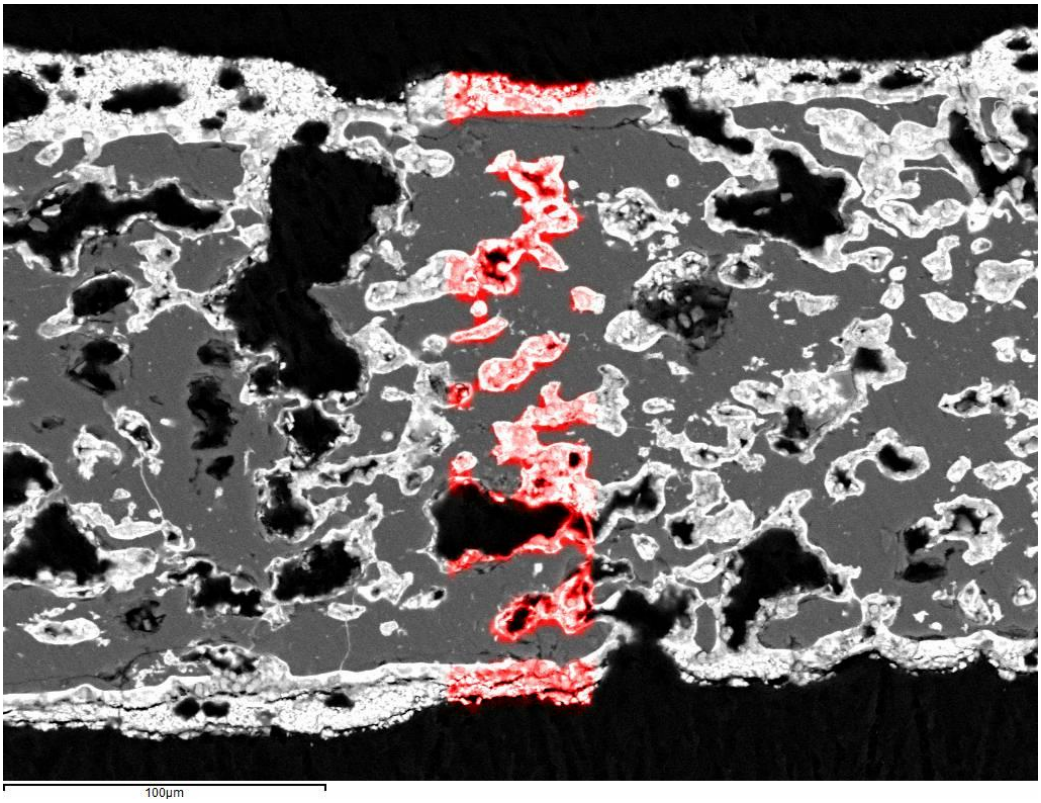

Figure 5.15 Cross section of monolith wall, with Sr highlighted from an area backscatter scan.

X-ray backscatter confirms that the white phase is strontium rich. The coating appears to be anchored very well to the support, which would be expected considering the performance of the coating in mechanical testing. Less expected, however, is the infiltration into the support by the strontium. The catalyst has coated the surfaces of many of the pores, presumably only missing those pores which were inaccessible.

5.2.4 Performance of Improved Slurry Coat

A batch of monoliths using this improved method was loaded into the reactor. Unfortunately, due to a few improperly coated pieces and breakage, only 18 pieces were available to put into the reactor. These had a total mass of 2.56g, and a strontium oxide content of approximately 0.64 g. The reactor was then operated at base conditions of 0.1 ml min^{-1} oil, 0.03 ml min^{-1} methanol, 195°C, and 20 bar, with intermediate experiments undertaken during the overall run. Under base conditions, the residence time was approximately 31 minutes. The results in terms of conversion of triglyceride during almost 300 hours of operation are shown in Figure 5.16.

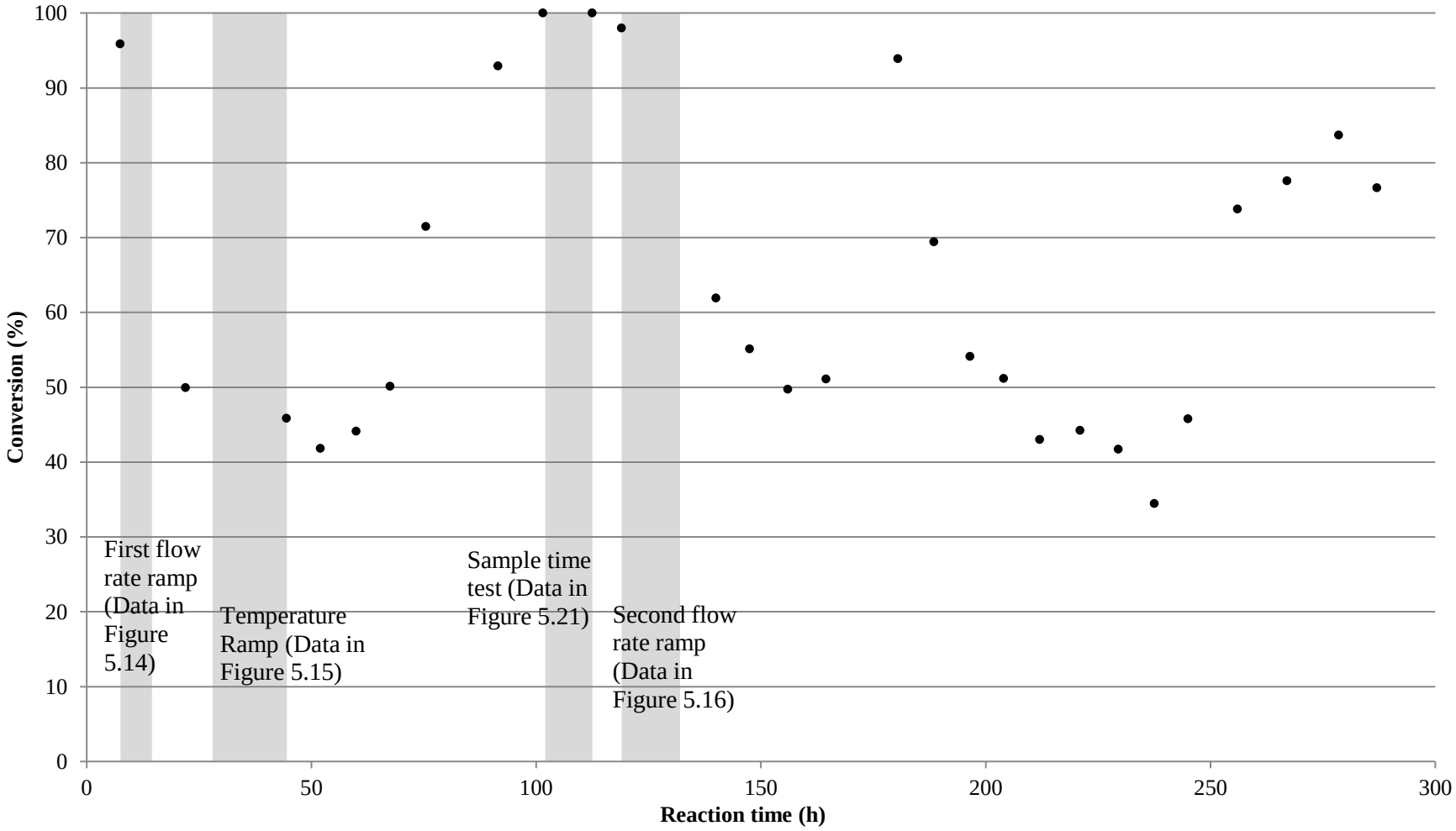

Figure 5.16 Improved slurry coat conversion with total time on stream, 0.1 ml min^{-1} oil, T= 195°C, P = 20 bar.

The most striking aspect of Figure 5.16 is obviously the repeated recovery and loss of catalytic activity. This unusual behaviour may be caused by a number of factors:

- First, the quality of the oil and methanol could have changed when the reservoirs were recharged. The most likely aspect of this that might influence the reaction is the water content of the feeds.

- A second cause could be the occurrence of leaching in some form of sequential manner – for example a species forming on the surface before becoming significantly unstable and dissolving into the liquid stream.

- A third possibility is experimental procedure – if the sample timing varied between individual runs, this may result in a variation in reactor output, depending on whether steady-state had been reached at the time of sampling. Although this would seem unlikely to produce non-random results, it is a possibility.

All of these factors were investigated, and are discussed in subsequent sections.

It was also hypothesised that operating the catalyst under low conversion conditions for prolonged periods (i.e. during the two flow rate ramps) contributed to activity loss. However, this would not explain initial activity, as the reactor was operated at 1 ml min^{-1} oil for the beginning of every run. However, as the experiment continues, it can be seen that it regains and loses activity twice more without the influence of flow-rate experiments.

5.2.4.1 First Flow Rate Ramp

The activity of the catalyst was investigated over a range of flow rates, using the first experimental run as a starting point. The flow rate was increased up to 1 mL min^{-1}, and the results are shown in Figure 5.17.

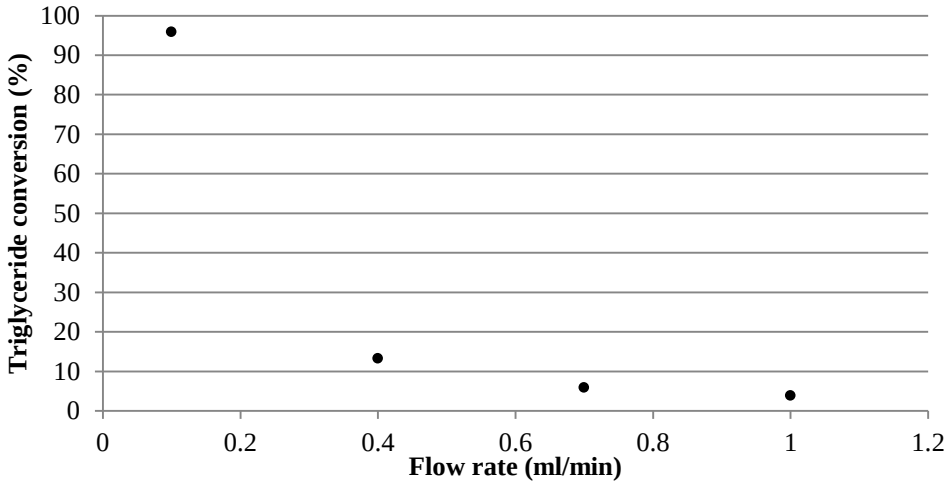

Figure 5.17a Effect of flow rate on conversion, T = 195°C, P = 20 bar.

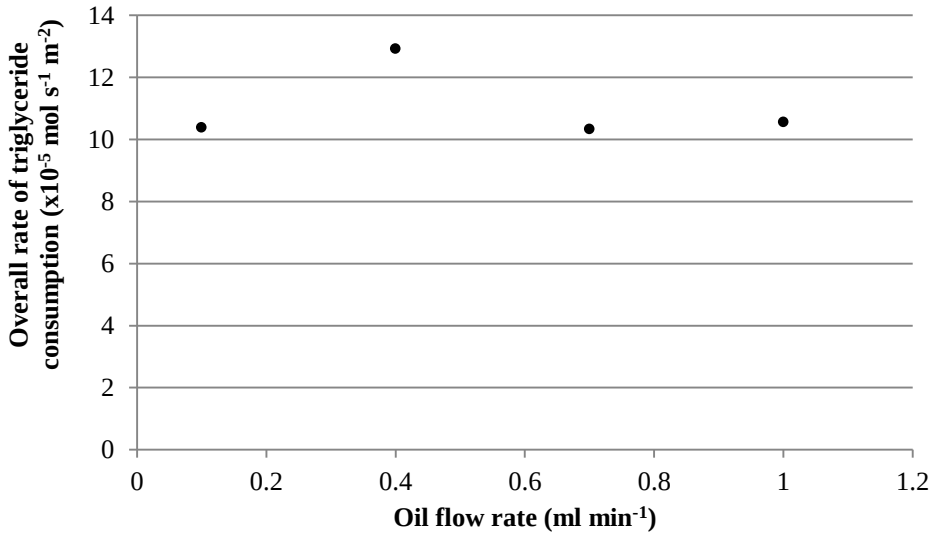

Figure 5.17b Effect of flow rate on overall rate, T = 195°C, P = 20 bar.

It should be noted that this experiment corresponds to the initial drop in catalytic activity seen in Figure 5.16. However, the trend seen with the original slurry coat is repeated – an initial increase in reaction rate with flow rate, which reduces at lower conversion.

5.2.4.2 Temperature Ramp

The effect of temperature on the activity of the catalyst was also observed by varying the temperature between 130°C and 195°C. The results of this are shown in Figure 5.18.

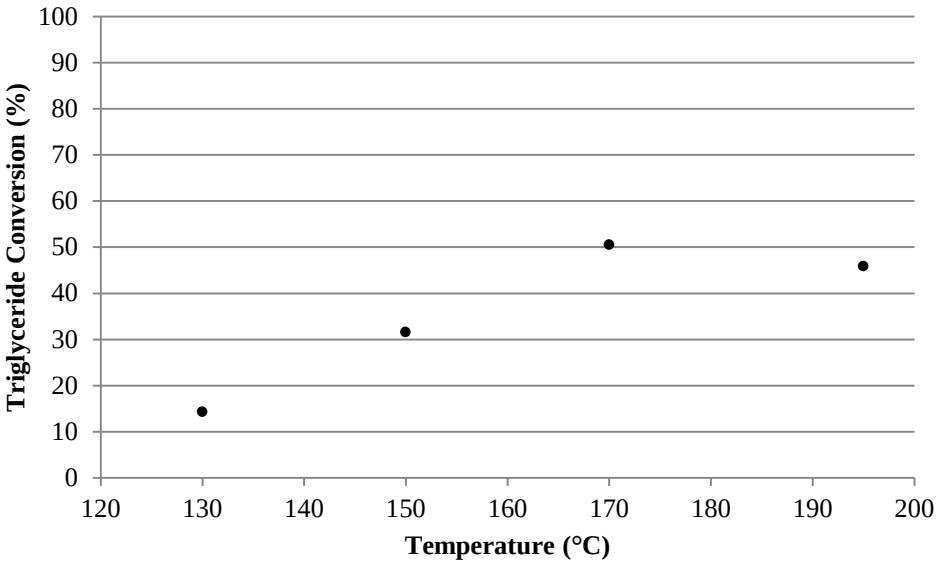

Figure 5.18 Effect of temperature on conversion, 0.1 ml min^{-1} oil, P = 20 bar.

The most notable aspect of this result is that the activity of the catalyst at 195°C appears out of line with the rest of the results. This seems to not simply be caused by a drop in the overall activity during this experiment, for two reasons. First, the other points increase in line with what one would expect to see from such an experiment. Secondly, comparing the activity prior to this experiment, as shown in Figure 5.16, the activity under the base conditions decreased only slightly, from a conversion of 50% to 45%. This also reveals that the activity at 170°C was higher than either at the start or the end of this experiment. It is possible that the catalyst regained and then lost some measure of its activity throughout this experiment.

As with the original slurry coat, the data was used to generate an Arrhenius plot:

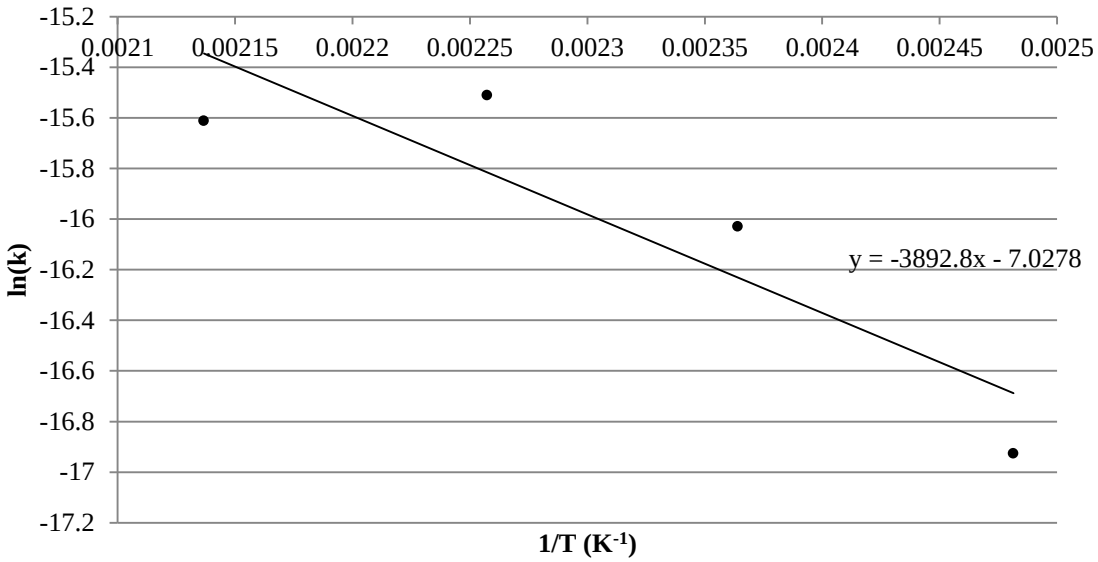

Figure 5.19 Arrhenius plot for the improved slurry coat

From this graph, the pre-exponential constant and the apparent activation energy are 8.87×10^{-4} m s^{-1} and 32.4 kJ mol^{-1}, respectively. However, considering that the result at 195°C appears to be a significant outlier, only considering the other three experiments gives a pre-exponential constant of 0.320 m s^{-1}, and an apparent activation energy of 52.7 kJ mol^{-1}, which are much more comparable to the values of 0.112 m s^{-1} and 49.7 kJ mol^{-1} from the original slurry coat. Indeed, the activation energies of the two catalysts are very similar.

5.2.4.3 Second Flow Rate Ramp

Once the catalyst had regained its activity, a second range of flow rates were tested. The results of this are given in Figure 5.20.

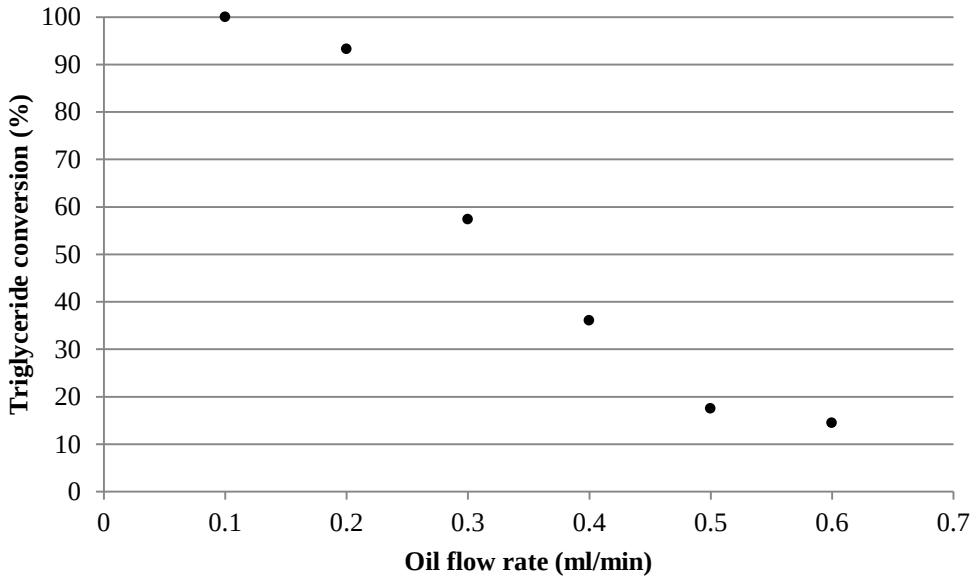

Figure 5.20a Effect of flow rate on conversion T = 195°C, P = 20 bar.

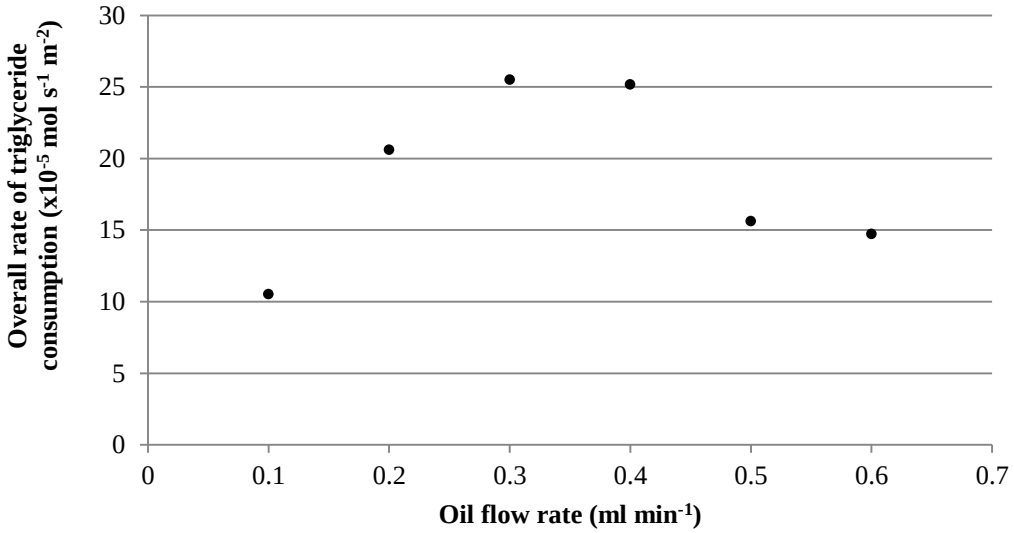

Figure 5.20b Effect of flow rate on reaction rate, T = 195°C, P = 20 bar.

The results indicate that there is an initial period at low conversion during which the rate of reaction is low, i.e. at 0.5 and 0.6 ml min^{-1} oil. After this, the rate increases substantially – and local reaction rates would rise even further, considering that the lower flow rates involve lower final triglyceride concentrations. This could be explained by a combination of factors. As triglyceride is converted, the bulk viscosity would decrease, and the diffusivity of the components would increase. Additionally, there would be reduced steric hindrance at the catalyst surface, as the amount of bulky triglycerides reduces.

It is possible that the increasing flow rate has an effect on the flow regime over the catalyst. However, it would be expected that this would improve mass transfer to the surface, and thus increase the reaction rate.

5.2.4.4 Effect of Water

In order to ascertain the effect of water on the catalyst activity, and to try to determine whether this was the cause of the variation in triglyceride conversion, selected product samples from the reactor were analysed using a Karl Fisher Titrator, follow the general procedure given in Section 3.1.2.3. The samples were shaken vigorously to mix the two phases as much as possible, and a 100 μL sample taken for titration. The results of these titrations are given in Figure 5.21.

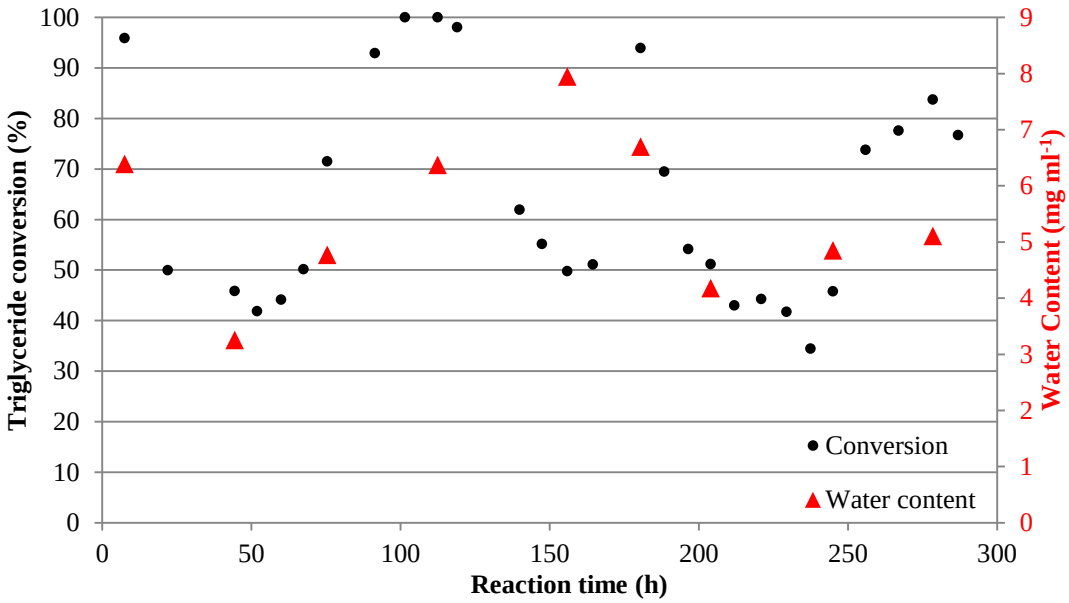

Figure 5.21 Conversion with time and water content of certain samples, 0.1 ml min^{-1} water, T = 195°C, P = 20 bar.

The presence of water in the product reached a maximum level of 8 mg ml^{-1}. For reference, the British Standard for biodiesel sold at a forecourt states that the maximum water content of the fuel is 500 mg kg^{-1} (BS EN 14214:2008 + A1:2009), or approximately 0.57 mg ml^{-1}. It should be noted that the reactor often contained more than 10 times this. Although it is likely that the majority of this water would separate into the methanol/glycerol phase after complete reaction, it is worth considering that an industrial process would need to remove the water at some point – either before or after the reaction. Thus it may be argued that this is an acceptable level of water tolerance for a transesterification catalyst.

The water content of the reaction mixture does not follow the same trend as the conversion, and would seem to be unrelated. Conversion plotted as a function of water content is given in Figure 5.22.

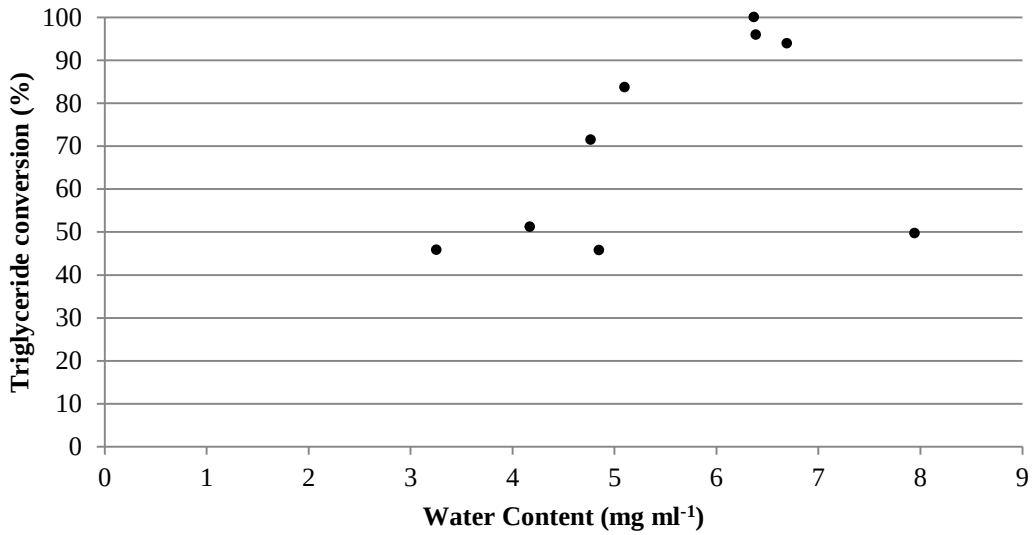

Figure 5.22 Triglyceride conversion as a function of water content.

Although there appears to be some kind of optimal water concentration, comparing this data with Figure 5.21 it can be argued that this may be a coincidence - because the water content was not random, but appears to have increased gradually in the reactant reservoirs until they needed to be filled, any overlap of the trends will create a correlation. However, taken in context, this correlation does not appear nearly as strong. The important fact demonstrated in Figure 5.22 is that the catalyst can operate with a moderate water content in the reactor, and does not appear to be inhibited by the increase up to 7 mg ml^{-1}.

Additionally, no evidence was found in the literature of water aiding a basic catalyst in the transesterification reaction, and it is widely reported that water is an inhibitor of the reaction. Indeed it would be expected that water would react with the SrO, and produce $Sr(OH)_2$, which would not revert to SrO under the experimental conditions. Thus water would be expected to cause permanent change to the catalyst activity, and almost certainly negative.

5.2.4.5 Catalyst Leaching

Another potential cause of activity variation could be the periodic release of a homogeneous catalyst species, and so the samples tested for water content, as well as a few others, were tested for strontium content, using inductively coupled plasma – optical emission spectroscopy (ICP-OES). Samples were prepared as follows:

- Samples were shaken vigorously, and a 1 ml aliquot was taken, added to an empty vial, and weighed;
- 3 mL of 65% nitric acid was added to the sample;
- The vial was closed, but vented slightly to prevent the build-up of pressure;
- The samples were then heated to 65°C and stirred for 24 hours;
- The vials were washed out 4 times with 10 ml of MilliQ water into a centrifuge vial;
- The samples were then centrifuged, and the aqueous supernatant removed and weighed;
- Standards were made from strontium nitrate and MilliQ water at strontium levels of 0.1, 0.5, 1, 5, 10, 50, 100, 500, and 1000 ppm (w/w);
- The aqueous samples were then analysed with a Varian Vista-Pro CCD Simultaneous ICP-OES, with the standards measured 4 times and the samples twice.

The results of the ICP-OES are given in Figure 5.23.

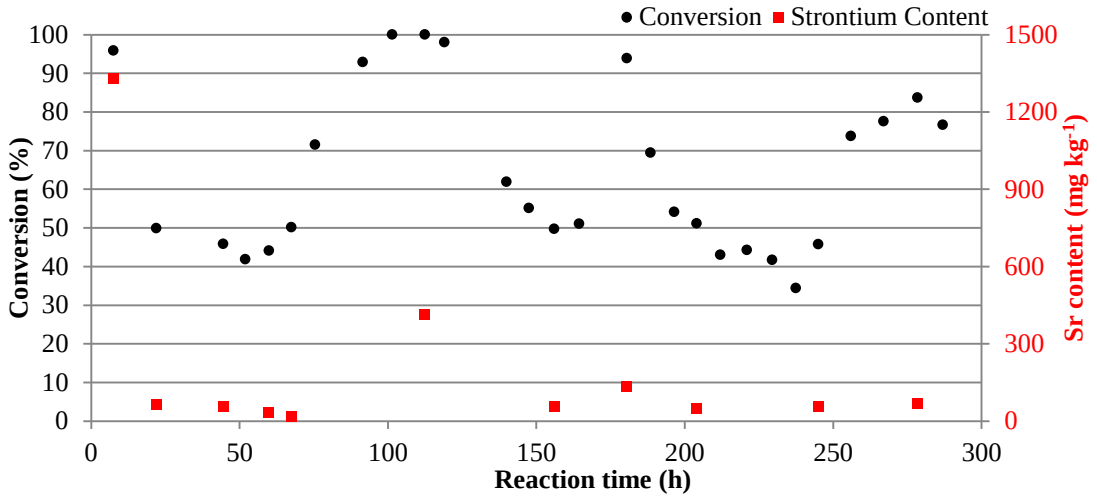

Figure 5.23 Strontium content of selected samples, plotted with conversion, 0.1 ml min^{-1} water, T = 195°C, P = 20 bar.

As can be seen in Figure 5.23, the leaching of the catalyst drops immediately after an initial high leaching, which can generally be expected from a fresh catalyst. There is a slight increase at 112 hours, which also corresponds to a high conversion. However, later activity increases do not correspond with a similar rise in leaching. It appears that the reaction is not dependent on the presence of a homogeneous strontium species, and can be considered to be heterogeneous. The mechanism of activity being regenerated as a result of leaching is not the case with this catalyst.

5.2.4.6 Sample Timing

The possibility that samples were taken at intervals in a way that contributed to the overall trend of activity as seen in Figure 5.16 was investigated by taking samples over a range of times, beginning approximately an hour earlier than was normally done, and extending over the course of about five hours. The results of this are shown in Figure 5.24.

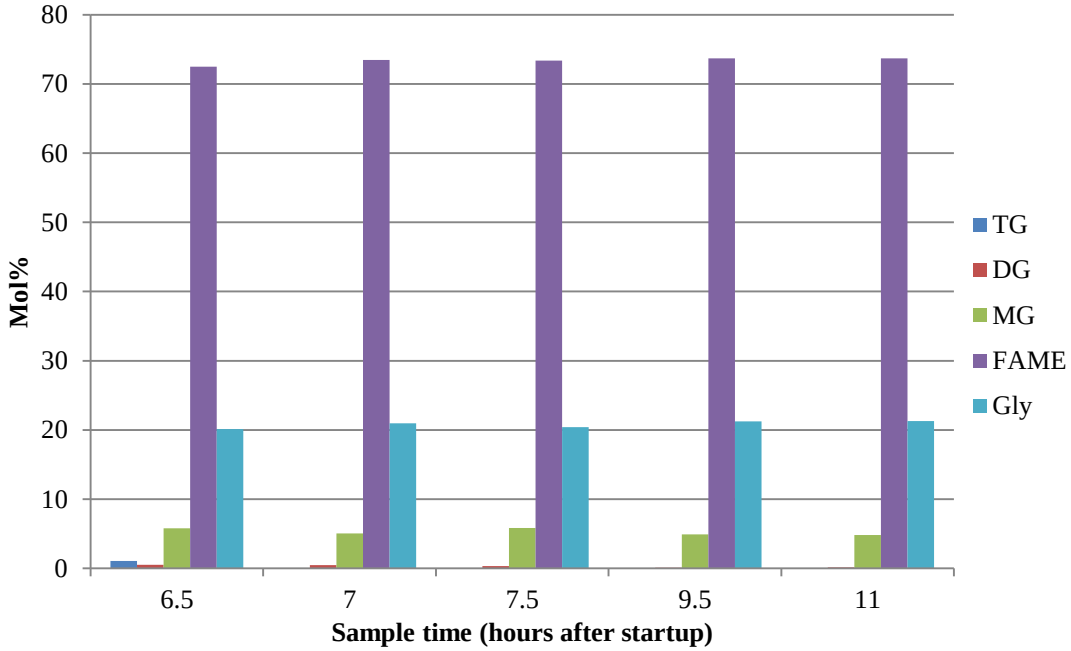

Figure 5.24 Continuous reactor products with sample time, T = 195, P = 20 bar.

As is clearly evident, there is no significant change in the end product with reaction time, and certainly no evidence of a change that could be related to the variation in catalyst activity.

5.2.4.7 Discussion of the Variable Activity

The potential experimental causes of the sequential loss and regeneration of catalytic activity discussed in Section 5.2.4 being ruled out, the question of the actual cause remains.

It is possible that the catalyst is inhibited by the potential adsorption of glycerol on the surface. This has been observed elsewhere in the literature (Xiao *et al.*, 2012). In such a case, it would be expected that the system would reach a steady state, where the formation, adsorption and desorption rates would reach equilibrium, reducing the overall activity of the catalyst from its maximum. However, due to the nature of the experiments, establishment of a steady state across multiple runs would be impossible. Thus, the proposed mechanism of the cyclic activity is as follows:

- Initially, the catalyst has no glycerol adsorbed to the surface, and the reaction rate is high
- The high reaction rate produces glycerol, some of which adsorbs to the surface.
- Subsequent experiments begin already inhibited by the glycerol, and thus have lower activities.
- As these experiments are not producing glycerol in similar quantities to the high conversion experiments, there is insufficient glycerol to replace desorbed molecules, and the catalyst regains its activity.
- These phenomena, combined with the methanol washing, and cooling and heating between each run, would make the system less likely to attain a steady operating condition.

5.2.5 Consideration of Experimental Errors

The primary sources of potential errors are considered here so that the reliability of the data presented may be considered.

Temperature

Temperatures in both the furnace and the reactor were monitored using type K thermocouples. These were calibrated in a professionally serviced thermocouple calibration furnace, and found to be accurate within 0.5°C across a range of temperatures. This would not affect the reliability of the results.

Flow rates

The flow rates of the HPLC pumps were calibrated by timed volume collection at experimental pressure into a 10 ml measuring cylinder with an accuracy of 0.2 ml, and were found to be accurate within this error. Additionally, sample collection size and time were noted throughout the experiments to guard against any change in pumping rates over time. This would not affect the reliability of the results.

Composition

The reaction compositions were monitored by GC. As shown in Section 3.1.1.2, the GC had a low standard deviation, 2.7% in the worst case. This would not affect the reliability of the results.

5.2.6 Interim Conclusions

- The slurry coating method developed in this chapter shows a great deal of promise, having maintained catalytic activity over a prolonged period of almost 300 hours of experimental runs, not including the time the apparatus was offline.

- The catalyst is capable of achieving complete conversion of triglycerides at 195°C and a residence time of just over half an hour. This is significantly shorter than the current industrial process, at similar conditions.

- This potential, however, is somewhat marred by the activity of the catalyst recovering at intervals. Although the cause of this activity is unknown, it appears to be an intrinsic property of the catalyst, and not caused by leaching or water content.

- In order to better analyse the catalyst, it would be helpful to track the reaction along the reactor bed. This would avoid the limitations of the single channel reactor, in that the flow rate effects cannot be separated from the changes in catalyst activity.

- A solution to this would be a reactor that allowed sampling along the bed length, which could provide insight into the activity of the catalyst, the effects of flow rate, and allow for these to be known at a single catalyst lifetime, which would compensate for any variability in catalyst activity.

5.3 Multiple Channel Monolithic Reactor

In previous work within the research group at the University of Bath, a multiple channel reactor was designed and built for the continuous production of pharmaceutical feedstocks (Al Badran, 2011). The basic design objectives of the reactor were to develop a scalable and flexible small pilot-scale process for the heterogeneous monolith-based catalysis of liquid phase reactants. The original design incorporated 10 parallel channels within a shared stainless steel heating jacket, although the rig was later modified into two separate reactors with five reactor tubes each.

The basic physical properties of the reactor are given in Table 5.3.

Table 5.3 Properties of the Multiple Channel Monolithic Reactor

Property	Value
Number of reactors	5
Single reactor dimensions	22mm i.d. x 550mm
Single reactor volume	235 mL
Design temperature	150°C
Design pressure	20 bar
Heating source	2x2 kW
Heating oil flow rate	8 L min-1
Heating oil pump maximum temperature	150°C

In order to effectively use the reactor for transesterification experiments, certain modifications were made:

- The autoclave used in Chapter 3 was used as a preheating and mixing device, in order to minimise the temperature gradients at the inlet of the reactor, and the formation of multiple phases.
- Sample valves were installed at the top of each reactor tube so that reactor profiles could be analysed.
- Thermocouples were installed at both ends of each reactor tube.

For the oil supply, a dosing pump rated up to 1.9 L min^{-1} with a 15 bar operating pressure was obtained (Liquid Metering Instruments), and the methanol pump used for the single channel reactor was used for the methanol. A piping and instrumentation diagram of the experimental rig is given in Figure 5.25, with a CAD drawing and a photograph of the reactor shown in Figure 5.26 and Figure 5.27, respectively.

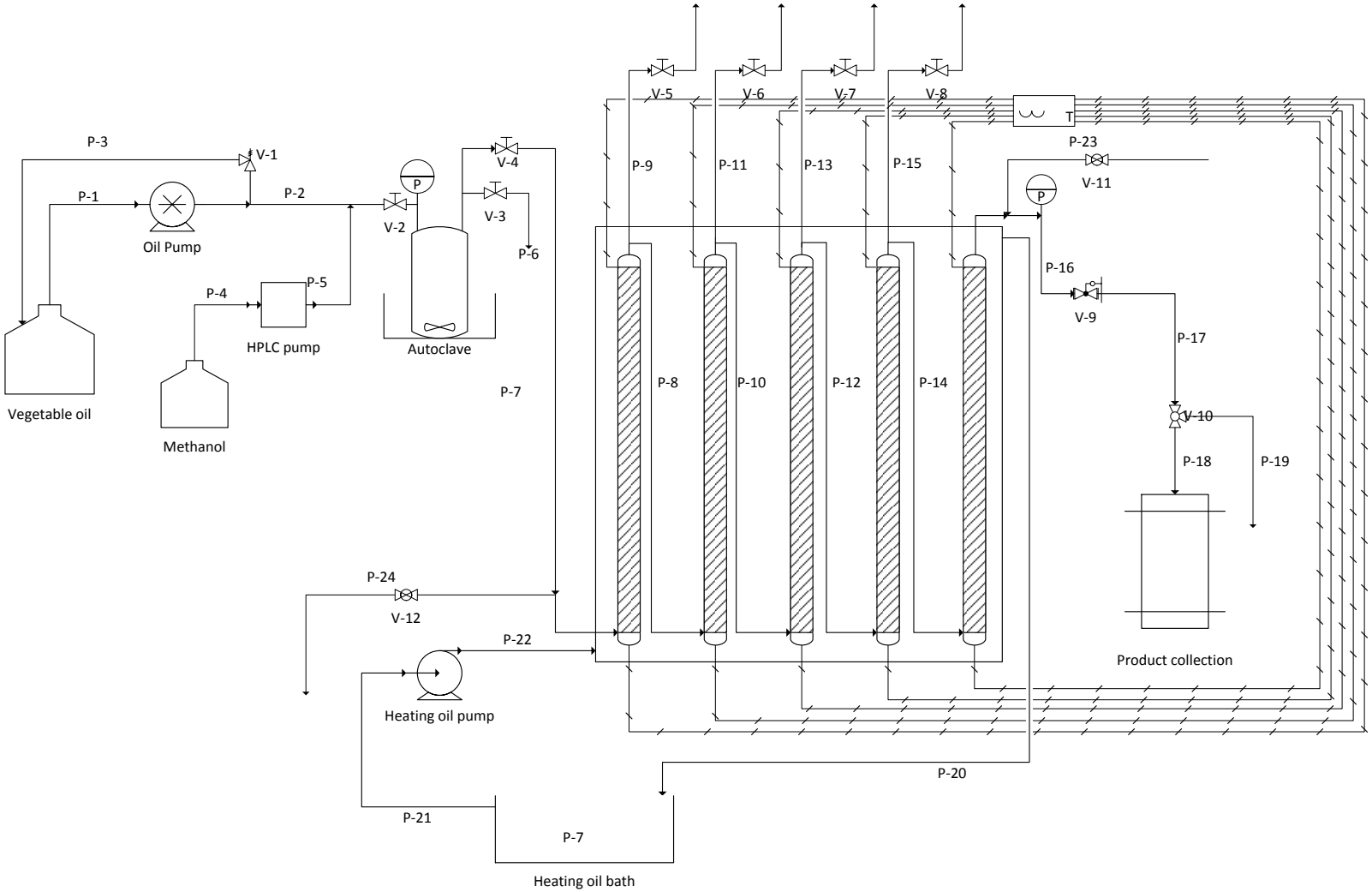

Figure 5.25 P&ID of the multiple channel reactor.

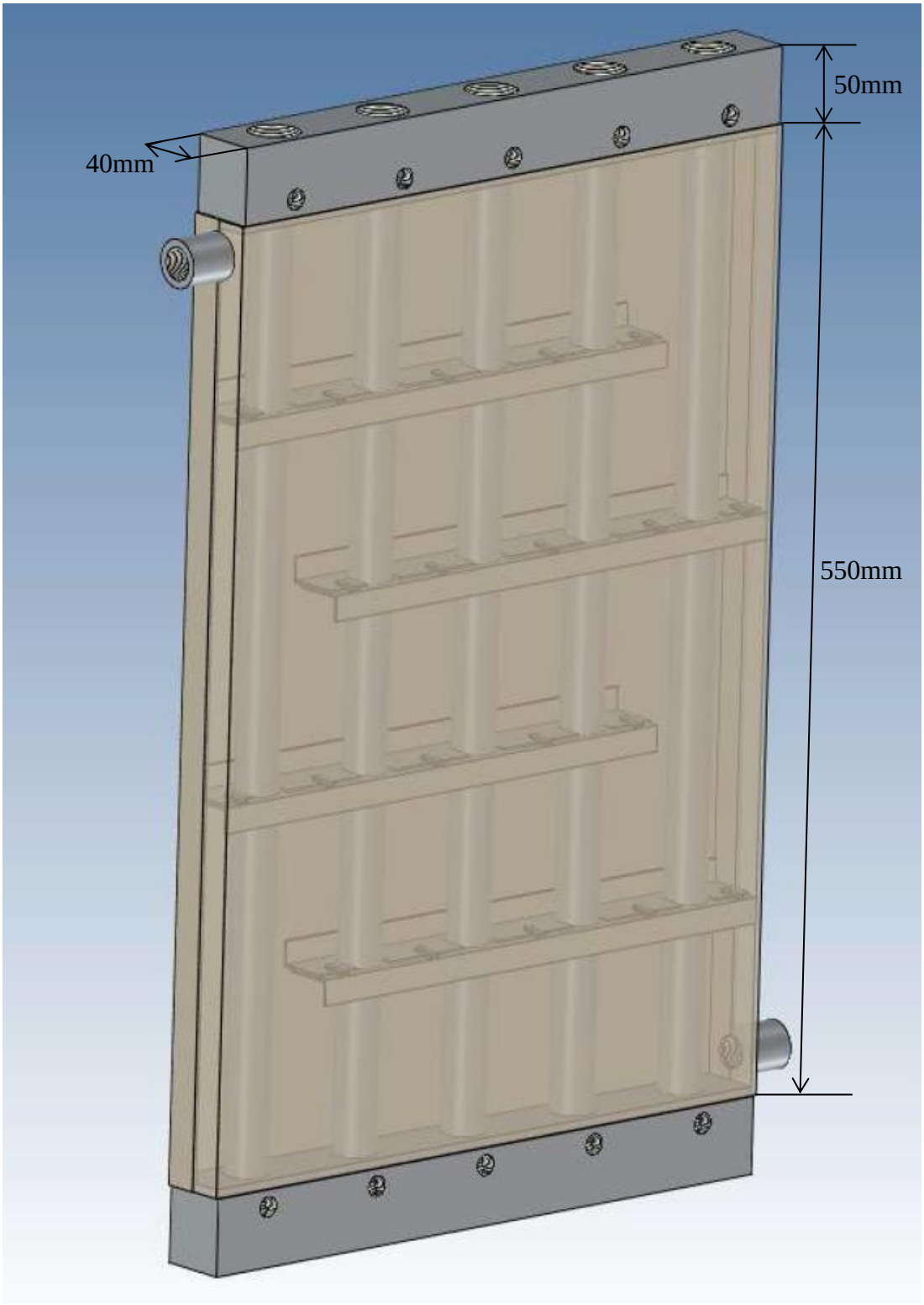

Figure 5.26 CAD drawing of multiple channel reactor, courtesy of S&C Thermofluids.

Figure 5.27 Photograph of uninsulated multiple channel reactor.

5.3.1 Residence Time Distribution

Residence time distribution (RTD) analysis was undertaken to develop some understanding of the fluid behaviour in the multiple channel reactor. The analysis was carried out on the reactor both with and without the monolith, in order to allow for the effects of the monolith to be observed. The experiment was carried out as described below, following the general procedure described by Levenspiel (1999).

- The thermocouple at the inlet of the reactor was replaced with an injection septum, and the outlet of the reactor was connected directly to a YSI in-line conductivity meter connected to a YSI Conductivity Instrument.
- Reverse-osmosis purified water was then pumped through the reactor at the desired flow rate, and the conductivity monitored until it fell to a stable level, at which point it was assumed that any contaminants had been flushed out of the reactor.
- Once the conductivity had stabilised, 1 mL of 200 mg mL^{-1} KCl solution was injected into the port at the bottom of the reactor. The injection was done quickly and steadily, with effort made to do this in a repeatable way.
- At the time of injection, the conductivity log was started, and the conductivity recorded.

A calibration curve was generated by measuring the conductivity of known concentrations of KCl. This allowed for the concentration to be found from the conductivity measurements taken throughout the experiment. The flow rate of the pumps was verified throughout the experiments by collecting the solution leaving the conductivity meter in a measuring cylinder, and using a stopwatch to calculate the flow rate. The experiments were carried out at a flow rate of 22.3 mL min^{-1}. For reference, total flow rates in the experimental runs ranged from 8.3 to 32.9 mL min^{-1}, although this does not account for any thermal expansion.

The results of the two injections are shown in Figure 5.28 and Figure 5.29.

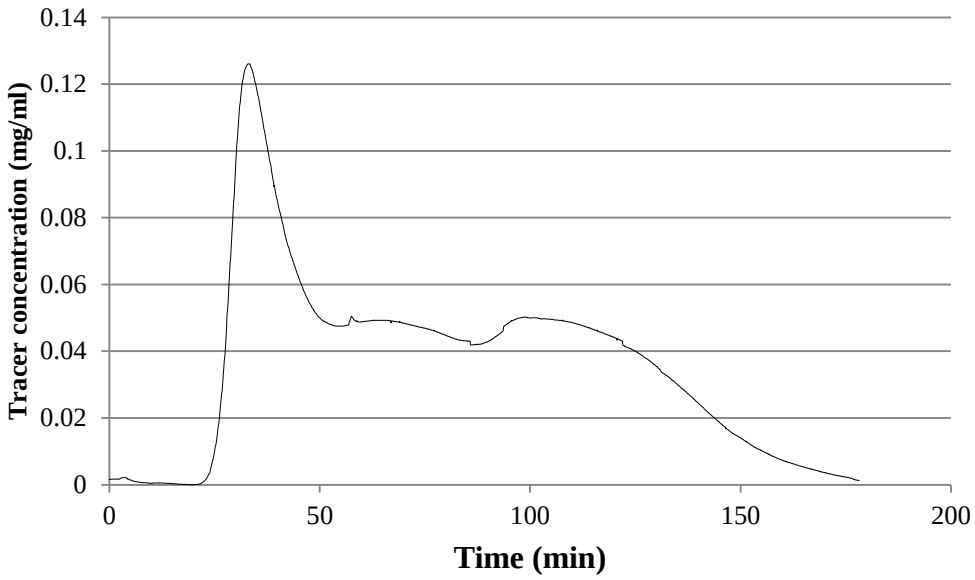

Figure 5.28 RTD curve of loaded reactor.

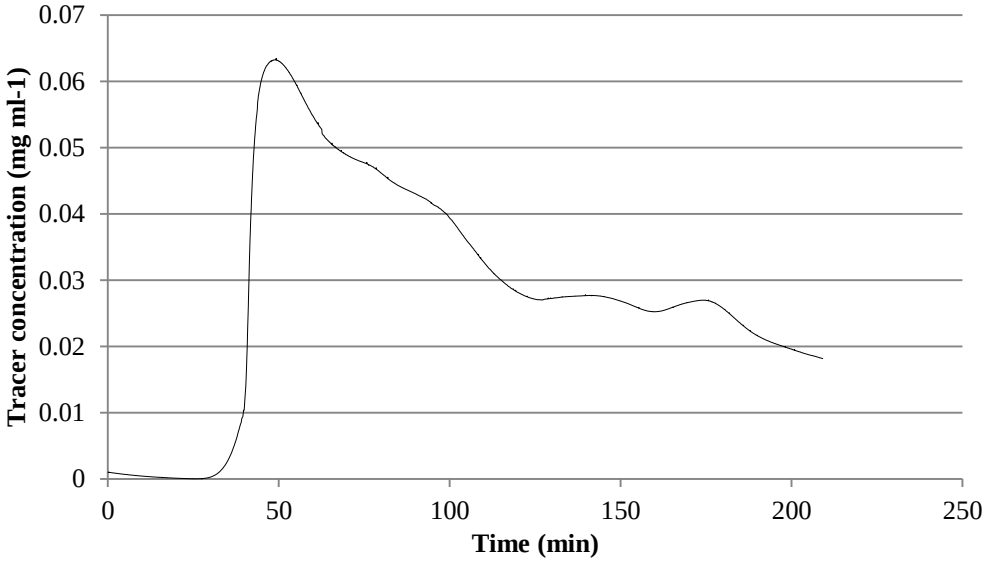

Figure 5.29 RTD curve of empty reactor.

The volume of the reactor is calculated as follows:

- **Five reactor tubes**: each is 22 mm in diameter, and 600 mm in length, for a total volume of **1140 ml**.

- **Four ¼" Swagelok tubes**: each is 560 mm long, with an i.d. of 3 mm, for a total volume of **16 ml**.
- **Four ¼" Swagelok union crosses**: an internal volume of 0.5 ml each.
- **Five ¼" Swagelok tees**: an internal volume of 0.4 ml each.
- **Outlet tube**: 6 mm i.d., 80 mm long, for a volume of 2 ml

Empty reactor total volume ≈ 1160 ml

The volume of the packed reactor excludes the volume of the catalyst:

- Catalyst bed is 22 mm in diameter and 2300 mm in total length, for a total empty volume of 874 ml.
- The voidage is 73.4%, and so the catalyst volume is 233 ml.

Loaded reactor total volume ≈ 930 ml

The data from the concentration curves can then be presented in terms of the age distribution function, E, with the equation (Levenspiel, 1999):

$$E = \frac{C_{Tracer}}{M/\upsilon} \tag{5.7}$$

Where:

E = Age distribution function ($min^{-1)}$

υ = Flow rate ($ml\ min^{-1}$)

M = Mass of tracer injected (mg)

C_{tracer} = Concentration of the tracer output ($mg\ ml^{-1}$)

The resulting curves are plotted below.

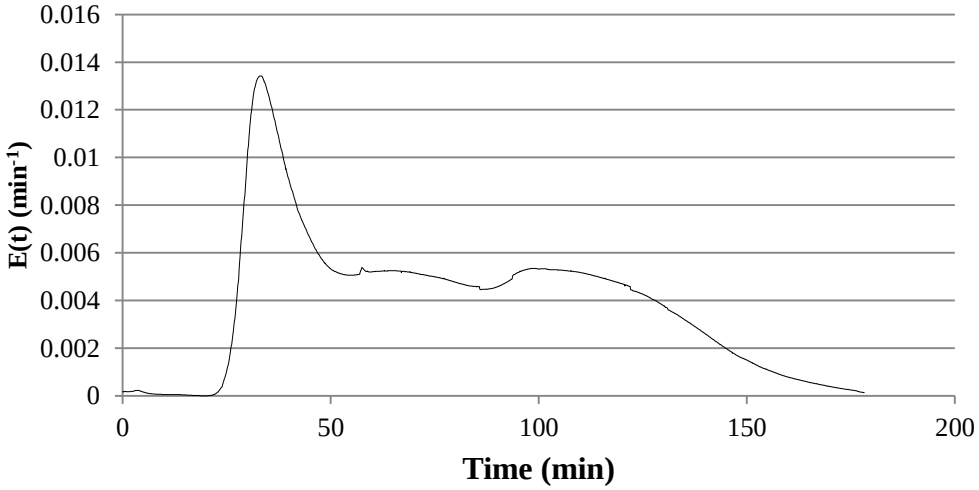

Figure 5.30 E curve of loaded reactor.

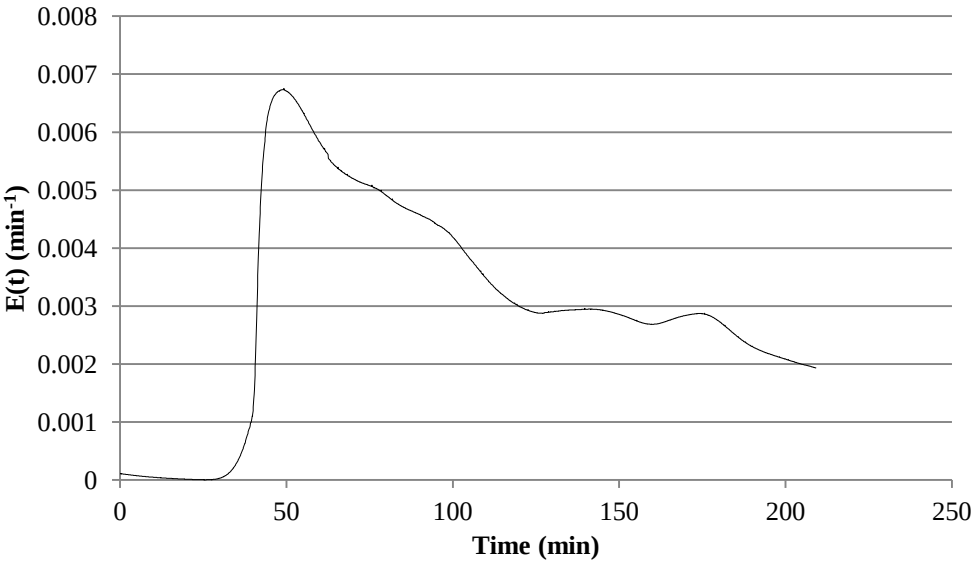

Figure 5.31 E curve of empty reactor.

The obtained concentration profile can be converted into an "E_θ-curve", where E_θ is the fluid element age function represented in terms of residence times. This allows for the loaded and empty reactor to be directly compared, as they are both presented in terms of a dimensionless number of residence times. The equation for obtaining E_θ is provided (Levenspiel, 1999):

$$E_\theta = \frac{V}{M} C_{tracer} \tag{5.8}$$

Where:

V = Reactor Volume (ml)

M = Mass of tracer injected (mg)

C_{tracer} = Concentration of the tracer output (mg ml^{-1})

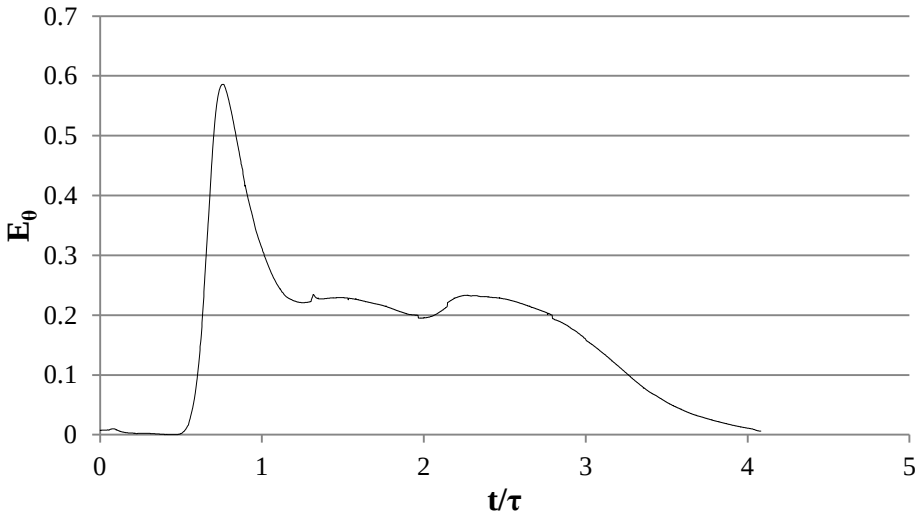

Figure 5.32 E_θ curve of loaded reactor, $\tau \approx 44$ min.

The RTD function of the loaded reactor is shown in Figure 5.32. The initial curve is the expected shape of a reasonable plug-flow reactor. However, the long tail with distinct "lumps" is characteristic of a reactor with back-mixing and stagnant dead zones (Levenspiel, 1999). This is unsurprising considering the number of fittings and expansion points along the total length of the reactor, as well as the relatively large diameter of the empty sections of the reactor tubes.

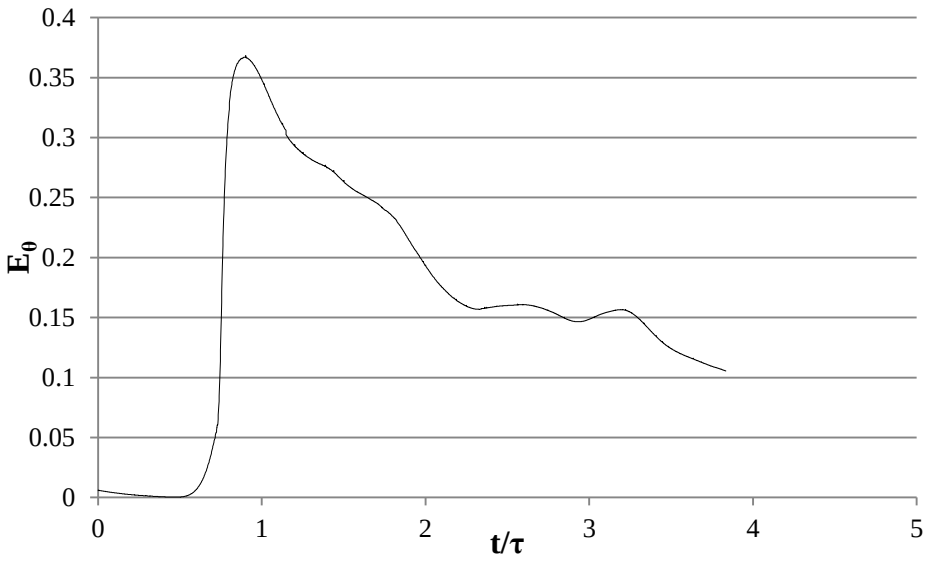

Figure 5.33 E_θ curve of the empty reactor, $\tau \approx 55$ min.

The RTD function of the empty reactor is shown in Figure 5.33. Once the initial pulse of tracer emerges from the reactor, there is a very long and unsteady tail. This shape is what is expected from a mixed flow reactor with sluggish, inadequate mixing (Levenspiel, 1999). This is to be expected from a completely empty tube of such large internal diameter compared to the relatively low flow rate. The lack of structure within the reactor leads to a lack of direction for the fluid, which is all amplified by any stagnant areas there may be at the fittings and reactor inlets.

A comparison of these two functions suggests that the monoliths in the packed sections of the reactor act with a relatively good approximation of plug flow, which makes sense considering the narrow channels will essentially eliminate radial diffusion and limit the extent of back-mixing.

The effectiveness of using a traditional single phase method to model a two-phase system is unclear, although it does provide some insight into the geometric effects within the reactor. Ideally, an in-situ RTD experiment would be carried out, wherein a tracer is introduced to the reactor during an actual reaction run. This would allow for the effects of convection currents, possible two-phase flows, and the actual reaction viscosity to be observed.

5.3.2 General Procedures

The reactor was operated under the follow procedures, with reference to Figure 5.25.

Reactor set-up

- The reactor tubes were filled with catalyst coated sections of monolith, with a 50 mm spring at the bottom to keep the monoliths in the heated section, and above the inlet;
- All valves were closed, with the exception of V-9 (the back-pressure regulator);
- A peristaltic pump was connected to pipe P-23, valves V-11 and V-12 were opened, valve V-9 was tightened slightly, and methanol was pumped into the reactor until liquid came out pipe P-24;
- Valves V-5 through V-8 were opened sequentially to bleed out any air pockets trapped in the reactors;
- Once all the air was purged, all the valves were shut, and V-9 was opened all the way.

Regulating the Back Pressure

- With the autoclave inlet (V-2) open, and the outlet (V-4) closed, the pumps were started at the desired flow ratio;
- Once the autoclave began to pressurise, valve V-4 was opened slightly, keeping the pressure in the autoclave constant (e.g. at ~ 2 bar);
- The back-pressure valve was closed, and once the system pressure had reached the autoclave pressure, V-4 was opened fully;
- The back pressure valve was then operated to achieve the desired system pressure (e.g. 15 bar).

Start of the reaction

- The flow-rates were adjusted to the desired levels;
- The autoclave was brought up to temperature, with stirring;
- The oil bath heaters were switched on and the temperature set to the reaction conditions (i.e. 150°C);
- The heating oil pump was started;
- The system pressure was monitored to ensure that it remained steady;
- The reaction was run for multiple residence times prior to any sampling.

Taking liquid samples

During the course of an experiment, small samples were taken:

- Product samples were taken by operating three-way valve V-10 to direct flow from the product collection vessel to a sample vial;
- Intermediate samples were taken by slightly opening valves V-5 through V-8 one at a time for collection into sample vials;
- The first part of each sample was discarded to clear the sample tubes.

Shutdown

- The oil bath heaters were switched off, as well as the oil pump;
- Both of the reactant pumps were switched off
- The system was left to cool overnight

5.3.3 Scale-up of catalyst production

With a total reactor length of over 2 m, the multiple channel reactor posed a significant challenge for catalyst preparation. Coating hundreds of smaller monolith sections was deemed impractical, and so whole 11.5 cm long monolith blocks were used. First, they were cut into sections of the correct diameter, 2.2 cm, as shown in Figure 5.34.

Figure 5.34 Monolith sections for the multiple channel reactor.

The primary challenge posed by the large monoliths was keeping the slurry suspended throughout the coating process. With smaller pieces, it was possible to use a beaker with a magnetic stirrer. However, a beaker large enough to accommodate the larger monoliths would require a significant increase in the amount of slurry prepared. Thus, the slurry was poured into a suitable measuring cylinder for dipping, as in Figure 5.35. Any extra slurry was kept in a stirred vessel, and the remaining slurry in the measuring cylinder was returned to this vessel after each monolith piece to maintain mixing.

Figure 5.35 Dip coating procedure for the larger monolith sections.

As before, the channels were cleared with compressed air, after which the monoliths were dried at 60°C for 1.5 hours. After three coatings, the monoliths were dried at 60°C overnight. They were then loaded into a quartz tube and heated in a furnace to 60°C under nitrogen for two hours. The pieces were then heated at approximately 5°C min^{-1} until the temperature prior to the first monolith reached over 700°C. This corresponded to an external temperature of 830°C. Two things must be noted here. First, the furnace used for the larger monoliths was not the same as for the smaller ones, as a larger furnace was needed. Second, this furnace did not have an automated temperature ramp, and so the temperature had to be adjusted manually.

On removal, each piece was inspected for a flaking coating; all were deemed satisfactory. The coating was performed in five batches of four pieces, and one batch of three. The catalyst loading of the monoliths is given in Table 5.4.

Table 5.4 Loadings of large monolith pieces

Batch number	Monolith Piece (wt % catalyst)				Average	St. Dev
	1	2	3	4		
1	18.6	16.7	19.4	-	18.2	1.1
2	19.9	19.1	19.3	16.7	18.8	1.2
3	20.6	20.9	21.5	19.1	20.5	0.9
4	20.6	20.4	20.9	21.0	20.7	0.2
5	18.6	18.5	20.0	19.7	19.2	0.7
6	21.8	20.7	22.1	16.7	20.3	2.2
Total					19.7	1.5

A large monolith piece was embedded in resin and ground down to provide a cross section for SEM. An example cross section is shown in Figure 5.36. As discussed in Chapter 3, the white areas represent the strontium rich phase.

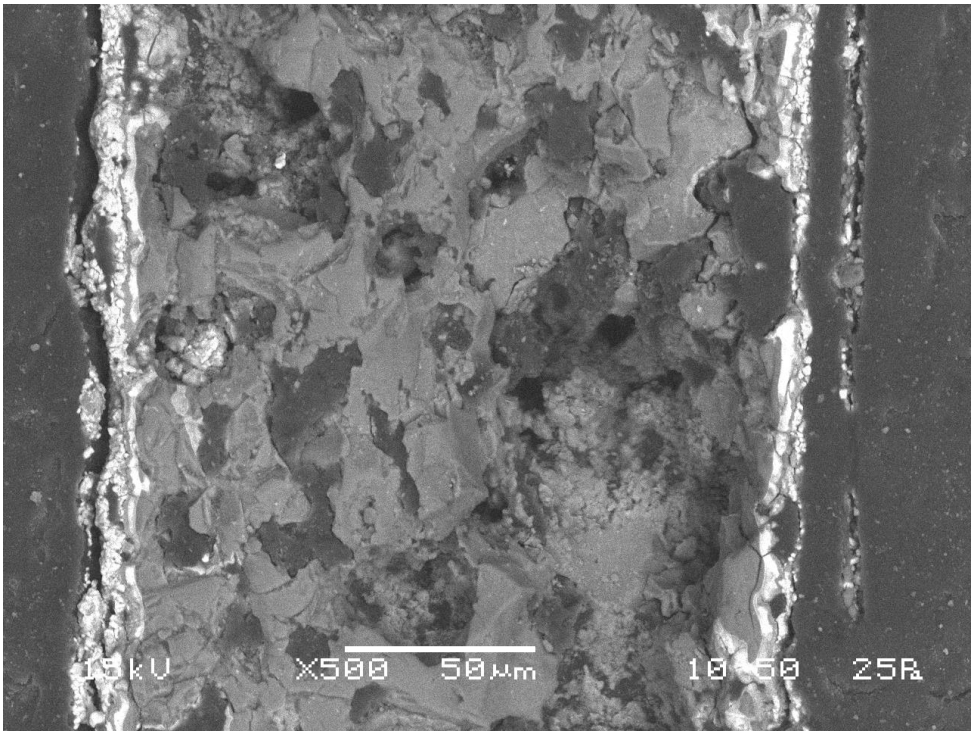

Figure 5.36 SEM of a catalyst cross-section.

As with the smaller catalyst, the coating appears to be well bound to the monolith surface. The cracks that do appear at the edge of the coating were believed to be caused by the resin embedding method, as there were bubbles of gas that formed and pulled at the surface. That aside, it is also clear from this that the catalyst did not infiltrate the monolith pores as it had in the smaller catalyst.

Across a larger range of the monolith, some variation was seen. Figure 5.37 shows a range of locations around the edge of the monolith.

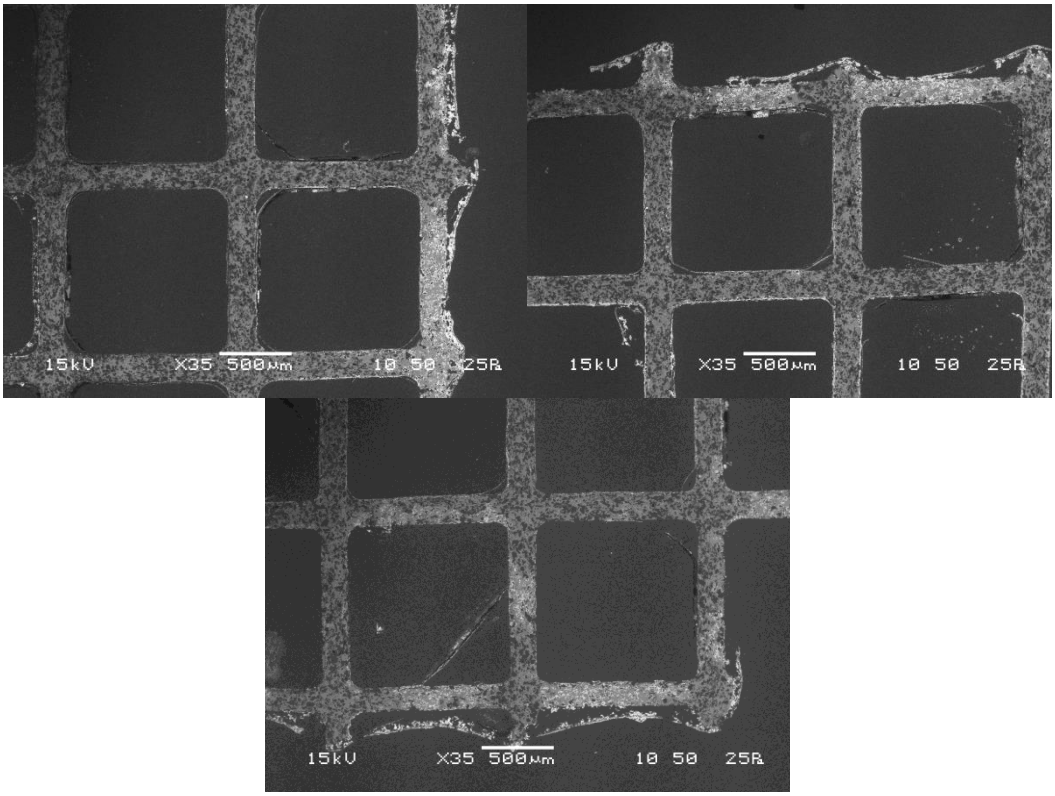

Figure 5.37 SEM images of various locations at the edge of a coated monolith.

These images show significantly more catalyst infiltration into the pores at the edge of the monolith, where the material had been cut and broken. It seems probable that the cutting step of the manufacturing process opened much more of the internal wall for access than was normally available further inside the monolith. This was not evident in the monoliths for the smaller reactor, as there was much less distance

between all of the broken surfaces, and thus much less distance for the catalyst to diffuse to fill the pores throughout.

Surface area data was also obtained *via* ASAP. The results of both the BET and Langmuir surface areas are given in Table 5.5.

Table 5.5 Surface area analysis of the scaled up catalyst

Material	BET surface area	Langmuir surface area
Blank cordierite	$0.0776 \pm 0.0128\ m^2g^{-1}$	$0.1121 \pm 0.0130\ m^2g^{-1}$
Calcined codierite	$0.0872 \pm 0.0117\ m^2g^{-1}$	$0.1264 \pm 0.0105\ m^2g^{-1}$
SrO coated cordierite	$0.2929 \pm 0.0187\ m^2g^{-1}$	$0.4326 \pm 0.0055\ m^2g^{-1}$

Although all of the samples exhibit general low surface areas, it is worth noting that there is a slight increase of surface area in the calcined monolith, implying that previously unavailable pores may be opened up during calcination. Additionally, the presence of the catalyst layer increases the surface area by about three times. At a loading of around 20%, this would imply that the surface area of the SrO layer is approximately 1 m^2g^{-1}. Although this would still not be considered a very porous material, it should be considered what implications this may have on the availability of catalyst surfaces within the SrO structure. This could be important for mass transfer and catalyst activity, as pore blocking could result in once active catalysts losing their activity.

5.3.4 Catalyst Performance

The five reactor tubes were each loaded with four catalyst sections from Batch numbers 2 to 6 (Batch one was held back for analysis), for a total bed length of 2.3 m, and an average loading of 19.9 wt%. There was approximately 16.4 g of catalyst in each reactor channel. The fluid volume in the each catalytic section can be calculated from Equation (5.2):

$$V = \frac{\pi d^2}{4} z\varepsilon \tag{5.2}$$

With a diameter of 2.2 cm and a length of 46 cm, the void volume of each catalytic section is about 128 ml, with a total volume of 642 ml. The residence time can again be calculated using Equation (5.3):

$$\tau = \frac{V}{v} \tag{5.3}$$

For an example flow rate of 25.3ml min^{-1} oil and 7.6 ml min^{-1} methanol, the residence time is 3.9 minutes in each catalyst section, for a total residence time 19.5 minutes.

The reactor was operated at 6 different flow rates, all at a heating oil temperature of 150°C and a molar ratio of 7.14:1. The flow rates were repeated three times each in order to track the overall level of activity throughout the timeframe of the experiments. An overview of the experimental runs is shown in Table 5.6.

Table 5.6 Overview of experimental conditions in the multiple channel reactor

Set	Experiment number	Oil flow (ml min^{-1})	MeOH flow (ml min^{-1})	Residence time (min)	Triglyceride conversion (%)
1	1.1	25.3	7.6	19.5	32.5
	1.2	12.6	3.78	39.2	39.2
	1.3	18.9	5.67	26.1	31.3
	1.4	6.35	1.91	77.7	49.0
	1.5	15.7	4.71	31.4	31.1
	1.6	9.47	2.84	52.1	34.9
2	2.1	25.3	7.6	19.5	19.3
	2.2	12.6	3.78	39.2	28.4
	2.3	18.9	5.67	26.1	20.5
	2.4	6.35	1.91	77.7	35.9
	2.5	15.7	4.71	31.4	26.0
	2.6	9.47	2.84	52.1	30.5
3	3.1	25.3	7.6	19.5	19.0
	3.2	12.6	3.78	39.2	25.2
	3.3	18.9	5.67	26.1	19.1
	3.4	6.35	1.19	77.7	34.5
	3.5	15.7	4.71	31.4	19.1
	3.6	9.47	2.84	52.1	27.9

Samples were taken after the reactor temperatures had been stable for at least two residence times.

Conversion of triglycerides was again calculated using Equation (5.1):

$$X = \left(1 - \frac{mol\%_{TG}}{mol\%_{TG} + mol\%_{DG} + mol\%_{MG} + mol\%_{Gly}}\right) \times 100 \qquad (5.1)$$

The temperatures at the inlet and outlet of each reactor were monitored. As an example, the temperatures from Experiment 1.1 are shown in Figure 5.38.

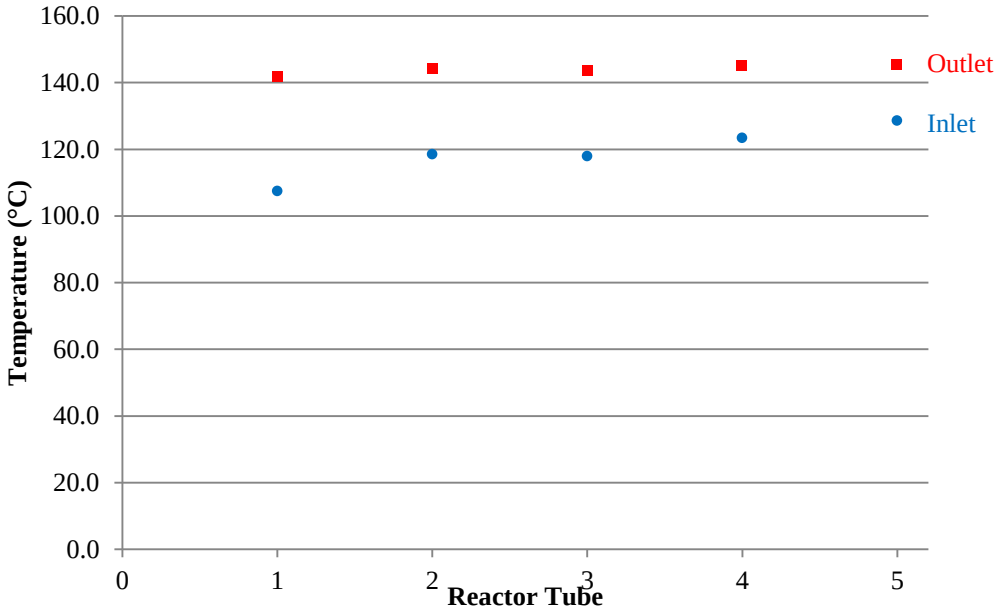

Figure 5.38 Inlet and outlet temperatures from Experiment 1.1.

The collated inlet and outlet temperatures from all the experimental runs are shown in Figure 5.39.

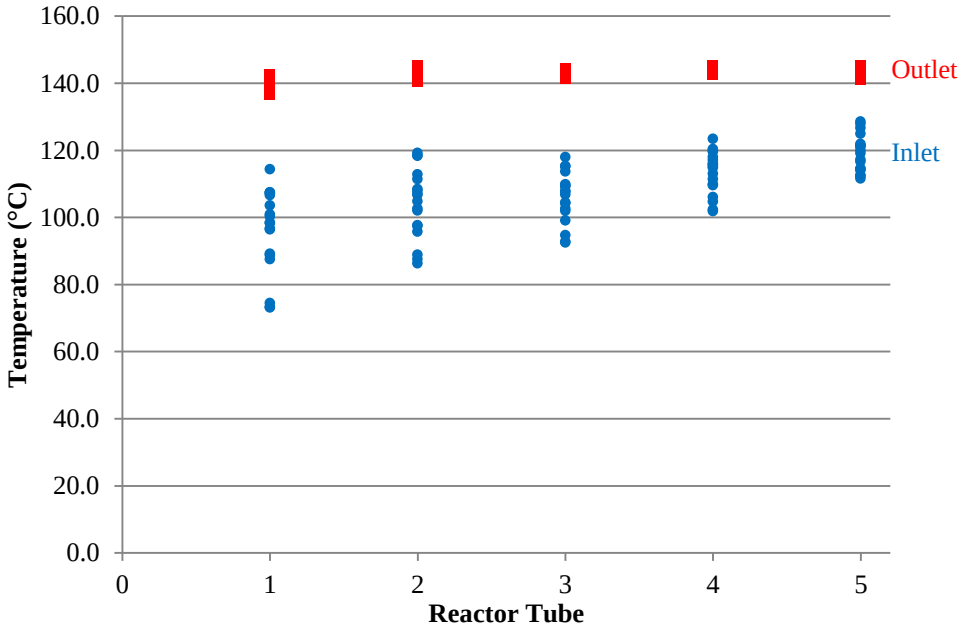

Figure 5.39 Temperature data from all experimental runs.

The outlet temperatures are reasonably stable across the five reactor tubes at all flow rates. The inlet temperatures vary more, with the highest temperatures corresponding to the highest flow rates, as the liquid had less time to cool in the external tubes between the reactors. The primary cause of the rise in inlet temperatures along the equipment is believed to be caused by increasing proximity to the oil bath, and thus increasing ambient temperature. Considering the fairly stable outlet temperatures, the high heating oil flow rate of 8 L min^{-1}, and the relatively low reactant flow rates, the temperatures within the reactor tubes are taken to be similar enough between experiments for the results to be comparable.

The full temperature data from these runs are given in Appendix B.

The reaction data obtained from the experiments has been collated in terms of triglyceride conversion, and are shown in Figure 5.40. The full data was checked to ensure the mass balance was satisfied, and the concentration data have been included in Appendix C.

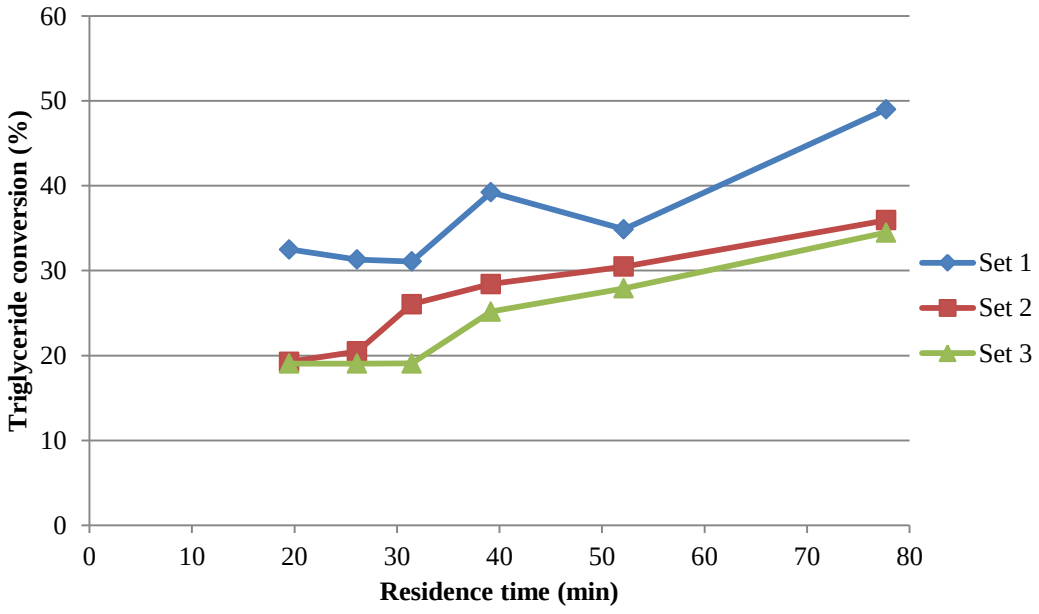

Figure 5.40 Conversion data from all the multiple channel reactor runs, T = 150°C, P = 15 bar.

There is steady loss of activity throughout the course of the experiments, although this appears to be abating towards the end. Although this is not an ideal situation for

obtaining reaction data, part of the rationale for using the multiple channel reactor was that it allows the user to take samples at a set catalyst lifetime, which can compensate for the variable catalyst activity. The results from the first set of experiments are displayed in Figure 5.41.

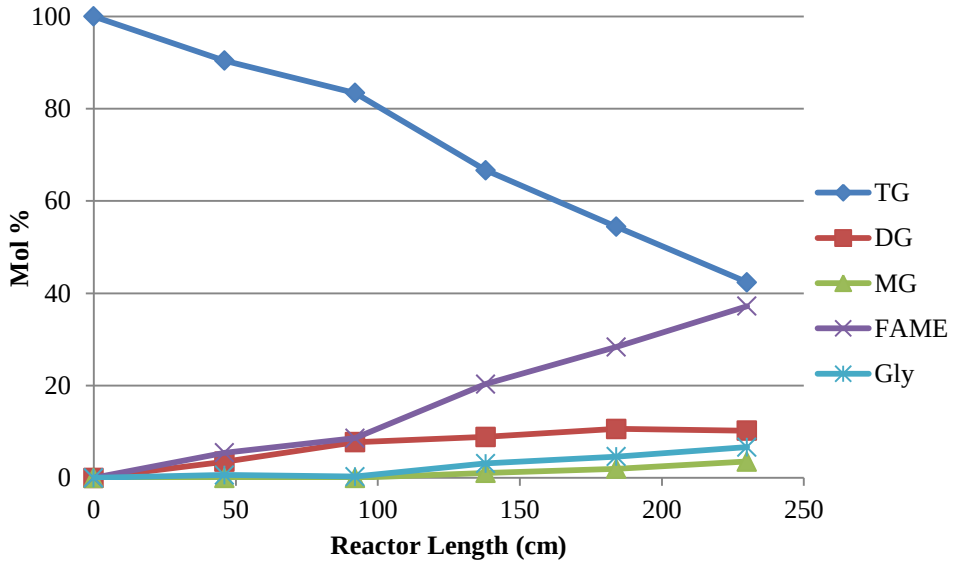

Figure 5.41a Example reactor profile for Experiment 1.1, 25.3 mL min^{-1} oil, T = 150°C, P = 15 bar.

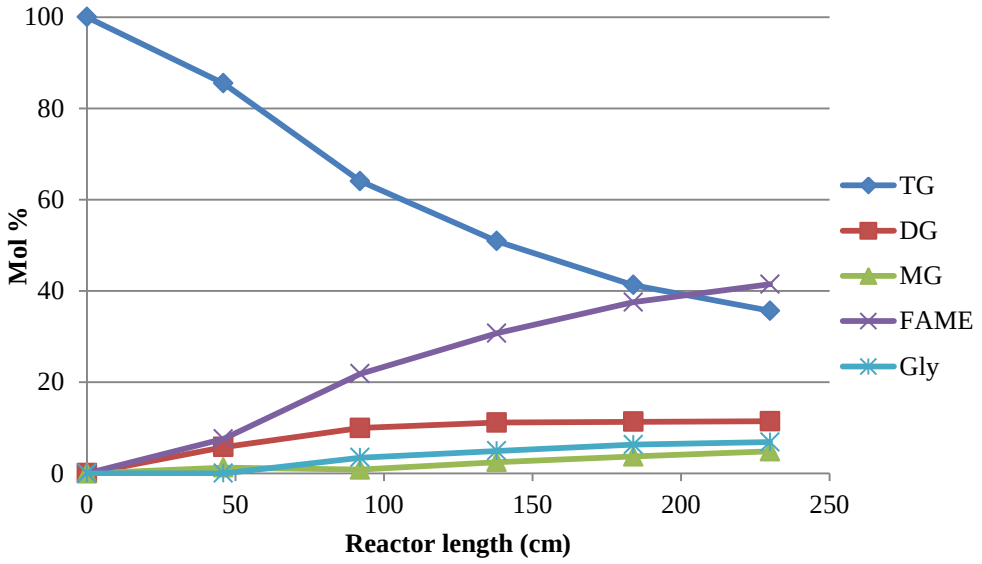

Figure 5.41b Example reactor profile for Experiment 1.2, 12.6 mL min^{-1} oil, T = 150°C, P = 15 bar.

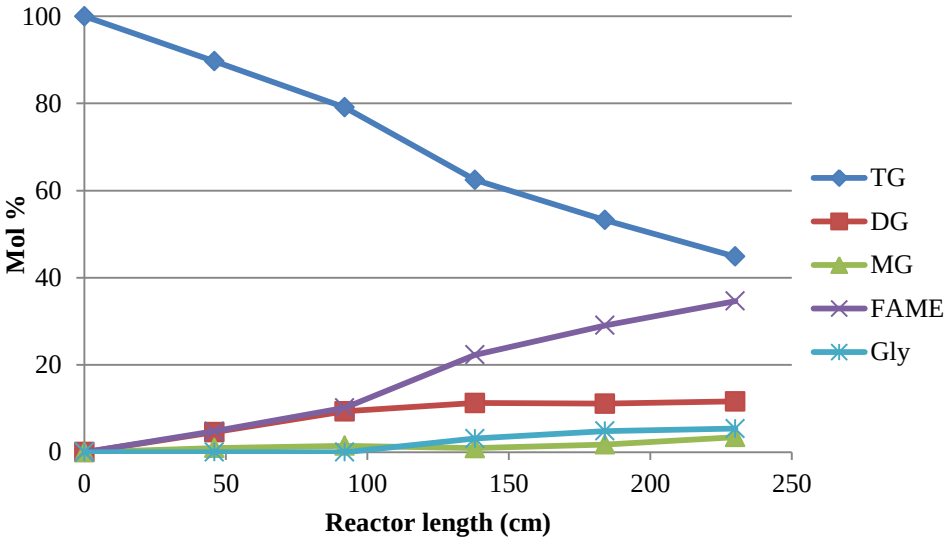

Figure 5.41c Example reactor profile for Experiment 1.3, 18.9 mL min^{-1} oil, T = 150°C, P = 15 bar.

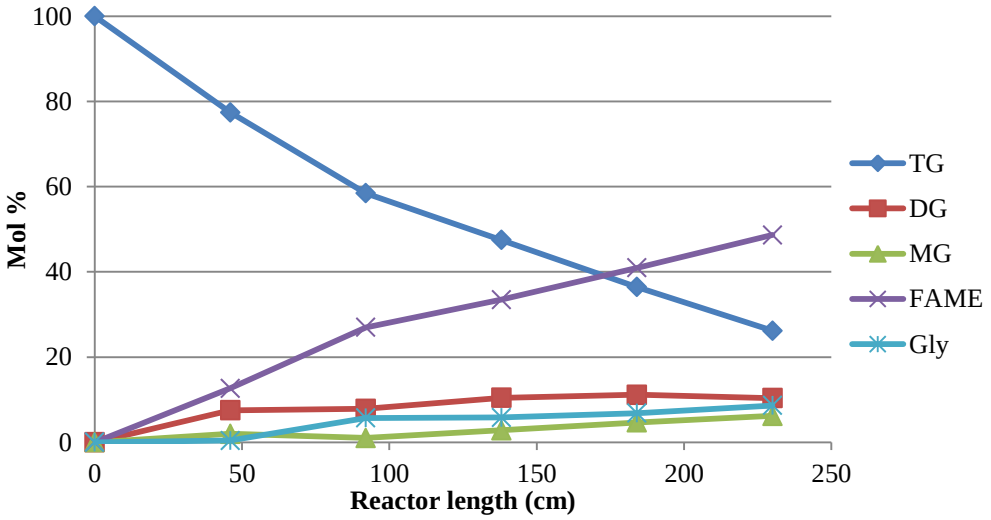

Figure 5.41d Example reactor profile for Experiment 1.4, 6.35 mL min^{-1} oil, T = 150°C, P = 15 bar.

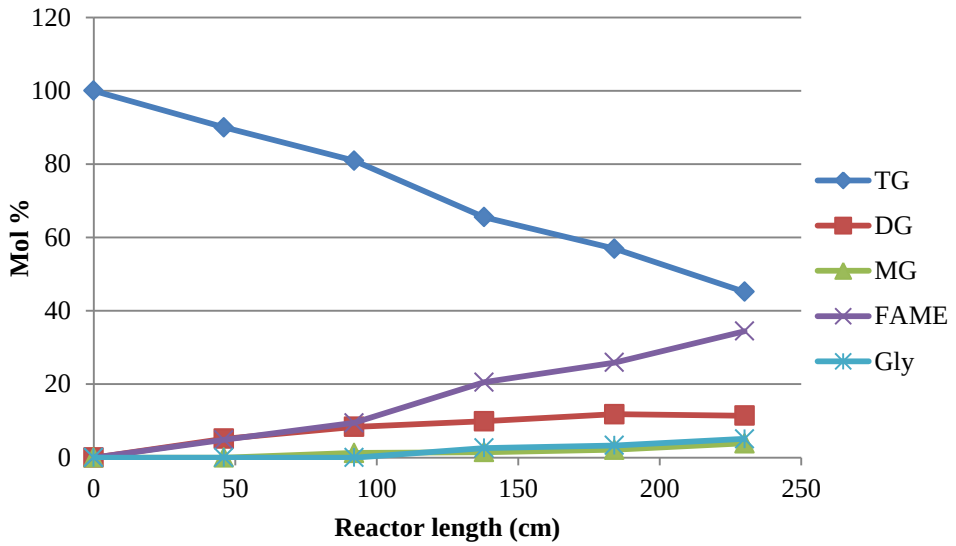

Figure 5.41e Example reactor profile for Experiment 1.5, 15.7 mL min^{-1} oil, T = 150°C, P = 15 bar.

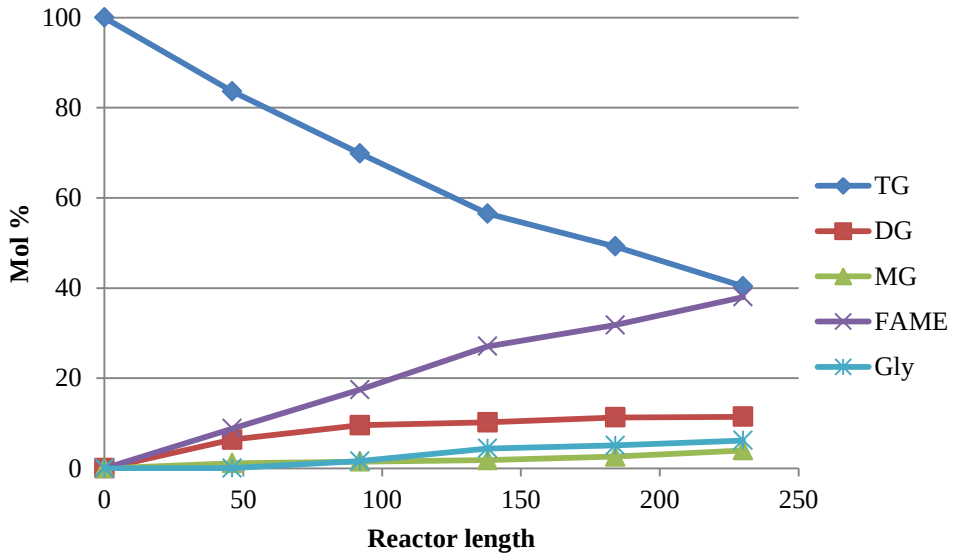

Figure 5.41e Example reactor profile for Experiment 1.6, 9.47 mL min^{-1} oil, T = 150°C, P = 15 bar.

The primary purpose of designing and commissioning the multiple channel reactor was to provide an experimental method whereby the reaction could be monitored along the length of the packed bed, and as the graphs in Figure 5.41 show, this objective was achieved. The reactor profiles also demonstrate that the catalyst was active throughout the packed length, and at all flow rates. This data could then be processed to obtain useful information about the reactor system and the catalyst.

5.3.5 Reaction Rates

This reactor profile can also be expressed in terms of molar flow of the individual components. Because there are three reactions which produce FAME, the overall reaction rate is best represented by the molar flow of FAME along the reactor. Figure 5.42 displays this data for Experiment 1.4. The reaction rate is thus represented by the initial slope of the curve.

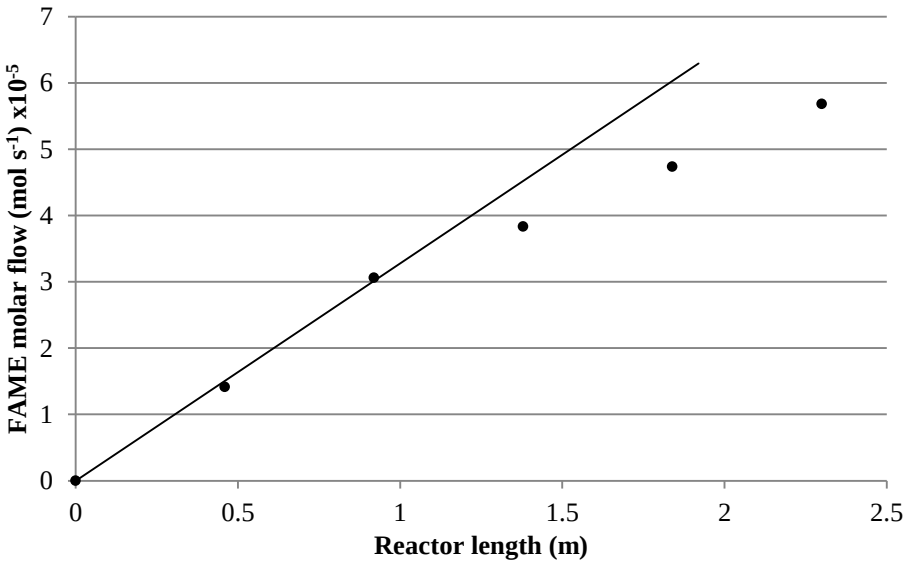

Figure 5.42 Example FAME concentration profile for estimating reaction rates, 6.35 ml min^{-1} oil, T = 50°C, P = 15 bar.

While this data follows the expected trend for a reaction, with an initial rate that reduces as the reactants are used, this pattern was not always observed. It was discussed in Section 5.2.4.3 that it was possible that there may be an initial period during which the rate is lower prior to a marked increase. This happened when the FAME concentration exceeded approximately 0.1 mol L^{-1}. This phenomenon was also observed in many of the multiple channel reactor experimental runs. An example (Experiment 2.5) of this is shown in Figure 5.43.

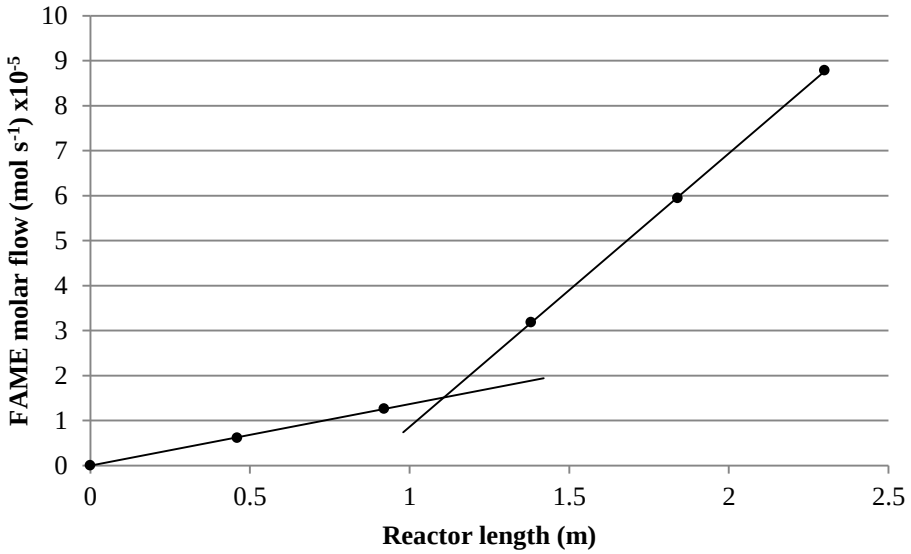

Figure 5.43 Example of rate increase after initial conversion, T = 150°C, P = 15 bar.

The reaction rate in this case appears to quadruple after an initially slow reaction. The cause of this is likely mass transfer limitations, as the triglycerides react and leave smaller, more mobile molecules in their place. This is supported by work in the literature, where it has been shown that the viscosity of an oil transesterification reaction mixture drops dramatically during the initial stages of reaction (Borges *et al.*, 2011). It is entirely feasible that this is a large contribution, along with steric hindrance at the catalyst surface, to the much smaller reaction rate. It seems unlikely that temperature is a cause of this increase in rate, considering the similarity of the temperature data of Reactor Tubes 2 and 3.

5.3.5.1 Location of the Maximum Rate

In order to locate the maximum observed rate in the system, the overall rate of reaction across each reactor tube was calculated. The change in molar flow of FAME across each tube was divided by the length of a single reactor, and normalised to the surface area of the catalyst, as follows:

$$r_{FAME} = \frac{F_{FAME,out} - F_{FAME,in}}{z\ a_s} \tag{5.9}$$

Where:

r = Overall reaction rate across a reaction tube (mol m^{-2} s^{-1})

$F_{FAME,\ in}$ = Molar flow of FAME at reactor inlet (mol s^{-1})

$F_{FAME,\ out}$ = Molar flow of FAME at reactor outlet (mol s^{-1})

z = Length of reactor section (m)

a_s = Geometric area of catalyst (m^2 m^{-1})

With a diameter of 0.022 m, the catalyst sections of the reactor have a specific area of 1.19 m^2 m^{-1}.

The individual reaction rates for each reactor in each experiment can then be compared. The rate data for each reactor across all 18 runs are given in Figure 5.44.

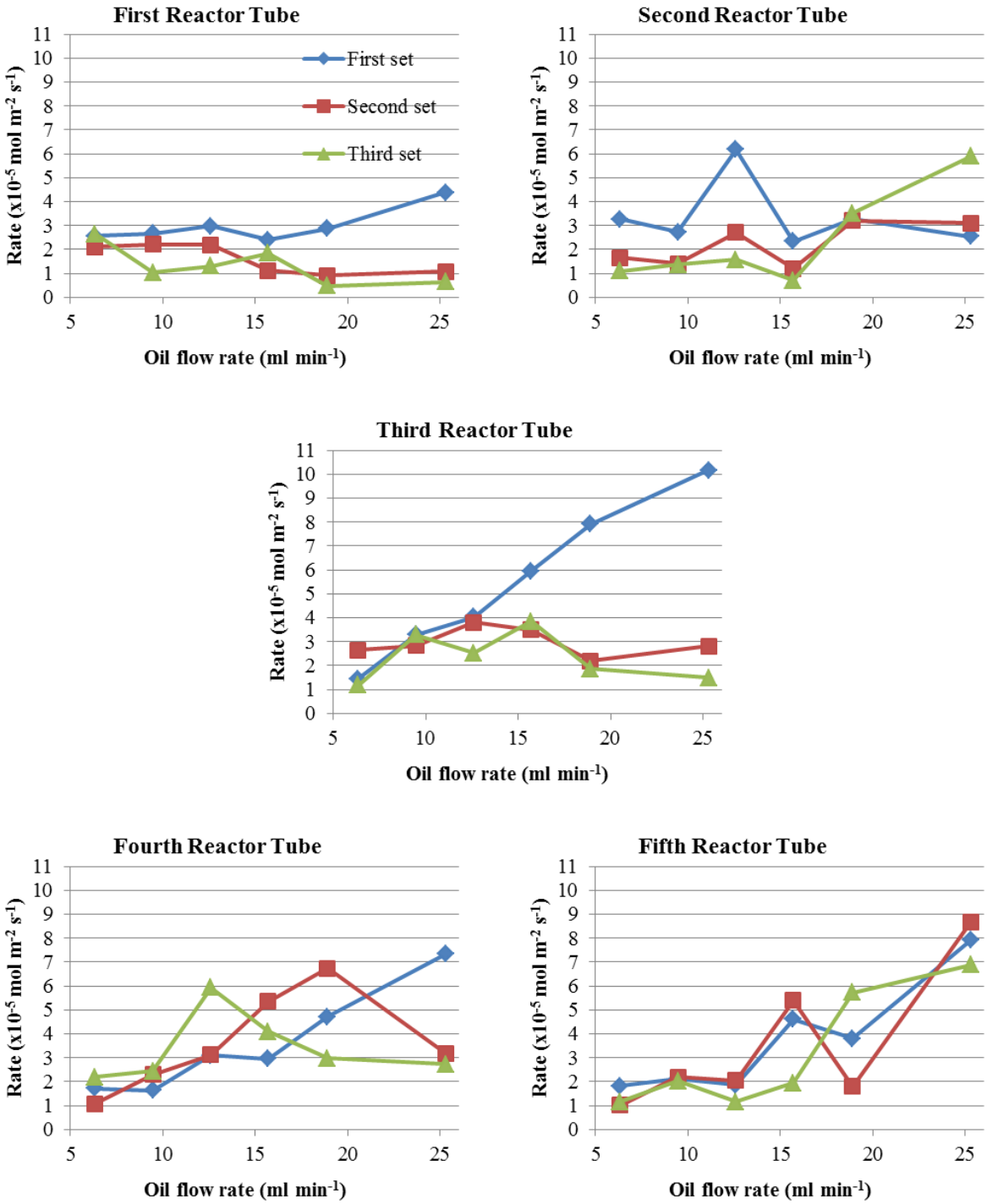

Figure 5.44 Overall average reaction rates (FAME appearance) across each reactor tube, T = 150°C, P = 15 bar.

In the first set of experiments, the flow rate does not appear to have a strong relationship to reaction rate in the first two reactors, but then has a strong influence on it in the final three tubes. Similarly, the second and third sets appear to show a positive correlation between flow rate and reaction rate in the fourth and fifth reactors – it should be pointed out that the experiments were not carried out in order of flow rate, and thus seemingly random increases or decreases in rate may be more subject to loss or gain of catalyst activity over time. This would suggest that the reaction is at a mass transfer limited stage.

However, in the first two reactors this effect is not as prominent – indeed it is reversed for the second and third sets of experiments in Reactor 1. In this case, it appears that the initial rate increases with decreasing flow rate. This is likely caused by the mixture having longer to react, and thus is able to reach a higher conversion, after which there is less inhibition from the triglycerides, increasing the rate. In other words, towards the entrance of the reactor the rate is extremely low, but by the end of the reactor the rate has increased enough to cause the observed rate to be higher than at higher flow rates.

Conversely, the higher flow rates in these cases do not have a large enough residence time in the first reactor for the triglyceride inhibition stage to be significantly masked. The inhibition would thus have to be substantial enough that the increased flow rates do not improve the mass transfer enough to overcome it. In the first experimental set this is not observed, likely because the catalyst was still active enough to reduce the duration of the strong inhibition. Considering that the inhibition appears transient, and specifically related to the extent of triglyceride conversion, it seems most likely that the inhibition is caused by a significantly high viscosity negating the flow rate effects within the range of flow rates possible on this experimental apparatus, as opposed to a chemical inhibition of reaction sites.

In order to gain further insight into the behaviour of this inhibition, the location of the highest rate is given in Table 5.7.

Table 5.7 Location of highest reaction rate

Experiment number	Reactor with highest reaction rate		
	Set 1	Set 2	Set 3
1	3	5	5
2	2	3	4
3	3	4	5
4	2	3	1
5	3	5	4
6	3	3	3

The location of the highest rate is spread across all of the reactors, which eliminates the possibility that the variable rate is primarily caused by poor distribution of catalyst among the reactors, or that one reactor was favoured due to e.g. higher temperatures. However, Reactor 3 is the most common location, with this occurring 8 times. This supports the notion that there is an initial inhibition stage, followed by a maximum rate after which the rate is limited by reactant availability.

In the first experimental set, the highest reaction rates all occur in Reactors 2 and 3. The two that occur in Reactor 2 are at lower flow rates. This further supports the theory of the inhibition being concentration dependent, and also shows that the temperature variations between the reactors do not play a major role in the data – as the lower flow rates correspond to lower temperatures in the inlets of the first reactors, the rate would be expected to be lowered in those reactors if this were detrimental.

The location also in general shifts to a later reactor with subsequent runs. This is likely due to a combination of lower catalyst activity and the effect of triglyceride concentration on rate – with reducing activity, the point where the threshold conversion for an increased rate is reached shifts further along the overall reactor length.

5.3.5.2 Effect of Flow Rate on Maximum Rate

In order to test the effect of flow rate on the reaction rate, the maximum reaction rate was plotted against the oil flow rate for the three experimental sets. This is shown in Figure 5.45.

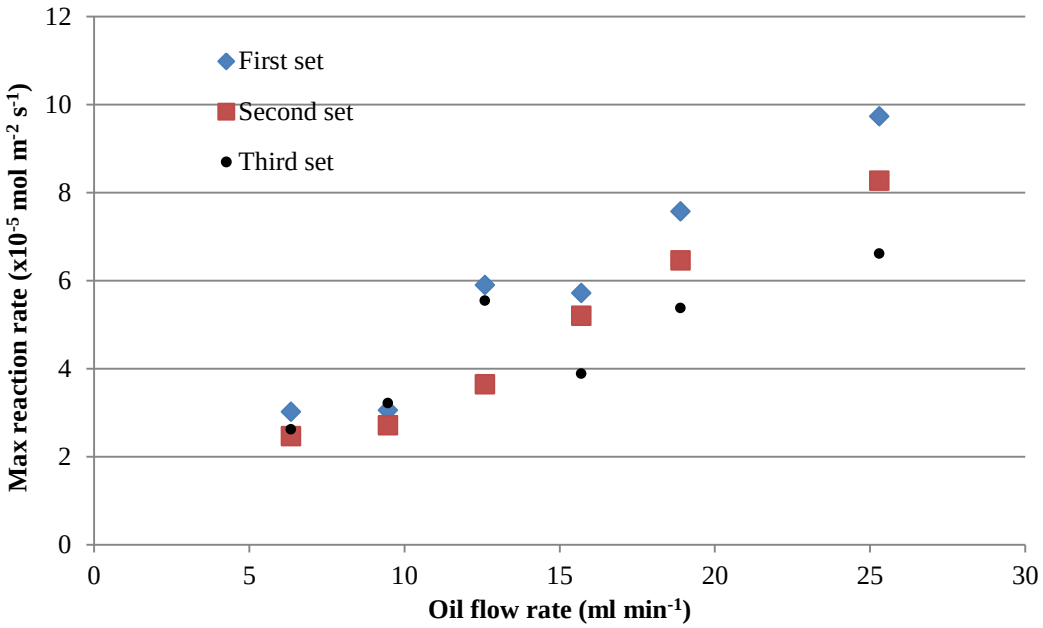

Figure 5.45 Maximum reaction rate (FAME appearance) with flow rate.

The clear trend in all three experimental sets is that the maximum reaction rate increases with flow rate, confirming the speculation in Section 5.3.5.1. This clearly demonstrates that mass transfer is a significant factor in the observed reaction rate. However, the decline in activity between the runs also suggests that the catalyst activity is a major contributor, meaning that the reactor was not operated in a regime where mass transfer limitations were overwhelmingly rate limiting.

5.3.5.3 Effect of Concentration on the Observed Rate

It has been hypothesised, both with the original continuous reactor and with the multiple channel reactor, that the reaction rate is initially inhibited until a certain amount of triglyceride has reacted. To achieve this it was simplest to compare the observed overall rate across each reactor with the average FAME concentration, as in Figure 5.46.

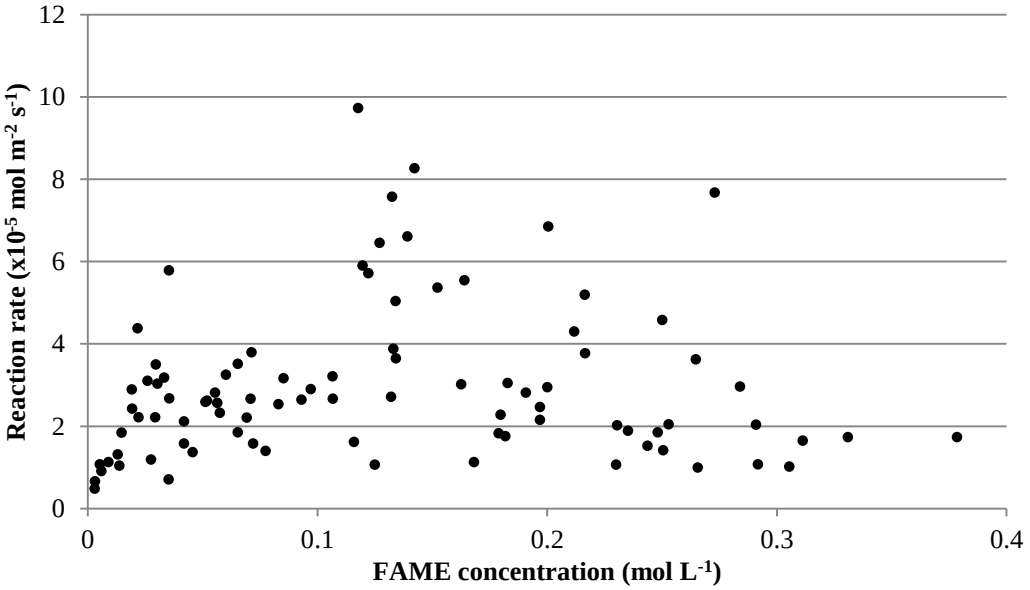

Figure 5.46 Effect of FAME concentration on reaction rate.

Although it is difficult to come to any certain conclusions based on this data, there are two pertinent observations that can be made. The first is that the lower concentrations correlate fairly well with a low reaction rate. Although this may be tautological to an extent (as the exit concentration is used here), it does further support the notion of an initial inhibited reaction period.

The second observation is that the maximum reaction rates predominately fall in a region between 0.15 and 0.25 mol L^{-1}. This region appears to be where the limiting effect of high triglyceride concentration has abated, and the supply of reactants to the catalyst has yet to have a major impact on the rate. In order to further analyse this situation, it is necessary to examine the effect of concentration for each flow rate, as shown in Figure 5.47.

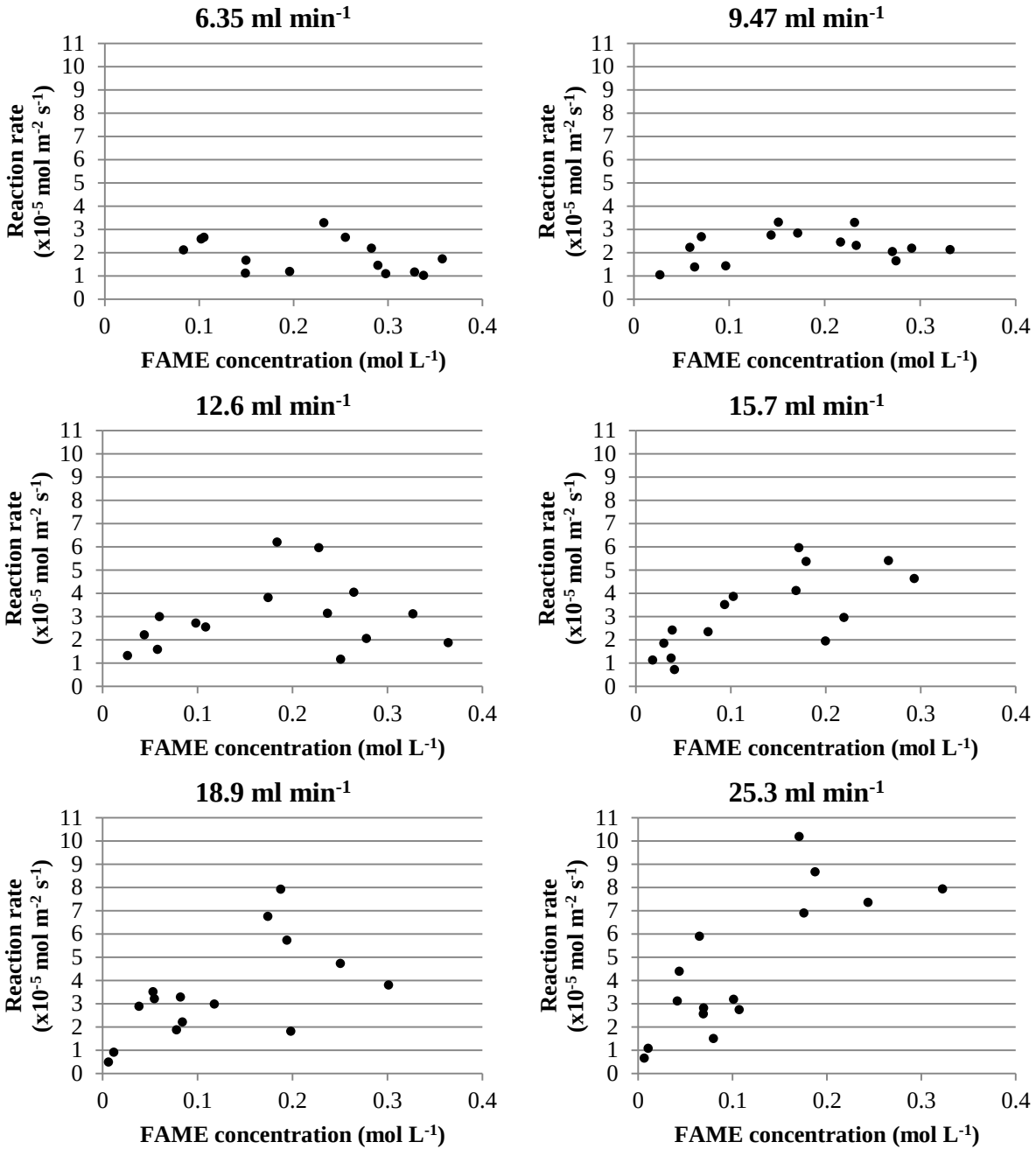

Figure 5.47 Comparison of effects of FAME concentration on overall reaction rate across a reactor tube at different oil flow rates.

At the lowest flow rate, there is no apparent effect of concentration on the observed rate, while as the flow rate is increased the effect become progressively larger. The cause of this is probably that at the lowest flow rate, the changes in viscosity along the reactor do not have a significant enough effect on the diffusion layer along the catalyst surface. This would imply that the effect is related to flow regime, as opposed to diffusivity – as if there were a dramatic improvement in diffusivity with increased FAME concentration, there would be a significant positive correlation between FAME concentration and reaction rate. At higher flow rates there is a very significant correlation between the FAME concentration and the reaction rate. This suggests that the flow rate changes are amplified by the lowering viscosity, possibly by reducing the diffusional layer between the bulk liquid and the catalyst.

Additionally, the results at a flow rate of 12.6 ml min^{-1}, being the only conditions where the flow rate is having a substantial effect on rate and sufficient conversion beyond the proposed optimum, corroborate the theory that this effect diminishes after a certain point, probably due to the decreasing availability of reactants.

Recalling the infiltration of catalyst into the monolith structure was mainly at the edges of the monolith pieces, as discussed in Section 5.3.3, it is not clear if this had any significant impact on the catalytic activity of the monoliths. It seems likely that the reaction would primarily take place at the outer surface, due to the large size of molecules involved and considering the dependence of reaction rate on fluid velocity. This would largely negate the effect of catalyst infiltration into the pores. However, if there is a significant contribution of activity from the inner catalysts, an improved coating method would be advantageous, perhaps including a pre-treatment to open the pores prior to coating. This could include a step such as acid washing (Shigapov *et al.*, 1999).

5.3.6 Consideration of Experimental Errors

The potential sources of error in the experiments were:

Temperature

The 10 thermocouples used in the rig were type K, and all of the same model as those used elsewhere in the work. Although these ten were not calibrated, all of the others used in this work were found to be accurate within 0.5°C. Additionally, no unexpected results were obtained, and so it can be said that this did not affect the reliability of the results.

Flow rates

Both pumps were calibrated by timed volume collection in measuring cylinders ranging from 25 ml, with a tolerance of 0.5 ml, to 250 ml, with a tolerance of 2 ml, depending on the flow rate used. This would not have an effect on the reliability of the results.

Compositions

As has already been discussed, the product compositions were monitored by GC. In the worst case, glycerol had a standard deviation of less than 2.7%. These errors would not affect the reliability of the results.

5.3.6.1 Effect of Temperature Variation on Reaction Rate

The effect of the temperature variations, as shown in Figure 5.39, on the rate of reaction can be estimated by considering the propagation of uncertainty through the Arrhenius equation.

$$k = Ae^{\frac{-E_A}{RT}} \tag{5.10}$$

Taking the variation in temperature to be ΔT, the subsequent variation in k, Δk may be written as:

$$\Delta k = \frac{\partial k}{\partial T}\Delta T \tag{5.11}$$

Thus, taking the partial differential of k and combining the equation yields:

$$\Delta k = A\frac{E_A}{RT^2}e^{\frac{-E_A}{RT}} \tag{5.12}$$

If it is assumed that the values as obtained in Section 5.2.4.2 for are correct, the variations in the reaction constant may be written as follows:

$$\Delta k = 0.320 \cdot \frac{52700}{8.314T^2}e^{-\frac{52700}{8.314T}} \tag{5.13}$$

Similarly, the effect of variations in k on the reaction rate may be found from the expression:

$$\Delta r = \frac{\partial r}{\partial k}\Delta k \tag{5.14}$$

Using first order kinetics leads to:

$$\Delta r = C\Delta k \tag{5.15}$$

Although it has been shown that the relationship between reactant concentrations and reaction rate is more complex than first order kinetics, these expressions are of use as they will allow an estimation of the effects of temperature. In order to find the maximum error caused by temperature, the initial concentration of triglyceride is used. Additionally, the temperature data from the five individual reactor tubes was used in order to demonstrate whether the tubes with larger temperature variations had a significantly larger error. The values for T and ΔT were taken as the average temperature and the standard deviation, respectively, for each tube. The results of this error analysis are given in Table 5.8.

Table 5.8 Calculated error ranges caused by variations in temperature in the five reactor tubes

Average Temperature (K)	Standard Deviation	Δr (mol m^{-2} s^{-1})
413.2	1.73	$3.58x10^{-6}$
416.0	1.20	$2.72x10^{-6}$
415.8	0.95	$2.12x10^{-6}$
416.7	0.93	$2.16x10^{-6}$
416.0	1.25	$2.83x10^{-6}$

Comparing this to the experimental data, the average reaction rate was $2.94x10^{-5}$ mol $s^{-1}m^{-2}$, thus the maximum expected experimental error represents 10% of this. Although this is a significant error, it should be stressed that this estimate of the error is under maximum rate conditions, using the highest possible triglyceride concentration. It would thus be expected that the actual error would be smaller than this, perhaps significantly so, although this is impossible to determine without a complete understanding of the complex relationships occurring throughout the reaction.

5.3.7 Conclusions

- The slurry coating technique was successfully scaled-up, achieving a catalyst loading of ~20 wt% across six batches.

- The system reached a highest conversion of 49%, which compares fairly well to the single channel reactor, considering the lower temperature the multiple channel reactor was operated under.

- The rate of reaction was found to be heavily dependent on flow rate and fluid composition.

- Generally speaking, with a higher flow rate, the rate of reaction increased. This effect was amplified by increased FAME concentration, implying that the rate limiting step is diffusion to the surface, which becomes easier with a less viscous liquid.

References

AL BADRAN, F. 2011. *Reactor design : compact & catalytic for speciality chemicals.* Ph.D., University of Bath.

ANTHONY, N. 2009. *Biodiesel refinery in Isanti is ready to rev* [Online]. Minneapolis: Star Tribune. Available: http://www.startribune.com/business/62453112.html [Accessed 30/08/2011].

ASLI, U. A. 2011. *Catalytic monoliths for biodiesel production.* Ph.D., University of Bath.

BORGES, M. E., DIAZ, L., ALVAREZ-GALVAN, M. C. & BRITO, A. 2011. High performance heterogeneous catalyst for biodiesel production from vegetal and waste oil at low temperature. *Applied Catalysis B: Environmental,* 102**,** 310-315.

BOURNAY, L., CASANAVE, D., DELFORT, B., HILLION, G. & CHODORGE, J. A. 2005a. New heterogeneous process for biodiesel production: A way to improve the quality and the value of the crude glycerin produced by biodiesel plants. *In:* International Conference on Gas-Fuel '05. Elsevier, 190-192.

BOURNAY, L., HILLION, G., BOUCOT, P., CHODORGE, J.-A., BRONNER, C. & FORESTIERE, A. 2005b. *Process for producing alkyl esters from a vegetable or animal oil and an aliphatic monoalcohol*. US6878837 (B2).

BS EN 14214:2008 + A1:2009 Automotive fuels - Fatty acid methyl esters (FAME) for diesel engines. Requirements and test methods. *British Standards Institute.*

KIM, M., DIMAGGIO, C., YAN, S., SALLEY, S. O. & NG, K. Y. S. 2011. The effect of support material on the transesterification activity of CaO-La2O3 and CaO-CeO2 supported catalysts. *Green Chemistry,* 13**,** 334-339.

KROHN, B. J., MCNEFF, C. V., YAN, B. & NOWLAN, D. 2011. Production of algae-based biodiesel using the continuous catalytic Mcgyan process. *Bioresource Technology,* 102**,** 94-100.

LEVENSPIEL, O. 1999. *Chemical reaction engineering,* Chichester, New York, Wiley.

MARSHALL, R. 2007. *39th Kirkpatrick Award Announced*. Chemical Engineering 12.

MCNEFF, C. V., MCNEFF, L. C., YAN, B., NOWLAN, D. T., RASMUSSEN, M., GYBERG, A. E., KROHN, B. J., FEDIE, R. L., *et al.* 2008. A continuous catalytic system for biodiesel production. *Applied Catalysis a-General,* 343**,** 39-48.

ONDREY, G. 2004. *Biodiesel production using a heterogeneous catalyst*. Chemical Engineering 10. p.13.

SHIGAPOV, A. N., GRAHAM, G. W., MCCABE, R. W., PAPUTA PECK, M. & KIEL PLUMMER, H. 1999. The preparation of high-surface-area cordierite monolith by acid treatment. *Applied Catalysis A: General,* 182**,** 137-146.

XIAO, Y., GAO, L., XIAO, G., FU, B. & NIU, L. 2012. Experimental and Modeling Study of Continuous Catalytic Transesterification to Biodiesel in a Bench-Scale Fixed-Bed Reactor. *Industrial & Engineering Chemistry Research,* 51**,** 11860-11865.

XIAO, Y., GAO, L. J., XIAO, G. M. & LV, J. H. 2010. Kinetics of the Transesterification Reaction Catalyzed by Solid Base in a Fixed-Bed Reactor. *Energy & Fuels,* 24**,** 5829-5833.

Chapter 6 Conclusions and Recommendations

As a reminder, at the start of the thesis, the main aim of the project was "to develop an improved heterogeneous catalyst system for the production of biodiesel from vegetable oils and to use this system in demonstrating a small scale continuous flow reactor." This goal has been progressed, and the following key conclusions have been formed.

6.1 Conclusions

6.1.1 Catalyst Screening and Selection

Following the literature review, two catalysts were chosen for investigation.

Modified Lanthanum Oxide:

Variations of the lanthanum oxide based catalysts were developed and tested, with higher activity resulting from a higher calcium content. With no cerium present, this relation was found to hold, although an intermediate level of calcium loading appeared to be best earlier in the reaction. Ultimately, however, the slow reactions achieved, with 24 hours required to reach 94% conversion for the best catalysts, were not sufficient to justify progressing the catalyst to the coating development stage.

Strontium Oxide:

Strontium oxide was tested, and found to be extremely active for the transesterification reaction. After an initial delay, the catalyst achieved a 95% theoretical yield within 5 minutes of the reaction starting. This confirmed the literature reports of catalytic activity, which included room temperature reactions in half an hour. Strontium hydroxide was also examined, as a probable product of catalyst poisoning. While it was active, it was not nearly as much as the oxide. The impressive activity of strontium oxide led to it being chosen for coating onto monoliths.

6.1.2 Catalyst Coatings on a Monolith Support

Having chosen strontium oxide as the catalyst for coating development, monolithic supports were coated with a SrO precursor and calcined. Two conventional coating methods were explored:

Catalyst Impregnation:

Conventional catalyst impregnation methods were used, coupled with thermal decomposition. The use of strontium nitrate required very high temperatures, and this led to the formation of strontium aluminate, which was not as active as strontium oxide. The loading using these methods was low, between 5.7 and 6.2% for the most active coating. The catalysts coated in this manner had inconsistent activity, with the best achieving a final yield of 12.6 mol% triglyceride and 60.9 mol% FAME after 24 hours at 120°C, but a repeat of this only coating only achieving 50.7 and 30.3 mol%, respectively.

Slurry Coating:

By coating the monoliths using a slurry of strontium hydroxide, a higher catalyst loading of around 20% was achieved, and this led to a substantially improved performance, with a final composition of 5.4 mol% triglyceride and 68.3 mol % FAME after 24 hours and 120°C. However, initial coats were mechanically unstable. A more stable method was developed, with higher loading of around 24 wt% and negligible weight loss in mechanical testing. Additionally, the coating method was successfully scaled up to much larger support pieces, resulting in a loading of 20 wt%.

6.1.3 Solubility Studies

The low solubility of methanol in vegetable oil at atmospheric reaction conditions was improved by raising the temperature of reaction in a pressurised reactor. In order to quantify this solubility, an experimental rig was designed and built which could take samples from a liquid phase at pressures up to 10 bar. It was found that at

typical reflux conditions of around 65°C the methanol dissolved at a 3:1 molar ratio, or just sufficient for the stoichiometric reaction. At 100°C this had increased to 6:1, and at 120°C it had reached 9:1. This data could be of use to the designers of a continuous reactor, where the temperature will determine if the mixture is two-phase, and thus more restricted by mass transfer.

6.1.4 Catalyst Characterisation

Catalysts were primarily characterised by SEM, combined with x-ray backscatter analysis. This allowed for the strontium rich phases to be identified against the cordierite. The slurry coated catalysts were found to have a good deal of strontium infiltration into the cordierite pores, although this was found to primarily be near to breakage points in the monoliths.

ASAP was also used to characterise the surface area of the monoliths, both blank and coated. It was found that calcination provides a small increase in monolith surface area, likely from the opening of access to existing pores. The catalyst coating has a substantially higher surface area than the cordierite.

6.1.5 Continuous Reactors

Two reactors from previous projects within the research group were obtained and modified for use in this work.

Single Channel Reactor:

A single channel reactor, with a 6.2 mm i.d. and a 400 mm heated length, was operated primarily at flow rates of 0.1 mL min^{-1} oil and 0.03 mL min^{-1} methanol, at 195°C, with a residence time of approximately 32 minutes. The first batch of slurry coated monoliths was tested for 100 hours, and maintained activity throughout, with a final triglyceride conversion of 65.4%. An experiment during this run where the flow rate was ramped over a range revealed that there was an exaggerated effect of flow rate on conversion – the increase in fluid velocity did not increase the rate as expected, and so the drop in conversion with residence time was larger than would be the case due to having less time to react. This suggested that there is some form of reaction inhibition at high triglyceride concentrations.

The reactor was then used for testing the improved slurry coating method. This batch of catalysts was used over the course of almost 300 hours of reaction time, primarily at flow rates of 0.1 mL min^{-1} oil and 0.03 mL min^{-1} methanol, with a residence time of approximately 29 minutes, at 195°C. Over this extended reaction time, the catalyst was found to regain its activity multiple times, ranging from full conversion to a minimum conversion of 34.4%. Although variations of water in the feedstocks and catalyst leaching were ruled out as causes of this, the actual cause was not determined. At its most active, the catalyst was capable of complete conversion of triglyceride with a residence time of half an hour, which is about four times less than the current industrial heterogeneous process, under similar conditions.

Multiple Channel Reactor:

The successfully scaled-up slurry coated catalyst was used in a multiple channel reactor, with five 22 mm i.d. tubes of 550 mm length in series in a shared heating jacket. This was carried out over the course of 18 experimental runs, involving three repeats of 6 different flow rates, all at a heating oil temperature of 150°C. The triglyceride inhibition of reaction that was hypothesised when using the single channel reactor was confirmed, as a lower FAME concentration was found to be associated with a lower reaction rate. Additionally the flow rate was found to be an important factor, with flow rates above 9.5 ml min^{-1} oil significantly improving the rate of reaction, once the initial triglyceride inhibited stage was finished. It was postulated that the triglyceride inhibition stage is primarily caused by the higher viscosity at those conditions.

6.1.6 Reaction Rates

Reaction rates were obtained from the various experimental runs of the multiple channel reactor. It was found that the initial reaction rate was significantly lower than the maximum rate, probably due to the high concentration of triglyceride slowing the reaction, mainly through viscosity effects. The diffusivity has less of an effect, as evidenced by the lack of change in rate with FAME concentration at the

lowest flow rate of 6.35 ml min^{-1} oil. The flow rate was found to have a strong effect on the rate of reaction, from which it was inferred that the reaction was still mass transfer limited, even after the initial triglyceride inhibition stage had been overcome.

6.2 Recommendations for Further Work

6.2.1 Arising from Chapter 3

i. While the slurry coating method was successful in producing an active and mechanically stable catalyst system, there is scope to improve the repeatability of the coating techniques.

ii. Further work is needed in characterising the slurry coated catalyst. In particular, the mechanism by which the catalyst is anchored to the support should be investigated.

iii. Additionally, further information should be obtained on the location and nature of catalytic sites.

6.2.2 Arising from Chapter 4

i. While the solubility of methanol was studied, there is still scope to investigate the time required to approach equilibrium. This would then allow for consideration of the required mixing time to be considered in any pre-mixing apparatus before a reactor.

ii. Although some work was identified in the literature examining the solubilities of oil, methanol, glycerol, FAME, and fatty acids, no work was found that studied the effects of di- and monoglycerides, and no works were found which examined temperatures as high as those in this thesis. Thus, a study of the effects of complex mixtures of these components would be of great use.

iii. There are also many alternative oils to rapeseed, and it would be beneficial for a set of experiments to be undertaken examining the effect of different oil compositions on the solubility of methanol. Potentially this could lead to the development of some kind of correlation between the fatty acid profile of the oils and the methanol solubility.

6.2.3 Arising from Chapter 5

i. The slurry coating was found to maintain activity over a prolonged period. Further examination of the cause of the variable activity, possibly including in-situ analysis, and subsequent development of a system where the activity is maintained at a maximum, could lead to a reactor with excellent performance.

ii. The flow rate was found to be a major influence on the observed reaction rate in both the single and the multiple channel reactors. As such, a project could be undertaken to determine the effect of flow rates, and methods of maximising the flow rate in order to achieve improved reactor performance. Such a project could design and commission an experimental rig with a variable rate recycle from the reactor outlet to the inlet. This would allow a wider range of flow rates to be analysed.

iii. The appearance of FAME in the reaction mixture also corresponded to an improvement in the reaction rate. Further experiments should be undertaken to determine if dosing the inlet stream with FAME, or recycling a small amount of product could improve the reactor performance by maximising the initial reaction rate at the reactor inlet.

iv. A full investigation into properties such as the density and viscosity of the reaction mixture at a range of temperatures would allow for a much more informed calculation of parameters such as the flow rate, as well as estimation of the Reynolds' number so that the flow regime can be hypothesised.

Appendix A – KOH Kinetics Calculations

Homogeneous transesterification has been successfully modelled as a series of first order reversible reactions (Vicente *et al.*, 2005). The reaction steps and constants are shown in equations (A.1) to (A.3):

$$\text{Triglyceride} + \text{Methanol} \underset{k2}{\overset{k1}{\rightleftharpoons}} \text{Diglyceride} + \text{FAME} \tag{A.1}$$

$$\text{Diglyceride} + \text{Methanol} \underset{k4}{\overset{k3}{\rightleftharpoons}} \text{Monoglyceride} + \text{FAME} \tag{A.2}$$

$$\text{Monoglyceride} + \text{Methanol} \underset{k6}{\overset{k5}{\rightleftharpoons}} \text{Glycerol} + \text{FAME} \tag{A.3}$$

Taking these reaction steps and constants, a kinetic model can be developed as a series of differential equations:

$$\frac{d[\text{TG}]}{dt} = \text{-k1[TG][Me]+k2[DG][F]} \tag{A.4}$$

$$\frac{d[\text{DG}]}{dt} = \text{k1[TG][Me]-k2[DG][F]-k3[DG][Me]+k4[MG][F]} \tag{A.5}$$

$$\frac{d[\text{MG}]}{dt} = \text{k3[DG][Me]-k4[MG][F]-k5[MG][Me]+k6[G][F]} \tag{A.6}$$

$$\frac{d[\text{G}]}{dt} = \text{k5[MG][Me]-k6[G][F]} \tag{A.7}$$

$$\frac{d[\mathrm{B}]}{dt} = \mathrm{k1[TG][Me]\text{-}k2[DG][F]+k3[DG][Me]\text{-}k4[MG][F]} \\ \mathrm{+k5[MG][Me]\text{-}k6[MG][F]} \tag{A.8}$$

$$\frac{d[\mathrm{Me}]}{dt} = -\mathrm{k1[TG][Me]+k2[DG][F]\text{-}k3[DG][Me]+k4[MG][F]} \\ \mathrm{-k5[MG][Me]+k6[MG][B]} \tag{A.9}$$

For comparison with experimental results, this modelling system was used, along with the kinetic constants at 65°C and 1% catalyst loading from Vicente *et al* (2006), to provide an ideal set of results. The concentrations of oil and methanol were taken to be 0.5 and 3.0 mol L^{-1}, respectively. The results of this are shown in Figure A.1.

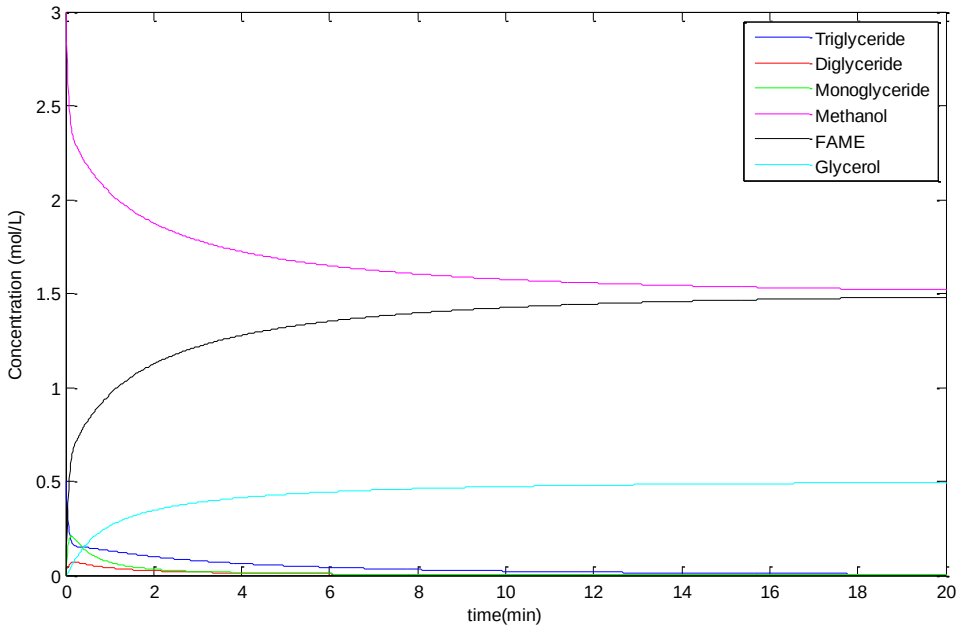

Figure A.1 Simulated reaction results from literature data.

VICENTE, G., MARTÍNEZ, M., ARACIL, J. & ESTEBAN, A. 2005. Kinetics of Sunflower Oil Methanolysis. Industrial & Engineering Chemistry Research, 44, 5447-5454.

VICENTE, G., MARTINEZ, M. & ARACIL, J. 2006. Kinetics of Brassica carinata oil methanolysis. Energy and Fuels, 20, 1722-1726.

Appendix B – Temperature Data from Multiple Channel Reactor

Temperatures were monitored using thermocouples at the inlet and outlet of each reactor. Figure B.1 shows the location of each thermocouple, with reference to the P&ID of the entire apparatus shown in Section 5.3.

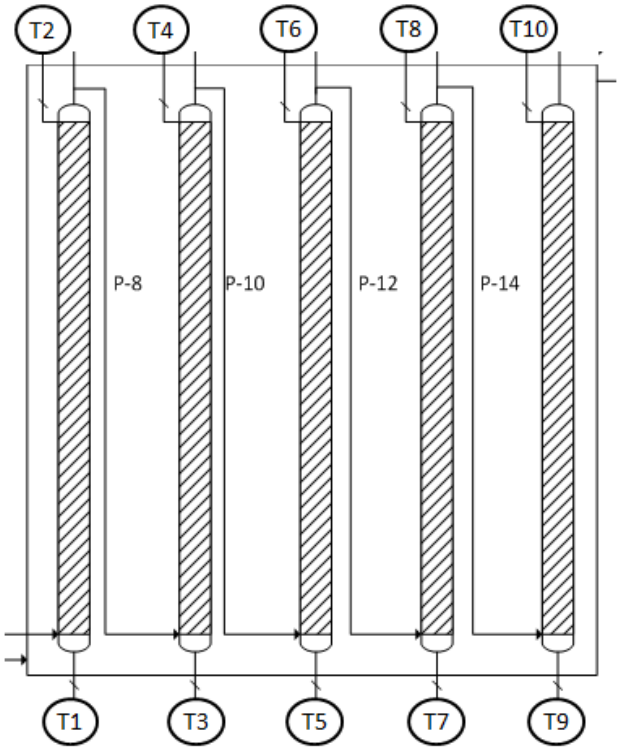

Figure B.1 Locations of thermocouples on multiple channel reactor.

Table B.1 Temperature data from experimental Set 1

	Experiment number					
	1.1	1.2	1.3	1.4	1.5	1.6
T1	107.4	98.3	106.5	74.4	100.8	88.8
T2	141.7	142.1	141.9	142.3	140.7	140.3
T3	118.4	104.7	112.8	88.8	107.0	97.6
T4	144.1	145.1	143.9	144.2	143.4	143.4
T5	117.9	109.2	113.6	94.6	107.8	102.5
T6	143.6	144.3	143.6	143.5	143.1	142.7
T7	123.4	115.8	119.9	104.7	116.9	109.8
T8	145.1	145.2	144.9	143.8	144.5	143.0
T9	128.5	120.0	124.9	114.5	121.3	114.0
T10	145.3	144.0	144.9	141.6	144.1	142.1

Table B.2 Temperature data from experimental Set 2

	Experiment number					
	2.1	2.2	2.3	2.4	2.5	2.6
T1	107.2	96.6	98.4	73.1	100.3	87.5
T2	137.6	139.2	138.3	141.5	139.7	136.4
T3	118.3	101.9	108.0	86.2	106.6	95.6
T4	140.3	142.6	141.3	143.3	141.9	142.5
T5	115.2	104.1	107.6	92.4	106.7	99.0
T6	141.3	142.5	141.7	143.3	141.4	141.5
T7	120.3	111.3	115.8	102.2	114.7	106.0
T8	142.9	142.6	143.0	143.4	142.7	142.3
T9	127.8	116.5	121.8	112.3	119.1	112.4
T10	143.0	142.1	143.1	141.1	143.0	141.4

Table B.3 Temperature data from experimental Set 3

	Experiment number					
	3.1	3.2	3.3	3.4	3.5	3.6
T1	114.3	96.4	107.3	73.3	103.5	89.1
T2	139.7	140.6	138.6	141.1	141.2	137.9
T3	119.1	102.5	111.3	87.4	108.3	97.4
T4	141.7	142.9	141.2	142.8	143.2	143.5
T5	115.1	104.4	109.5	92.7	109.8	101.9
T6	141.6	142.8	141.2	142.9	143.2	143.2
T7	119.5	112.9	115.2	101.7	117.9	109.5
T8	143.2	143.8	142.4	142.9	144.4	144.0
T9	126.6	117.1	121.4	111.5	121.0	114.4
T10	143.6	142.3	142.7	141.1	144.1	142.4

Appendix C – Material Balances from Multiple Channel Reactor

The following tables contain the full concentration data from each experimental run from the multiple channel reactor.

Table C.1 Concentration data from Experiment 1.1

Reactor Length (m)	0	0.46	0.92	1.38	1.84	2.3
[TG] (mol L^{-1})	0.7982	0.7266	0.6729	0.5456	0.4501	0.3545
[DG] (mol L^{-1})	0.0000	0.0282	0.0623	0.0725	0.0879	0.0855
[MG] (mol L^{-1})	0.0000	0.0000	0.0000	0.0087	0.0163	0.0296
[FAME] (mol L^{-1})	0.0000	0.0436	0.0693	0.1663	0.2347	0.3113
[Gly] (mol L^{-1})	0.0000	0.0051	0.0023	0.0255	0.0381	0.0555
[MeOH] (mol L^{-1})	5.6994	5.6940	5.6909	5.6790	5.6706	5.6611

Table C.2 Concentration data from Experiment 1.2

Reactor Length (m)	0	0.46	0.92	1.38	1.84	2.3
[TG] (mol L^{-1})	0.7982	0.6886	0.5253	0.4221	0.3453	0.2993
[DG] (mol L^{-1})	0.0000	0.0464	0.0814	0.0921	0.0943	0.0957
[MG] (mol L^{-1})	0.0000	0.0100	0.0065	0.0203	0.0309	0.0402
[FAME] (mol L^{-1})	0.0000	0.0607	0.1789	0.2544	0.3138	0.3484
[Gly] (mol L^{-1})	0.0000	0.0000	0.0282	0.0406	0.0526	0.0575
[MeOH] (mol L^{-1})	5.6994	5.6919	5.6774	5.6681	5.6608	5.6566

Table C.3 Concentration data from Experiment 1.3

Reactor Length (m)	0	0.46	0.92	1.38	1.84	2.3
[TG] (mol L^{-1})	0.7982	0.7201	0.6392	0.5126	0.4408	0.3742
[DG] (mol L^{-1})	0.0000	0.0368	0.0755	0.0923	0.0920	0.0970
[MG] (mol L^{-1})	0.0000	0.0075	0.0117	0.0073	0.0145	0.0287
[FAME] (mol L^{-1})	0.0000	0.0386	0.0820	0.1832	0.2406	0.2890
[Gly] (mol L^{-1})	0.0000	0.0000	0.0000	0.0254	0.0399	0.0449
[MeOH] (mol L^{-1})	5.6994	5.6947	5.6893	5.6769	5.6698	5.6639

Table C.4 Concentration data from Experiment 1.4

Reactor Length (m)	0	0.46	0.92	1.38	1.84	2.3
[TG] (mol L^{-1})	0.7982	0.6279	0.4828	0.3952	0.3062	0.2223
[DG] (mol L^{-1})	0.0000	0.0610	0.0649	0.0868	0.0938	0.0880
[MG] (mol L^{-1})	0.0000	0.0161	0.0082	0.0234	0.0390	0.0525
[FAME] (mol L^{-1})	0.0000	0.1027	0.2226	0.2787	0.3441	0.4129
[Gly] (mol L^{-1})	0.0000	0.0031	0.0471	0.0484	0.0575	0.0733
[MeOH] (mol L^{-1})	5.6994	5.6868	5.6720	5.6651	5.6571	5.6487

Table C.5 Concentration data from Experiment 1.5

Reactor Length (m)	0	0.46	0.92	1.38	1.84	2.3
[TG] (mol L^{-1})	0.7982	0.7229	0.6536	0.5368	0.4693	0.3766
[DG] (mol L^{-1})	0.0000	0.0412	0.0675	0.0808	0.0972	0.0951
[MG] (mol L^{-1})	0.0000	0.0000	0.0102	0.0119	0.0175	0.0324
[FAME] (mol L^{-1})	0.0000	0.0389	0.0763	0.1682	0.2134	0.2870
[Gly] (mol L^{-1})	0.0000	0.0000	0.0000	0.0212	0.0271	0.0424
[MeOH] (mol L^{-1})	5.6994	5.6946	5.6900	5.6787	5.6732	5.6641

Table C.6 Concentration data from Experiment 1.6

Reactor Length (m)	0	0.46	0.92	1.38	1.84	2.3
[TG] (mol L^{-1})	0.7982	0.6748	0.5699	0.4665	0.4089	0.3381
[DG] (mol L^{-1})	0.0000	0.0513	0.0781	0.0843	0.0938	0.0958
[MG] (mol L^{-1})	0.0000	0.0092	0.0124	0.0151	0.0217	0.0335
[FAME] (mol L^{-1})	0.0000	0.0712	0.1422	0.2235	0.2640	0.3182
[Gly] (mol L^{-1})	0.0000	0.0005	0.0132	0.0364	0.0423	0.0518
[MeOH] (mol L^{-1})	5.6994	5.6906	5.6819	5.6719	5.6670	5.6603

Table C.7 Concentration data from Experiment 2.1

Reactor Length (m)	0	0.46	0.92	1.38	1.84	2.3
[TG] (mol L^{-1})	0.7982	0.7642	0.7230	0.6775	0.6209	0.5145
[DG] (mol L^{-1})	0.0000	0.0247	0.0374	0.0514	0.0777	0.0857
[MG] (mol L^{-1})	0.0000	0.0000	0.0000	0.0068	0.0094	0.0129
[FAME] (mol L^{-1})	0.0000	0.0106	0.0415	0.0696	0.1011	0.1836
[Gly] (mol L^{-1})	0.0000	0.0000	0.0014	0.0015	0.0016	0.0240
[MeOH] (mol L^{-1})	5.6994	5.6940	5.6909	5.6790	5.6706	5.6611

Table C.8 Concentration data from Experiment 2.2

Reactor Length (m)	0	0.46	0.92	1.38	1.84	2.3
[TG] (mol L^{-1})	0.7982	0.7072	0.6348	0.5341	0.4538	0.4038
[DG] (mol L^{-1})	0.0000	0.0433	0.0629	0.0815	0.0907	0.0947
[MG] (mol L^{-1})	0.0000	0.0089	0.0097	0.0095	0.0176	0.0251
[FAME] (mol L^{-1})	0.0000	0.0443	0.0977	0.1707	0.2297	0.2667
[Gly] (mol L^{-1})	0.0000	0.0000	0.0052	0.0234	0.0346	0.0406
[MeOH] (mol L^{-1})	5.6994	5.6939	5.6874	5.6784	5.6712	5.6666

Table C.9 Concentration data from Experiment 2.3

Reactor Length (m)	0	0.46	0.92	1.38	1.84	2.3
[TG] (mol L^{-1})	0.7982	0.7542	0.7048	0.6529	0.5376	0.4997
[DG] (mol L^{-1})	0.0000	0.0335	0.0412	0.0613	0.0756	0.0887
[MG] (mol L^{-1})	0.0000	0.0000	0.0000	0.0084	0.0127	0.0150
[FAME] (mol L^{-1})	0.0000	0.0120	0.0545	0.0840	0.1702	0.1936
[Gly] (mol L^{-1})	0.0000	0.0000	0.0044	0.0020	0.0230	0.0249
[MeOH] (mol L^{-1})	5.6994	5.6979	5.6927	5.6891	5.6785	5.6756

Table C.10 Concentration data from Experiment 2.4

Reactor Length (m)	0	0.46	0.92	1.38	1.84	2.3
[TG] (mol L^{-1})	0.7982	0.6516	0.5695	0.4394	0.3827	0.3282
[DG] (mol L^{-1})	0.0000	0.0602	0.0684	0.0820	0.0901	0.0941
[MG] (mol L^{-1})	0.0000	0.0129	0.0116	0.0196	0.0300	0.0386
[FAME] (mol L^{-1})	0.0000	0.0839	0.1481	0.2459	0.2854	0.3258
[Gly] (mol L^{-1})	0.0000	0.0000	0.0188	0.0416	0.0451	0.0515
[MeOH] (mol L^{-1})	5.6994	5.6891	5.6812	5.6692	5.6643	5.6594

Table C.11 Concentration data from Experiment 2.5

Reactor Length (m)	0	0.46	0.92	1.38	1.84	2.3
[TG] (mol L^{-1})	0.7982	0.7530	0.7106	0.6370	0.5289	0.4228
[DG] (mol L^{-1})	0.0000	0.0294	0.0486	0.0672	0.0842	0.0828
[MG] (mol L^{-1})	0.0000	0.0000	0.0064	0.0091	0.0052	0.0232
[FAME] (mol L^{-1})	0.0000	0.0181	0.0371	0.0937	0.1747	0.2582
[Gly] (mol L^{-1})	0.0000	0.0000	0.0000	0.0028	0.0267	0.0430
[MeOH] (mol L^{-1})	5.6994	5.6972	5.6948	5.6879	5.6779	5.6677

Table C.12 Concentration data from Experiment 2.6

Reactor Length (m)	0	0.46	0.92	1.38	1.84	2.3
[TG] (mol L^{-1})	0.7982	0.6966	0.6377	0.5378	0.4589	0.3840
[DG] (mol L^{-1})	0.0000	0.0411	0.0612	0.0787	0.0892	0.0977
[MG] (mol L^{-1})	0.0000	0.0085	0.0102	0.0129	0.0197	0.0295
[FAME] (mol L^{-1})	0.0000	0.0589	0.0961	0.1683	0.2257	0.2802
[Gly] (mol L^{-1})	0.0000	0.0002	0.0048	0.0213	0.0324	0.0411
[MeOH] (mol L^{-1})	5.6994	5.6921	5.6876	5.6787	5.6717	5.6650

Table C.13 Concentration data from Experiment 3.1

Reactor Length (m)	0	0.46	0.92	1.38	1.84	2.3
[TG] (mol L^{-1})	0.7982	0.7704	0.7038	0.6523	0.6226	0.5239
[DG] (mol L^{-1})	0.0000	0.0221	0.0250	0.0672	0.0657	0.0927
[MG] (mol L^{-1})	0.0000	0.0000	0.0000	0.0086	0.0095	0.0119
[FAME] (mol L^{-1})	0.0000	0.0065	0.0643	0.0800	0.1063	0.1723
[Gly] (mol L^{-1})	0.0000	0.0000	0.0131	0.0000	0.0072	0.0186
[MeOH] (mol L^{-1})	5.6994	5.6986	5.6915	5.6896	5.6863	5.6782

Table C.14 Concentration data from Experiment 3.2

Reactor Length (m)	0	0.46	0.92	1.38	1.84	2.3
[TG] (mol L^{-1})	0.7982	0.7329	0.6930	0.6109	0.4701	0.4392
[DG] (mol L^{-1})	0.0000	0.0424	0.0529	0.0775	0.0843	0.0907
[MG] (mol L^{-1})	0.0000	0.0000	0.0000	0.0132	0.0186	0.0211
[FAME] (mol L^{-1})	0.0000	0.0262	0.0578	0.1085	0.2195	0.2409
[Gly] (mol L^{-1})	0.0000	0.0000	0.0016	0.0015	0.0327	0.0360
[MeOH] (mol L^{-1})	5.6994	5.6962	5.6923	5.6861	5.6724	5.6698

Table C.15 Concentration data from Experiment 3.3

Reactor Length (m)	0	0.46	0.92	1.38	1.84	2.3
[TG] (mol L^{-1})	0.7982	0.7679	0.7072	0.6637	0.6107	0.5125
[DG] (mol L^{-1})	0.0000	0.0248	0.0373	0.0577	0.0641	0.0809
[MG] (mol L^{-1})	0.0000	0.0000	0.0055	0.0057	0.0114	0.0118
[FAME] (mol L^{-1})	0.0000	0.0063	0.0531	0.0778	0.1165	0.1882
[Gly] (mol L^{-1})	0.0000	0.0000	0.0016	0.0029	0.0099	0.0279
[MeOH] (mol L^{-1})	5.6994	5.6986	5.6929	5.6898	5.6851	5.6763

Table C.16 Concentration data from Experiment 3.4

Reactor Length (m)	0	0.46	0.92	1.38	1.84	2.3
[TG] (mol L^{-1})	0.7982	0.6373	0.5730	0.5074	0.4006	0.3430
[DG] (mol L^{-1})	0.0000	0.0481	0.0670	0.0819	0.0909	0.0956
[MG] (mol L^{-1})	0.0000	0.0092	0.0114	0.0167	0.0284	0.0375
[FAME] (mol L^{-1})	0.0000	0.1039	0.1461	0.1905	0.2707	0.3131
[Gly] (mol L^{-1})	0.0000	0.0125	0.0188	0.0251	0.0410	0.0475
[MeOH] (mol L^{-1})	5.6994	5.6866	5.6814	5.6760	5.6661	5.6609

Table C.17 Concentration data from Experiment 3.5

Reactor Length (m)	0	0.46	0.92	1.38	1.84	2.3
[TG] (mol L^{-1})	0.7982	0.7439	0.7124	0.6342	0.5487	0.5086
[DG] (mol L^{-1})	0.0000	0.0277	0.0443	0.0572	0.0714	0.0755
[MG] (mol L^{-1})	0.0000	0.0000	0.0056	0.0080	0.0093	0.0149
[FAME] (mol L^{-1})	0.0000	0.0296	0.0409	0.1018	0.1643	0.1936
[Gly] (mol L^{-1})	0.0000	0.0006	0.0000	0.0096	0.0247	0.0294
[MeOH] (mol L^{-1})	5.6994	5.6958	5.6944	5.6869	5.6792	5.6756

Table C.18 Concentration data from Experiment 3.6

Reactor Length (m)	0	0.46	0.92	1.38	1.84	2.3
[TG] (mol L^{-1})	0.7982	0.7323	0.6750	0.5514	0.4776	0.4107
[DG] (mol L^{-1})	0.0000	0.0417	0.0601	0.0948	0.0903	0.0932
[MG] (mol L^{-1})	0.0000	0.0000	0.0072	0.0078	0.0181	0.0304
[FAME] (mol L^{-1})	0.0000	0.0276	0.0639	0.1495	0.2102	0.2604
[Gly] (mol L^{-1})	0.0000	0.0000	0.0000	0.0130	0.0279	0.0355
[MeOH] (mol L^{-1})	5.6994	5.6960	5.6915	5.6810	5.6736	5.6674